Pilot-Scale Oxy-Fuel Combustion of Victorian Brown Coal

Dr Lian Zhang

Department of Chemical Engineering,

Monash University, Clayton,

Vic 3800, Australia

Tel: 61-3-9905-2592, Fax: 61-3-9905-5686

Email: lian.zhang@monash.edu

March 24, 2014

Disclaimer

Copyright

Acknowledgement

The authors are grateful to Australian National Low Emission Coal (ANLEC) R&D and Brown Coal Innovation Australia (BCIA) for the support. The project partners including Shanghai Boiler Works Co Ltd, Chubu University, and Shanghai Jiao Tong University are acknowledged for their support and collaboration throughout the project. The Shanghai University of Electric Power and Huazhong University of Science and Technology are also thanked for on-site flue gas analysis.

Table of Contents

1. Research Summary

The project was supported by Australian National Low Emission Coal (ANLEC) R&D and Brown Coal Innovation Australian (BCIA) in 2011-13. It aims to clarify the science and engineering characteristics of oxy-fuel combustion of Victorian brown coal in a pilot-scale furnace, to provide the performance and emission data in an industry relevant facility, and eventually to provide a basis for design and scale-up of this low emission coal technology to commercial scale in the foreseeable carbon-constrained future.

Victorian brown coal is the single largest source for the power generation in Victoria, meeting over 85% of the electricity needs of the State. Due to the presence of high levels of inherent moisture, its greenhouse gas emission rate is much higher than that of Australian black coals and natural gas. The oxy-fuel combustion technology is a process of burning coal in the mixture of pure or highly pure oxygen and recycled flue gas (RFG) to deliver a CO2-rich gas stream which is ready for direct storage/sequestration with minimal further purification. It is cost-effective when compared with post-combustion capture. It is also energy-efficient when the supercritical or ultra-supercritical steam condition and advanced coal drying techniques are implemented in a retrofitted or purposed-designed oxy-firing plant. The oxy-fuel combustion was generally tested focus on black coals which possess high heating values and are used as the major feedstock for most the power plants worldwide. Through this project, we successfully conducted the first pilot-scale research of brown-coal-fired oxy-fuel combustion around the word. Apart from the retrofit case, a new purpose-designed oxy-firing scheme was proposed and examined intensively with independent external/internal coal drying coupled to address the potential of offsetting the energy penalty of air separation and thus achieving high-efficiency for this process.

The project has been completed successfully. It was commenced from the techno-economic analysis to confirm that the integration of pre-drying and super-critical steam condition is essential to compensate for the energy penalty related to air separation unit and CO2 compression. It also clarified that the use and installation of Chinese equipment in an Australian-own brown coal oxy-firing power plant is critical in reducing the cost of electricity and cost of CO2 avoidance significantly. Moreover, the techno-economic analysis suggested that coal pre-drying is a key factor affecting the cost of electricity and cost of CO2 avoidance. The use of low-cost and effective coal drying technique such as those developed in China is effective in reducing the

capital cost for the construction of a purpose-designed oxy-fuel power plant in the Latrobe Valley.

A variety of experiments have been conducted successfully in a 3MW pilot-scale facility, which provides sufficient information and knowledge on the performance of oxy-fuel combustion of Victorian brown coal, as closer to the level of industrial demonstration. The pilot-scale experiments have proven the easiness for the shift of the combustion of Victorian brown coal, either dry or as-mined wet, from air-firing to oxy-firing. Under an estimate air ingress rate of about 2%, the purity of CO2 in flue gas has been confirmed to reach approximately 80% in dry flue gas basis, with moisture reaching 40% in wet flue gas basis, SO3 being negligible and NO3 (mg/MJ) being reduced remarkably. To complete and interpret the experiments conducted in the 3 MWth pilot-scale facility, the lab-scale studies in a flat-flame burner reactor for oxy-fuel fundamental mechanism have also been approached. Plus the commercial CFD modeling program has been refined to address the distinct radiation property of abundant tri-atomic gases, CO2 and steam, the higher char-CO2 and char-steam gasification reactivity of Victorian brown coal, and the different reaction rate for volatiles in oxy-firing mode. The model has been fully verified by a good agreement with the experimental observations.

The deployment of oxy-fuel combustion technology for brown coal is the ultimate goal of the authors. We do believe it will play a significant role in cutting the high carbon emission of Victoria by 2020 and maintain the sustainability and competitiveness of the industry in Victoria.

2. Techno-economic analysis on Victorian brown coal oxy-firing

One final goal of this part is to clarify if the integration of coal drying, namely the use of externally dried coal instead of the as-mined wet coal and supercritical steam condition in the boiler can offset the large energy penalty (~ 9%) related to the air-separation unit (ASU) in an oxy-firing boiler. Moreover, we are interested in knowing if the use and installation of low-cost, Chinese-made equipments in an Australian-own oxy-firing power plant can remarkably reduce the levelised cost of electricity (LCOE) and the cost of CO_2 avoidance. In this part, we also aim to reveal the variation of net efficiency for oxy-firing power plant with the change on a number of key operating parameters.

The process flowsheeting was conducted through the use of commercial software, namely Thermoflex 24. Two unit sizes, 300 MWth and 600 MWth with subcritical and supercritical steam conditions respectively have been simulated. For each unit, the air-firing was first simulated, by the use of the built-in process flowsheet in the software. For an oxy-fuel boiler system, it can be simply described as a process that eliminates nitrogen from the oxidant by burning the fuel in a mixture of nearly pure oxygen and a CO_2-rich recycled flue gas (RFG), resulting in a product flue gas from the boiler containing mainly carbon dioxide and water vapour. For the use of either dried coal or wet coal, the accumulation of water vapour is a critical issue the condensation of which has to be considered from the boiler operating perspective. With the use and recirculation of wet flue gas discharged from economiser, the latent heat of water vapour within it could be used so as to slightly increase the boiler thermal efficiency. However, the high-temperature (~400 ^{o}C) hot flue gas from economiser requires large energy consumption for the induced fan (IF) to recirculate it back into coal mill and boiler, which in turn could deteriorate the net efficiency of the oxy-firing power plant. Moreover, the recirculated flue gas has to been split into two streams, primary gas into mill to entrain coal particle into the boiler, and secondary gas into the boiler straight away to ensure a complete burnout of coal particles. In light of this, three cases have been considered for the process simulation, namely

(a) Dry recycle for the condensation of steam and removal from both primary and secondary gases,

(b) Wet recycle for the recirculation of hot wet flue gas without condensation, and
(c) Half - dry (or half-wet) recycle for the condensation of steam out of primary gas only.

In the case of dry recycle, all the primary and secondary recycled flue gas are desulphurised and dehydrated prior to being recirculated, in the half-dry recycle, only the primary recycled flue gas is desulphurised and dehydrated, whereas the secondary gas remains wet; in wet recycle case, desulphurization and water removal are not implemented for both two streams of the RFG.

The use of dried coal (*e.g.* as-mined black coal or pre-dried brown coal) for oxy-firing is easy to be simulated in the Thermoflex, because coal drying is not necessarily integrated into the overall process. However, for the as-mined wet Victorian brown coal with up to 70 *wt%* inherent moisture, an effective integration of external dryer into the overall process, through the use of waste heat, is pivotal for improving the net efficiency of the process. In light of this, four scenarios have been considered for wet Victorian brown coal oxy-firing, that is:

a) *Direct oxy-firing* of wet Victorian brown coal through the use of fan mill in which a portion of hot flue gas, sucked from the exit of combustion zone, is injected for coal drying;
b) *Pre-drying of coal by flue gas from economiser* which has a temperature of around 300-400oC;
c) *Pre-drying of coal by the use of low-pressure steam* which is extracted from the turbine system instead of using any external steam, and
d) *Pre-drying of coal by the combined use of steam and flue gas*.

The boiler system with an output of 600 MW for supercritical steam condition was simulated for above four different coal drying scenarios.

Apart from the analysis on process efficiency, the LCOE and cost of CO_2 avoidance for purpose-designed Victorian brown coal oxy-firing were also calculated, based on the methods based on the methods from "CCS economics methodology and assumptions" (Guy Allinson, Peter Neal, Minh Ho, Dianne Wiley and Geoffrey McKee, 2006, CO2CRC Report No: RPT06-0080) and the data from "Pulverized Coal Oxycombustion Power Plants" (2008, DOE/NETL-2007/1291). Calculation on these two costs was conducted for three scenarios:

a) *The full use of Western countries' equipments* for the construction of an oxy-firing power plant in the Latrobe Valley;
b) *The hybrid use* of Chinese equipments including boiler, turbine and auxiliary facilities, and Western countries' facilities including air-separation unit (ASU) and CO_2 compressors for the oxy-firing plant; and
c) *The full use of Chinese equipments* for the oxy-firing power plant construction.

For each scenario, an external fluidized-bed dryer based on Germany RWE technology was employed for coal pre-drying. The cost related to this process was also estimated based on RWE report.

2.1 Net efficiency of Victorian brown coal oxy-firing boiler

As mentioned above, the boiler system with an output of 600 MW for supercritical stream conditions was simulated, with four different coal pre-drying scenarios. The results are summarised in table 2.1, and all the process flowsheets are illustrated in figure 2.1. In table 2.1, the four coal pre-drying scenarios are listed in the first column and numbered as 0, 1, 2, and 12 for direct firing, pre-drying by flue gas from economiser, pre-drying by steam from low-pressure steam turbine, and pre-drying by the combined use of flue gas and steam, respectively. Instead, the four flue-gas condensation modes, from air to oxy-dry, oxy-half-dry and oxy-wet are labelised as A, D, HD and W, respectively. All the cases simulated here are symbolized as the combination of these numbers and letters. For instance, case A-0 refers to direct combustion of Victorian brown coal in air. The case of A-1 was not simulated, because there is insufficient heat from the flue gas to pre-dry the wet Victorian brown coal.

Due to the employment of energy-intensive ASU and CO_2 compressors, the efficiencies of the oxy-firing scenarios are significantly lower than that of reference (air-firing) case for any pre-dry method. For the oxy-fuel systems of bituminous coal and fully dried brow coal, half-dry model has higher efficiency than the dry model and the system of wet model has the highest efficiency among the three models. For any system of reference case and oxy-fuel cases for Victorian brown coal, the pre-dry methods of using flue gas alone, steam alone and the combination of flue gas and steam can exert an effect on efficiency improvement. The effect of flue-gas pre-dry method is apparently better than that of steam. The efficiency improvement of about 2% for flue gas and about 0.2% for steam can be achieved. Nevertheless, the pre-dry method of combining flue gas and steam has the greater effect of efficiency improvement. The achieved net efficiency is also comparable to the existing

subcritical air-firing boiler in the Latrobe Valley, which is reportedly around 25-30% LHV based. This proves the necessity of the combined use of pre-drying and ultra-supercritical steam condition for the ASU-related energy penalty compensation for brown coal oxy-fuel combustion process. Otherwise, the efficiency drop would be too significant to afford.

Table 2.1 Net efficiency of brown coal oxy-fuel combustion by the combination of pre-drying and ultra-supercritical steam condition in the boiler system, %LHV based.

Coal process type	Air [A]	Oxy-dry [D]	Oxy-half-dry [HD]	Oxy-wet [W]
Direct [0]	39.47	25.9	26.08	26.22
Pre-drying (flue gas) [1]	-	27.84	28.17	28.23
Pre-drying (steam) [2]	39.89	26.03	26.25	26.41
Pre-drying (steam & flue gas) [12]	41.7	27.95	28.29	28.48

Table 2.2 Basic financial parameters for the cost estimation

Item	Unit	Value
Plant lifetime	year	20
Plant occupancy	hour	7500
Discounted cash flow	%	8
Cost allocation for year 1	%	20
Cost allocation for year 2	%	30
Cost allocation for year 3	%	40
Cost allocation for year 4	%	10
CO_2 capture rate (for OF cases)	%	95
Price of standard coal (LLV=29270 kJ/kg)	$/t	47.1
Rate of fixed capital formation	-	0.95
Net residual value	-	0.05
Depreciation year	year	15
Amortization year	year	5

Case A-0: Direct firing of coal in air – reference power plant

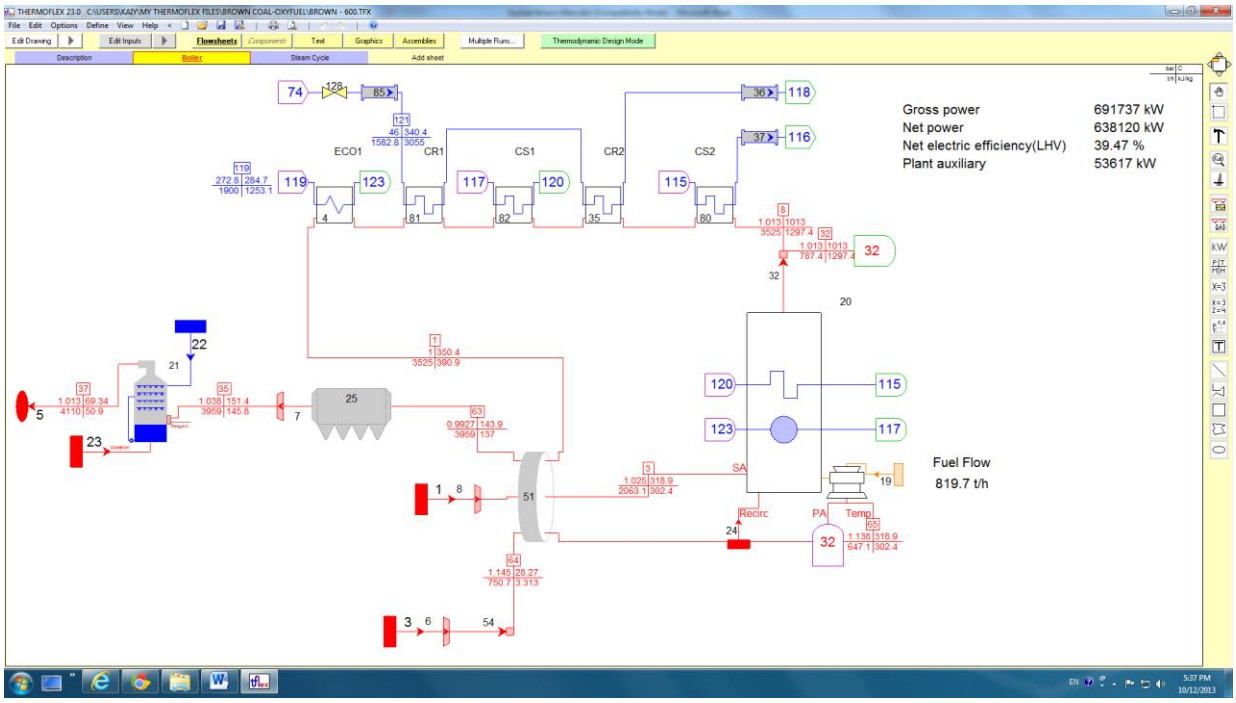

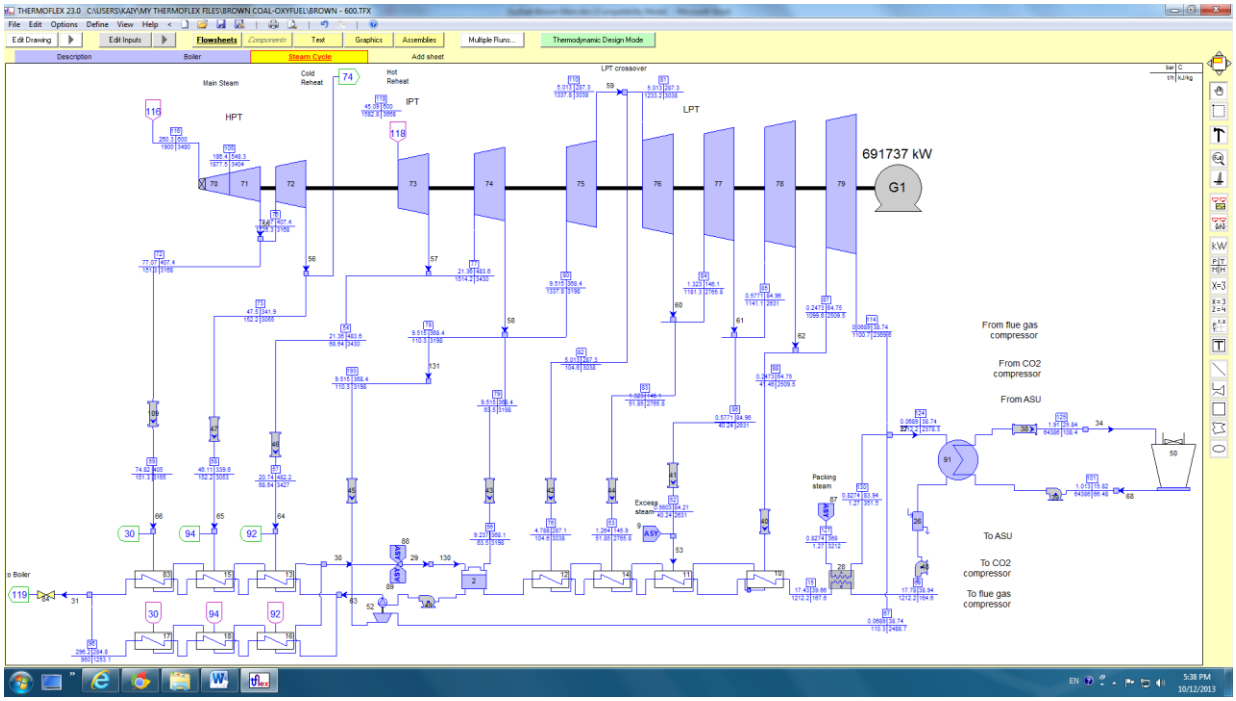

Case A-2: Air-firing system integrated with a pre-dryer using steam from low-pressure turbine

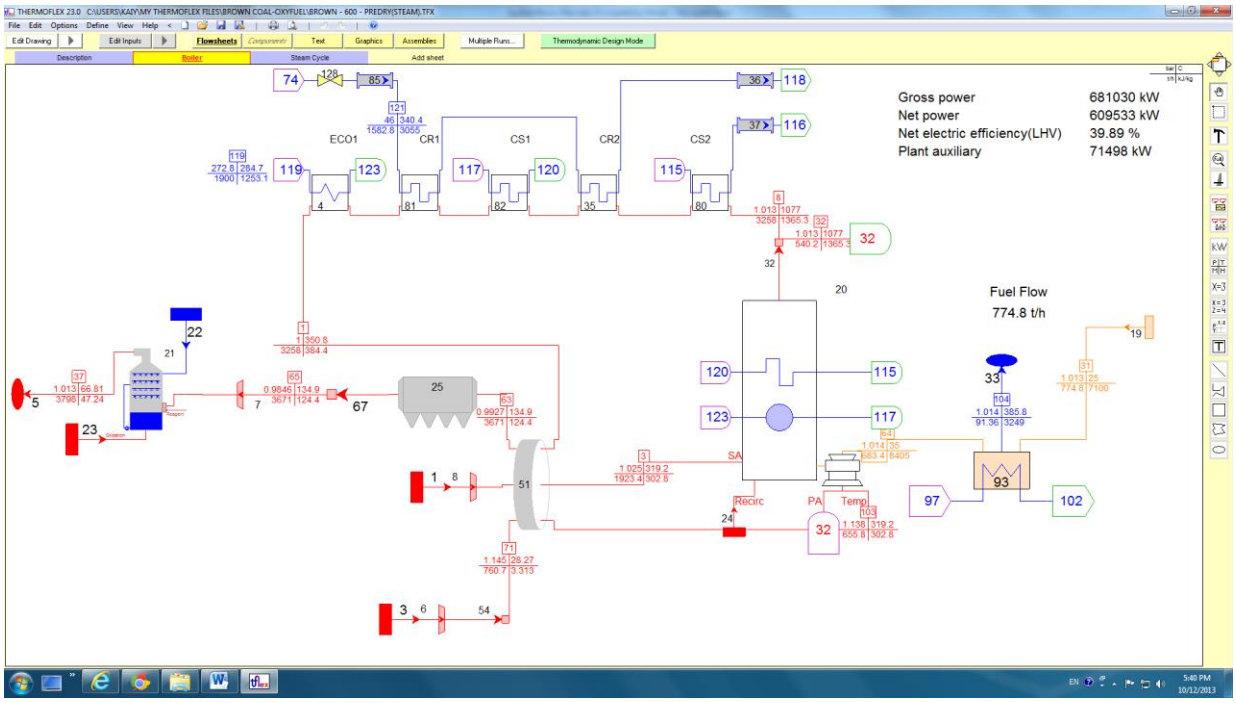

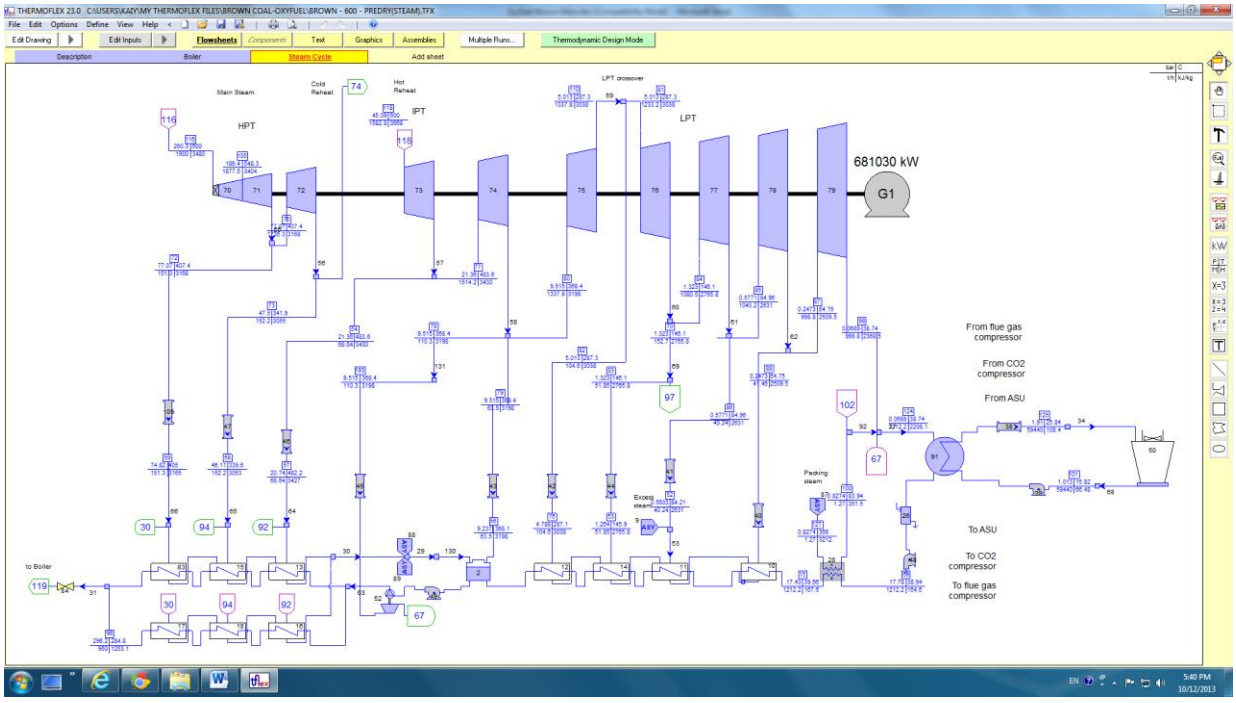

Case A-12: Air-firing system integrated with a pre-dryer using both flue gas and steam

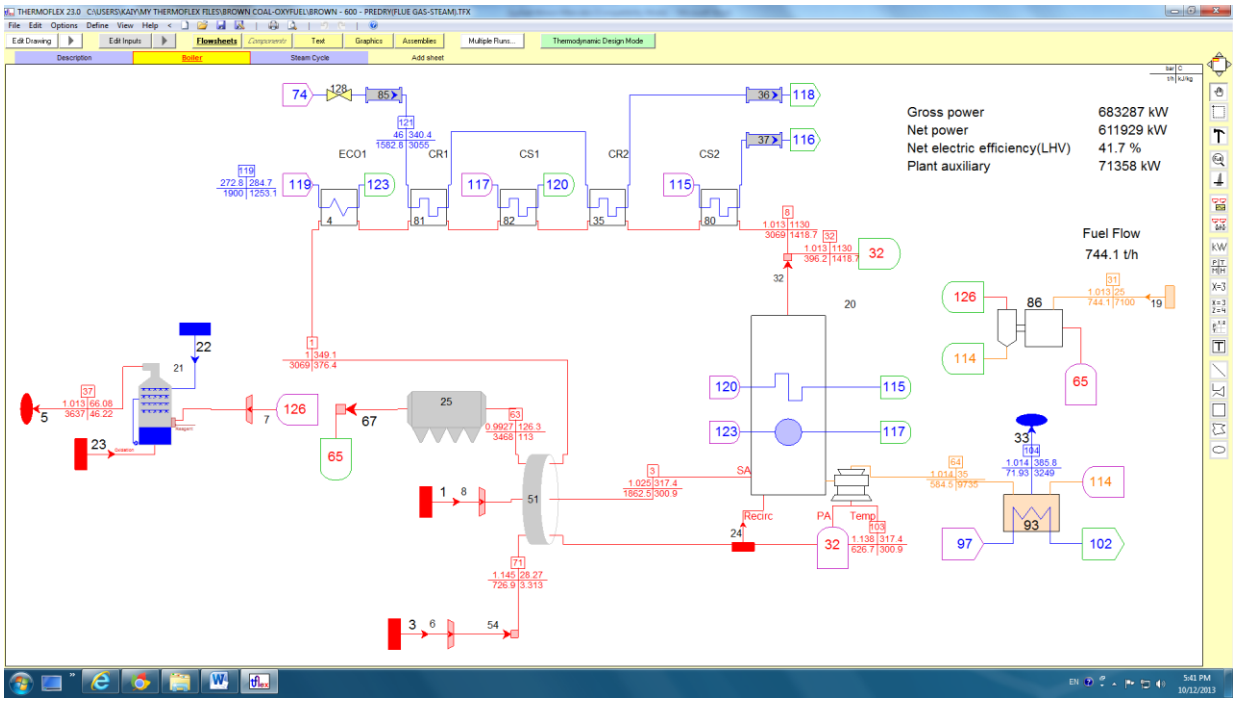

Case D-0: Oxy-firing of as-mined wet brown coal using fan mill, and both streams of recirculated flue gas are dried

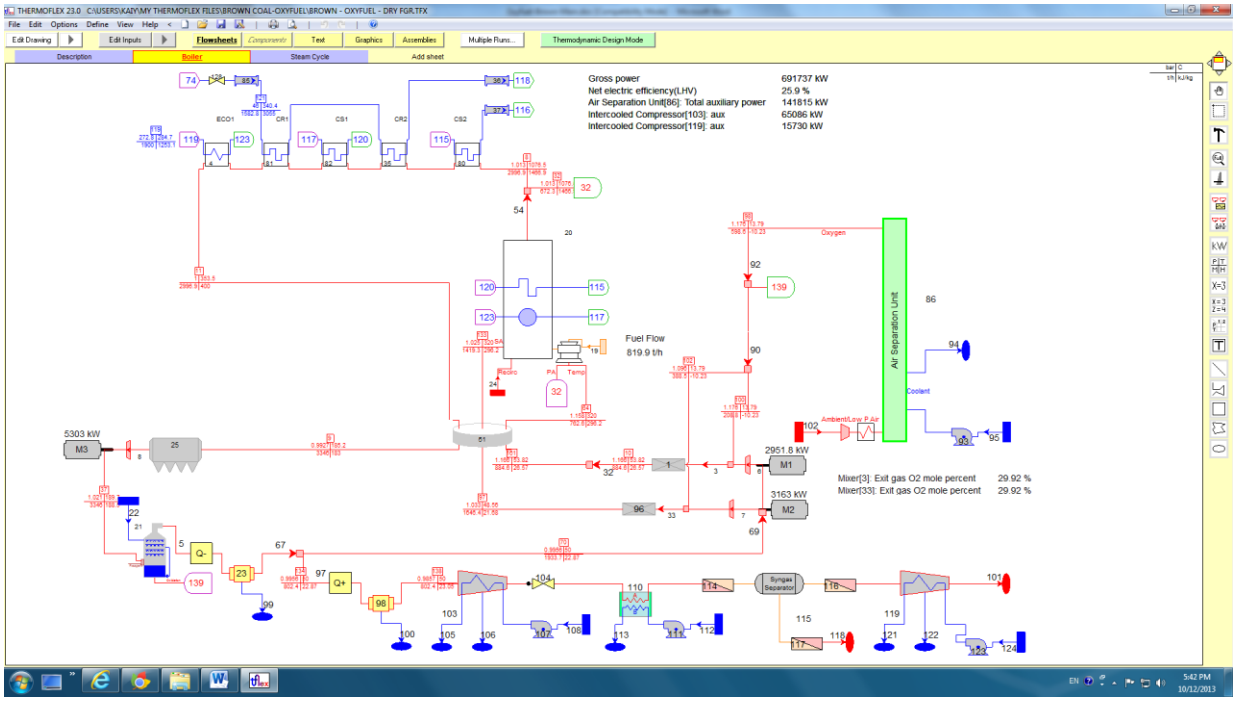

Case D-1: Oxy-firing of pre-dried brown coal using fan mill; both streams of recirculated flue gas are dried, and coal is pre-dried by flue gas from economiser

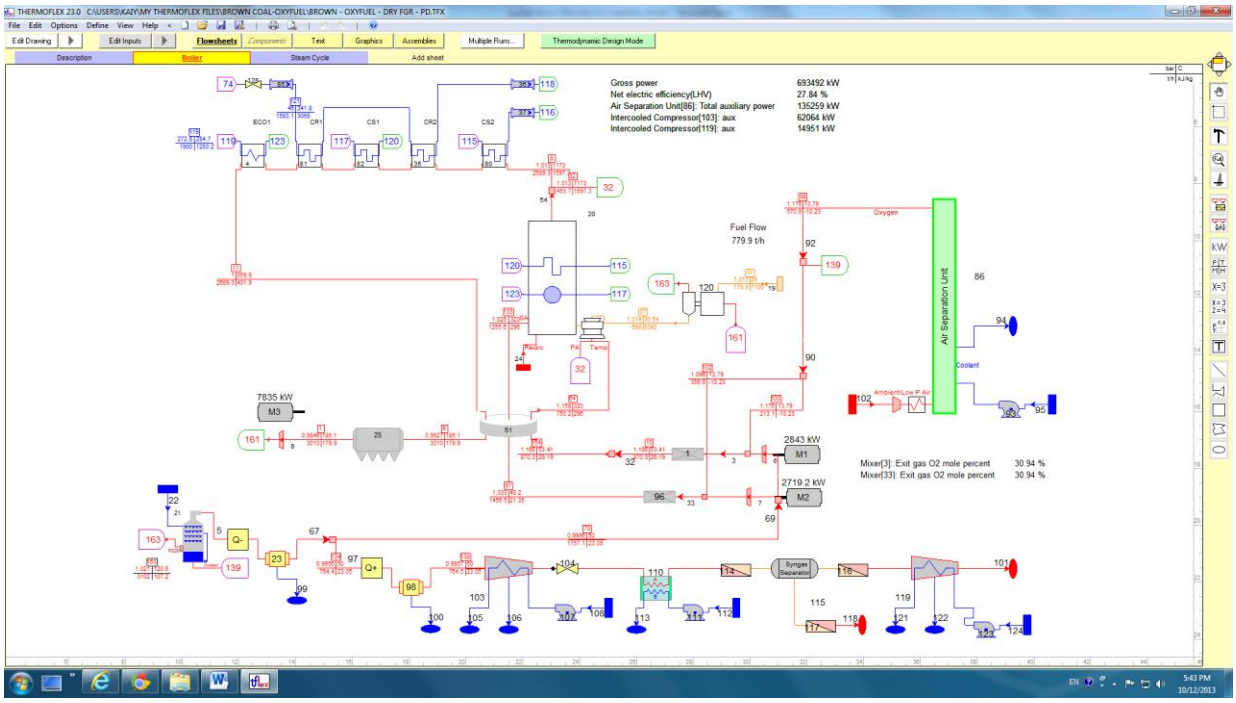

Case D-2: Oxy-firing of pre-dried brown coal using fan mill; both streams of recirculated flue gas are dried, and coal is pre-dried by steam from low-pressure turbine

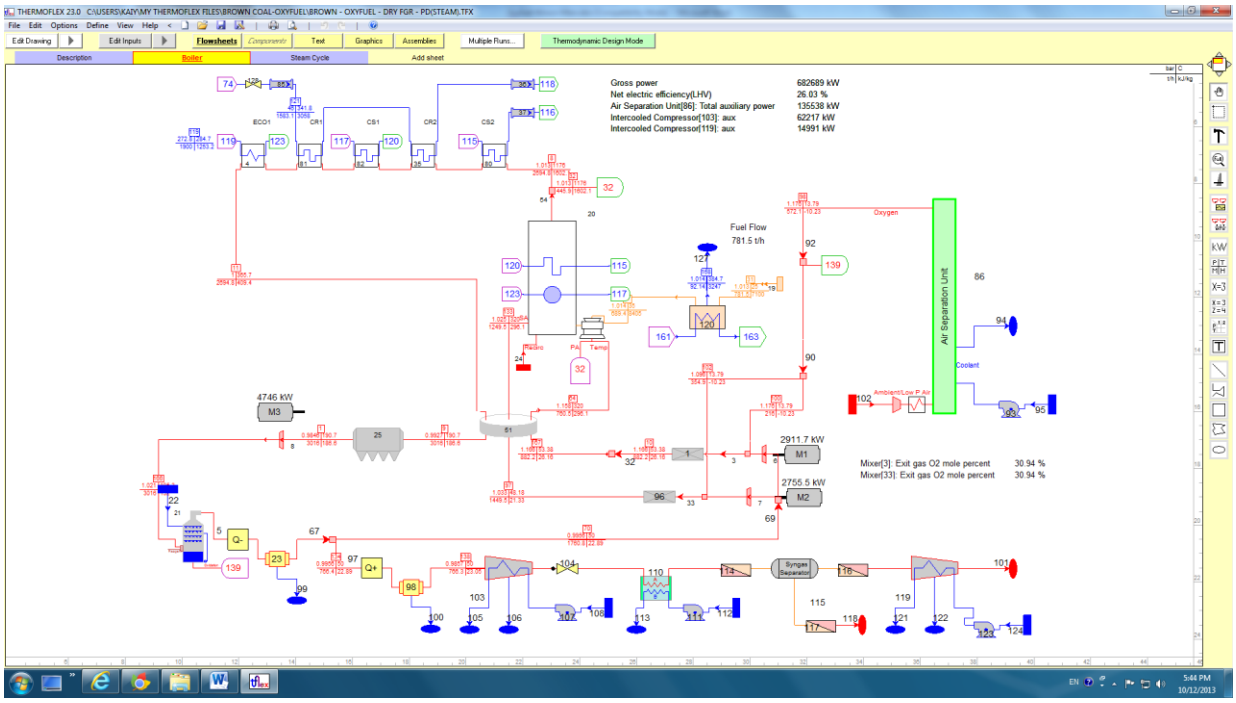

Case D-12: Oxy-firing of pre-dried brown coal using fan mill; both streams of recirculated flue gas are dried, and coal is pre-dried by both flue gas from economizer and steam from low-pressure turbine

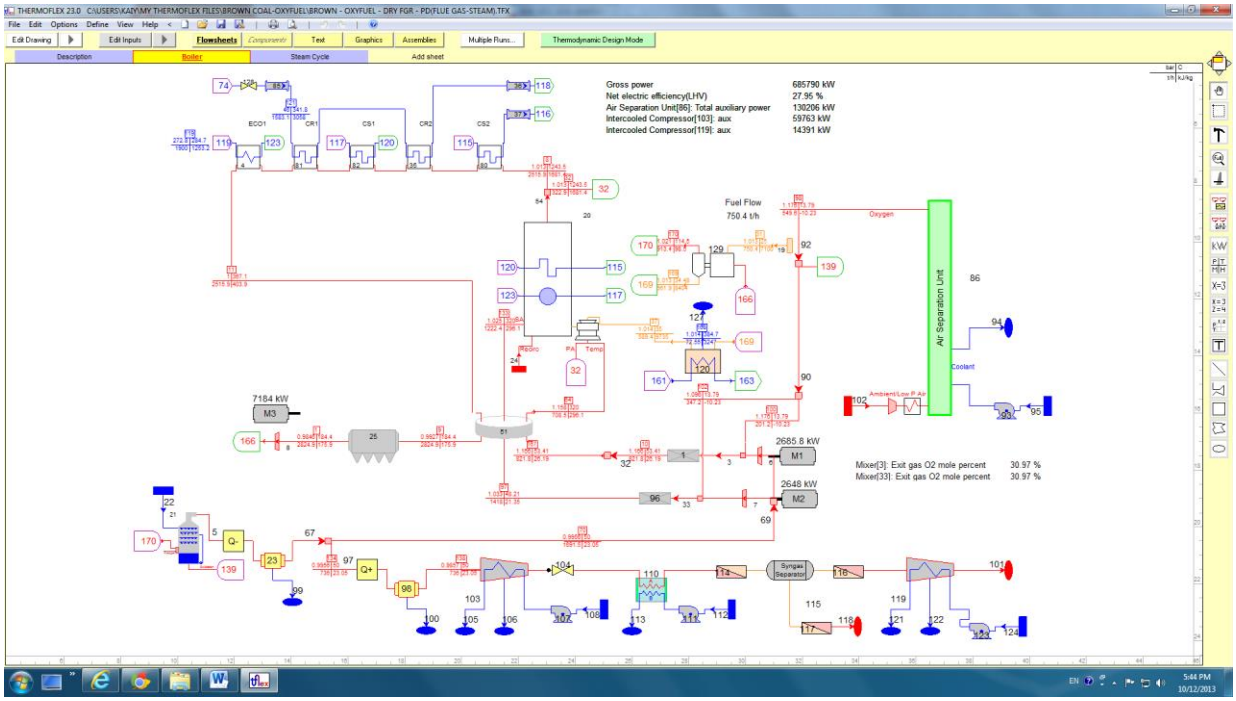

Case HD-0: Oxy-firing of as-mined wet coal using fan mill; the primary stream of recirculated flue gas is dried, and coal is pre-dried by both flue gas from economizer and steam from low-pressure turbine

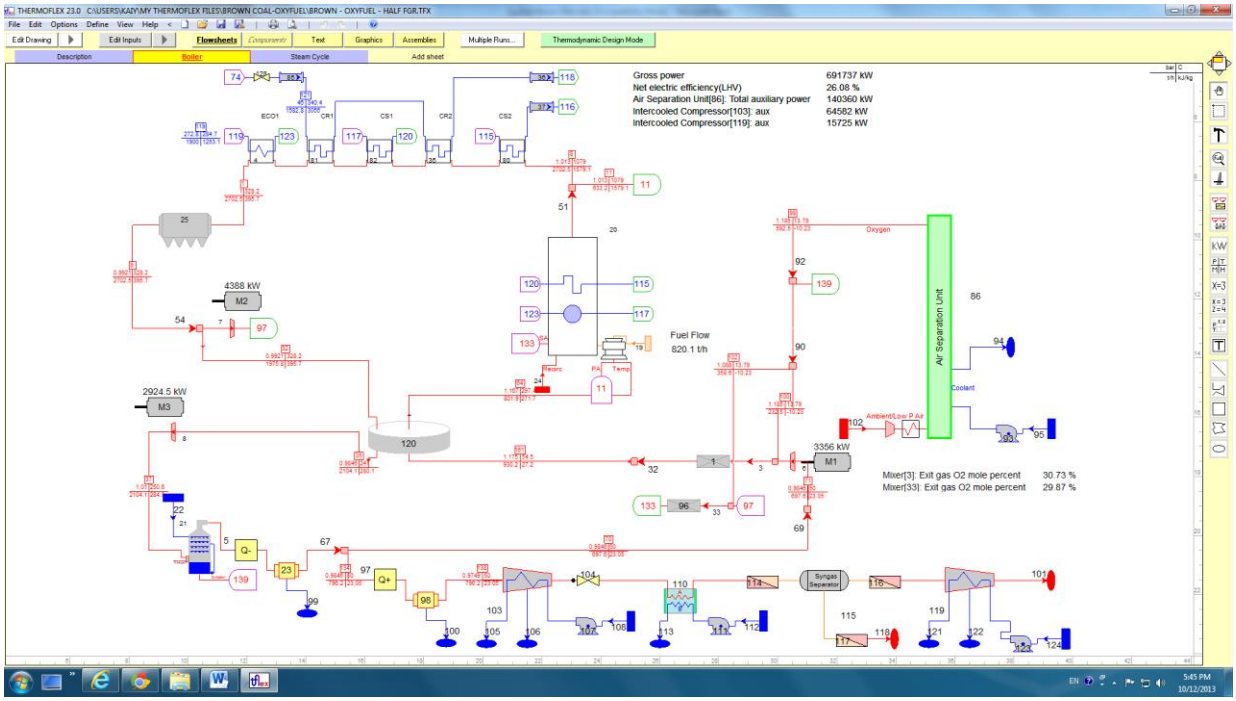

Case HD-1: Oxy-firing of pre-dried coal using fan mill; the primary stream of recirculated flue gas is dried, and coal is pre-dried by flue gas from economiser

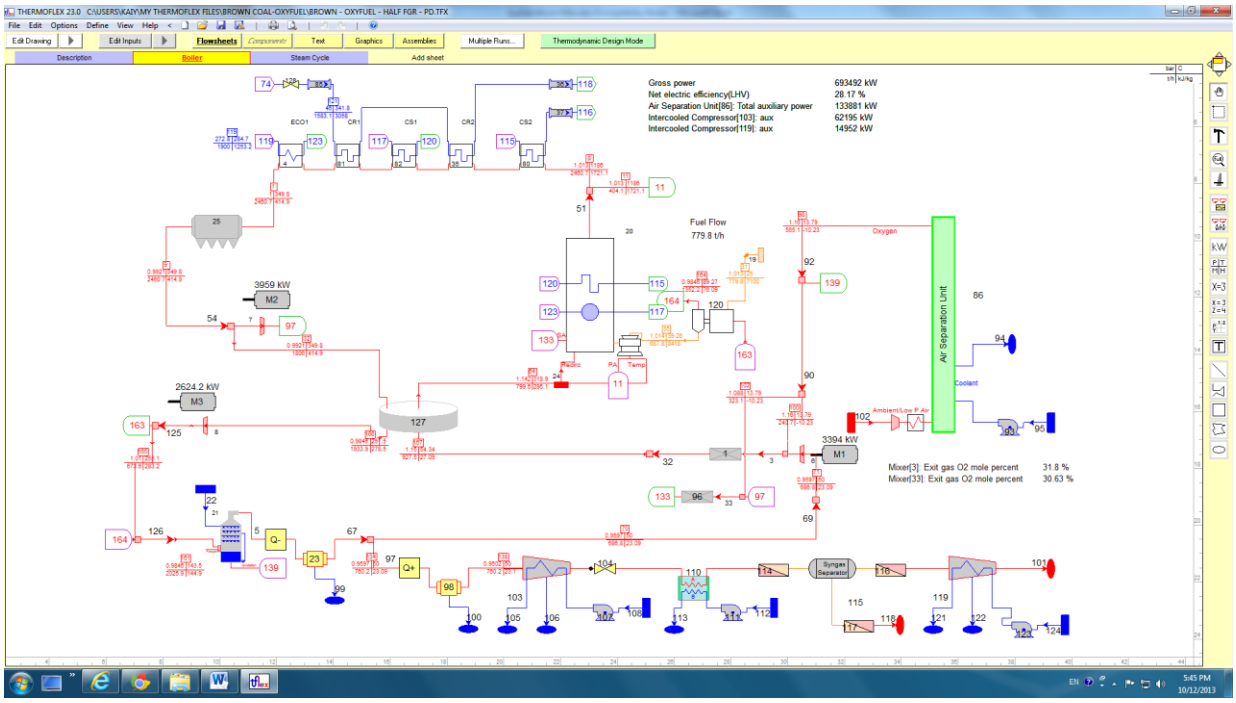

Case HD-2: Oxy-firing of pre-dried coal using fan mill; the primary stream of recirculated flue gas is dried, and coal is pre-dried by steam from low-pressure turbine

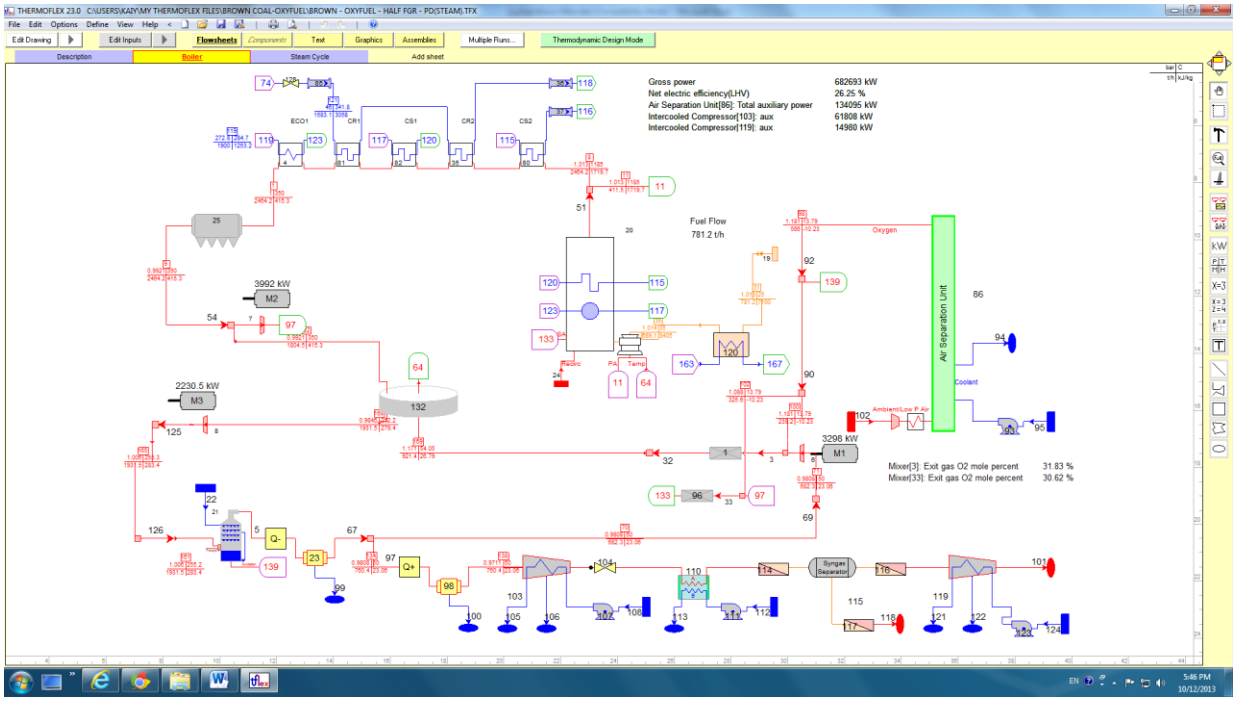

Case HD-12: Oxy-firing of pre-dried coal using fan mill; the primary stream of recirculated flue gas is dried, and coal is pre-dried by both flue gas from economizer and steam from low-pressure turbine

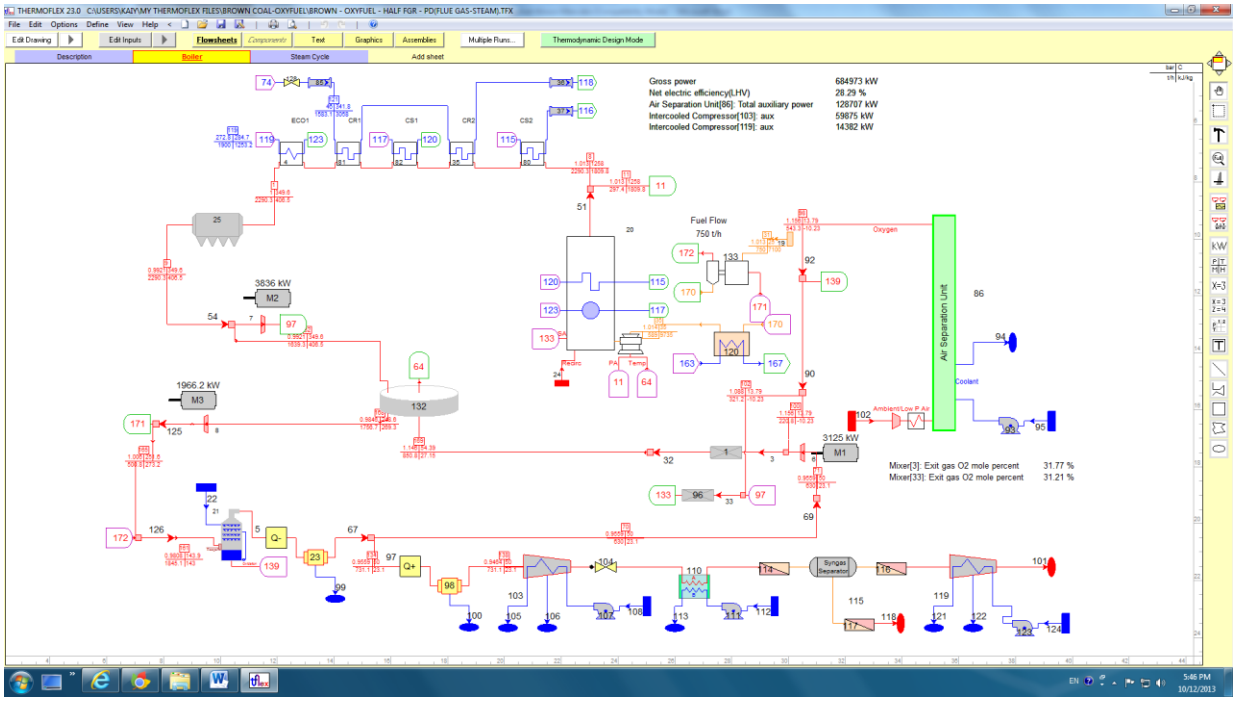

Case W-0: Direct oxy-firing of as-mined wet brown coal, and the recirculated flue gas remains wet without being condensed to remove water

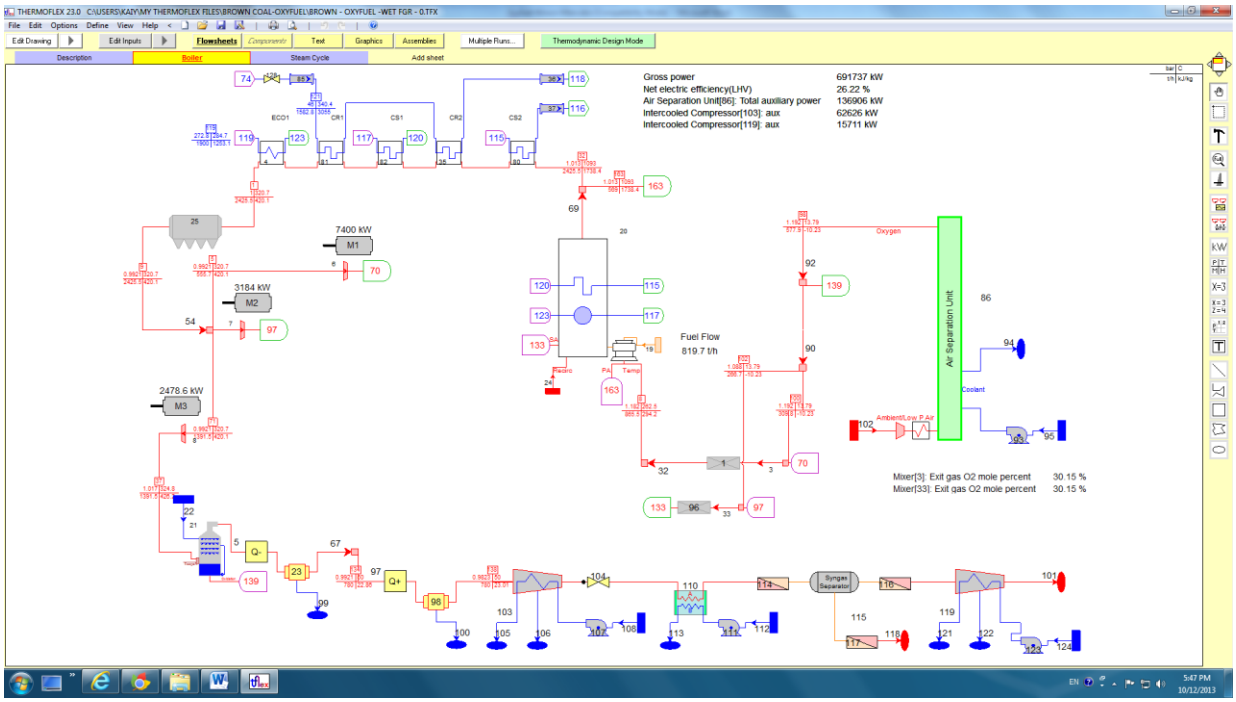

Case W-1: Oxy-firing of pre-dried brown coal; the recirculated flue gas remains wet without being condensed to remove water, and coal is pre-dried by the use of flue gas from economizer.

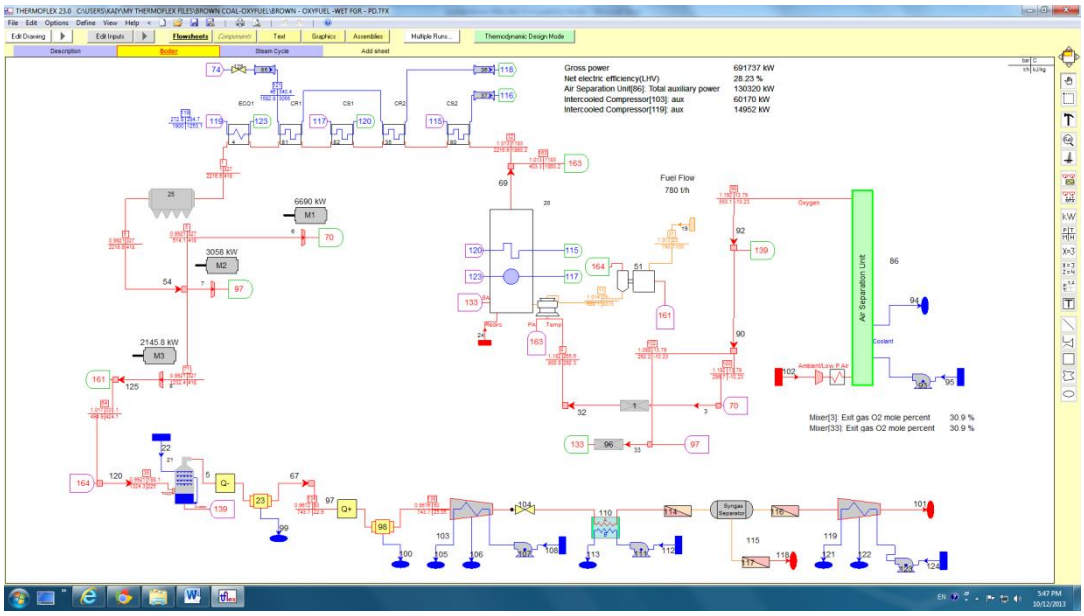

Case W-2: Oxy-firing of pre-dried brown coal; the recirculated flue gas remains wet without being condensed to remove water, and coal is pre-dried by the use of steam from low-pressure gas turbine.

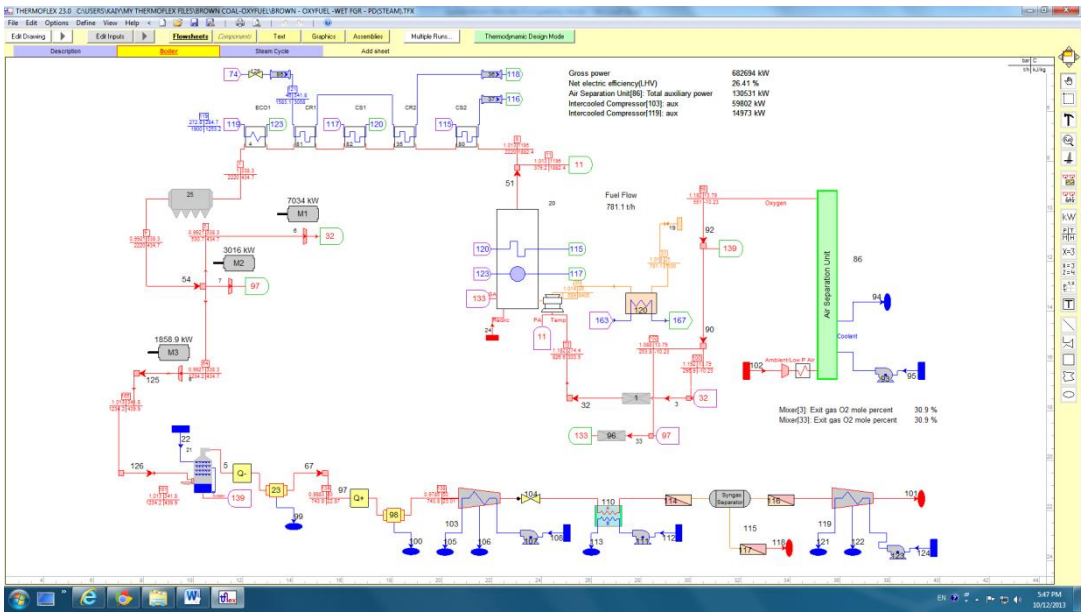

Case W-12: Oxy-firing of pre-dried brown coal; the recirculated flue gas remains wet without being condensed to remove water, and coal is pre-dried by the use of flue gas from economizer and steam from low-pressure gas turbine.

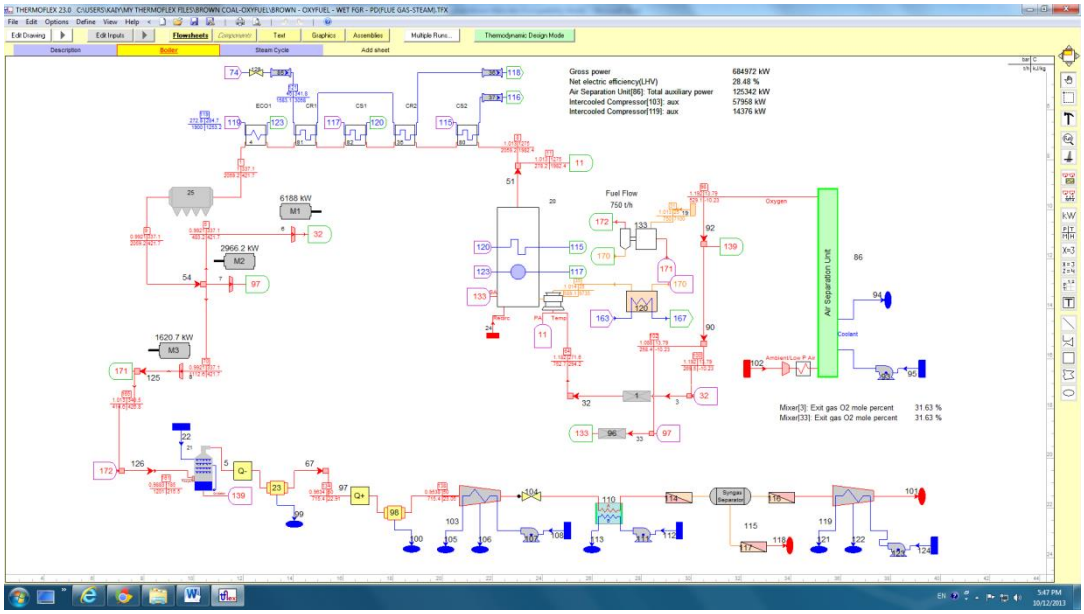

Figure 2.1 Thermoflex process flowsheet for all the cases studied for Victorian brown coal oxy-fuel combustion

2.2 LCOE and Cost of CO2 Avoidance for Victorian brown coal oxy-firing

Estimation of these two costs were only conducted for the case of integration of oxy-firing system with a fluidized bed pre-dryer which uses the steam extracted from low-pressure steam turbine. The boiler unit size is 600MWth, with a net power output of 550 MW for air-firing and the fuel consumption rate is defined as 204.2 t/h. For oxy-firing, the fuel consumption rate remains the same as the air-firing reference case, and the average 30% vol O_2 in the boiler was assumed. Due to the use of ASU and CO_2 compressors, the oxy-firing power plant has a net power output of 409 MW. The CO_2 emission amount for air-firing and oxy-firing mode reaches 3,579,881 and 178,994 ton/y, respectively. The CO_2 capture rate for oxy-firing plant was estimated to be around 95%. The CO_2 emission rate for air-firing plant and oxy-firing plant is 0.87 and 0.06 t/MWh, respectively.

The basic financial parameters for cost estimation are summarised in ***table 2.2.*** In brief, the plant lifetime was assumed as 20 years, and its occupancy was set at 7500 hrs. An 8% discounted cash flow was assumed, with the cost allocation to years 1-4 setting at 20%, 30%, 40% and 10%, respectively. The CO_2 capture rate for oxy-firing was defined at 95%. Since the drying cost for Victorian brown coal is unknown in any published literature, we used the price of USD $47.1 for international standard coal (LLV = 29270 Kj/kg) as the initial guess for the dried Victorian brown coal. This value was varied to estimate the sensitivity of LCOE and cost of CO_2 avoidance upon the change on fuel price. The rate of fixed capital formation was set at 0.95, and the depreciation and amortization years are of 15 and 5, respectively.

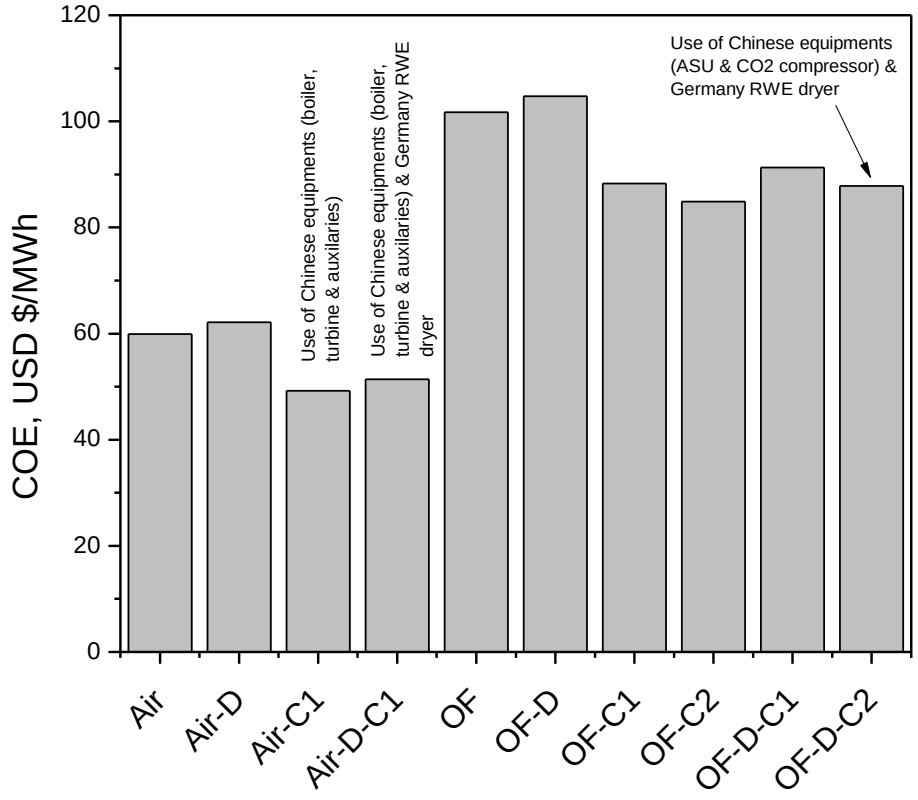

Figure 2.2 COE for the combustion of Victorian brown coal in air-firing and oxy-firing power plants installed with Germany RWE dryer and/or Chinese equipments including boiler, turbine, auxiliaries, ASU and CO_2 compressor.

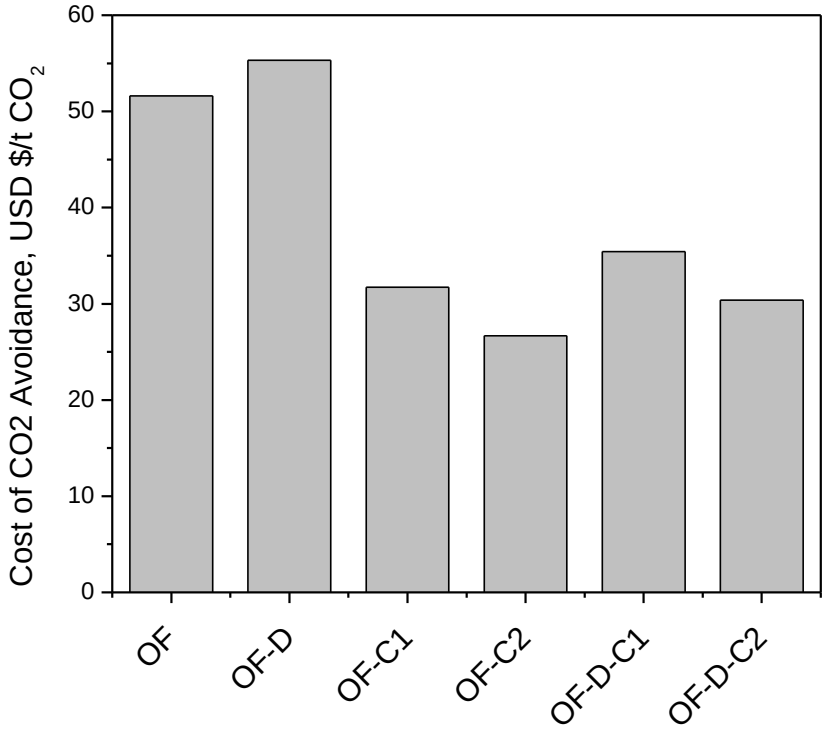

Figure 2.3 Cost of CO_2 avoidance for oxy-firing of Victorian brown coal through the use of Germany and/or Chinese equipments. The symbols are the same as those in figure 2.2.

As summarised in figure 2.2 for the LCOE, the integration of Germany RWE coal drying technology in the existing air-firing power plant slightly increases the COE from USD $59.9 for the reference baseline to 62.1. The use of Chinese equipments (C1) including boiler, turbine and boiler auxiliary facilities decreases the COE to USD $49.2 and 51.4 for the case integrated without and with Germany RWE coal dryer, respectively. The use of Chinese equipments (C1 and C2) is more influential in reducing the COE of oxy-firing system. For the oxy-firing boiler integrated with a Germany RWE dryer, the COE was estimated to be around USD $104.7, which dropped to USD $88.3 and $84.9 or oxy-firing using Chinese equipments C1 (boiler, turbine and auxiliary facilities) and C2 (ASU and compressors), respectively. The integration of Chinese equipments C2 and Germany RWE dryer into oxy-firing plant is also cost-effective, reaching a COE of USD $87.8 that is far lower than the control case OF-D with a COE of USD $104.7. The use of low-cost Chinese equipments is also beneficial in reducing the cost of CO2 avoidance for the oxy-firing of Victorian brown coal. As substantiated in figure 2.3, the reference oxy-firing power plant bears

a cost of CO2 avoidance of approximately USD $51.6, which is increased slightly to $55.3 for the integration of Germany RWE dryer into the power plant. However, the use of Chinese equipments, from C1 to C2 and the combination of C1/C2 and Germany dryer, is able to reduce the cost of the CO2 avoidance by around half. This is clearly a positive indicator for promoting the deployment of oxy-firing technology in the Latrobe Valley.

The breakdown cost ratio for the COE of different case is summarised in ***table 2.3***. Irrespective of the process mode, the total plant cost is the largest factor affecting the final COE of the plant, which accounts for 0.35-0.47. The second largest source affecting the final COE is fuel price (consumption amount), which is followed by depreciation ratio, operating and maintenance cost, and amortization in a descending sequence.

Table 2.3 Breakdown cost ratio of electricity for different cases

Item	Total plant cost	Depreciation	Amortization	Operating & maintenance	Fuel consumption
Air	0.41	0.18	0.01	0.13	0.26
Air-D	0.42	0.19	0.01	0.13	0.25
Air-C1	0.35	0.16	0.01	0.16	0.32
Air-D-C1	0.36	0.16	0.01	0.16	0.30
OF	0.46	0.21	0.02	0.11	0.21
OF-D	0.47	0.21	0.02	0.10	0.20
OF-C1	0.42	0.19	0.01	0.13	0.25
OF-C2	0.41	0.19	0.01	0.13	0.26
OF-D-C1	0.43	0.20	0.02	0.12	0.24
OF-D-C2	0.42	0.19	0.01	0.13	0.25

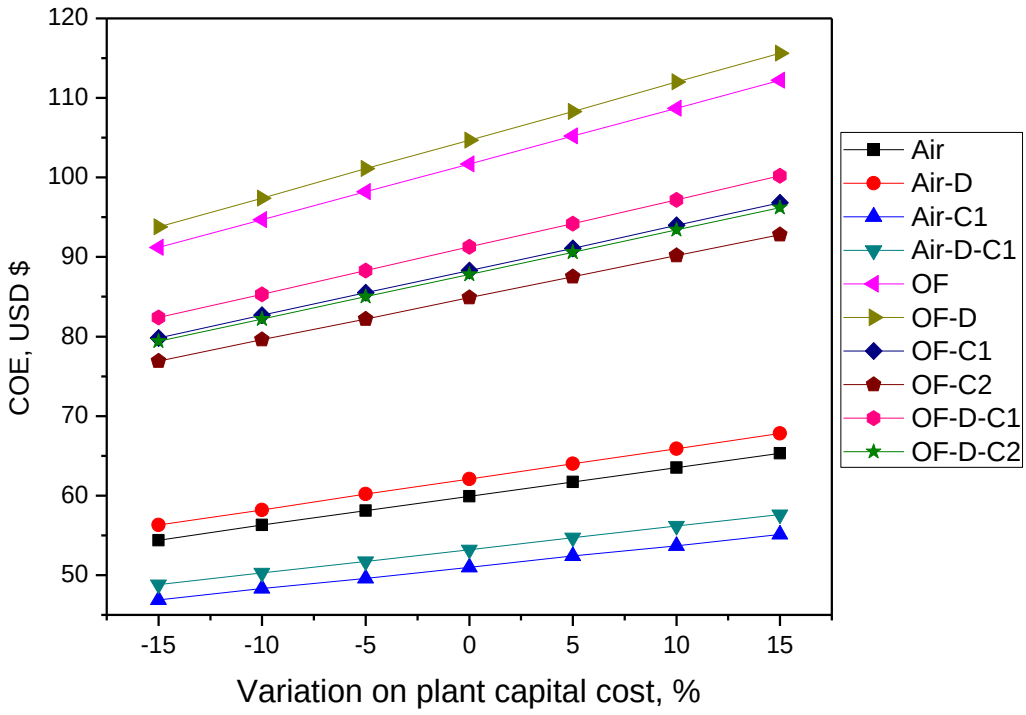

Figure 2.4 Sensitivity on COE variation with the percentage change on total plant capital cost

The sensitivity analysis on the COE variation as a function of four key parameters (i.e. plant capital cost, fuel price, discounted cash flow and plant occupancy) was further carried out. Figure 2.4 summarises the variation of COE with the change on plant capital cost, the largest influential factor. This factor is most influential for the oxy-firing plant coupled with a pre-dryer, which has the steepest slope with the change of plant cost from -15% to 15%. The change on COE for the case of air-C1 (air-firing using Chinese equipment) is the least, which is due to a much lower price for the Chinese equipments C1 that change narrowly on the prices. As shown in table 2.3, the ratio of total plant cost in the overall COE only accounts for 0.35 in the case of air-C1, which is much lower than the case OF-D with a ratio of 0.47 for the total plant cost. The sensitivity of COE upon the percentage change of dried brown coal fuel price is shown in figure 2.5. Decreasing the fuel price by 20% has a marginal effect on reducing the overall COE. This is because the influence of fuel consumption amount is marginal for the overall COE, as shown in table 2.3. Taking the OF-D case with the highest COE as an example, decreasing the fuel price by 20% only results in an COE of approximately USD \$100/t CO_2, which is even far higher than the case OF-D-C1 (using Chinese equipment and Germany RWE dryer) at a fuel consumption increment of 20%.

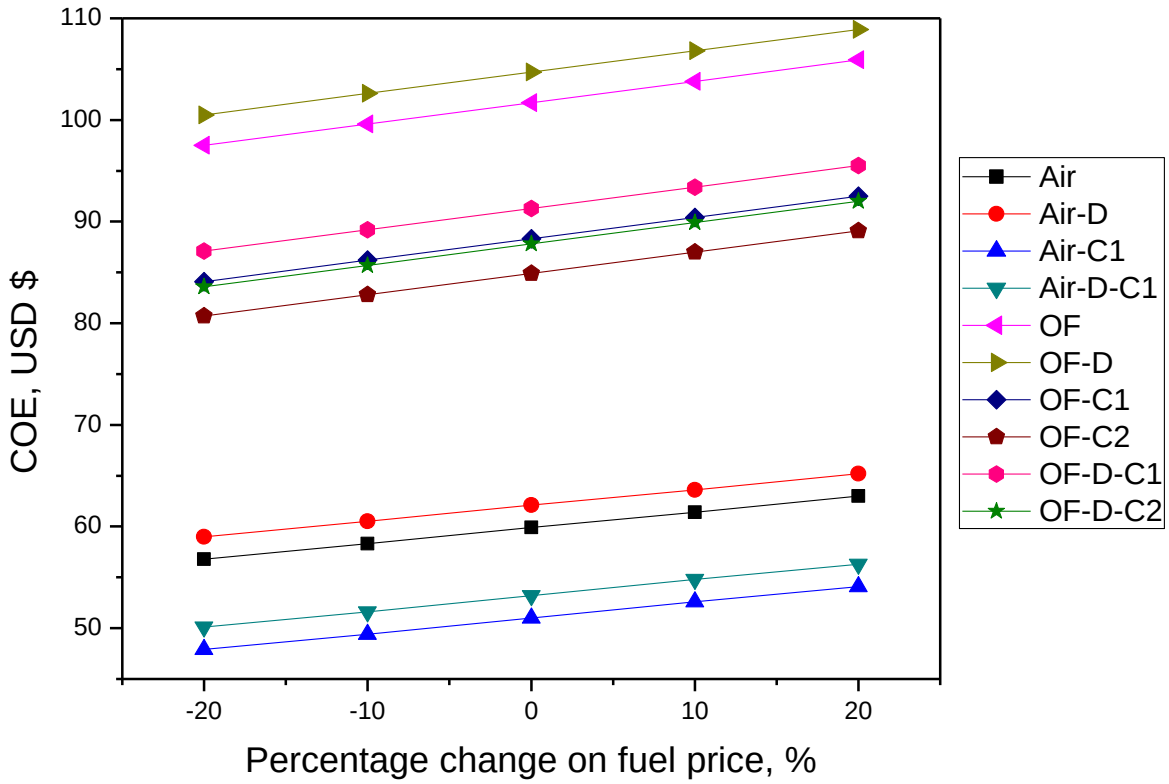

Figure 2.5 Sensitivity on COE variation with the percentage change on fuel price

The influence of discounted cash flow on COE variation is remarkable. As shown in figure 2.6, an increment from 4% to 12% on this factor can increase the COE for OF-D case to around USD $120/t CO_2, which is even higher than the maximum value of USD $110/t CO2 upon 20% rise in fuel price for this case in figure 2.5. The increase in plant occupancy time is also effective in reducing the COE, as demonstrated in figure 2.7.

The sensitivity variation of COE as per unit for the four key parameters is further summarised in table 2.4. For each case, the discounted cash flow has the largest influence on COE variation, which is fllowed by plant occupancy, capital cost and fuel price in a descending sequence. Interestingly, the price of fuel is insignificant in the air-firing cases. However, its influence is larger than that of plant occupancy and even capital cost for the oxy-firing cases. Apparently, for the oxy-firing of Victorian brown coal, choosing a cost-effective and efficient dryer to reduce the final price for the dried coal is critical in reducing the COE for the overall process.

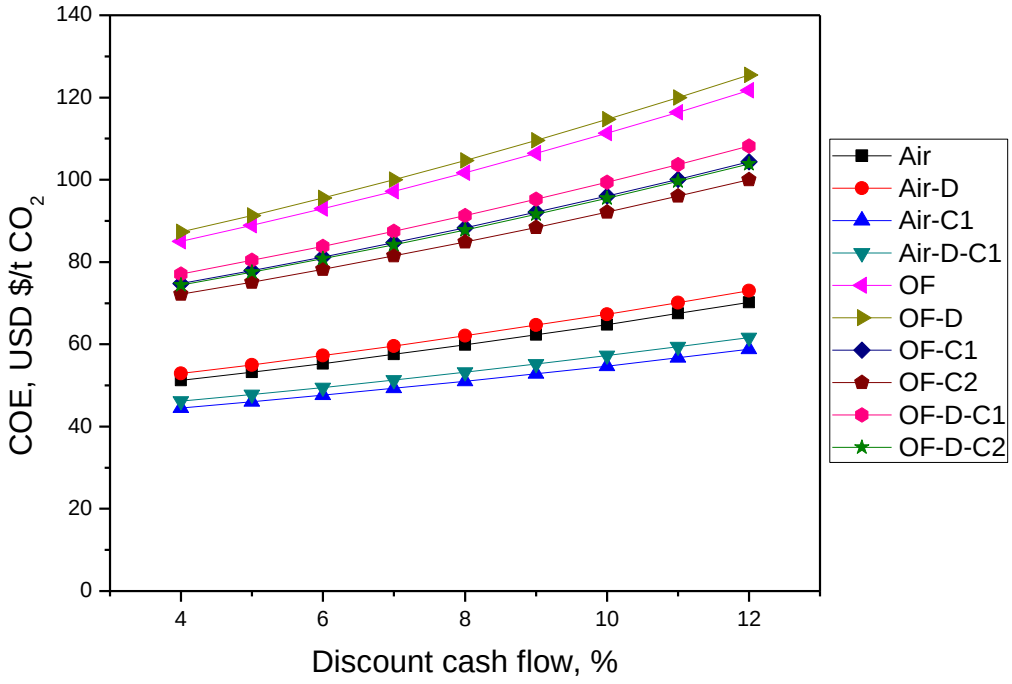

Figure 2.6 Sensitivity on COE variation with the change on discount cash flow

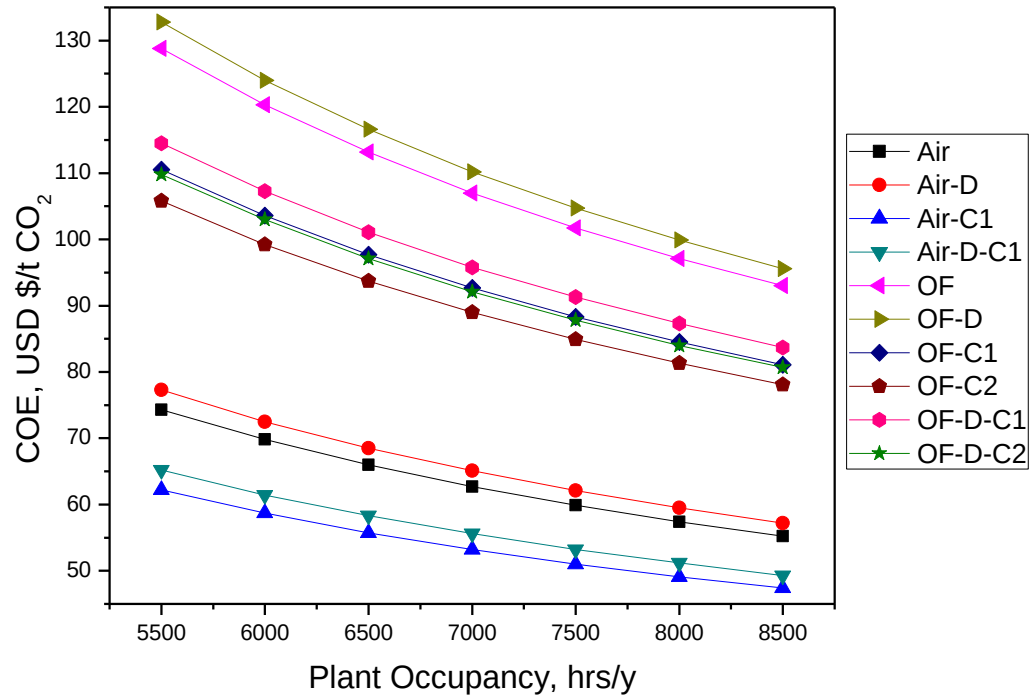

Figure 2.7 Sensitivity on COE variation with the change on plant occupancy time

Table 2.4 COE sensitivity analysis of power plant for cases-Cent/(kWh)

Item	Discounted cash flow	Fuel Price	Plant Occupancy	Capital Cost
	Absolute 1%	Relative %	100 hr	Relative %
Air	0.21	0.0155	-0.06	0.04
Air-D	0.23	0.0155	-0.07	0.04
Air-C1	0.16	0.0155	-0.05	0.03
Air-D-C1	0.17	0.0155	-0.05	0.03
OF	0.41	0.021	-0.12	0.07
OF-D	0.43	0.021	-0.12	0.07
OF-C1	0.33	0.021	-0.10	0.06
OF-C2	0.31	0.021	-0.09	0.05
OF-D-C1	0.35	0.021	-0.10	0.06
OF-D-C2	0.33	0.021	-0.10	0.06

2.3 Influence of individual operating parameters on the net efficiency of brown coal oxy-firing plant

2.3.1 Basic assumptions

Following the above two analysis on the efficiency and cost related to oxy-firing of Victorian brown coal, we further examined the influence of individual operating parameters on the process net efficiency. The use of pre-dried coal was only simulated here, considering the influence of these parameters is rather similar for the combustion of wet coal and semi-dried coal. The main parameters adjusted and optimised are as follows:

a) Flue gas circulation rate

b) Oxygen concentration from ASU

c) Excess oxygen rate

d) Air leakage into furnace

e) Fan power consumptions

f) Gas leakage in gas heater

g) Temperature of moisture removal

h) SO_x and acid dew point

The reference air-firing power plant, with a schematic shown in figure 2.8 is a pulverised coal-fired supercritical power plant coupled with a single reheat steam turbine system. The module 'boiler' in fig 1 consists of furnaces, superheaters, reheaters and economizers, which together produce the steam required to drive the turbines. Note that, in the component "Boiler", the economizer is located at the outlet of "Boiler", which restrains the flue gas temperature level at "Boiler" outlet not to be too low. The air excess ratio applied in the furnace of the reference power plant is set at 1.2. The air leakage coefficient is set at 8%. The other main thermal parameters for the power plant system are listed in table 2.5.

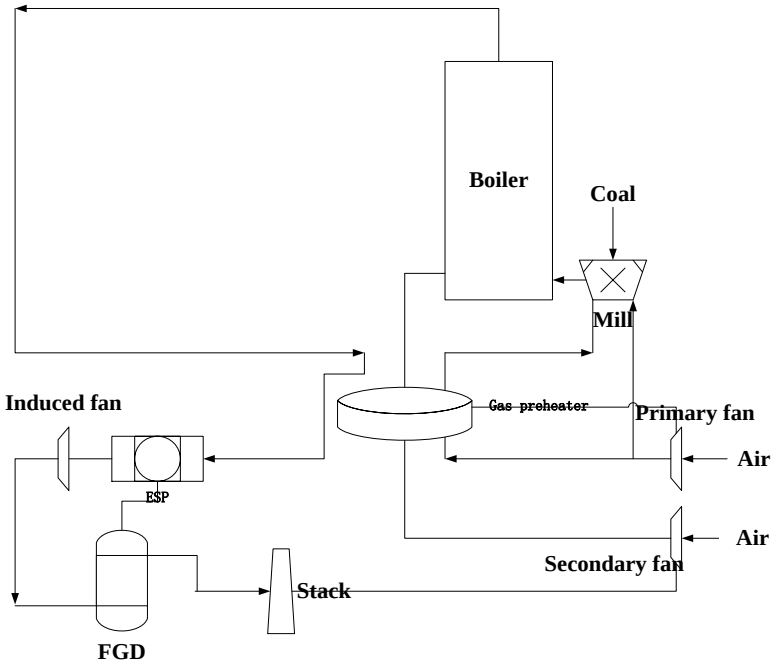

Figure 2.8. The boiler system of the reference air-firing power plant

Table 2.5 Thermal parameters of reference power plant

Item	Value
Superheater steam	600 ℃, 260 bar, 1900 t/h
Reheater steam	600 ℃, 45.1 bar, 1582.8 t/h
Feed water	284.7 ℃, 272.8 bar, 1900 t/h
Fuel consumption	257.8 t/h
Gross power	691737 kW
Gross electric efficiency(LHV)	43.93%
Net power	656455 kW
Net electric efficiency(LHV)	41.69%
Plant auxiliary	35282 kW
Gross calorific value (HHV)	23.1 MJ/kg

The turbine system of the reference power plant is shown in figure 2.9. There are eight feed water heaters and eight steam extractions in the turbine system. The packing steam of the turbine system is used as the first feed water heater. The feed water with a certain pressure and temperature flows out of the turbine system from "feed water outlet" into the boiler system. The superheat steam is introduced back into the turbine system from "superheat steam inlet" to do work by volume expansion. The inlet and outlet of the reheat steam in the turbine system are "reheat steam inlet" and "reheat steam outlet", respectively. The feed water is first pressurized by feed water pump after the condenser and cooling tower and then is pressurized again by feed water pump 2 after the deaerator, and finally is pressurized again by steam-driven pump system. In the steam-driven pump system, a small portion of steam is introduced from one of the middle-pressure turbines, T1, to drive the pump, and then is extracted from T2 with a very low pressure and temperature to the condenser.

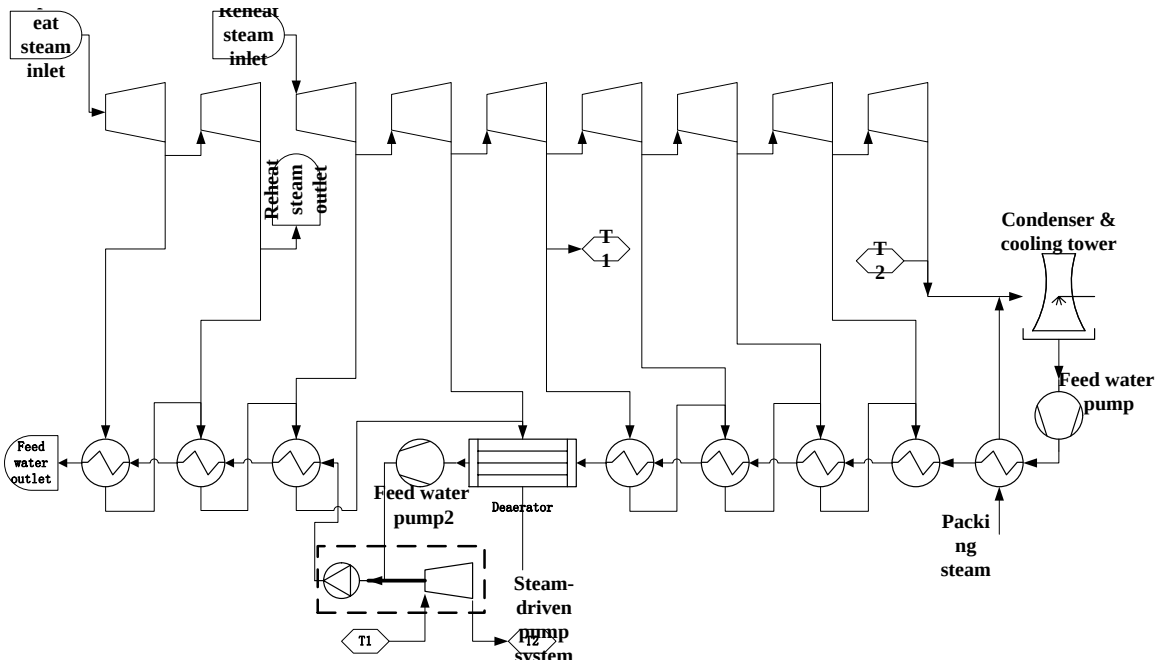

Figure 2.9 The turbine system of the reference power plant

Based on whether the flue gas is dried via condensation or not, three modes for the recirculation of flue gas back into the boiler were examined hereafter, *i.e.* dry mode, half-dry mode and wet RFG mode.. The schematic representations of the three systems are illustrated in figure 2.10. In the dry mode, the RFG is processed through the components electrostatic precipitator (ESP), Flue gas desulphurization (FGD), and heat exchanger (HX) for water removal and dust removal prior to being introduced into the primary and secondary fans. In the half-dry system, only the FG introduced into primary fan is processed through FGD and HX for purity and condensation, respectively, whereas the RFG into secondary fan mixes with the oxygen from ASU directly and is fed into the furnace. Clearly, a smaller gas preheater is required for the half-dry system than the dry RFG one. The location of ESP (Electrostatic Precipitator) is also different for the above two systems. The ESP is located behind the gas preheater for the dry mode, whereas it is located after the economizer to remove the dust in the hot RFG prior to it flowing into the secondary fan. In the wet RFG system shown in Fig. 3 (c), a component "HX2" is allocated in front of coal mill to reduce the flue gas temperature and volume flow rate to the design values required by the mill system. Certainly some heat has to be lost in HX2. The gas preheater is also omitted in the wet mode, because it is unnecessary for the heat-up of the hot flue gas.

It is noteworthy that, here we just focused on a system design or the state parameter sensitivity analysis of a whole thermal system, where only the appropriate state parameters are considered. In component design, however, special structure size for each component, such as the width and depth of furnace and the heating areas of heating surfaces, are determined by the state parameters which have been decided in system design. The influence of flue gas temperature at furnace outlet is also beyond the scope of this study. The energy needed for turbine doing work, including superheating and reheating steam systems, remains constant for all the systems examined. The flue gas outlet temperature exerts no effect on the performance of the power plant system. For a real boiler design, the flue gas temperature at the outlet of the combustion zone is merely determined by the ash fusion temperature and the cost of boiler manufacturing. In this study, the component "Boiler" is considered as a black box unit.

It is proposed that in an oxy-fuel unit, the excess oxygen ratio is reduced due to the high flue gas recirculation flow rate and a furnace stoichiometry of 1.05–1.07 is considered as appropriate. Meanwhile, a reduced furnace stoichiometry is beneficial for reducing the ASU power consumption. Thus, the excess oxygen ratio into furnace is chosen as 1.05 and changes from 1 to 1.1.

The process of CO_2 compression and purity occurs in two stages. CO_2 is compressed with multiple-stage intermediate cooling in the two stages. The TEG dehydration system is placed after the first CO_2 compression stage with its pressure of 33.5 bar for the removal of non-condensable gas. The final pressure of CO_2 compression and storage reaches 150 bar.

The purity of oxygen discharged from ASU is set at 95% by volume, with Ar of 0.5% and the remaining N_2. Due to the gas compression process in the ASU, The exit pressure of O_2 usually has a higher pressure which can naturally satisfy the pressure demand of the primary fan. As a result, no primary fan is used in the oxy-fuel system for the oxidant, in contrast to the air-firing boiler.

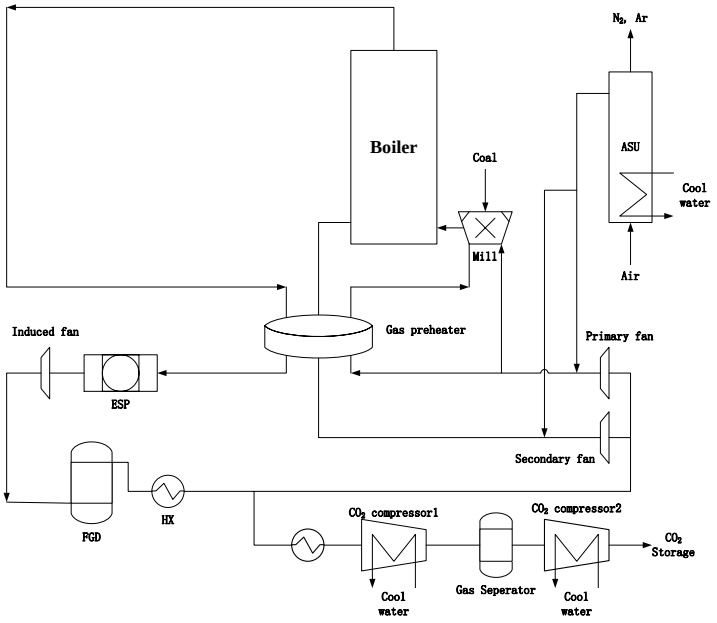
N2, Ar
Boiler
Coal
ASU
Cool water
Mill
Air
Induced fan
Gas preheater
Primary fan
ESP
Secondary fan
FGD
HX
CO2 compressor1
CO2 compressor2
CO2 Storage
Cool water
Gas Seperator
Cool water

(a)

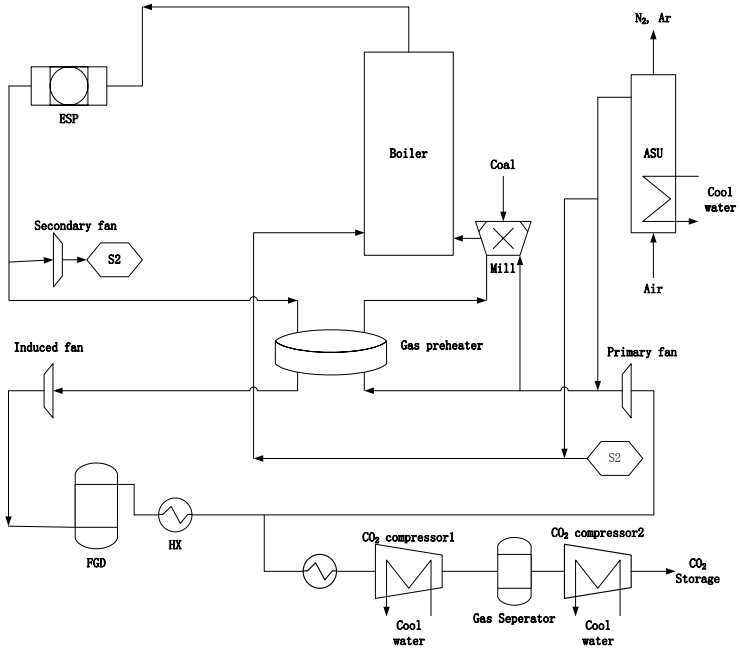
N2, Ar
ESP
Boiler
Coal
ASU
Cool water
Secondary fan
S2
Mill
Air
Induced fan
Gas preheater
Primary fan
S2
FGD
HX
CO2 compressor1
CO2 compressor2
CO2 Storage
Cool water
Gas Seperator
Cool water

(b)

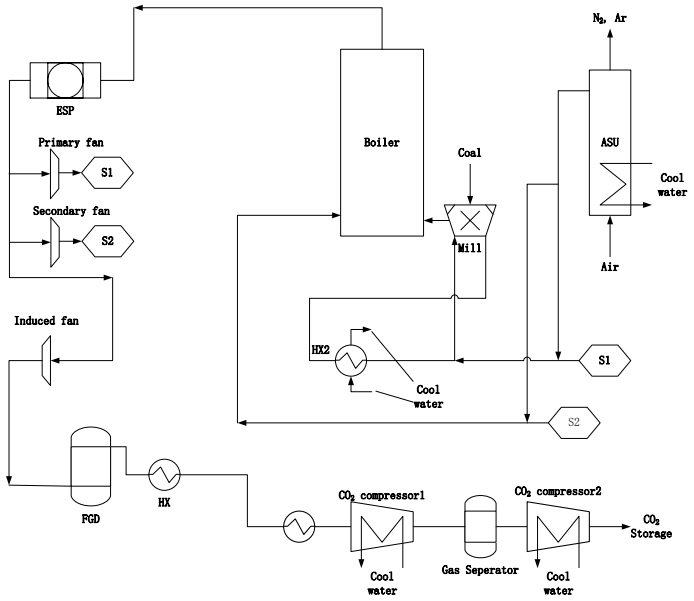

(c)

Figure 2.10 The boiler system of three oxy-fuel power plant systems, dry-mode *(a)*, half-dry mode *(b)* and wet-mode *(c)*.

2.3.2 Sensitivity analysis of a half-dry RFG system

The half-dry RFG mode was first analysed to reveal the influences of invidiual parameters on the performance of the oxy-fuel system. This mode was chosen because it has the largest output efficiency than the other two modes, as will be detailed later. In addition, this mode is apparently more practical as the condensation of primary gas assists to avoid the blockage of coal transportation pipe as well as the corrosion in the coal mill system.

The thermal parameters of the half-dry RFG oxy-fuel power plant are listed in table 2.6, where the fuel consumption rate of the oxy-fuel system is set identical with the reference air-firing case. The gross power and the gross electric efficiency of the two systems are almost the same. The plant auxiliary of oxy-fuel system is about six times as much as that of the reference plant, due to the power consumptions of ASU and the two CO_2 compressors. This induces a great reduction of the net power output and the net electric efficiency. The net electric efficiency is decreased by about ten percent points, accounting for 25% of the original value. The power consumption of ASU

accounts for approximately half of the total auxiliary power consumption. It is nearly twice that of the CO_2 compression process.

The oxygen-rich gas from ASU is distributed proportionally between the primary and secondary streams to ensure the same oxygen concentration in the two gas streams. There is no air leakage into furnace. Here the air leakage ratio is defined as the ratio of the volume of leaked air into furnace and the gross volume flowing into furnace when there is no air leakage into furnace. The temperature of flue gas after the outlet of the FGD drops to 50 ℃ by an additional heat exchanger "HX" to remove a portion of moisture within it.

Table 2.6 Thermal and design parameters of the half-dry RFG oxy-fuel power plant

Item	Value
Fuel consumption	257.8 t/h
Gross power	691737 kW
Gross electric efficiency(LHV)	43.92%
Net power	485974 kW
Net electric efficiency(LHV)	30.85%
Plant auxiliary	205763 kW
ASU consumption	114072 kW
CO_2 Compressor consumption	61365 kW
Oxygen concentration in furnace	30%
Excess oxygen ratio in furnace	5%
Air leakage ratio into furnace	0%
Oxygen concentration from ASU	95%
Gas leakage ratio of Gas preheater	8%

A total of eight factors have been considered for the sensitivity analysis. However, in terms of significance, the results detailed below only include five influential factors, flue gas recirculation rate, air leakage ratio, fan pressure rise distribution, temperature in the primary gas condenser, and the oxygen distribution ratio between primary gas and secondary gas.

The flue gas recycle rate, denoted by *Rc* hereafter, is linearly dependent on the average oxygen concentration in the furnace. The O_2 concentration range is chosen as 25% - 35% here, based on the consideration that ~27% O_2 is essential to match the reference air-firing case in terms of in-flame temperature and gas concentration levels. The other design parameters are unchanged.

The main results are shown in figure 2.11. With increasing O_2 concentration into furnace, both the *Rc*-hot (for the flue gas to secondary fan) and the *Rc*-cold (for the flue gas to primary fan) decrease linearly, as expected, as shown in panel (a). The variation of *Rc*-hot is obviously much greater than that of *Rc*-cold. The reason is that the cold recirculated flue gas into primary fan is mainly determined by the design requirements of the mill system, in terms of gas volume flow rate and coal-gas mixing ratio and temperature. The design requirements of the mill system are kept unchanged with increasing O_2 concentration. Thus, the variation of the required recirculated flue gas into furnace is mainly reflected by the hot recirculated flue gas to secondary fan.

The outlet of gas preheater is selected to demonstrate the influence of O_2 concentration on flue gas composition, as shown in *figure 2.11 (b)*. With the increase of O_2 concentration in the furnace, the concentrations of O_2 and H_2O vapor in flue gas increase, whereas the concentrations of N_2 and CO_2 decrease. However, the variations of the concentrations of the all four component gases are trivial, suggesting the insignificant impact of oxygen concentration on flue gas composition. The largest variation observed for CO_2 only accounts for 1.3% with the oxygen concentration changes from 25% to 35% in the furnace.

The increase of the power consumptions of ASU and CO_2 compressors at elevated oxygen concentration in the furnace, as shown in *figure 2.11 (c)* is also marginal. The increase in the ASU power consumption is induced by the worsen leakage of flue gas (and thus oxygen within it) in the gas heater unit. Thus, more fresh O_2 has to be supplied by ASU to achieve the constant excess oxygen ratio in the furnace. Similarly, more exhausted O_2 makes the CO_2 compressors consume more power.

Figure 2.11 (d) shows the variation of the power consumption for three fans, primary fan, secondary fan and induced fan as a function of oxygen concentration in the furnace. The largest variation was confirmed for the secondary fan, as expected. The

oxygen is mainly mixed with the secondary flue gas. A reduction on the averaged oxygen concentration in the furnace certainly reduces the amount for the flue gas to be recirculated. The power consumptions of the other two fans have very little change, since less of oxygen is charged through them. The volume flow rates of the three fans are also shown. Similarly, the volume flow rate of the three fans has similar variation profiles to their power consumptions. The volume flow rate of the secondary fan changes intensively compared to the other two fans. Upon the increase on the oxygen concentration in the furnace, the reduction on the power consumption for the second fan is even great enough to offset the increase in the power consumption for the ASU and CO_2 compressors. As a result, the net efficiency of the plant is even slightly increased by 0.05 % LHV based, as demonstrated in panel (e).

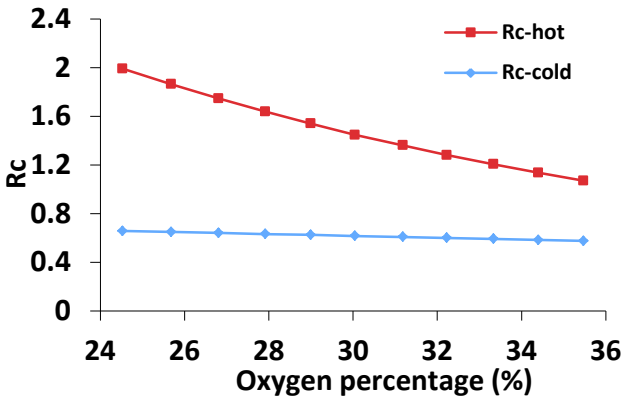

(a)

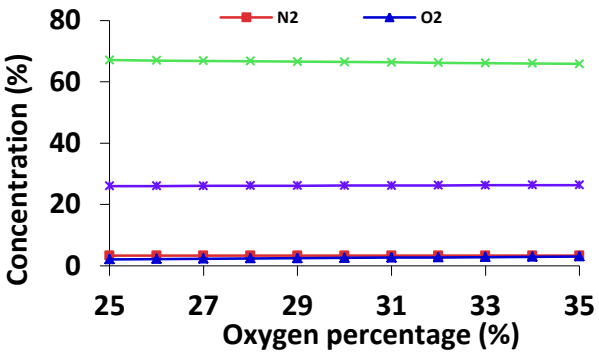

(b)

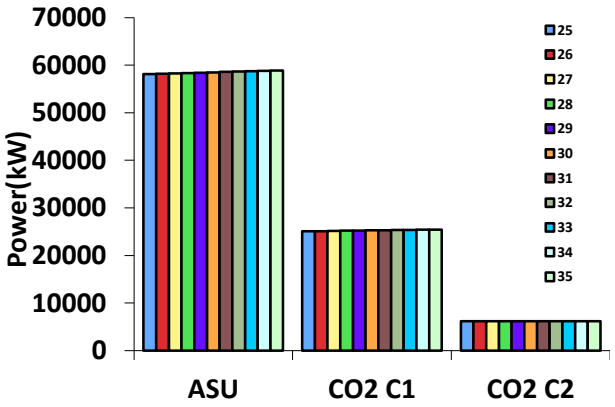

(c)

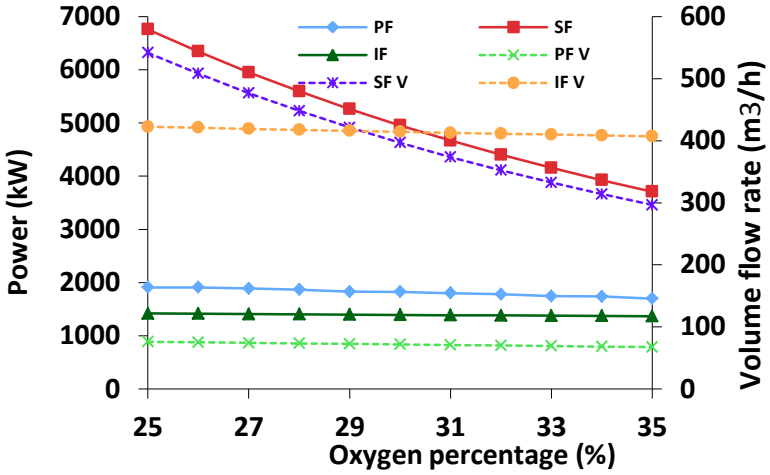

(d)

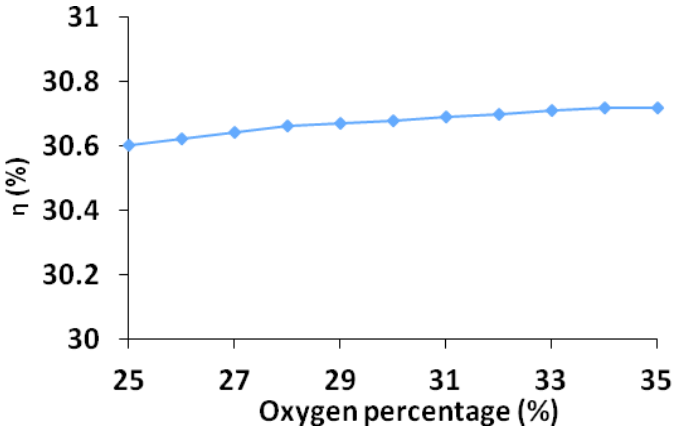

(e)

Figure 2.11 The influence of flue gas recirculation rate on (a) oxygen concentration in boiler, flue gas composition (b), power consumption (c) and (d) and net efficiency (e)

2.3.3 Air leakage ratio

The calculation was performed with all design parameters remaining unchanged except the air leakage ratio. The outlet of gas preheater is selected to manifest the influence of this factor on flue gas composition. For the flue gas composition shown in figure 2.12 (a), The concentration of O_2 in the exhaust flue gas has little change with air leakage ratio. This is because its input, oxygen excess ratio in the furnace is set at a rather fixed value here. In contrast, with increasing air leakage ratio, the concentration of N_2 is increased quickly, reaching up to 20% at the air leakage ratio of 10%. As a consequence, the purity of CO_2 in flue gas drops rather linearly, being around 50% at the air leakage ratio of 10% versus 70% for the zero air ingress. The concentration of H_2O in the exhaust flue gas is decreased slightly, due to the dilution effect of the ingress air.

Upon a fixed excess oxygen ratio and flue gas recirulation ratio, the increased amount of the air entering the system reduces the amount of oxygen required from the ASU, since the air will bring extra air into the boiler as well. Figure 2.12 (b) confirms a nearly linear reduction on the mass flow rate of ASU oxygen with the increase in air leakage ratio. As a result, the power consumption for AUS is decreased, as demonstrated in panel (c). However, the decrease in the ASU power consumption is much smaller than the increase in the power consumed by the primary CO_2 compressor. This is due to the ingress of a large amount of N2 that is compressed as well. Therefore, the net efficiency of the system drops quickly with the increase in the air leakage ratio, as shown in figure 2.12 (d).

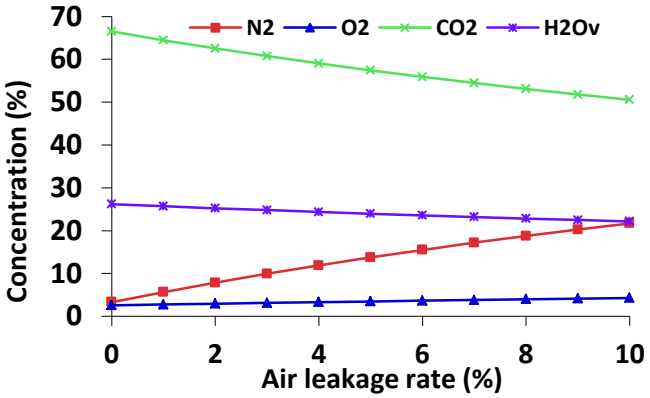

(a)

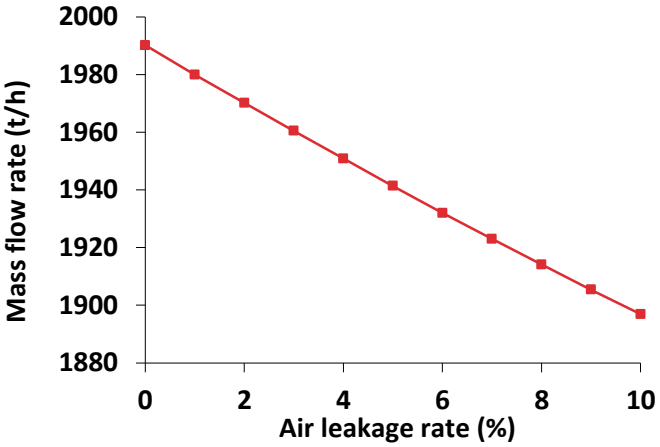

(b)

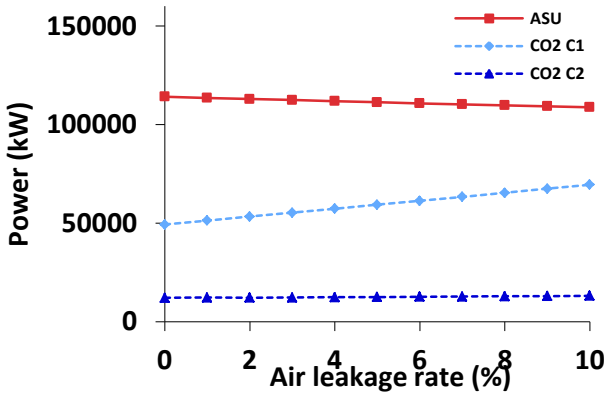

(c)

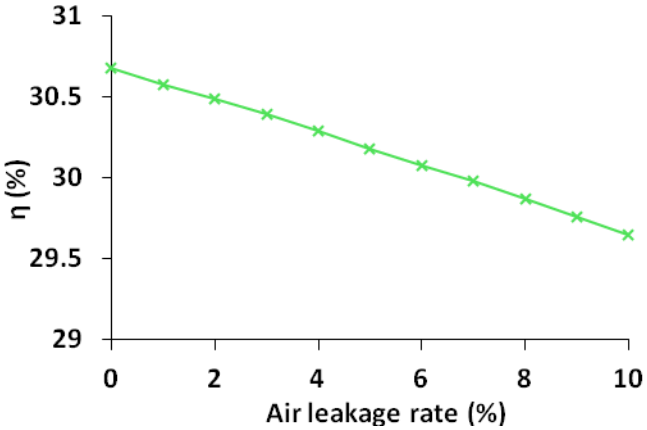

(d)

Figure 2.12 The influence of air leakage into furnace on (a) flue gas concentration, (b) mass flow rate of gas in furnace, (c) power consumption for major equipment, and (d) net efficiency

2.3.4 Pressure rise of fans

The boiler system of a half-dry RFG oxy-fuel power plant includes three fans, primary fan (PF), secondary fan (SF) and induced fan (IF). The secondary fan is used to balance the pressure between the RFG from the secondary fan and the primary RFG sent through the burner. From the perspective of system design, the pressure difference between the two parts are kept constantunchanged. Thus, the pressure rise of the secondary fan is almost constant. For the other two fans, the sum of their pressure rise is used to balance the pressure between the mill system and the flue gas at the outlet of the boiler's heating surface. Here we analysed five different cases with different pressure rise distributions between the primary fan and the induced fan, as shown in table 2.7, where the pressure rise of the secondary fan is set at a fixed value.

The power consumptions of the main auxiliaries are shown in *figure 2.13 (a)*. For a given case, the larger power consumed by the induced fan than the primary fan is due to the fact that the induced fan has to pump a hot flue gas of approximately 300^{o}C which thus has a larger volume than at room temperature. With increasing the pressure rise of the induced fan, the power consumption of the induced fan increases and the power consumption of the primary fan decreases correspondingly. Meanwhile, since the increase in the pressure rise for the induced fan induces a higher pressure at the inlet of the primary CO_2 compressor, whereas its outlet pressure remains constant at 33.5 bar, the power consumption of the primary CO_2 compressor also decreases slightly with increasing the induced fan pressure rise. However, since the decrease extents of the power consumed by CO_2 compressor and even the primary fan are smaller than the increase for the induced fan upon increasing its pressure rise, the net efficiency of the whole system drops slightly at the elevated pressure rise for the induced fan.

Table 2.7 The design pressure rise of fans

No.	Pressure rise of PF (mbar)	Pressure rise of IF (mbar)
1	200	24.88
2	179.9	44.86
3	160	64.85
4	140	84.83
5	120	104.8

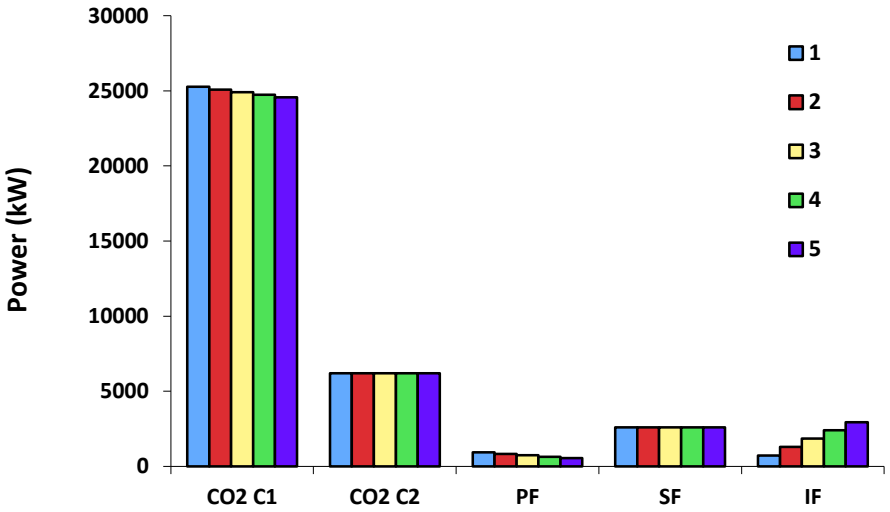

(a)

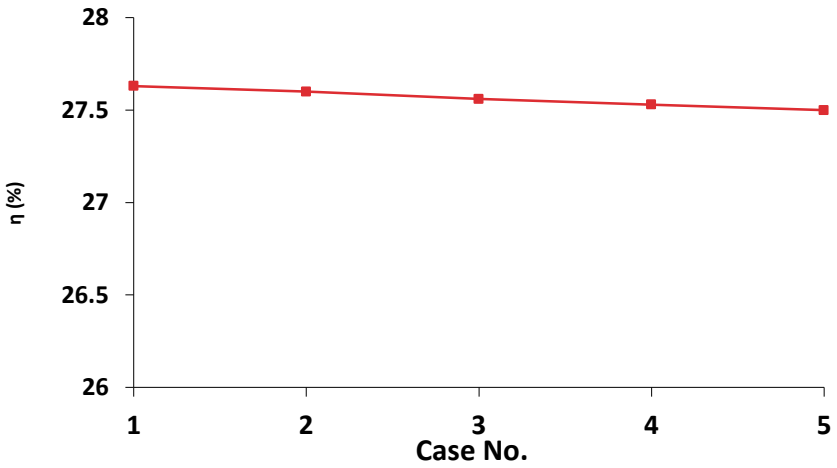

(b)

Figure 2.13. The influence of pressure rise of fans on power consumption (a) and net efficiency (b)

2.3.5 Flue gas condensation temperature

For the half-dry RFG model, the moisture in the primary flue gas needs to be removed prior to entering the mill system to mix with coal particles to avoid the corrosion and blockage of the pipelines. The moisture removal is achieved in the desulfurization unit FGD, where the wet type mode with the use of limestone is adopted. A wet slurry or by-product is produced and the flue gas leaving the absorber is saturated

with moisture. In this sense, the moisture is removed in a saturation way. The absorber SO_2 removal efficiency is specified as 98%.

Figure 2.14(a) confirms a remarkable increase in the H_2O% in the primary flue gas, with increasing the condensation temperature from 50 ℃ to 80 ℃. This is reasonable, as the high temperature in the FGD improves the extent of the water that can be saturated in flue gas. Simultaneously, the CO_2% in the primary gas entering coal burner decreases. Moreover, the absolute flow rate of the primary gas will be increased as well, due to more of water being saturated within it. To maintain a constant oxygen excess ratio at a given air leakage ratio in the boiler, more of oxygen thus needs to be generated from the ASU, as demonstrated in panel (b). The influence of this factor on the power consumption of three fans is very marginal, if not negligible. As shown in panel (c), a slight increase in the power consumption of primary fan would occur, in the case the FGD outlet temperature rises up. This is because the elevated temperature induces an expanded large volume for the flue gas to be pumped through the fan, as mentioned in the last subsection.

With increasing the condensation temperature, the volume flow rate and temperature of the secondary fan all decrease, then the power consumption of the secondary fan decreases. The power consumption of the induced fan has a slight increase. On the whole, the total power consumption of the three fans increases with increasing the condensation temperature. With the variations of the power consumptions of ASU, the two CO_2 compressors and the three fans, the net electric efficiency is slightly dropped down, as shown in figure 2.14 (d). The variation of H_2O% in flue gas before, in the FGD and after the moisture removal process, are also concerned. As shown in figure 2.14 (e), with increasing the condensation temperature, both the "before" and "after" concentrations of H_2O in the flue gas increase. The "after" concentration is increased much faster than that of "before". For the case of 50 ℃, the "after" concentration is only half of the "before" one, suggesting the removal of more than half of the H_2O vapor in flue gas. In contrast, for the case of 80 ℃, the "after" concentration even is greater than that of "before", indicating an actual water absorption by the flue gas. The turning point for water removal appears at about 70 ℃, beyond which the water removal does not occur. The variation of CO_2% concentrations as a function of FGD outlet temperature is opposite to that of H_2O%, as shown in panel (e).

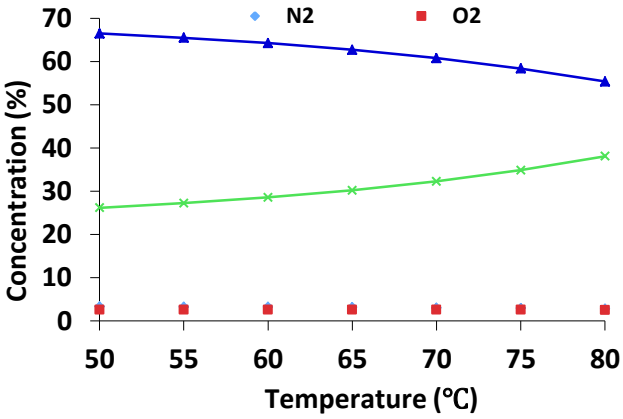
N2
O2
Concentration (%)
70
60
50
40
30
20
10
0
50
55
60
65
70
75
80
Temperature (℃)

(a)

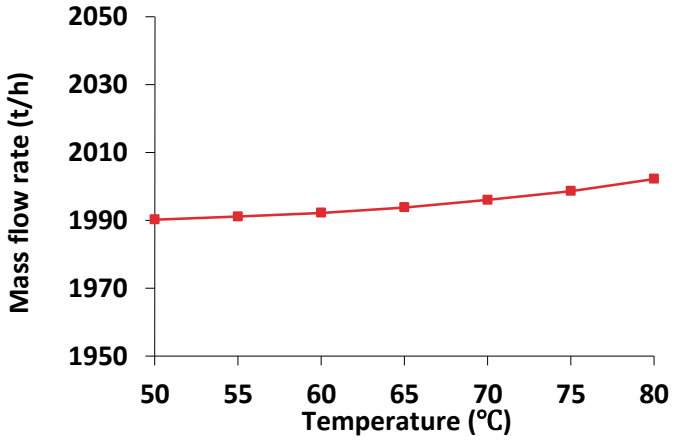
Mass flow rate (t/h)
2050
2030
2010
1990
1970
1950
50
55
60
65
70
75
80
Temperature (℃)

(b)

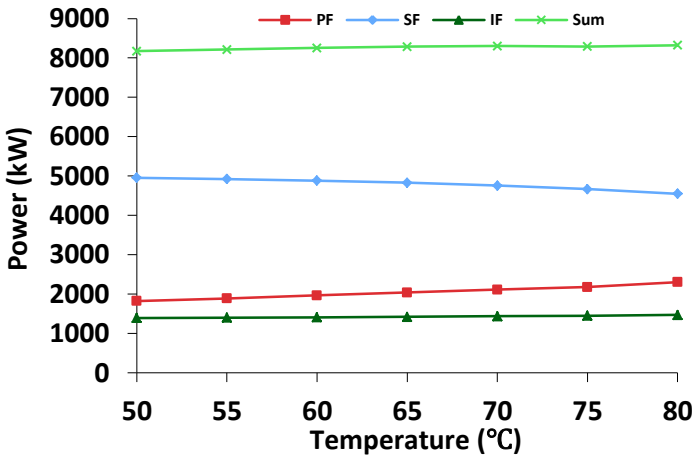
PF
SF
IF
Sum
Power (kW)
9000
8000
7000
6000
5000
4000
3000
2000
1000
0
50
55
60
65
70
75
80
Temperature (℃)

(c)

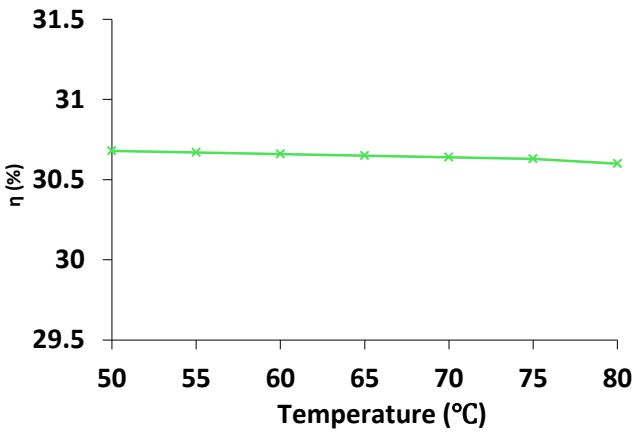

(d)

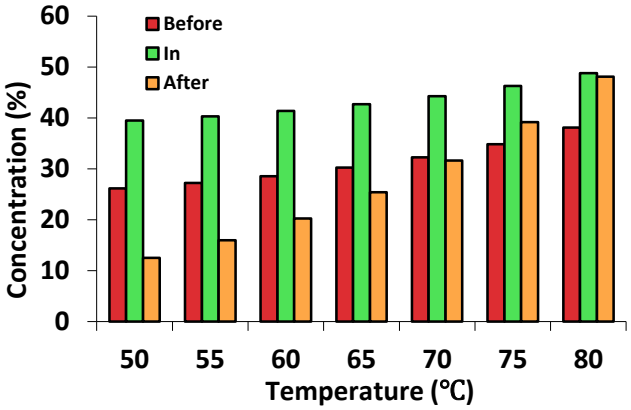

(e)

Figure 2.14 The influence of flue gas condensation temperature on flue as composition (a), mass flow rate in furnace (b), power consumption for major equipment (c), net efficiency (d), and moisture content in flue gas (e)

2.3.6 Oxygen distribution ratio between the primary fan and the secondary fan

One of the major differences between air-firing boilers and oxy-fuel boilers is that the oxygen-rich gas is produced from ASU, which brings extra cost for air separation. However, the ratio on how oxygen is introduced into furnace may bring great influence in design and operation of burners. It should be expected that control systems for oxy-fuel burners would be more complex than that for typical air-fired burners. For example, it is desirable that excess oxygen level is kept as low as

possible without affecting the performance and safety of boilers. When some portion of oxygen-rich gas is employed as transport gas in mill system, safety problem should be concerned, because the concentration of O_2 would be limited to a maximum of 21-25% by volume. Besides, for burner design some critical criteria should also be considered, such as flame length, ignition, flame stability, heat transfer profile, CO emission, unburnt carbon in ash and so on.

In this section, to study the influence of oxygen distribution ratio between the primary fan and the secondary fan, the concentration of O_2 after the primary fan is chosen as the independent variable and the air leakage ratio into furnace and gas leakage ratio in gas preheater are specified as 0 to avoid the influences of other factors.

The relationship between the O_2 concentration at the primary fan outlet and that at the secondary fan outlet is shown in figure 2.15 (a). With increasing the O_2 concentration at the primary fan outlet, the concentration of O_2 at the secondary fan outlet decreases linearly. It is noted that the variation degree for the primary fan is dominantly larger than that for the secondary fan. It is induced by the fact that most of the gas is introduced into furnace through the secondary gas. The same variation degree of oxygen-rich gas has a smaller effect on the secondary recirculated flue gas than on the primary recirculated flue gas.

Due to the constant thermal design requirements of mill, with increasing the O_2 concentration at the primary fan outlet, the power consumptions of the primary fan and the secondary fan drop down and rise, respectively, as shown in panel (b). It is noted that the flue gas temperature before the secondary fan is as high as 400 ℃. Although the secondary fan has a smaller pressure rise to flue gas than the secondary fan, this high temperature still leads to greater variation of volume flow rate through the secondary fan due to the great volume expansion of flue gas at high temperature. Thus, the power consumption variation of the secondary fan is significantly greater than that of the primary fan. The power consumption of induced fan has a slight change due to the slight changes of flue gas temperature and volume flowing through the induced fan. Finally, the total power consumption of the three fans rises with increasing the O_2 concentration at the primary fan outlet. For different oxygen-rich gas distribution ratios between the two fans, the power consumptions of ASU and the two CO_2 compressors are kept unchanged. Thus, the net electric efficiency decreases, as shown in the panel (c). It is suggested that oxygen should be introduced into the secondary fan as much as possible for higher efficiency. Meanwhile, this also satisfies the requirement of reducing the safety risk of high O_2 concentration in mill system. This is a dominant advantage of a half-dry RFG oxy-fuel boiler system.

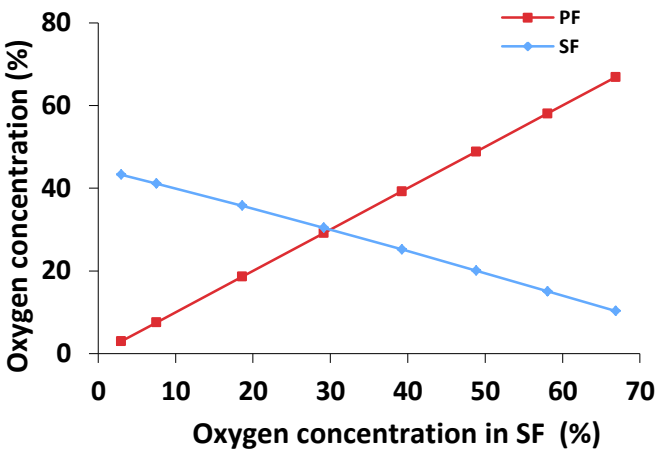

(a)

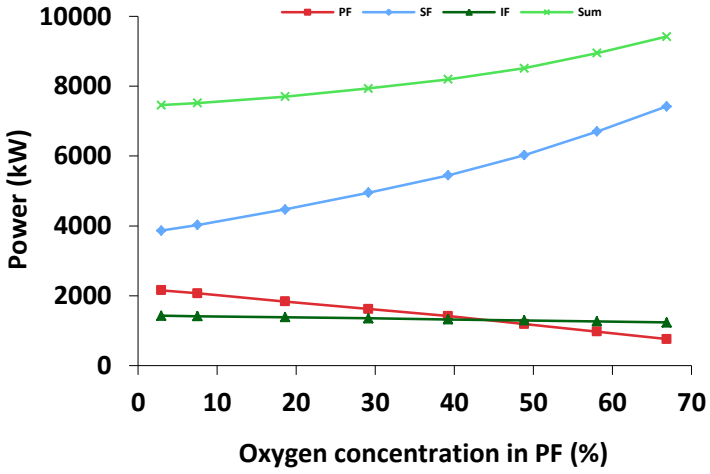

(b)

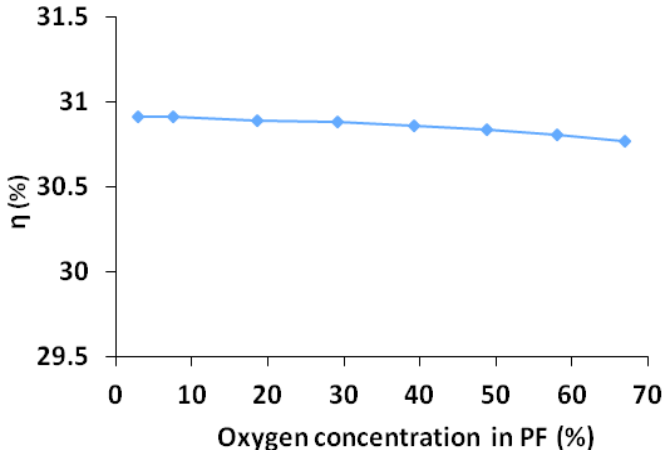

(c)

Figure 2.15 The influence of oxygen distribution ratio on oxygen concentrations in flue gas (a), power consumption (b) and net efficiency (c)

2.3.7 Sensitivity comparisons of net electric efficiency for three types of oxy-fuel boiler systems

The influences of eight factors on the net electric efficiency for the dry, the half-dry and the wet RFG oxy-fuel boiler systems are performed. For comparing in a direct way, the influences of these factors are shown through the conception of efficiency sensitivity, i.e. the variation of efficiency per unit change. The so-called "unit change" has different meanings for different influence factors. For all influence factors except "fan distribution" and "flue gas condensation temperature", the unit change means per percentage change. For the two exceptional factors, the meanings of the unit change are substituted by every ten-milli-bar pressure rise of the induced fan and every ten Celsius degree variation of temperature, respectively. For the factor of "Flue gas recirculation rate", the unit change means per percentage change of the O_2 concentration at the outlet of the primary fan or the secondary fan. All the "unit changes" are specified purposely in view of both the convenience of comparison and the possible variation extents of influence factors in engineering.

The results of efficiency sensitivities for the three systems are shown in Table 2.8. The efficiency sensitivity of flue gas recycle rate becomes greater from the dry RFG system to the wet RFG system. For the dry RFG system, the increase of the recirculated flue gas into furnace by one percentage has only the energy at the temperature of moisture removal. For the wet RFG system the increasing energy corresponds to higher temperature. The half-dry RFG system is between the two systems. This leads to the most sensitive efficiency change for the wet RFG system.

For the factor of oxygen concentration from ASU, the efficiency sensitivity of O_2 concentration from ASU become smaller from the dry RFG system to the wet RFG system, despite the very little change of the efficiency sensitivity. This difference among three systems is due to different gas leakages in gas preheater. In view of the flue gas before the primary fan and the secondary fan all conduct water removal process in dry RFG system, its volume rate of gas leakage in the gas preheater is the most. For the half-dry RFG system, the fact that water removal process is conducted only for the primary fan flue gas means only the flue gas in the primary fan is heated by the gas preheater. Apparently, there is no gas preheater in the wet RFG system.

The difference of gas leakage degree in gas preheater for the three systems can also be employed to understand the efficiency sensitivities due to the two factors of air leakage into furnace and gas leakage in gas preheater among the three systems.

The factor of excess oxygen in furnace has the lowest efficiency sensitivity for the dry RFG system and the highest one for the wet RFG system. In the dry RFG system, the process of water removal for the primary fan and the secondary fan recirculated flue gas leads to the recirculated flue gas having the highest O_2 concentration among the three systems. It requires the least oxy-rich gas from ASU and then the lowest power consumption variation of ASU.

The factor of fan distribution is referred to only in the dry and the half-dry RFG system. The factor of fan distribution can only bring the variations of ASU and the two CO_2 compressors, and the variations of these components are almost equal among the three systems. Thus, the variation of the induced fan pressure rise of the induced fan has no effect on the efficiency sensitivity for the three systems.

For the factor of flue gas condensation temperature, the process of moisture removal in the dry RFG system takes more heat away than the half-dry system, which results in higher efficiency sensitivity for the dry RFG system.

The sensitivity of oxygen concentrations distributed ratio has a great difference for both the dry the half-dry RFG systems. With more oxygen-rich gas being introduced into the primary fan, the net electric efficiencies of the dry RFG system and the half-dry RFG system increase and drop down, respectively. For higher efficiency and higher safety, the half-dry RFG system may be a more practical system. The distributed ratio has almost no influence on the net electric efficiency of the wet RFG system. The influence of oxygen distribution ratio on efficiency sensitivity is reflected by the power consumption variations of the three fans with different working conditions.

In view of the characteristics of the wet RFG system, the studies on the factors of fan distribution, gas leakage in gas preheater and flue gas condensation temperature for this system are not performed.

From the results listed in Table 2.8, it can be seen that the factor of air leakage into furnace has the greatest influence on the efficiency sensitivity for all the three systems. Besides, the four influence factors of oxygen concentration from ASU, excess oxygen in furnace, gas leakage in gas preheater and flue gas condensation temperature can also not be negligible. In the four factors, for the dry RFG system, the factor of flue gas condensation temperature has the highest efficiency sensitivity, the two factors of oxygen concentration from ASU and gas leakage in gas preheater have a little lower efficiency sensitivity and the three factors have equivalent efficiency sensitivity; for the half-dry RFG system, the factor of oxygen concentration from ASU has the highest efficiency sensitivity, the factor of excess oxygen in furnace has a little lower efficiency sensitivity and the efficiency sensitivities of the two factors are dominantly higher than the other two factors. It is noted that the efficiency sensitivity of flue gas recirculation rate is very small for the three systems.

In these factors, the influence of flue gas condensation temperature is necessary and inevitable for both the dry and the half-dry RFG systems. Correspondingly, air leakage into furnace and gas leakage in gas preheater are not needed but inevitable, which suggests that avoiding air and gas leakages as possible as we can is a key point when designing an oxy-fuel boiler. Through adjusting the other factors, the optimized design proposal for an oxy-fuel boiler system can be achieved.

Table 2.8 Sensitivity comparisons of the net electric efficiency for three systems

Item	Unit	Dry RFG	Half-dry RFG	Wet RFG
Flue gas recirculation rate	1/P	0.002	0.012	0.02
Oxygen concentration from ASU	1/P	0.05	0.044286	0.041429
Excess oxygen in furnace	1/P	-0.036	-0.041	-0.045
Air leakage into furnace	1/P	-0.112	-0.103	-0.097
Fan pressure rise distribution	1/(10mbar)	-0.016	-0.016	-
Gas leakage in gas preheater	1/P	-0.066	-0.025	-
Flue gas condensation temperature	1/(10 ℃)	-0.0786	-0.0267	-
Oxygen distribution ratio	1/P	0.000724	-0.00219	0

Note: the letter “P” in column “Unit” means percentage.

2.3.8 The acid dew point

For the flue gas system of an oxy-fuel power plant, the acid dew point is still an important research focus as for an air-firing power plant due to the knowledge limitation to the acid dew point of exhausted flue gas in oxy-fuel condition. For an oxy-fuel power plant system, the impacts of acid dew point on RFG pipe and mill system should also be concerned.

To determine the acid dew point, not the SO_2 concentration but the SO_3 concentration should be paid more attentions. Current literatures on this topic mainly focus on the mechanisms of sulphur conversion. However, the calculating methods for the acid dew point in oxy-fuel conditions are still very limited. In this section, based on the conventional mechanisms of sulphur-related conversion in air-firing conditions, a calculating method for the acid dew point is proposed to evaluate its performance and sensitivities of various influence factors.

The SO_3 conversion rate of SO_2 can be obtained by *figure 2.16*. It can be seen from this figure that the upper and lower limits of SO_3 conversion rate has been shown by their respective curves. For simplicity, the middle-value curve of the two limit curves is selected to calculate the SO_3 conversion rate of SO_2 in this study.

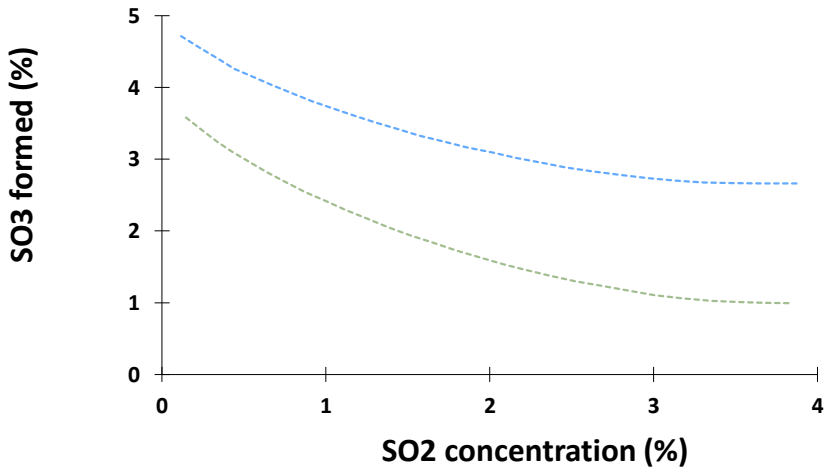

Figure 2.16 SO_3 **conversion rate of** SO_2

The acid dew point can be obtained according to the SO_3 concentration through the relationship proposed by A. G. Okkes and Badger B. V., which is written as:

$$T = 203.25 + 27.6 \lg p_{H_2O} + 10.83 \lg p_{SO_3} + 1.06(\lg p_{SO_3} + 8)^{2.19}$$

where T is the acid dew point, ℃; p_{H_2O} and p_{SO_3} are the partial pressures of H_2O and SO_3, respectively in flue gas, bar.

In this proposed method, all sulphur element in fuel is supposed to become SO_2 in the process of combustion and only a small portion of SO_2 finally converses SO_3 through the further reaction. Here the effect of sulphur retention in ash is ignored due to both simplicity and the lack of essential knowledge. It can be expected that the value from this proposed method is a little lower than the real one. However, this method still has enough accuracy to perform in this study.

The influences of the partial pressures of H_2O and SO_2 on acid dew point are shown in figure 2.16. The parameters of p_{H_2O} =20% and p_{SO_2} =0.2% is chosen as the benchmark condition. The results for the cases of the relative changes of the partial pressures of H_2O and SO_3 in flue gas from -70% to 70% are shown. It can be seen that the acid dew point sensitivity of the partial pressure of H_2O is greater than that of SO_2. In practice, the partial pressure of H_2O has a greater relative change than that of SO_2, which leads to a consequence that the partial pressure of H_2O are usually paid more attentions.

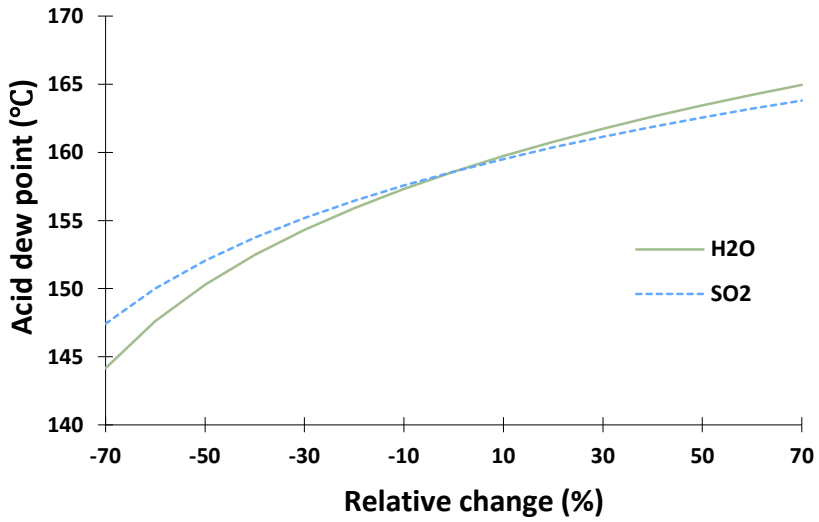

Figure 2.17 The influences of the partial pressures of H_2O and SO_3 on acid dew point

The influences of various design parameters on the acid dew point for the three different RFG type oxy-fuel boiler systems are shown in figure 2.18. The outlet of gas preheater is selected to manifest these influences.

In figure 2.18, with increasing O_2 concentration into furnace, the acid dew points rise in the dry and the half-dry RFG system. The rises of the acid dew points are induced by the increases of the partial pressures of H_2O and SO_3 in the flue gas. The flue gas conducted by the processes of desulphurization and water removal in the dry RFG system is much more than that in the half-dry RFG system, which leads to the greater sensitivity of the acid dew point. For the wet RFG system, O_2 concentration into furnace has almost little impact on the partial pressures of H_2O and SO_3, thus the acid dew point is almost kept unchanged.

With increasing air leakage rate into furnace, the acid dew points rise in all the three systems, as shown in panel (b)). The drops of the acid dew points are induced by the decreases of the partial pressures of H_2O and SO_3 in the flue gas. Air leakage rate into furnace has the most impact on the wet RFG system and the least impact on the dry RFG system. In fact, the influence of air leakage rate into furnace is resulted in mainly by the change of the partial pressure of H_2O. The air leakage into furnace can have an impact on the system because some portion of the recirculated flue gas is substituted by the leaked air into furnace. For the wet RFG system, the recirculated

flue gas is not processed by FGD and HX and has highest H_2O concentration. The similar analysis can be used for the other two systems. The recirculated flue gas in the half-dry RFG system has the intermediate H_2O concentration and in the dry RFG system the least H_2O concentration.

With increasing gas leakage rate in gas preheater, the acid dew points drop in the two systems, as shown in panel (c), the dry and the half-dry RFG systems. The result for the wet RFG system is not shown in view of the absence of gas preheater. With increasing gas leakage rate in gas preheater, more mixing gas of the recirculated flue gas and oxidant gas is leaked to the flue-gas side of the gas preheater. The lower H_2O concentration of the mixing gas leads to the lower H_2O concentration of the flue gas at the flue-gas side of the gas preheater, then lower acid dew point. With a certain gas leakage rate in gas preheater, more leaked gas in the dry RFG system than the half-dry RFG system leads to greater sensitivity of the acid dew point.

In figure 2.18 (d), with increasing flue gas condensation temperature, the acid dew points rise in the dry and the half-dry RFG system. As in panel (c), the result for the wet RFG system is not shown. With increasing flue gas condensation temperature, the recirculated flue gas introduced into furnace from the primary fan and the secondary fan contain more moisture, which directly induces the rise of the acid dew point. Because the flue gas conducted by the processes of desulphurization and water removal in the dry RFG system is much more than that in the half-dry RFG system, flue gas condensation temperature have greater influence on the acid dew point in the dry RFG system.

Overall, under the same condition, the acid dew point of the wet RFG system is the highest and the dry RFG system the lowest, which corresponds to the process degree of desulfurization and moisture removal for the recirculated flue gas in the three systems, the least in the wet RFG system and the most in the dry RFG system. The acid dew point of the half-dry RFG system is usually higher about 10 ℃ than that of the dry RFG system and lowers about 5 ℃ than that of the wet RFG system. Besides, the acid dew points of the three oxy-fuel RFG system are higher about 20-35 ℃ than that in the air-firing system.

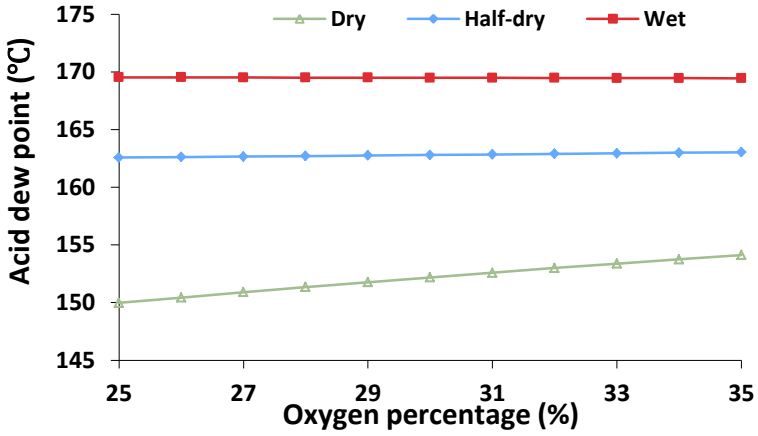
Dry
Half-dry
Wet
Acid dew point (℃)
175
170
165
160
155
150
145
25
27
29
31
33
35
Oxygen percentage (%)

(a)

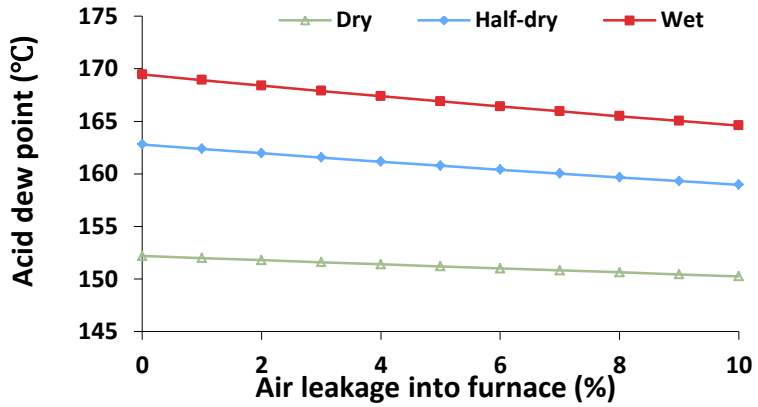
Dry
Half-dry
Wet
Acid dew point (℃)
175
170
165
160
155
150
145
0
2
4
6
8
10
Air leakage into furnace (%)

(b)

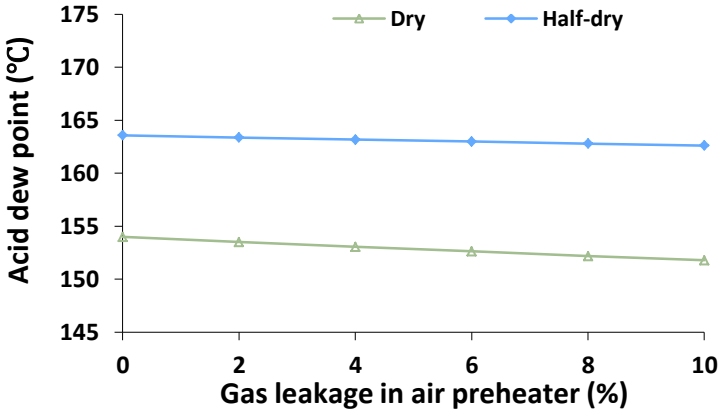
Dry
Half-dry
Acid dew point (℃)
175
170
165
160
155
150
145
0
2
4
6
8
10
Gas leakage in air preheater (%)

(c)

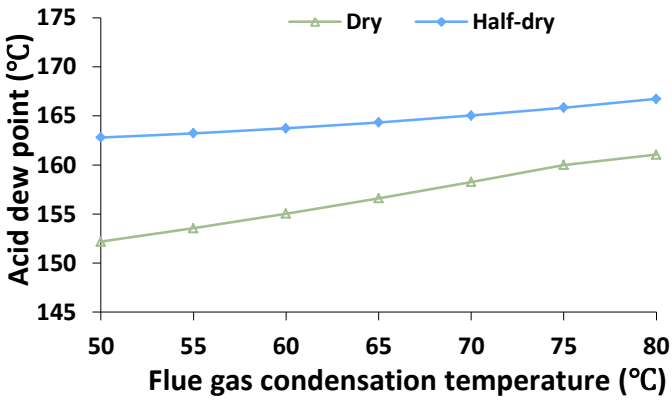

(d)

Figure 2.18 The influences of various design parameters on acid dew point. Panels (a) – (d) are for oxygen percentage, air leakage, gas leakage ratio in air preheater and flue gas condensation temperature, respectively.

2.4 Conclusions

The achieved major conclusions from techno-economic analysis are drown as follows:

1) The integration of pre-drying and supercritical steam condition has proven to be able to compensate for the energy penalty related to ASU and CO2 compression, leading to a net efficiency of 25-29% LHV based, which is comparable with and even higher than the existing sub-critical steam boiler for Victorian brown coal.
2) The use of Chinese equipments including boiler, turbine, auxiliaries, ASU and/or CO_2 compressor is pivotal in reducing the cost of electricity and cost of CO_2 avoidance for the oxy-firing combustion of Victorian brown coal in the Latrobe Valley. Through the use of Chinese equipment, the cost of electricity is expected to decrease to approximately USD $80/MWh, relative to around USD $100/MWh based on the use of facilities manufactured in western countries. The cost of CO_2 avoidance drops from USD $50-60/t CO_2 to 20-30/t CO_2.
3) The plant capital cost and discounted cash flow are the most influential factors affecting the cost of electricity and cost of CO_2 avoidance for the oxy-fuel combustion of Victorian brown coal. The fuel price, i.e. cost of coal drying technique, is less significant in air-firing mode. However, for the oxy-firing mode, this factor is also crucial. Getting a cost-effective and efficient coal dryer, e.g. from China, is a essential in further reducing the cost of electricity

and cost of CO_2 avoidance for the deployment of oxy-fuel technology in the Latrobe Valley in the future.

4) The operation of fans and mill system has a noticeable effect on the net efficiency f the overall oxy-firing process. Flue gas recirculation rate has a trivial effect. The influence of flue gas recirculation rate is reflected by the power consumption of the secondary fan. The factor of air leakage into furnace has the greatest influence on the efficiency sensitivity for all the three oxy-fuel RFG modes. The four factors from O2% from ASU, excess ratio of oxygen in furnace, gas leakage rate in gas preheater and flue gas condensation temperature cannot be neglected for process design. With employing wet type FGD for flue gas condensation, its outlet temperature is crucial in terms of water removal extent and process net efficiency. From the perspective of the sensitivity of oxygen concentrations distributed ratio, the half-dry RFG system have a relative high efficiency and higher safety and can be considered as a more practical system compared the other two systems.

3. 3MWth experimental investigations of oxy-fuel combustion of Victorian brown coal

3.1 Experimental facility

A 3.0 MWth boiler with a schematic in figure 3.1 and details in figure 3.2 has been employed throughout this project. The furnace is approximately 10.5 m in height, and its square cross- section is 1.2 m in width. For the oxy-fuel combustion mode, RFG system was implemented by taking a portion of flue gas out after bag filter back to the burners. The boiler is coupled with an air separate unit (ASU) providing oxygen with a purity of 95%, which is partitioned into two fractions into primary and secondary gases for flexibly adjustment of the local oxygen concentration in the burners. The boiler is also coupled with gas preheater, flue gas and oxygen mixer, bag filter for fly ash collection, a dry lime scrubbing unit for desulphurisation, and pipelines for flue gas recirculation.

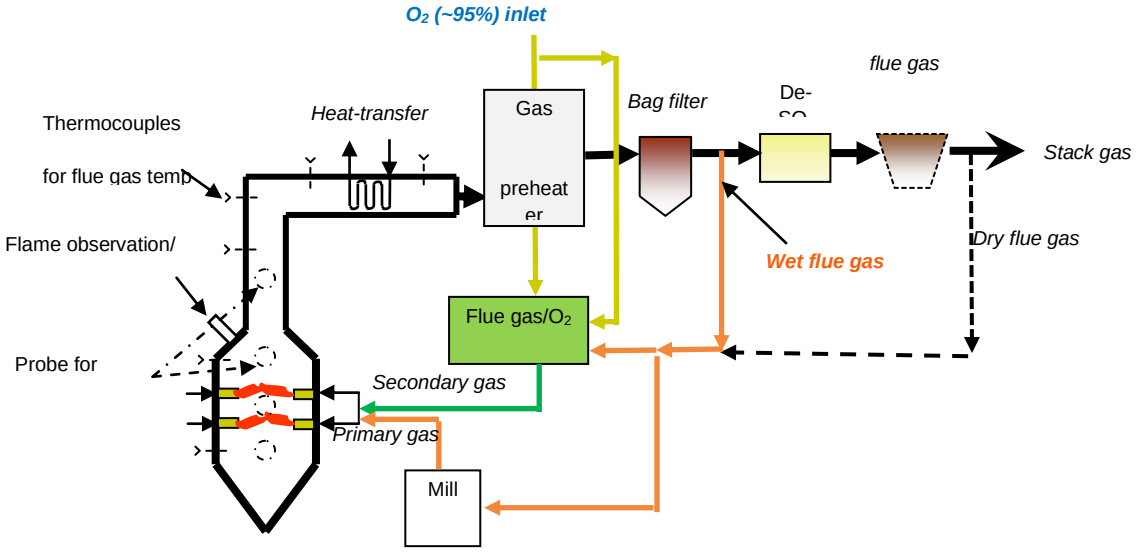

Figure 3.1 schematic of the 3 MWth air-firing/oxy-firing facilities at SBWL

Figure 3.2 Front views of the SBWL 3 MWth oxy-firing facility and different units

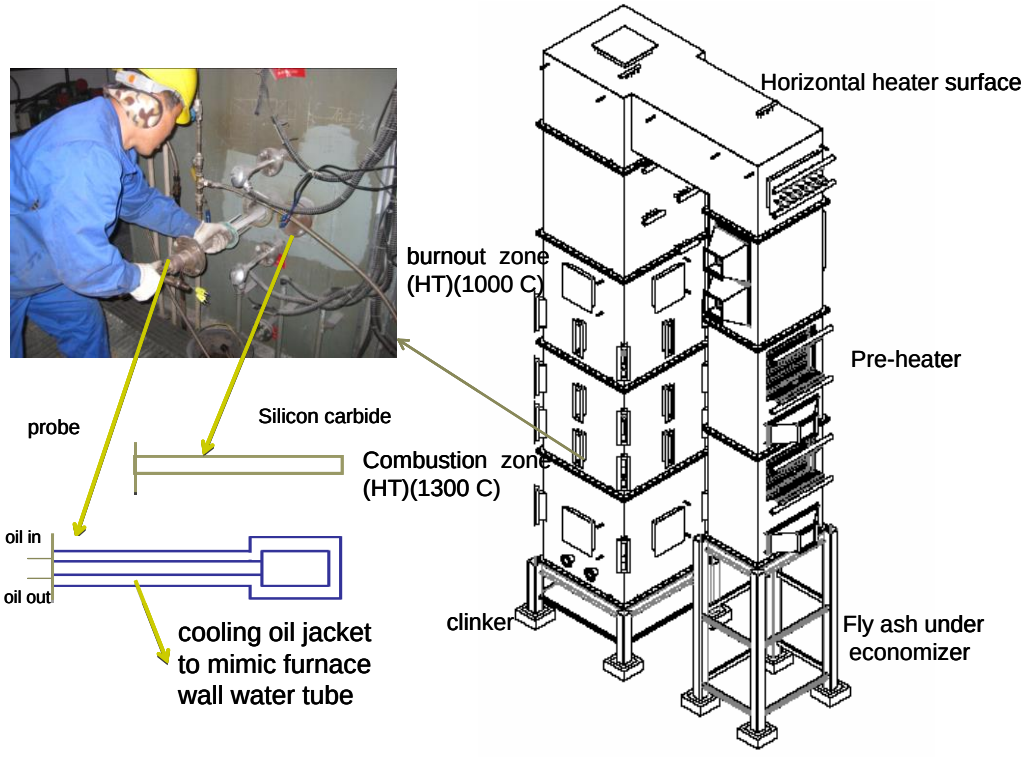

Figure 3.3 Ash deposition probes used for ash collection through the boiler

The charge-coupled device (CCD) camera is located on the upside of front wall to obtain the real-time flame photography. A variety of B-type thermocouples are used to measure flue-gas temperature profile above the burner area. The furnace wall temperatures are recorded by thermocouples mounted inside. Ash deposition probes (detailed in figure 3.3) were inserted for ash sampling with an oil jacket to simulate real pipe temperatures in boiler. Regarding the different pipelines of primary gas, secondary gas, recycled flue gas and exhaust flue gas, the gaseous concentrations of CO_2, O_2, CO, SO_2 and NOx were measured by a flue-gas analyzer. And a gas impinger train system is applied for the collection of SO3 and trace metals except Hg, and mercury analyser is also used.

3.2 Transportation and test of Victorian brown coal

The successful transportation of three Victorian brown coals (Morwell, Loy Yang and Yallourn) has been achieved in the end of February 2012. Approximately 50 tons coals (17 tons of each coal) were transported, among which 40 tons were sent to Shanghai Boiler Works Ltd for pilot-scale testing and the remainder was sent to IHI Co Ltd for ash deposition testing. The photos in figure 3.4 prove the safe arrival of coals to the two companies.

Figure 3.4 Successful transportation of Victorian brown coal

The coal properties are all tabulated in table 3.1 below. Apart from these three Victorian coal samples, two local coal samples, namely Xinjiang lignite and Shenhua bituminous coal, were also tested for reference and comparison.

Table 3.1 Proximate and ultimate properties of three Victorian brown coal samples tested

Coal	Victorian brown coal			Auxiliary coal used for practice and comparison	
	Hazelwood	Yalloum	Loy Yang	XJ coal (lignite)	SH coal (bituminous coal)
Proximate analysis, % air-dried basis					
Moisture	12.3	16.2	16.6	16.0	10.5
Volatile Matter	51.1	50.7	49.9	25.9	27.24
Fixed Carbon	46	46.2	49.4	51.7	47.84
Ash content	2.8	3.2	0.7	6.4	14.42
Ultimate analysis, % dry basis					
Carbon	66.3	64.5	70.2	72.9	69.11
Hydrogen	4.6	4.3	4.7	3.84	3.73
Nitrogen	0.48	0.51	0.52	0.58	0.89
Sulphur	0.26	0.28	0.35	0.62	0.56

Table 3.2 Kinetic data of Victorian brown coal tested

Reaction kinetics	Raw coal	Ammonia acetate washed coal
(1) Devolatilisation rate		
Pre-exponential coefficient (s^{-1})	5.18×10^{16}	1.92×10^{11}
Activation energy (kJ/mol)	217.27	152.22
(2) Char oxidation rate		
Pre-exponential coefficient ($kgm^{-2}s^{-1}Pa^{-1}$)	0.0024	0.0014
Activation energy (kJ/mol)	69.06	68.54
(3) Char gasification rate with CO_2		
Pre-exponential coefficient ($kgm^{-2}s^{-1}Pa^{-1}$)	0.0053	1.2659
Activation energy (kJ/mol)	125.5	195.0

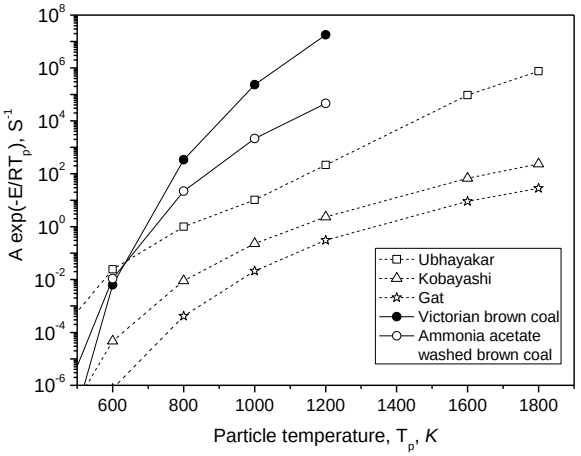

(a)

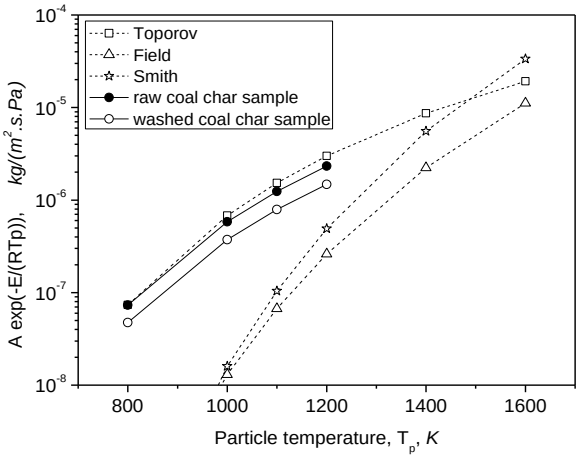

(b)

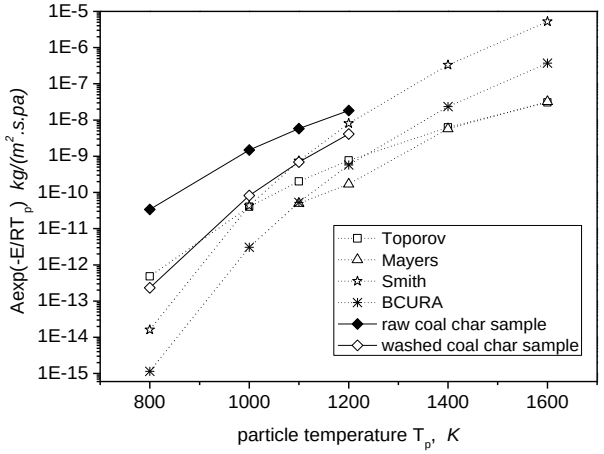

(C)

Figure 3.5 Comparison of measured kinetics of Victorian brown coal and those reported in reference *Panels (a), (b)* and *(c)* are for devolatilisation, char oxidation and char gasification reaction with CO_2, respectively.

The kinetic data was tested for Victorian coal-sample with a size range of 106 - 153 μm (mean size 130 μm) and air dried prior to use. On the dried mass basis, the volatile matter content is comparable to fixed carbon. The devolatilisation, char-O_2 oxidation and char-CO_2 gasification reaction occur fast for the coal tested here, as shown in Table 3.2. The kinetics of coal devolitilisation and char surface reactions were measured by a non-isothermal heating program, with the heating rate varying from 10 K/min to 50 K/min in a thermal gravimetric analyzer (TGA, Shimadzu – 60H).

Once being dried, the Victorian brown coal bears a very high reaction rate for both devolatilisation and char oxidation. Figure 3.5 summarises the kinetic parameters for this coal, its ammonia acetate-washed residue and the bituminous coals reported in. Ammonia acetate was used to remove the alkali and alkaline earth metals that are supposed to be the catalysts for brown coal oxidation. In panel (a) showing the devolatilisation rate, one can see that both Victorian brown coal and its washed residue were pyrolysed quickly from 800 K onwards. Their devolatilsation rates are 10^2-10^6 faster than the bituminous coals. This is due to the youngest age and shortest coalification time for this brown coal. Its volatile matter is mainly composed of light/gaseous hydrocarbons accounting for more than half on the mass basis of the total volatiles. Regarding the brown coal char-O_2 oxidation rate in panel (b), it is close to that reported by Toporov, being fast compared to the bituminous coal char. The ammonia acetate washing affected little on the char-O_2 oxidation rate. For char-CO_2 gasification rate, it is obviously higher than the reported high-rank coal at the temperatures below 1200 K. The removal of the ash-forming metals by ammonia acetate washing dropped the magnitude of this reaction to the same level as the reported bituminous coals, which substantiates the catalytic role of ash-forming metals on the high char-CO2 reactivity of this coal.

3.3 Experiments on air-firing combustion of air-dried Victorian brown coals

The purpose of this experiment suite is to clarify the air-fired combustion characteristics of dried coal, its ash fouling and slagging propensities and pollutant emissions. On the one hand, the comparison of these results with the existing wet coal-fired boiler will help clarify the impact of coal pre-drying on ash slagging and fouling. The pre-drying is expected to improve the flame/particle temperature and hence promote the melting/slagging of ash particles. On the other hand, these results will be used as baseline to compare with the oxy-fuel combustion results to elucidate the influence of gas substitution on ash formation and pollutant emissions. Upon

being exposed in air for the duration of around one month in the summer season at Shanghai, the moisture content drops at ~ 24 wt%, reaching its equilibrium state.

On Sept 15 – Oct 15 2012, four conditions have been done for the combustion of three Victorian brown coals and one lignite coal (for both practice and comparison) at a boiler capacity of 1.0-1.4 MW, experimental cases shown in Table 3.3. For each condition, two replicates have been done as one single run lasted maximum 5 hrs due to the blockage of coal feeder and feeding pipelines. One run was used to do the measurements including gas compositions, dust and SO3 concentrations; and another run for the production and samples of ash samples. The flame photographs were observed for three Victorian brown coals, shown in Figure 3.6.

Generally one experiment was conducted per week. Its timeline is:
Day 1
7:30 am, commence the preparation;
12:00 pm, commence the ignition of natural gas and move coal to the bunker;
14:00 pm, commence coal milling;
16:00 pm, commence coal combustion;
17:00 pm, commence the samplings for fly ash and SO3/trace metals;
21:00 pm, coal combustion finished;
24:00 pm, shut down the furnace;

Day 2
Leave furnace to cool down;

Day 3
Ash samples collection.

Table 3.3 Air-firing experimental conditions conducted

Coal	Moisture in coal (wt%)	Thermal power, Mw	Coal feeding rate, kg/h	total air, Nm^3/h
Yalloum	23.1	0.95	185.4	1060.0
		1.2	246.6	1360.0
Hazelwood	24.6	0.8	155.6	910.0
		1.0	189.5	969.0
		1.2	240.0	1361.0
Loy Yang	24.0	1.2	222.0	1359.0
		1.4	260.0	1590.0
XJ coal (lignite)	16.0	1.05	196.3	-

Figure 3.6 Flame pattern and intensity for the three air- dried Victorian brown coal samples under air-firing conditions of 1.2 MW

For each condition, apart from on-line sampling of flue gas components, around 20-36 ash samples was generated, all of which are being characterised by the combination of a number of advanced facilities including XRD, XRF, ICP-OES, TMA and XAS, as detailed in Chapter 6 below.

3.4 Experiments on oxy-fuel combustion of air-dried and wet Victorian brown coals

The oxy-fuel combustion of one air-dried Victorian brown coal was successfully commissioned. As it is our first time and even the first trial in the world for Victorian brown coal oxy-fuel combustion, we actually faced up with many uncertainties that have not been explored in the literature. In light of this, we simplified the questions by testing air-dried coal (moisture ~24wt%) first, and then tried the oxy-fuel cases of semi-dried/wet coal (moisture content up to ~42wt%) which yields too much steam in the boiler. The details are shown in Table 3.4.

The experimental tests include three different patterns in terms of shifting the combustion from air to oxy-fuel mode:
1) complete the recirculation of flue gas (secondary gas only) during the initial natural gas combustion;
2) complete the recirculation of flue gas (secondary gas only) during the coal combustion in air;
3) complete the recirculation of the flue gas for the primary gas after the secondary gas is shifted from air to oxy-fuel mode.

Table 3.4 Experimental conditions conducted of oxy-fuel combustion

Coal	Moisture in coal (wt%)	Thermal power, MW	Coal feeding rate, kg/h	Pure O2 flux, Nm3/h	Recycled gas flux, Nm3/h	O2 in furnace, vol%
Hazelwood	24.6	0.5	74.3	130		30
		0.8	156	200		26
		1.0	210	220		30
Hazelwood	38.0	1.0	250	226		35
Yallourn	34.0	0.6	155.8	302	1055	33
		0.8	195.7	340		34
Yallourn	42.0	0.9	220	202		26
		0.9				30
		1.0				35
		1.0				40
Loy Yang	40.0	1.0	242	226		35

For the oxy-firing cases, a variety of trials for four different scenarios in terms of flue gas recirculation sequence and the shift between air and O2/FRG had been conducted. The four different scenarios include: primary gas (air) + secondary gas (O2+RFG), primary gas (RFG) + secondary gas (O2 + air), primary gas (RFG + O2) + secondary gas (RFG), primary gas (RFG) + secondary gas (O2+RFG). As bas been confirmed by the trial-and-error method, for the air-dried brown coal, the use of RFG only for the primary gas is enough to maintain the stability of coal volatile flame. However, for the semi-dried wet coal, the presence of oxygen in the primary gas is essential, which otherwise caused the complete extinction of coal flame over a very short time.

3.5 Experimental results – CO_2 purity in flue gas

A typical run procedure for the shift from air-firing to oxy-firing is illustrated in figure 3.7. For a combustion trial, the natural gas burner was first ignited to warm up the whole furnace. Once the furnace temperature reached 800^{o}C, coal feeding for air combustion was commenced, which lasted around five hrs to ensure that the coal flame is stable and the sampling of flue gas and fly ash for three times is accomplished. Once this is done, the secondary gas is first replaced by the mixture of RFG and pure oxygen from ASU. By monitoring the flame stability, the primary gas is shifted from air to RFG mixed with or without oxygen. The overall oxygen fraction is also adjusted to ensure coal flame is stable and intense enough to avoid the formation of unburnt carbon in flue gas. The whole shift process usually took around 30 min until the flame was stabilised. The flue gas temperature was maintained at around 160^{o}C to avoid the condensation of acidic species within flue gas. The experiment was continued for another five hours.

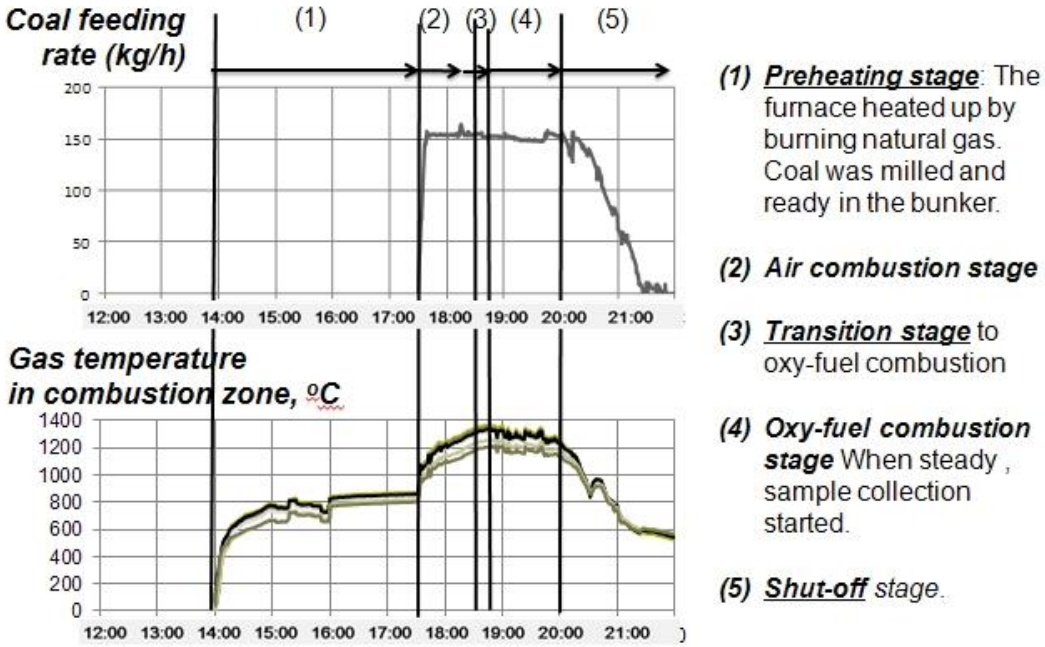

Figure 3.7 A typical combustion profile for Hazelwood coal in air versus oxy-fuel combustion

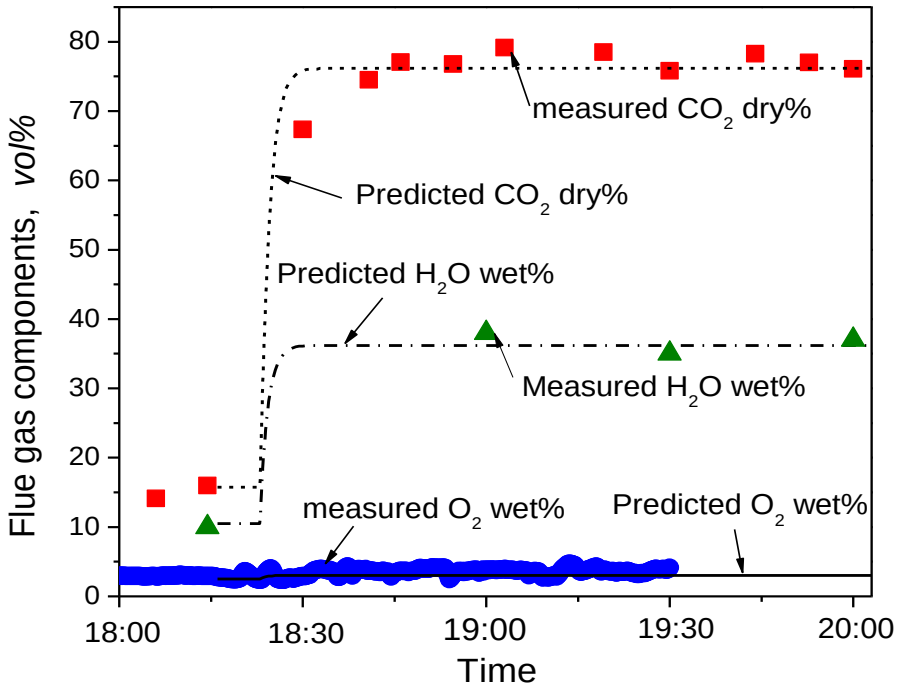

Figure 3.8 Flue gas components for the combustion of dried coal from air mode to oxy mode

As has been confirmed, a maximum purity of 80% (dried) can be achieved for the combustion of Victorian brown coal under the oxy-31 condition for the presence of ~30% O_2 mixed by RFG in the boiler, as shown in figure 3.8. The remaining impurities mainly include ~4% oxygen. Compared to air-firing flue gas containing about 15% steam, the oxy-firing wet flue gas contains up to 40% moisture, which caused the blockage tendency of the coal-feeding pipelines after a continuous operation for maximum five hours.

The nitrogen in flue gas is believed to derive from ASU and the air ingress from natural gas burner, bag-filter and pre-heater. Stopping these leakages is an engineering problem that needs to be solved by the boiler maker in the future scale-up. Operating the oxy-firing boiler at a positive pressure like natural gas boiler could be one useful option.

Regarding the CO2 level achieved in this study, it is also comparable to the reported literature values, e.g. emitted CO_2 content reached 78% (dry) in Calide oxy-fuel project with black coal burned, the CO_2 emission of 81.34% (dry) was observed during oxy-firing of dried European lignite with 15 wt% moisture, as demonstrated in table 3.5 below.

Table 3.5 CO_2 purity in oxy-firing flue gas

	Coal	CO_2, dry%	O_2, wet%	H_2O, wet%
This study	Hazewood coal (24.6%, moisture)	80.0 (air 15.0)	5.0 (air 5.0)	35.0 (air 10.0)
Callide oxy-fuel project	Australian black coal	78.0	4.0	-
Energy Conversion and Management 2007, 48, 2879-87.	Dried lignite (15% ,moisture)	81.34	1.25	18.81

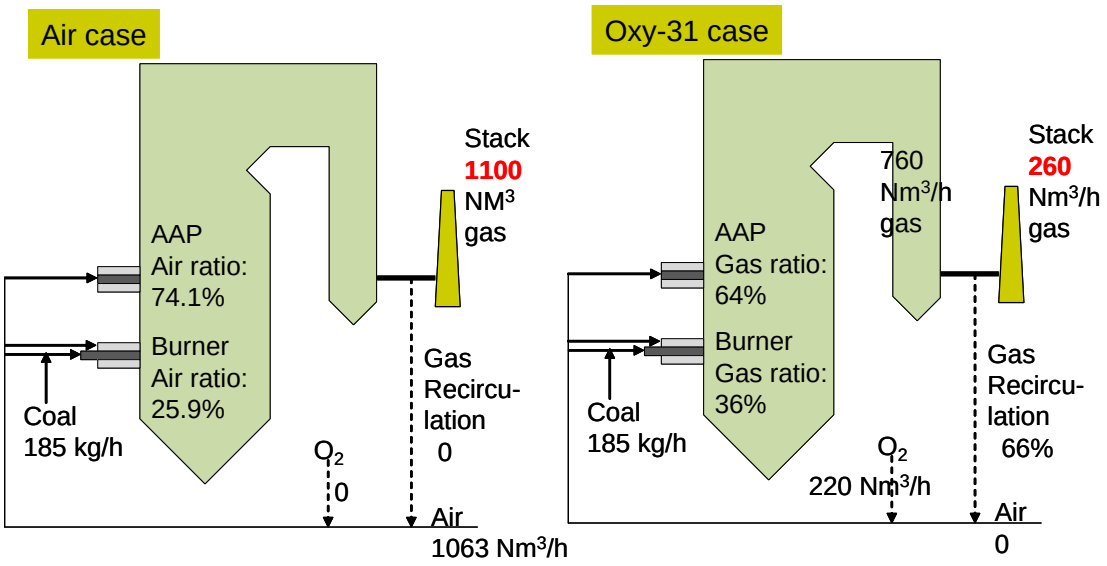

Figure 3.9 Comparison of flue gas amount from air-firing and oxy-firing modes for the air-dried Hazelwood coal

The flue gas amount in the oxy-firing boiler and its fraction discharged out of the chimney are remarkably lower than the air-firing case. As demonstrated in figure 3.9 for the oxy-firing of air-dried Hazelwood coal in oxy-31 versus air, the total flue gas amount in the air-firing boiler approximates 1100 m^3N/h for the coal feeding rate of 185 kg/h, which is reduced to 760 m^3N/h and 260 m^3N/h in the oxy-firing boiler and out of the oxy-firing chimney, respectively. This is a large advantage of a purpose-designed oxy-firing boiler, which can be 1/3 smaller than the air-firing boiler with the same thermal capacity. The flue gas amount to be treated will also be around 1/5 of that derived from the air-firing case.

3.6 Experimental results – coal flame stability, gas temperature and radiation profiles

Flame stability is the primarily significant index in burner design and operation because burners must stay ignited through a reasonable range of fuel and oxidizer flow characteristics and over a range of heat release rates, avoiding the flame extinction phenomena.

Fig.3.10(a) visualises the predicted gas temperature distributions (CFD modeling approach is stated in Chapter 5, which used to interpret the experimental data here.) on a vertical mid-plane and a horizontal burner plane, in which the comparison was made between air-firing case and two oxy-fuel cases of 27% and 30% O_2 for air-dried coal. When the oxygen concentration in the feed gas stream is increased, the whole flame temperature increases, which result in the pulverised coal ignition position closer to the burner. For the flame formed at oxy-21% O2, its flue gas temperature is around 100-300^{o}C cooler than the air case, supporting the negative effect of the larger specific heat capacity of CO_2. The flame from each burner also does not attach to one another, indicating the non-stability of coal ignition. At 27% O2 in oxy-fuel mode, the flue gas temperature profile formed is rather identical with the air-case. Increasing the oxygen content to 30% induces a strong attachment between the flames formed from the burners opposite each other. The flue gas is thus a bit hotter than the air case. Clearly, 27% O2 is the best option in terms of matching the flue gas temperature achieved in the air-firing case. Figure 3.10 (b) illustrates the real flame photographs observed in the corresponding experiments. These photos support the CFD modeling prediction results. The same conclusion for the optimum oxygen content of 27%O2 was also found in our previous laboratory experimental observation in a drop-tube furnace for air-dried Victorian brown coal. Victorian brown coal bears a very high reactivity for both devolatilisation and char oxidation, once being dried.

For the wet coal containing 42 wt% moisture, the red zone referring to coal flame is not formed in the oxy-21% O2 case, as shown in Fig.3.11 (a). Improving the O2 content to 27% still fails to match the reference air-firing case. Its flue gas temperature in flame zone is still considerably lower. The use of 30% and 35% O2 balanced by RFG is clearly essential to match the air-case. Through on-line flame surveillance in Fig.3.11(b), one can witness an unstable, dark and extinguished flame formed in oxy-21% O2 compared to the air case. The bright fireball for the flame in air is another evidence supporting the rapid drying and high reactivity of the brown coal tested here. For the oxy-27% O_2 flame, it is rather shaking and fails to attach together to form a stable fireball. Apparently, apart from the large heat loss caused by moisture evaporation, the combined effect of CO_2 and evaporated steam (due to their larger specific heat capacity than nitrogen) negated coal ignition and flame propagation even in 27 % O_2 that is sufficient for the dried coal. Increasing the oxygen content in flue gas outweighed the negative influence of coal moisture and CO_2, thus leading to the formation of stable and bright fireball as visualised in fig. 3.11 (b).

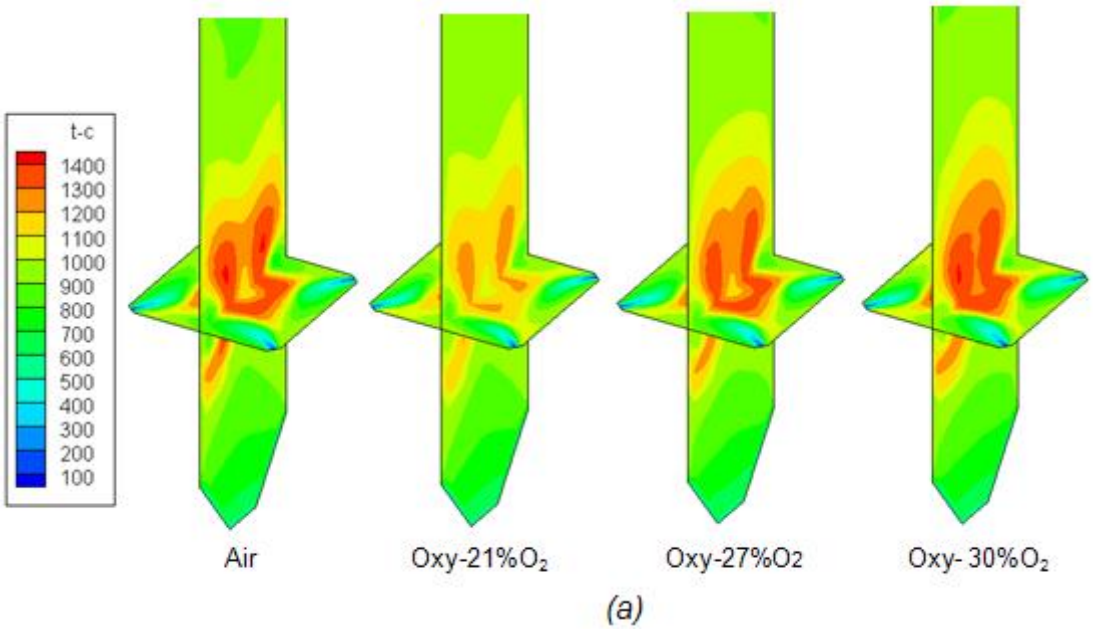

(a)

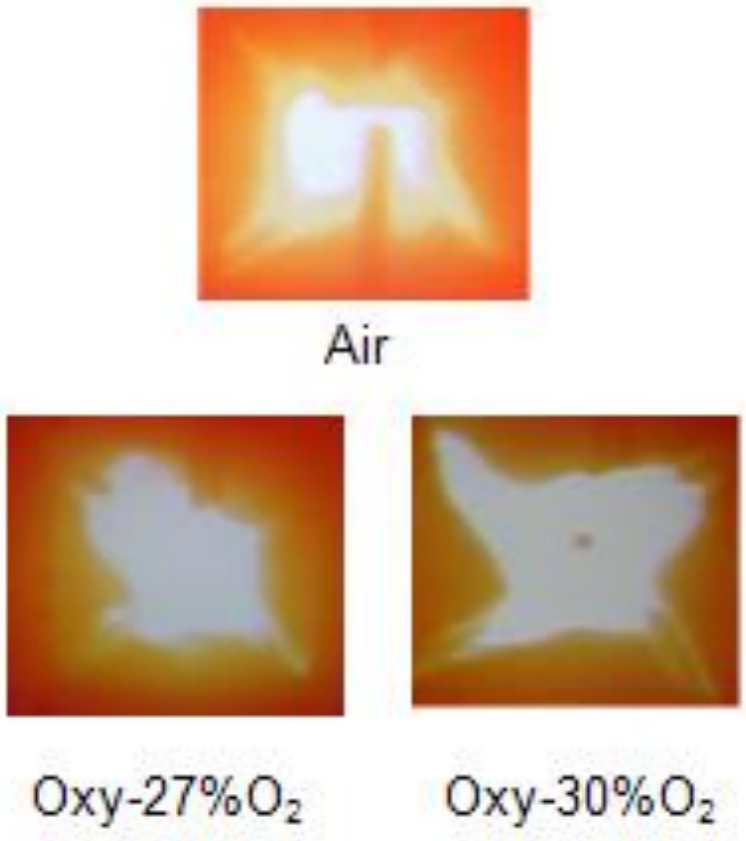

(b)

Fig.3.10 Flame stability analysis of air-dried coal, (a) Modeling results of gas temperature, ^{o}C; (b) Flame photographs in burner cross section.

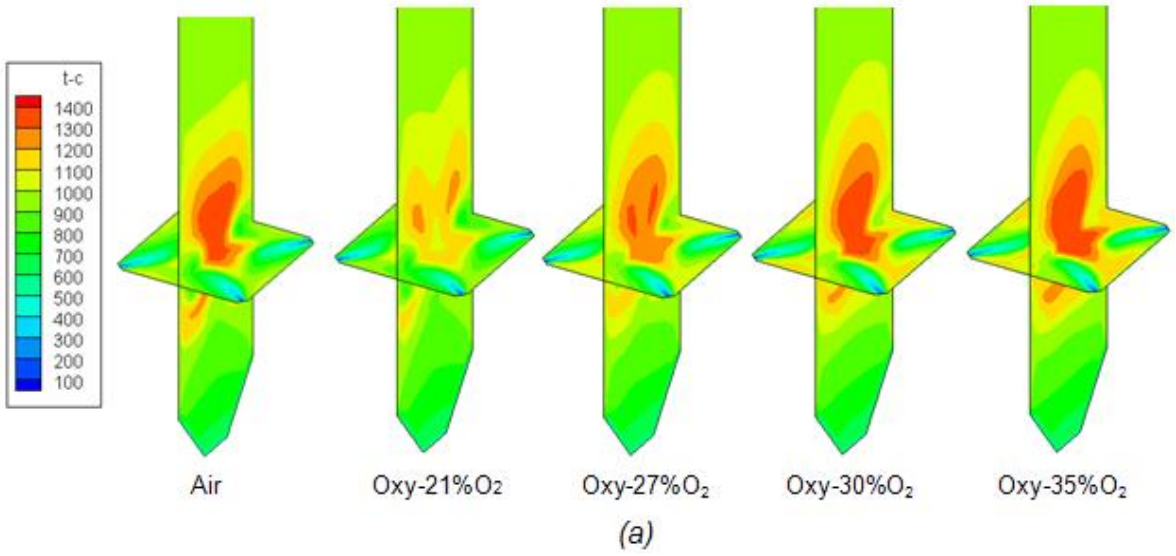

(a)

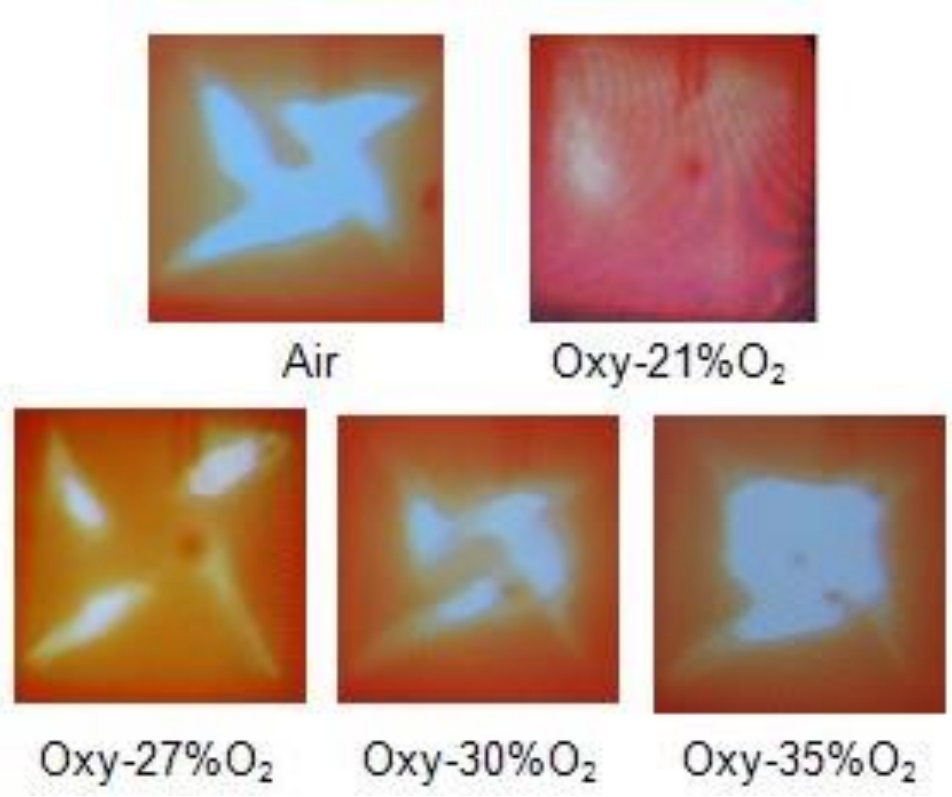

(b)

Figure 3.11 Flame stability analysis of wet coal, (a) Modeling results of gas temperature, ^{o}C; (b) Flame photographs in burner cross section.

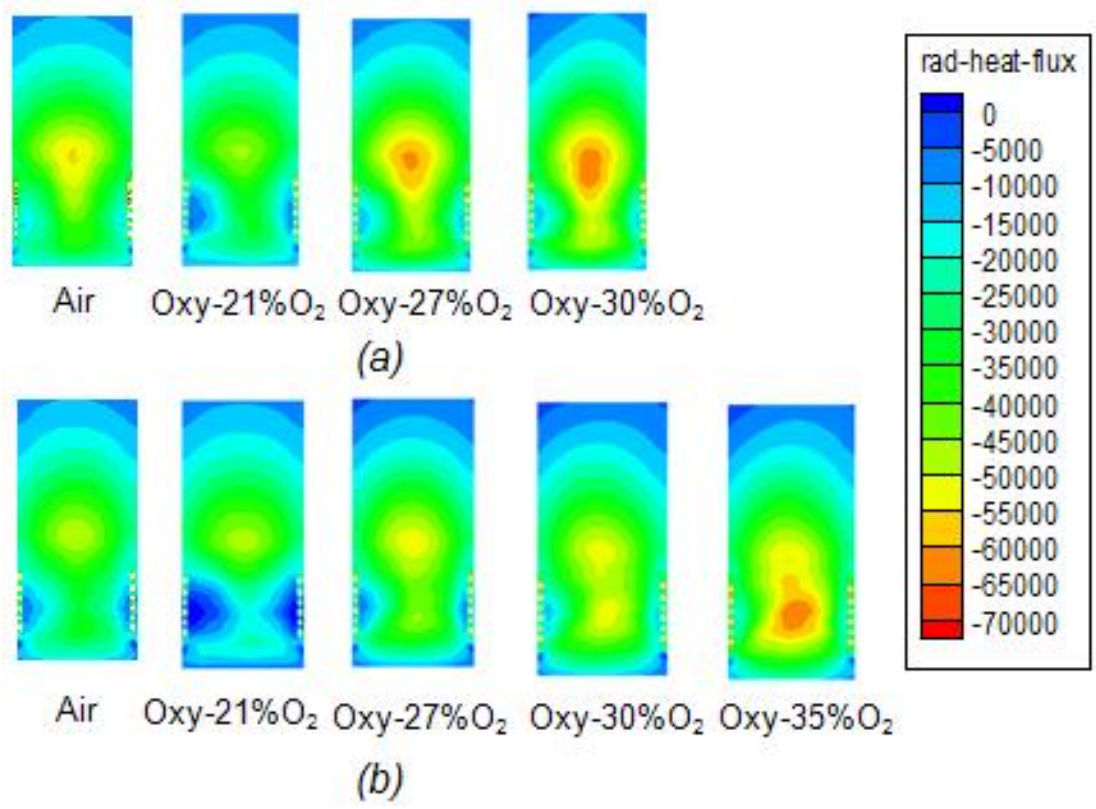

Figure 3.12 Radiative heat transfer on the furnace wall, W/m2
(a) air-dried coal; (b) wet coal.

In a pulverised coal fired furnace, the bulk of heat transfer is dominantly accomplished by radiation. For oxy-fuel retrofit application, the radiative heat transfer needs to remain identical to air-firing case. The modeling results are illustrated in Figure 3.12, where the increase in oxygen level in oxy-fuel flue gas results in enhanced radiative intensity at the central upside of oxy-fuel flame, irrespective of coal moisture content. For the dried coal, its radiative heat transfer at oxy-27% O2 is clearly intensified compared to the air case, although their flue gas temperature and flame pattern match each other. This phenomenon is even worse for the wet coal, where the raditive heat transfer at oxy-30% O2 is much more intense than the air case. In particular, the intense radiation occurs in the burner vicinity in oxy-30% O2 case, whereas the most intense radiation heat transfer occurs above coal burner for the air case. This can be largely attributed to a low flue gas velocity and the improved oxygen content near coal burner. Moreover, by comparing the dried and wet coal under the same oxy-fuel condition, e.g. oxy-30% O_2, one can see a weak but broad distribution for the radiative heat in the wet coal case. In particular, the radiative heat transfer near coal burner was enhanced, which is apparently beneficial for the initial

drying of wet coal particles. The enhanced radiative heat transfer should be caused by the co-existence of abundant CO_2 and coal moisture - derived steam, which is able to absorb more heat from coal flame due to their large specific heat capacity. This is a clear sign of the distinct combustion characteristics of wet brown coal.

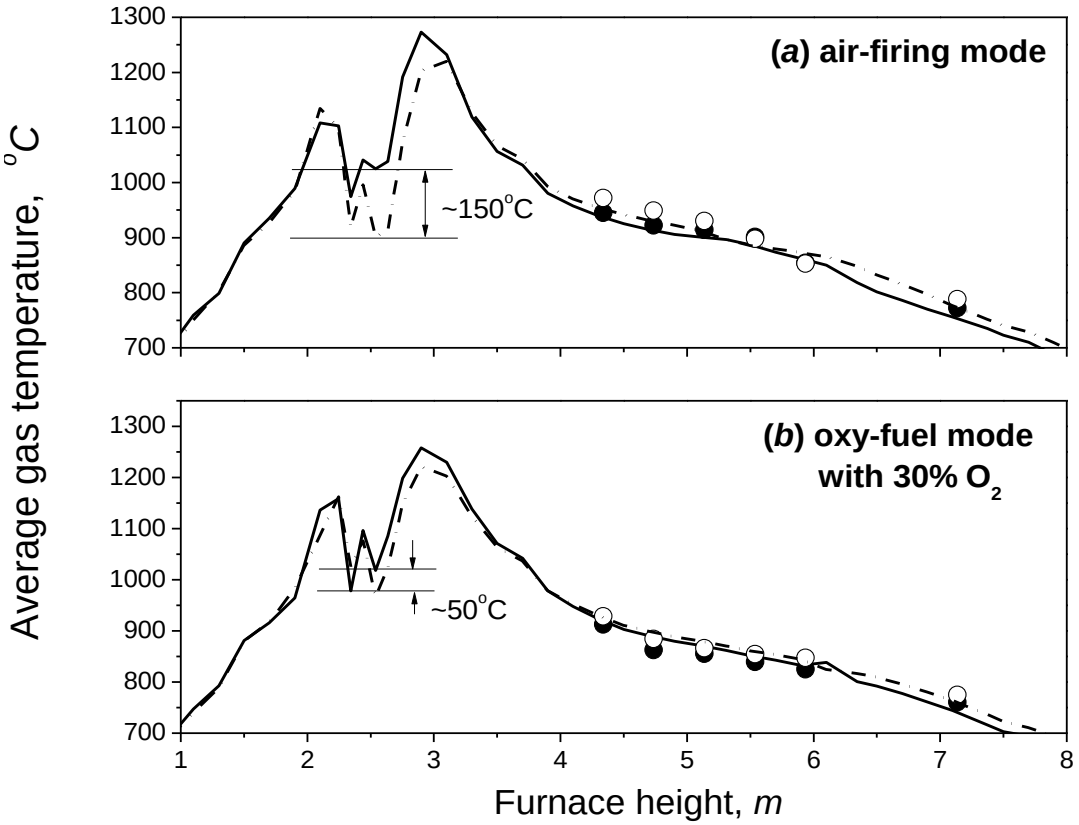

Figure 3.13 Flue gas temperature profiles along furnace height Open symbol is experimental data for air-dried coal; Filled symbol is experimental data for wet coal; Solid line and dash line are predictions for air-dried and wet coals, respectively

The temperature profiles were also measured and predicted through the use of CFD modeling. Figure 3.13 indicates a good agreement between predicted and measured results in the burnout zone, which increase the level of confidence in our CFD modeling work. For the air-firing case in panel (a), the temperature gap between dried coal and wet coal particles reaches around 150°C in the burner vicinity, which should be attributed to the heat loss for the evaporation of coal moisture in the wet coal case. Interestingly, with the substitution of oxy-30% for air, the temperature gap in burner zone is narrowed to ~ 50°C. This can be explained by an enhanced radiative heat transfer for the wet coal near coal burner, as shown in Fig3.12 (b). This is another

distinct feature for the oxy-fuel combustion of wet brown coal that has yet to be revealed in the literature.

3.7 Experimental results – Emission of pollutants (trace metals, SO2/SO3, Hg)

The flue gas emitted from oxy-firing of three brown coals is rather clean, due to the low concentrations of the ash-forming elements within the original coal. Victorian brown coal is internationally renowned for it slow sulphur (0.5-1.0 wt%) and low ash (~2.0 wt%) contents. For the concentrations of SO2 and NO in oxy-firing flue gas, they are higher than the air-firing case (see table 3.6), due to the smaller amount of flue gas generated.

Table 3.6 Concentrations of SO_2 and NO in oxy-firing flue gas

Coal (moisture)	Flue gas temperature, °C	O_2, vol%	NO, ppm	SO_2, vol%	H_2S, Vol%
Yallourn (23.1%)	144.0	4.3	327	332	26
Hazewood (24.6%)	120.0	5.0	300~453	-	-
Loy Yang power station (as minded)	~150	3.9	218.58	-	-

The other pollutants including SO_3 (table 3.7) and trace metals except Hg (see table 3.8) in the oxy-firing flue gas are also extremely low. For SO3, its measured values are lower than a concentration of 2-16 ppm reported for the Australian black coal in the Callide project. This can be due to the abundance of alkali and alkaline earth metals that are good sorbent capturing SO3 in the original brown coal. The dust concentrations are very low, most of which are captured by the bag filter. Moreover, most of the trace metals bear a concentration in the ppb level that is maximum 300 ppb. This indicates a negligible accumulation of these impurities upon flue gas

recirculation in the system. Regarding mercury, its measured total concentration in flue gas reached 3.5036 μg/Nm3 at 6% O2 in flue gas, which corresponding to the vaporisation of 99.65% Hg in the original coal, and an emission factor of 3.52E-5 kg Hg/tonnes as-received raw coal (see table 3.9). Such an emission factor is even comparable to the NPI reported value for black coal, which is also higher than NPI reported value for brown coal in Jan 2012. Measurement of the three raw coal samples independently by Idemistsu Kosan (Japan) and Shanghai University of Electric Power (China), as tabulated in table 3.8, indicates the high Hg contents in the air-dried three brown coal samples that were transported to China. These values are even higher than that reported for the Australian brown coals. These measurements are contradictory to the commonly accepted "fact' that Hg is negligible for Victorian brown coal. The coal sample heterogeneity could be one of the major reasons. If yes, an appropriate sampling and measurement for the three brown coals is necessary in the future, to further confirm this hypothesis and the measurements achieved in this study.

Table 3.7 Concentrations of SO_3, HCl and mercury in flue gas derived from oxy-firing

	SO_3 (ppm)	Cl (ppm)	dust (mg/l)	Hg^0 ($\mu g/Nm^3$)	Hg^{2+} ($\mu g/Nm^3$)	Hg^T ($\mu g/Nm^3$)
Hazelwood	0.053	0.027	0.4	2.7525 ($6\%O_2$) 3.3163 ($3\%O_2$)	0.7511 ($6\%O_2$) 0.9049 ($3\%O_2$)	3.5036 ($6\%O_2$) 4.2211 ($3\%O_2$)
Yallourn			0.5			
Chinese lignite	0.082					

The measured total Hg concentration in flue gas is also higher than that reported for the Australian black coal in the IHI oxy-firing pilot-scale facility, as shown in table 3.9. Moreover, back to table 3.7, one can deduce that the elemental mercury (Hg0) accounts for 78.56% of the total Hg in flue gas. Such a proportion is much higher than the black coal mercury emission in which most of the vaporised Hg is in the form of oxidised Hg2+, as demonstrated for Australian black coals tested in the IHI pilot-scale oxy-firing facility. Such an observation is very interesting, which, if correct, is a strong cause for a detailed investigation on the mode of occurrence of Hg in brown coal and its transformation routes during air-firing and oxy-firing modes. Moreover, how to effectively oxidise Hg0 into Hg2+ is critical. Otherwise, the water-insoluble

Hg0 will cause severe corrosion problems during the CO2 compression. It is also highly toxic and easily released into the air, due to its extremely low solubility in the aqueous system.

Table 3.8 Concentrations of trace metals in flue gas versus raw coal, ppb

	Hazelwood		Yalloum	
	raw coal	Flue gas	raw coal	Flue gas
	ppm	ppb	ppm	ppb
Al	4225±90	8.44	849.1±116	130
As	0.3±0.4	0.75	0.1±0.1	10
Ba	17±12	7.28	198.3±18.6	20
Be		-0.15		0
Ca	935±69	613.27	1795±142.5	1390
Co	8.9±1.1	0.58	5.9±1.8	0
Cr	3.9±0.6	0.93	2.6±0.3	0
Cu	1.3±0.3	118.52	2.1±0.3	30
Fe	1113.7±74	168.38	8644±795.6	210
K	52.2±8.6	79.63	98.5±10.2	260
Mg	740±47	19.37	2391±207	80
Mn	15.4±1.1	1.57	103±10	10
Na	570±36	299.56	941.6±92	740
Ni	3.1±0.2	1.96	2.5±0.2	0
Pb	2.4±0.4	0.83	2.9±0.4	10
Sr	13.6±0.9	0.86	28.5±2.8	0
V		-0.38		0
Zn		43.72		80

Table 3.9 Mercury concentrations in three Victorian brown coals (air-dried), ppb

	Mercury content (ppb)	Cl (ppb)
Moura	16	
Newlands	72	
Blackwater	25	
Ulan U/G	31	
Ulan O/C	50	
Wallarah	78	
Hunter Valley	50	
Blair Athol	32	
Yallourn	84	800
Hazelwood	110 (85*)	710
Loy Yang	85	480

*: measured by Shanghai University of Electric Power. The rest

Numbers for three coals were reported by Idemitsu Kosan Co Ltd

3.8 Conclusions

The scale-up experiments have been conducted to clarify the oxy-fuel combustion characteristics of Victorian brown coal, dried and wet, in a 3MWth pilot-scale facility. This is the first successful trial of brown coal oxy-fuel combustion around the word. The major conclusions achieved are drawn as follows.

(1) Oxy-fuel combustion of Victorian brown coal has been successfully achieved, irrespective of dried or wet coal. The mode shift process is smooth, safety and reliable. The CO2 purity reached 80% (dry) with a varying recycle ratio from 48% to 64% for flue gas.

(2) For dried brown coal, the optimum oxygen content to match flue gas temperature profile in its air case was found to be 27%, same as bituminous coals tested in the literature. For wet coal with 40 wt% moisture, the presence of 30% O_2 in flue gas is essential to match air for an identical flue gas temperature profile, due to the extra heat loss caused by coal drying. However, under the optimised oxygen content, the radiative heat transfer is stronger than the air case, and CO emission due to gasification reaction is also more intense, for both dried and wet coal.

(3) The enhanced radiative heat transfer in oxy-fuel mode facilitates the drying of wet coal, which narrows down the discrepancy of its flue gas temperature with the dried coal case. For a timely and stable ignition of wet coal, the presence of 30% O_2 above in primary stream is essential.

(4) The experiments provide the oxy-fuel performance and emission data in an industry relevant facility, which provide a basis for design and scale-up of this low emission coal technology to commercial scale in the foreseeable carbon-constrained future.

4. Lab-scale oxy-fuel foundational studies in flat flame burner reactor

4.1 Experimental setup

The abundant moisture is a specific issue for Victorian brown coal, yielding ~20% and ~55% of steam by volume in bulk flue gas for air-firing and oxy-firing of as-mined wet coal, respectively. The influence of coal moisture is complex in an oxy-fuel case, as it will negatively affect coal ignition and flame temperature through increasing radiative heat transfer by the large specific heat capacity of steam and CO_2. The adsorbed heat is subsequently released in convective zone to increase the heat flux there. A careful adjustment of the recycle ratio of flue gas and oxygen proportion in furnace is thus essential to 'compensate' the complex influence of steam.

To clarify the combustion of dried and wet coal in air versus oxy-fuel mode, the lab-scale flat flame burner reactor (FFBR) was employed. The FFBR used has a schematic as shown in figure 4.1. Note that, the FFBR used is coupled with a high-speed camera and a two-color pyrometer for particle imaging and temperature measurement, respectively.

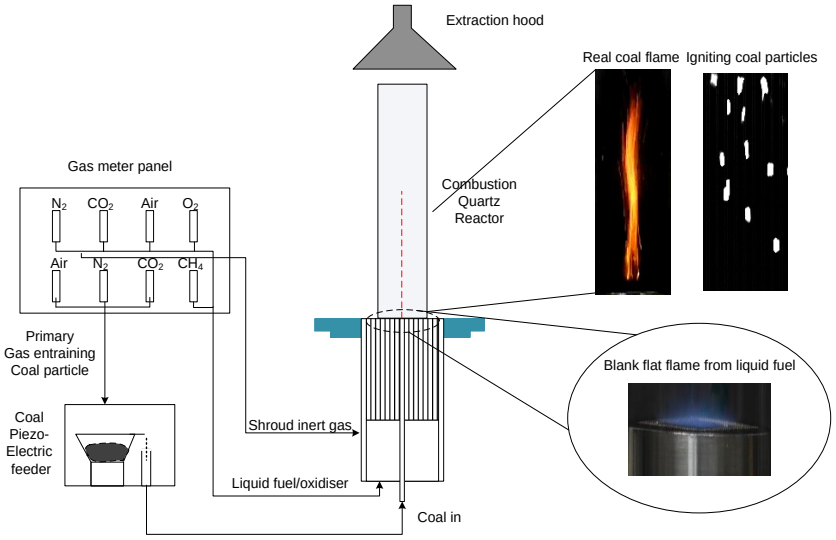

Figure 4.1 Schematic of lab-scale FFBR used for coal combustion diagnosis

4.2 Optical diagnosis on ignition and combustion of Victorian brown coal

Compared to the air-firing case with the abundant bi-atomic components (e.g. N2 and O2) in flue gas, the tri-atomic gases including CO_2 and H_2O possess a very high concentration in the oxy-firing flue gas. In comparison to bi-atomic N2 and O2, CO2 and H2O possess a high specific heat capacity (1.7 times of N_2) that potentially slow down flame propagation speed as well as reduce flame temperature. Moreover, these tri-atomic gases are heavier than air at the same volume, thus exhibiting a low velocity at the same mass flow rate in the coal burner. All these unique features for the tri-atomic gases can affect coal flame stability and flue gas radiation significantly.

The representative images for the combustion of all coal samples are visualised in figure 4.2. For each coal sample, the five photos were taken from their combustion in air and oxy-fuel modes with the oxygen fraction varying from 16% to 31% in sequence. In the case of the combustion of dried coal in air, the flame was observed to attach closely to the burner base, suggesting a quick ignition and stable oxidation of the dried brown coal in air. Its volatiles should be released quickly, forming a yellowish segment near the burner base. Above the yellowish segment is a bright part with strong luminosity, referring to the homogeneous oxidation of the abundant volatiles releasing the strongest radiative heat. The tail of the flame, possessing a rather reddish and less luminous intensity, should refer to the stage for the heterogeneous oxidation of char particles. Clearly, the boundary between the two oxidation stages is rather vague and overlapped here, suggestive of a high reactivity of the dried Victorian brown coal, same as that observed previously. By changing the gas composition to oxy-fuel mode with 16% O2, the flame length was enlarged, and its intensity was reduced remarkably. The enhanced flame length is attributed to the longer yellow segment near the burner base, substantiating the delayed ignition of volatiles in the CO_2-rich environment due to the large specific heat capacity of CO2, as has been well confirmed elsewhere. The bright part denoting volatile oxidation nearly disappeared, which should be attributed to the lower bulk oxygen fraction and the slower diffusivity of oxygen in CO_2. Increasing the oxygen fraction in CO2 gradually shortened flame length and increased its luminosity, as expected. For the highest oxygen content 31% tested here, its flame clearly bears a similar and even stronger brightness/intensity than the air case. Even so, one can still see that, a rather longer yellowish segment was present in the flame pattern formed in 31% O2/CO2. This should be caused by the absence of oxygen in the primary gas entraining coal particle in the oxy-fuel mode. Instead, the 21% O2 is present in both primary and second streams in air mode, which thus favours coal ignition near the burner base.

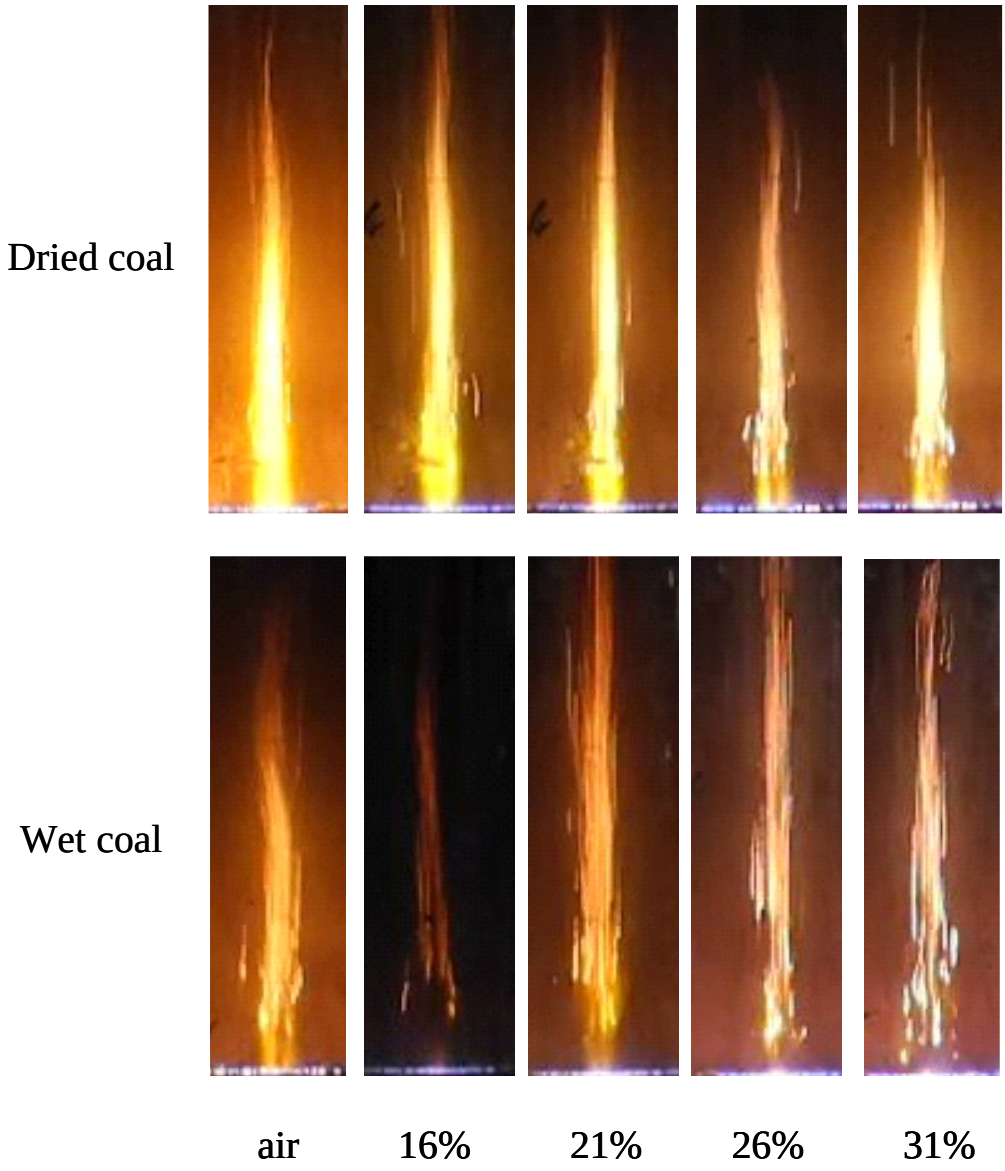

Figure 4.2 Representative flame patterns for dried and wet coal combustion in air and oxy-fuel mode in lab-based flat flame burner reactor

As can be seen, to match coal volatile flame in air, the oxygen fraction in O_2/CO_2 needs to be increase to 26% and above. For the fully dried brown coal, the substitution of O_2/CO_2 with O_2 fraction being 16% caused little change on the flame intensity, although the flame length was increased due to coal ignition delay. The similar flame is observed in 26% O_2/CO_2 when compared to air-firing.

In contrast, for the wet coal with 31 wt% moisture, the use of 16% O_2 in CO_2 in place of air caused a complete extinction of coal ignition and its volatile flame. Even for the case of 21% O2 in CO2, the flame was lifted up obviously, which was also unstable and weak in intensity. Using a higher oxygen fraction such as 31% is essential. Observation of coal flame in the 3MWth pilot-scale also conformed to the necessity of minimum 30% oxygen in boiler to ensure a stable and complete combustion of the semi-dry or wet brown coal, shown in Figure 3.11, which is consistent with the results in flat flame burner reactor.

4.3 One-dimensional mathematical description of brown-coal drying and combustion

For the commercial computational fluid dynamic (CFD) software like ANSYS Fluent, it does not have the capability to accurately predict coal drying and the influence of drying on the combustion process. The drying model namely 'wet coal combustion' is embedded in the program. However, it is only useful for coal-water-slurry in which the coal is high-rank bituminous coal. Coal drying is assumed to occur initially upon particle heating, having no overlapping with the subsequent coal devolatilisation process. This is the case for bituminous coal, because its devolatilisation usually occurs from 400^{o}C onwards, whereas drying occurs at 100^{o}C. For brown coal drying, the initial temperature plateau referring to its moisture evaporation is usually around 200oC. Moreover, compared to the majority of moisture being surface water in black coal, the moisture in brown coal is largely associated chemically as mono-layer or multi-layer within coal capillary and/or pores. They are also bound with oxygen-containing functional groups, the decomposition of which requires a higher temperature than 100oC, the boiling point for bulk water. Due to this reason, coal drying overlaps greatly with devolatilisation and even particle ignition for Victorian brown coal. Thus, the conventional 'wet coal' code in CFD can not be used, and the new code for brown coal drying and wet brown coal combustion has to be developed.

(1) Gas Transport Properties

The complete computation of one-dimensional coal combustion model requires the evaluation of gas-phase properties, including density, heat capacity, thermal conductivity, viscosity as well as diffusivity. The properties of the gaseous species were taken from the literature. The density and heat capacity of gas mixtures are calculated by:

$$\rho_m = \sum_i W_i \rho_i \quad \ldots(4\text{-}1)$$

$$C_{p_m} = \sum_i X_i C_{p_i} \quad \ldots(4\text{-}2)$$

The diffusivity of gaseous species in the mixtures was calculated using statistical theory. Thermal conductivity of gas mixture was estimated using Wassiljewa's equation with Mason-Saxena formulation. The gas mixture viscosity was determined from Wilke's mixture rule with Chapman-Enskog approximation. The summary of these equations is given as follows:

$$\mu_m = \sum_i \frac{\mu_i}{\sum_k (1 + \varphi_{ik}(\frac{X_k}{X_i}))} \quad \ldots(4\text{-}3)$$

$$k_m = \sum_i \frac{k_i}{\sum_k (1 + 0.85\varphi_{ik}(\frac{X_k}{X_i}))} \quad \ldots(4\text{-}4)$$

$$D_{im} = \frac{(1 - X_i)}{\sum_{k \neq i} (\frac{X_k}{D_{ik}})} \quad \ldots(4\text{-}5)$$

$$\varphi_{ik} = (\frac{1}{8})^{\frac{1}{2}} [1 + \frac{M_i}{M_k}]^{-\frac{1}{2}} [1 + (\frac{\mu_i}{\mu_k})^{\frac{1}{2}} (\frac{M_k}{M_i})^{\frac{1}{4}}]^2 \quad \ldots(4\text{-}6)$$

The variable φ_{ik} is defined as the interaction parameter between two gaseous species, i and k. The calculated values, μm and km describe the viscosity and thermal conductivity of gas mixtures, respectively, and Dim represents the diffusivity of species gas i in the mixture. For Mason-Saxena formulation, the interaction parameter for thermal conductivity calculation is slightly modified as follow:

$$\varphi_{ik} = (\frac{1}{8})^{\frac{1}{2}} [1 + \frac{M_i}{M_k}]^{-\frac{1}{2}} [1 + (\frac{\mu_i}{\mu_k})^{\frac{1}{2}} (\frac{M_i}{M_k})^{\frac{1}{4}}]^2 \quad \ldots(4\text{-}7)$$

(2) Single Coal Particle Drying Model

The brown coal moisture evaporation behaviour is modelled as a receding wet-core, dry-shell model. The detailed equation describing the model has been reported elsewhere.As the coal particle size is in the range of pulverized coal range, the drying rate could be assumed constant and equals to the initial drying rate, corresponding to drying of non-shrinking water droplet.

$$MC = MC_0 (1 - nt) \quad \ldots(4\text{-}8)$$

Where MC and MC_0 are current moisture content in the coal and initial moisture content, respectively, t is the drying time required to achieve current moisture content and n is an empirical constant obtained by equating the initial heat transfer rate with the product of the initial evaporation rate and latent heat of vaporization. The expression for n is described as:

$$n = \frac{6h(T_g - T_a)}{\frac{H_L ?? _{wc}[MC_0]\, d}{(1+ MC_0)}} \quad \ldots(4\text{-}9)$$

Where h = convective heat transfer coefficient, T_g= gas temperature, T_a = coal wet bulb temperature, HL is the latent heat of vaporization, ρwc is the density of wet coal and d is the particle diameter. The wet-bulb temperature of hot gas, Ta is a function of ambient gas temperature and is set at 360 K for the hot gas temperature of 1200 K in this study.

(3) Devolatilisation and Volatile Combustion Model

The coal devolatilisation is modelled by a single kinetic rate model that assumes the rate of devolatilisation as first order, and expressed as:

$$q_{devol} = A_{devol} \exp\left(-\frac{E_{devol}}{RT}\right)[m_p - (1 - f_{vol,o})m_{p,o}] \quad \ldots (4\text{-}10)$$

The kinetic data for Arrhenius form of the equation was determined from the thermo-gravimetric analyser. It was assumed that the volatiles, once being released, burn instantly on the particle surface, thus providing heat feedback to coal particle to ensure the continuation of the volatiles combustion within the particle vicinity. The hypothetic model for volatile combustion is expressed as:

$CwHxNyOz + O_2 \rightarrow CO_2 + H_2O$ …Reaction (a1)

While the coefficient w, x, y and z are obtained from the ultimate analysis of dried coal and its corresponding char generated from pyrolysis in drop-tube furnace.

(4) Char Combustion Model

All the probable surface reactions for char particles are included in this study, as listed below.

$C + O_2$	$\rightarrow CO_2$	….. Reaction (1)
$C + ½\ O_2$	$\rightarrow CO$	….. Reaction (II)
$C + CO_2$	$\rightarrow 2CO$	….. Reaction (III)
$C + H_2O$	$\rightarrow CO + H_2$	….. Reaction (IV)

The rate of char burning is described using the conventional single-film model, assuming that the above-listed multiple reactions occur in a frozen boundary layer at the particle surface with no gas-phase reactions. The burning behaviour is assumed to be kinetic-diffusion limited. This model has been suggested to work well for pulverized coal combustion for the particle size less than 100 μm. For the combustion of particles larger than 100 μm, Mitchell suggested that conversion of CO to CO2 in the boundary layer could not be neglected that will significantly change the particle temperature and burning rate. The char combustion rate can be written as:

$$q = \frac{P_{O_2}}{\frac{1}{k_{c,o}} + \frac{1}{k_{d,o}}} + \frac{P_{CO_2}}{\frac{1}{k_{c,c}} + \frac{1}{k_{d,c}}} + \frac{P_{H_2O}}{\frac{1}{k_{c,s}} + \frac{1}{k_{d,s}}} \quad \ldots(4\text{-}11)$$

$$k_c = A \exp\_(-\frac{E}{RT}) \quad \ldots (4\text{-}12)$$

$$k_d = C_2 \frac{(\frac{T_p + T_\infty}{2})^{0.75}}{d_p} \quad \ldots(4\text{-}13)$$

The rate of changes in the particle diameter is formulated as follows:

$$\frac{\partial d}{\partial t} = -\frac{2q}{\rho} \quad \ldots(4\text{-}14)$$

With kc and kd are chemical reaction rate coefficient and diffusion reaction rate coefficient, respectively. The chemical reaction rate coefficient is expressed in an Arrhenius form with A is the pre-exponential factor and E as the activation energy for reaction I –IV. The kinetic parameters for reaction I-III are obtained from the thermo-gravimetric analyser experiments conducted at different heating rate (10-50 K/min) for devolatilised char at both air and CO_2 atmosphere, which have proven accurate in our previous work.

For the char-steam gasification reaction IV, it is considered to include two reactions for wet coal combustion, one being induced by the external steam in the bulk gas, and another one occurring within char matrix that is triggered by the internal moisture. The latter reaction was accounted for the hypothesis that the inherent moisture might be strongly held and remained permanently on char surface. The partial pressure of the inherent steam was determined based on the amount of moisture remaining after the drying and ignition steps, it was assumed to be saturated and the saturation water vapour pressure was calculated by the Clausius-Clapeyron equation.

The modelling of single coal particle combustion here was based single-film model. The code employed in this study only focused on one-dimensional particle-phase calculation, neglecting any gas-phase transport phenomena. The coal combustion is divided into three steps in sequence, drying, volatile release/ignition/oxidation and char combustion, and no overlapping between the latter two steps.

(5) Particle Temperature Profile

The coal particle temperature profile in the furnace was calculated by using an unsteady-state energy balance equation shown below, considering both the heat transfer by radiation and convection from the surroundings.

$$m_p c_p \frac{dT_p}{dt} = hA_p\left(T_\infty - T_p\right) + \varepsilon\sigma A_p\left(T_w{}^4 - T_p{}^4\right) + H_{gen} \quad \ldots(4\text{-}15)$$

Where mp is the particle mass (kg), cp is the heat capacity of coal particle (kJ/kgK), h is the convective heat transfer coefficient calculated assuming Nusselt number of 2. Tw is the wall temperature (773 K), Tg is the gas temperature measured with thermocouple, ε is the particle emissivity (0.8) and σ is the Stefan Boltzmann constant.

The term Hgen is the total heat generated/released from the reactions and can be expressed as follows:

$$H_{gen} = -q_d H_d + \varphi q_c H_{CO} + (1-\varphi) q_c H_{CO2} - q_{g,co2} H_{CO2,g} - q_{g,h2o} H_{h2o,g} \quad \ldots(4\text{-}16)$$

With Hgen is the total heat generated from the contributing reaction I-IV. The heat generated from the char oxidation reaction is calculated from the amount of the CO/CO2 produced. The ratio of CO2/CO production at the particle surface is calculated based on the coefficient suggested by Arthur et al. At low temperature, little amount of CO2 is produced at the particle surface, while at higher temperature CO is the sole oxidation product and will react with O2 to form CO2 in the gas phase boundary layer.

(6) Solution Techniques

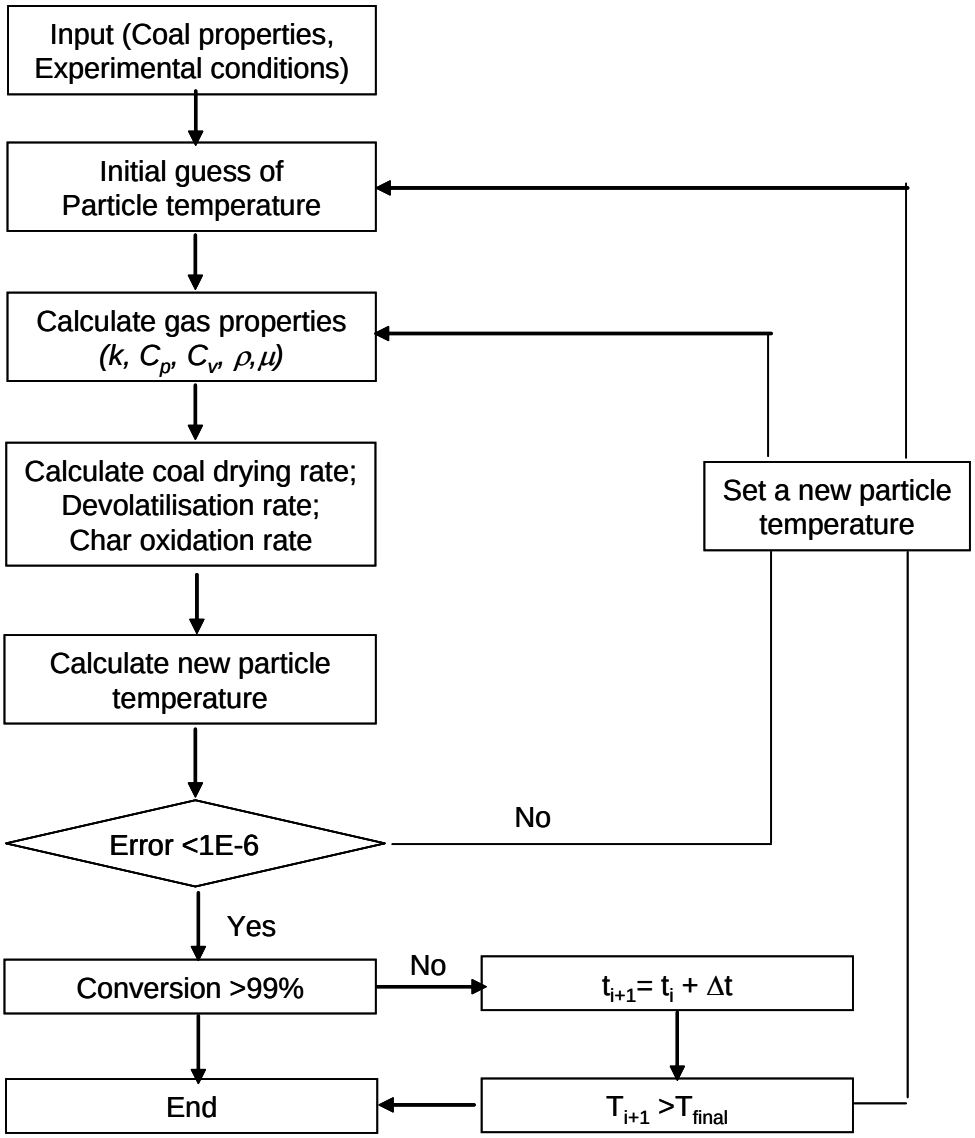

Figure 4.3 Pseudo – steady state modeling program approach.

The series of differential equations to describe the transient change in particle temperature was written and solved numerically using MATLAB, taking into account the ignition delay caused by the change in the gas composition. The particle temperature and the burning rate were calculated at any instantaneous time using Euler's method with increasing time step as shown in the equation below. The time step chosen in this study was determined based on the trial and error method to ensure that the solution stabilizes. A pseudo-code algorithm has been developed to solve the particle temperature history and is shown in Figure 4.3.

$$y(t + \Delta t) = y(t) + dt \times \frac{\partial y}{\partial t} \quad \ldots(4\text{-}17)$$

The effect of inherent moisture on coal gasification is evaluated on the following method. Firstly, the coal drying model is used to evaluate and compare the ignition time from the experiments. The amount of inherent moisture in the coal is adjusted in the model to match that of the experimental data for air-dried coal. For wet coal cases, the delay in the ignition time between air-dried coal and wet coal is caused by the additional time to evaporate the surface moisture. The remaining inherent moisture calculated is assumed to contribute to the char-steam gasification reaction at the later stages.

4.4 Experimental result - Effect of Inherent Moisture on Coal Drying and Ignition

To Figure 4.2, the addition of extra moisture into coal matrix for the combustion of semi-dried coal changed the combustion flame pattern significantly. For the semi-dried coal in air, a yellowish segment appeared near the burner base, and the bright flame was lifted up accordingly. This is apparently attributed to the evaporation of the extra moisture, fully or partially, prior to the devolatilisation and ignition. The substitution of air by O2/CO2 enlarged the flame length, particularly the initial yellow segment for semi-dried coal, suggesting the longer ignition delay. More interestingly, the flame intensity for the oxidation of volatiles and char was decreased dramatically. These phenomena were more obvious for the wet coal with 30 wt% moisture. A stable flame in air was still observed to attach to the burner baser closely, its intensity was however reduced further significantly compared to dried and semi-dried coal samples. By the substitution of O2/CO2 for air, the wet coal particle ignition was even distinguished in 16% O2. Its flame was detached far from the burner base, substantiating the significant delay by the evaporation of added moisture prior to particle ignition. Upon the increment of oxygen fraction in CO2, the flame was gradually brought closer to the burner base. Even so, the flame detachment was still visible in 31% O2. The flame intensity was weaker than the dried coal, and even its pattern observed differed distinctively from both dried and semi-dried coals.

Following the classic hypothesis on coal drying that is a separate stage to be accomplished completely prior to devolatilisation and ignition, the flame formed for wet coal should be identical with the dried coal in terms of flame intensity and shape, except an initial delay to accommodate a short period for the evaporation of coal moisture. Moreover, the steam created by the evaporation of coal moisture is swept rapidly into bulk gas, its interference to the subsequent coal combustion should be negligible, since its amount (maximum 0.03 g/min here) is trivial, compared to the presence of 18 vol% steam in the 15 L/min bulk gas produced from the burning of liquid fuel. This is clearly not the case observed here. By the statistical analysis of hundreds of flames same as that observed in figure 4.2, figure 4.4 provides the quantitative time for the duration of particle ignition, volatile combustion and char oxidation as the function of bulk gas composition and moisture content in coal. Clearly, the ignition time in air was delayed by the magnitude of 2-4 ms from dried coal to semi-dried and wet coal. The use of O_2/CO_2 mixtures, irrespective of oxygen fraction, clearly diminished the discrepancy of the ignition of three coal samples, indicative of the overweighing effect of CO_2 over external moisture on coal ignition in the oxy-fuel mode. The duration of volatile combustion is opposite against coal ignition, that is, insignificant difference between the three coals in the air case, whilst remarkable delay on the oxidation of semi-dried and wet coal volatiles in the oxy-fuel case. The similar phenomenon was also observed for the char oxidation stage. Obviously, the steam created from the evaporation of coal moisture must partially or even fully reside in the vicinity of burning coal particle surface, which in turn could exert the influence on coal combustion through three probable aspects including, altering the volatile composition (by chemical reactions) and concentration (by dilution), and hence, the flammability and ignition potential of volatiles on particle surface; moving the flame front outwards away from particle surface and hence providing less heat feedback for the continuation of particle combustion; and increasing the resistance against oxygen diffusion to char surface. The three aspects are discussed separately below.

As shown in figure 4.2 the length of the yellowish segment in a flame refers to the initial flame front to the burner base, which is made up of the duration for moisture evaporation and the time for volatile release. The high-speed camera observation on this are was further conducted to detect the distance of the igniting bright spots to the burner for the calculation of coal ignition time. In addition, the modelling prediction for the sum of coal drying and devolatilisation were carried out and compared with experimental data to deduce the percentage of the moisture released prior to particle ignition.

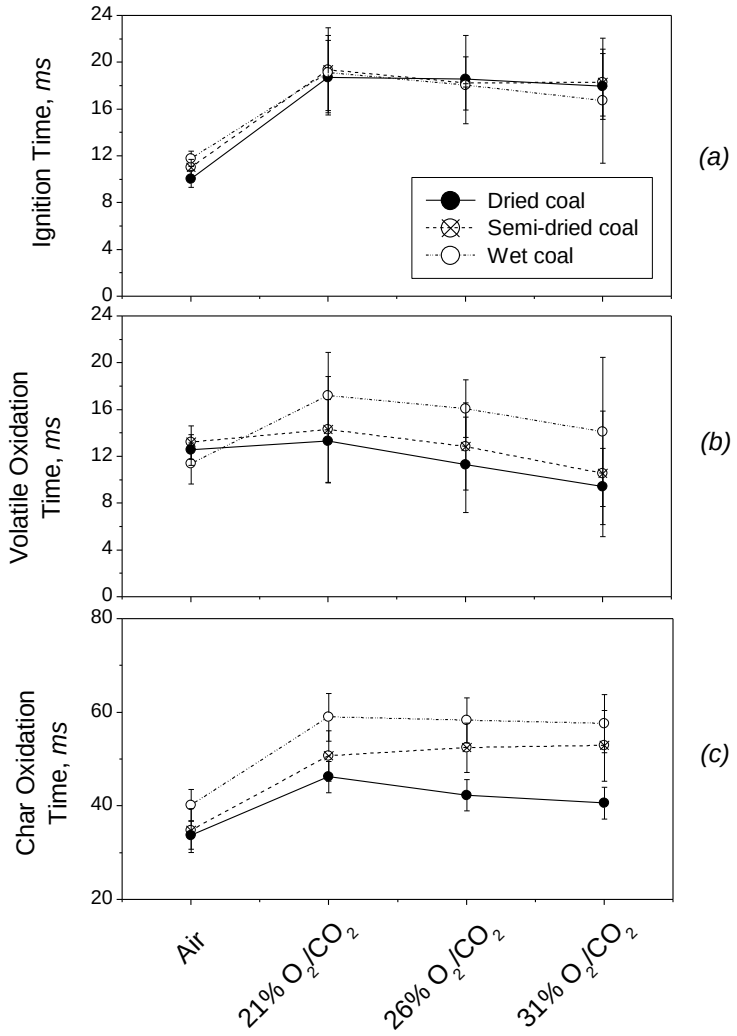

Figure. 4.4 Influence of coal moisture on particle ignition time, volatile oxidation duration and char oxidation time

Figure 4.5 plots the predicted ignition time versus the extent of coal moisture evaporated for air-firing mode. Irrespective of the moisture content in coal, the ignition time increases proportionally with the coal moisture evaporation extent increases. This is due to the drying equation used which describes a linear relationship between the moisture evaporation rate as a function of the drying time required. By the match between experimental data and the prediction curve, one can quantify the extents of 65%, 58% and 45% for the moisture to be evaporated prior to the ignition of dried coal, semi-dried and wet samples, respectively. These results clearly substantiate the above hypothesis for an incomplete coal drying prior to particle ignition. In other words, the coal drying step and devolatilisation overlap considerably for the wet brown coal sample studied here, which also agree with the observations in the combustion of wet brow coal in fluidised bed reactor. In addition, the descending

trend for the moisture evaporation extent from dried to wet coal indicates the enveloping of most of the moisture in the igniting wet coal particle. This can be explained by a slow motion of the moisture evaporation front towards the core of wet coal particle, due to less of heat feedback generated from its igniting surface. This is certainly not the case for dried coal.

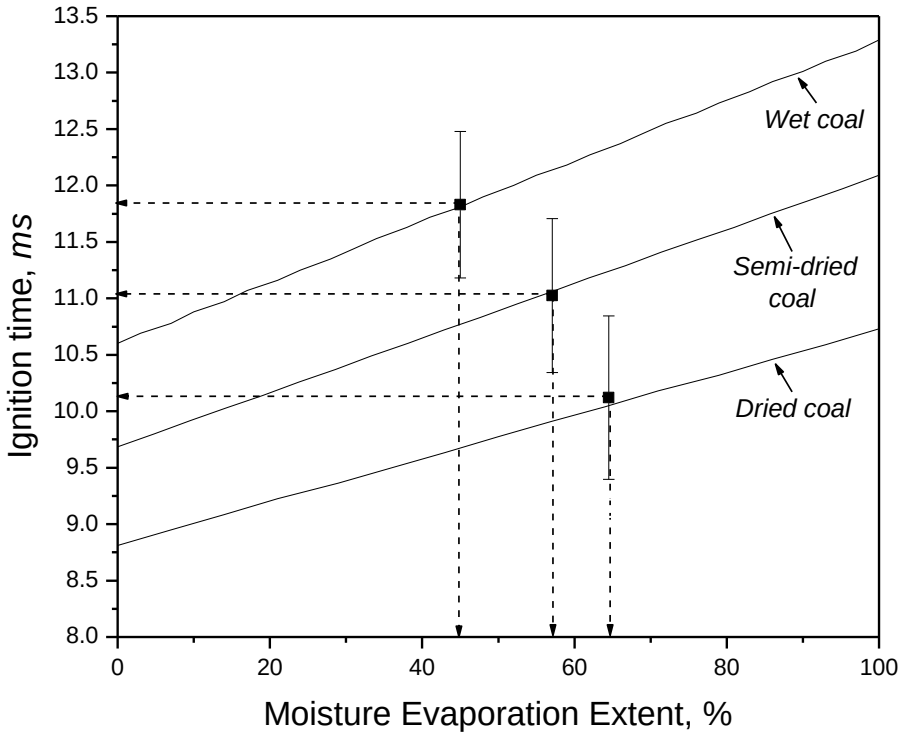

Figure 4.5 Correlation between moisture evaporation extent and particle ignition time

The substitution of CO_2 for N_2 to dilute oxygen affects little on coal particle drying time, because the molar thermal conductivity of these two gases are identical. In equation (4-15), the thermal conductivity is the only property of a bulk gas affecting coal moisture evaporation. Indeed, figure 4.5 even indicates that the use of CO_2 is able to shorten the drying time by 1.5 ms for the complete evaporation of 30% moisture out of coal matrix. In this sense, the ignition delay upon shifting air to O2/CO2 in figure 4.6(a) is mainly caused by the large specific heat capacity of CO_2 and any other factors that are not relevant to coal drying time.

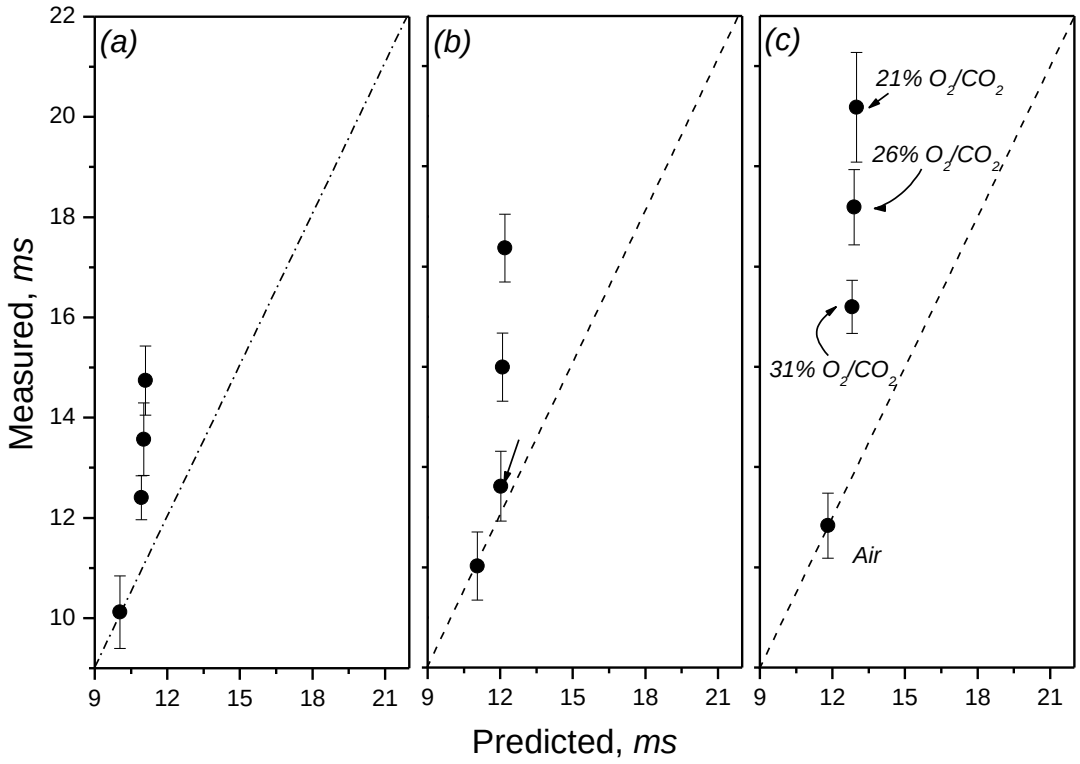

Figure 4.6 predicted particle ignition time versus measured values, Panels (a) – (c) are for dried coal, semi-dried and wet coal, respectively.

Figure 4.6 plotted the measured ignition times for the oxy-fuel combustion of three coal samples, versus the predicted values for the sum of drying time plus devolatilisation duration. The drying time in O2/CO2 was fixed as the same as in air in the model. The dashed curve in each panel refers to the parity line for the match between measured and the respective prediction value. The air-firing results were also included as reference. Compared to the air-firing points falling on parity lines, the oxy-fuel results deviate remarkably from the parity lines. For a given O2/CO2 ratio, the prediction on wet coal is underestimated the most, whereas increasing the oxygen fraction in CO2 narrowed down the discrepancy between prediction and the measurement. The ignition of dried and semi-dried coal in 31% O2/CO2 was predicted satisfactorily. In contrast, the gap is still noticeable for the wet coal ignition in 31% O2. Apparently, apart from the large specific heat capacity of CO2 that has been incorporated into the model, there are extra factors negating the wet coal ignition under the oxy-fuel mode. As mentioned above, these factors may include the altered volatile composition and concentration, and/or the enhanced resistance against the diffusion of oxygen through particle boundary layer, upon the co-existence of coal moisture and CO2 on particle surface.

4.5 Conclusions

This chapter has provided the observations on the combustion behaviour of brown coal that contains a high amount of moisture under oxy-fuel versus air-firing cases. The experiments in a flat flame burner reactor have proven that indeed inherent moisture has a significant role in both volatile combustion and char combustion regime. Then main conclusions include:

(1) From both lab-scale experiments in DTF, it is clear that the use of 27vol% O2 in recalculated flue gas is essential to match air combustion to achieve the identical particle temperature profile regarding air-dried brown coals. However, the use of 30% O2 in CO2 is essential for wet Victorian brown coals to match the identical and stable air-firing flame.

(2) A one-dimensional numerical modeling method was developed to describe the influence of residual moisture in brown coal. During the initial drying and heating up stages prior to ignition, the drying mechanism is controlled by the temperature of the surrounding gases. The coal inherent moisture is determined based on the amount of coal remains prior to the ignition stage.

(3) During the devolatilisation and volatile combustion stages, wet coal has slightly larger volatile cloud compared to the dried coal due to more volatiles being released as a result on increasing inherent moisture. At 31%O2 in oxy-fuel, the size of volatile clouds is similar for both air-dried and wet coal as volatiles are consumed in a much faster rate.

(4) Inherent moisture char gasification occurs as the secondary reactions at a much slower rate compared to ambiance CO_2 and H_2O gasification. At high temperature, this reaction could occur in parallel with CO_2 and atmospheric steam gasification.

5. CFD modeling research on oxy-fuel combustion of Victorian brown coal

The commercial CFD software, Ansys FLUENT 13.0, has been employed to predict brown coal combustion. The sub-models chosen and the other methods incorporated into Fluent are summarized as follows. The modeling was first used to predict the air-airing and oxy-firing characteristics of Victorian brown coal measured in a drop tube Furnace (DTF), which is used to verify the modeling methods and the accuracy of developed sub-models in codes. After then, the verified method will also be applied to predict the oxy-fuel combustion characteristics in the 3MW facility.

5.1 CFD modeling approach

Under the oxy-firing mode, the coal combustion route and reactivity are supposed to alter dramatically when compared with the air-firing mode. On the one hand, coal ignition will be delayed due to the larger specific heat capacity of CO_2 than N_2. On the other hand, apart from C-O_2 oxidation reaction, the C-CO_2 and C-H_2O gasification reactions could be triggered due to the abundance of CO_2 and H_2O in flue gas.

$$C + O2 = CO \qquad \Delta H < 0$$

$$C + CO2 = CO \qquad \Delta H > 0$$

$$C + H2O = CO + H2 \qquad \Delta H > 0$$

The endothermic gasification reactions above are very likely to happen for Victorian brown coal, given the fact that the abundant alkali and alkaline earth metals are catalytic in oxygen shuttling for coal gasification. If this is the case, the coal particle temperature will drop due to the self consumption of its oxidation heat by the gasification reactions on the particle surface. Accordingly, the char burnout rate by C-O2 reaction would be slowed down. However, the proceedings of two gasification reactions are in favour of char consumption by the formation of reducing gases.

The commercial CFD software, Ansys FLUENT 13.0, has been employed to predict coal combustion in DTF. The sub-models chosen and the other methods incorporated into Fluent are summarized as follows.

5.1.1 Turbulent flow model

The gas-phase time-averaged continuity equation and conservation equations of momentum, turbulent kinetics energy/dissipation, enthalpy and species fraction in 3-D coordinates are given as

$$\frac{\partial}{\partial t}(\rho\phi)+\frac{\partial}{\partial x_j}\left(\rho u_i\phi\right)=\frac{\partial}{\partial x_j}(\Gamma_\phi\frac{\partial\phi}{\partial x_j})+S_\phi+S_p \qquad (5\text{-}1)$$

Where φ denotes the generalised variables, S_ϕ and S_p refer to gas and discrete phase source term, respectively.

The k-ε model is the most popular turbulent model based on the Reynolds time-averaged Navier-Stokes (RANS) equations. Realizable k-ε Model, an improved k-ε Model, is able to rationally predict the strong swirling flow, and so applicable for the numerical simulation in a tangentially-fired furnace.

5.1.2 Particle trajectory model

Coal particle trajectory was simulated by the Discrete Phase Model (DPM). The impact of drag force and gravity force acting on particle phase was taken into account during calculation. In the prediction of Drop-tube furnace, a total of 800 coal particle trajectories were tracked at each-step DPM coupling. During combustion, coal particle size was assumed to remain constant, while its particle density varies. The particle size was assumed to obey the Rosin-rammler distribution with a spread parameter of 3.5 and 10 groups. During combustion, coal particle size is assumed to remain constant, while the particle density varies. The particle motion is described below.

$$\frac{du_{pi}}{dt}=F_D(u_i-u_{pi})+\frac{g_i}{\rho_p}(\rho_p-\rho) \qquad (5\text{-}2)$$

Where $F_D = \frac{C_D \mathrm{Re}_p}{24\tau_r}$, $\tau_r = \frac{d_p^2 \rho_p}{18\mu}$, $\mathrm{Re}_p = \frac{\rho d_p \left|\vec{u} - \vec{u}_p\right|}{\mu}$, $C_D = \frac{24}{\mathrm{Re}_p}(1 + b_1 \mathrm{Re}_p{}^{b_2}) + \frac{b_3 \mathrm{Re}_p}{b_4 + \mathrm{Re}_p}$

With regard to the influence of random turbulence on particle motion, the gas fluctuation velocity (u_i'), obeying a stochastic distribution of Gaussian PDF, is used to calculate real particle trajectories.

$$u_i' = \zeta(\overline{u_i'^2})^{1/2} = \zeta\left(\frac{2k}{3}\right)^{1/2} \qquad (5\text{-}3)$$

Where ζ is random number with Gaussian distribution.

5.1.3 Radiation model

In the power plant furnace, the fraction of radiative heat-transfer could achieve as high as approximately 95%. The Discrete Ordinates (DO) model was applied here for radiation modeling, in which gas was assumed being a gray body. The radiative transfer equation using DO model is written as

$$\nabla \cdot \left(I\left(\vec{r},\vec{s}\right)\vec{s}\right) + \left(a + \sigma_s\right) I\left(\vec{r},\vec{s}\right) = an^2 I_{b\lambda} + \frac{\sigma_s}{4\pi}\int_0^{4\pi} I\left(\vec{r},\vec{s}\right)\Phi\left(\vec{s},\vec{s}'\right)d\Omega' \qquad (5\text{-}4)$$

Considering the effect of green gases (CO_2 and H_2O), the weighted-sum-of-gray-gases model (WSGGM) is used for computation of a variable absorption coefficient, which helps improve the accuracy of radiative heat transfer in an oxy-fuel furnace. The WSGGM was originally proposed by Hottel and Sarofim, which was used to calculate the total emissivity as a weighted sum of Jth grey gases and one clear gas. The air-firing modeling results of Smith et al. were widely used, which was also employed in ANSYS-FLUENT. However, the spatial variations in the mean H2O/CO2 ratios within the flame are supposed to vary widely and even beyond the range of the WSGGM parameters. Due to this consideration, a refined WSGGM has been developed by CG Yin, which is applicable to both air-firing and oxy-firing, as well as to both gray and non-gray gases. The model extends its applicability to cover a broader range of parameters, 0.001 $\leqslant$ L $\leqslant$ 60 m, 0.001 $\leqslant$ PL $\leqslant$ 60 atm.m, 500 $\leqslant$ Tg $\leqslant$3000 K, and includes broader conditions to accommodate the variation of the molar ratio of H_2O to CO_2 in oxy-fuel flame. The new modeling results have

witnessed a significant difference from the Smith's model in particular at large beam length under oxy-enriched mode. The refined WSGGM was therefore implemented in the CFD model via the user defined function in ANSYS FLUENT, the detailed shown in Chapter 5.4.2.

The total emissivity and the effective absorption coefficient of flue gas are described as

$$\varepsilon = \sum_{i=0}^{I} a_{\varepsilon,i}(T_g)(1-e^{-k_i PL}) \qquad (5\text{-}5)$$

$$a_{\varepsilon,i}(T) = \sum_{j=1}^{J} b_{\varepsilon,i,j}\left(\frac{T_g}{1200.0}\right)^{j-1} \qquad (5\text{-}6)$$

$$\bar{k}_a = -\frac{1}{\bar{L}}\ln(1-\varepsilon) \qquad (5\text{-}7)$$

Where $b_{\varepsilon,i,j}$, k_i were given in the ten suites of the refined WSGGM database, including the cases of variable H_2O/CO_2 ratios of 0.125, 0.25, 0.5, 0.75, 1, 2 and 4 for oxy-firing mode, and the H_2O mole fractions of 0, 0.1 and 0.3 in the air-firing mode.

The total emissivity and the absorption coefficient of flue gas were determined on the basis of the characteristic length of the computational domain, a mean beam length, which is calculated as $\bar{L} = 3.6V/A$, where V is the volume of the domain and A the corresponding surface area. The domain-based length is normally recommended, since the other method (cell-based length) could bring up more grid-dependent error as the grid is refined. Regarding the lab-scale DTF, its domain length was determined by its inner diameter of 0.05 m and the height of 2 m.

5.1.4 Drying modeling of inherent moisture in brown coal

The moisture in coal is defined according to the manner in which they are measured. Broadly, the moisture in a coal can be either inherent moisture embedded chemically within a coal matrix, or free moisture remaining on coal surface. The former portion is held within the pore and capillaries of coal, requiring more energy to break the chemical ponds for the release. In contrast, the surface moisture is the portion to be released spontaneously once the coal particle temperature reaches the water

evaporation/boiling point. The coal particle temperature remains at a plateau of 373 K during the evaporation of the surface moisture. This is also the methodology for the wet combustion model in FLUENT.

Regarding Victorian brown coal, inherent moisture can be simplified to release with volatile matter in coal pyrolysis process, as is due to higher volatilization rate of brown coal. And the release rate of surface moisture follows the wet combustion model in FLUENT. Generally inherent moisture is 8~10wt% in air-dried brown coal sample, and others belongs to surface moisture then.

5.1.5 Devolitilisation modeling of coal particle

The devolatilisation process is determined by first order model. The rate of volatile matter loss from coal is expressed as

$$\frac{dV}{dt} = k_{0,v} \exp(-E_v / RT_p)(V_\infty - V) \qquad (5\text{-}8)$$

The volatile hydrocarbon fuels, assuming a single hypothetic component CxHyOz, can be oxidised to produce essentially water vapor and carbon dioxide as final products. The reaction stoichiometric calculation was deduced from coal proximate and ultimate analysis. The combustion rate of volatiles was simplified as the oxidation rate of methane.

5.1.6 Single-film model with multiple surface reactions

The three heterogeneous reactions, as listed below, were assumed to occur at particle external surface with first-order global Arrhenius kinetics. The overall carbon consumption rate equals the sum of the rates from each individual surface reaction.

$C(s) + 0.5O2 \rightarrow CO$ (5-9)

$C(s) + CO2 \rightarrow 2CO$ (5-10)

$C(s) + H2O \rightarrow CO+H2$ (5-11)

$$q=\sum_{j=1}^{3} q_j = \frac{P_{g,O_2}}{\frac{1}{K_{s,1}}+\frac{1}{K_{d,1}}} + \frac{P_{g,CO_2}}{\frac{1}{K_{s,2}}+\frac{1}{K_{d,2}}} + \frac{P_{g,H_2O}}{\frac{1}{K_{s,3}}+\frac{1}{K_{d,3}}} \quad (5\text{-}12)$$

Where Kinetic and mass diffusion coefficients for each reaction above were decided by

$$K_{s,j} = k_{0,j} \exp\left(-\frac{E_j}{RT_p}\right) \quad (5\text{-}13)$$

$$K_{d,1} = \frac{2D_{m,O_2} M_C}{r_p R T_m} \quad (5\text{-}14)$$

$$K_{d,2} = \frac{D_{m,CO_2} M_C}{r_p R T_m} \quad (5\text{-}15)$$

$$K_{s,3} = \frac{D_{m,H_2O} M_C}{r_p R T_m} \quad (5\text{-}16)$$

$$K_{d,i} = C_{diff} \frac{\left[(T_p + T_g)/2\right]^{0.75}}{d_p} \quad (5\text{-}17)$$

Note that, the gas-phase diffusion coefficients ($D_{O_2}, D_{CO_2}, D_{H_2O}$) are different in the diluent CO_2 and N_2. Once the diffusion coefficients are determined, the Cdiff is calculated by equation (5-17), as tabulated in Table 8 below.

Table 5.1. Global mechanisms of char surface reactions

No.	Reactions	A, *kg/(m²sPa)*	E, *J/kmol*	C_{diff}, in air	C_{diff}, in CO_2
1	$C+0.5O_2 \rightarrow CO$	In Table 3.2		5.0×10^{-12}	4.0×10^{-12}
2	$C+CO_2 \rightarrow 2CO$	In Table 3.2		2.0×10^{-12}	1.8×10^{-12}
3	$C+H_2O \rightarrow CO+H_2$	0.00635	162.0	3.4×10^{-12}	2.2×10^{-12}

The particle temperature was calculated by considering heat transfer from convection, radiation and surface heat gain/loss due to char heterogeneous reactions, using the following equation:

$$m_p c_p \frac{dT_p}{dt} = \frac{2\lambda}{d_p} A_p (T_\infty - T_p) + A_p \varepsilon_p \sigma(\theta_R^4 - \sigma T_p^4) + f_h A_p (q_1 H_1 - q_2 H_2 - q_3 H_3) \quad (5\text{-}18)$$

5.1.7 Gaseous homogenous reactions

The primary gaseous products yielded from char surface reactions burn further in the bulk gas, shown as

$CO + 0.5O_2 \rightarrow CO_2$ (5-19)

$H_2 + 0.5O_2 \rightarrow H_2O$ (5-20)

The turbulent combustion of volatile matter and char surface primary products are predicted by a Finite-rate/ eddy-dissipation model, considering two mechanisms of Arrhenius laminar reaction and turbulent fluctuation. The eddy dissipation model (EDM) as detailed in was employed, which was developed from the eddy break-up (EBU) model and firstly proposed by Spalding. The reaction kinetic data are listed in Table 5.2.

Table 5.2 Global mechanisms of gas-phase reactions

No.	Reactions	Rate equations, *Kmol/(m^3s)*	*A*	*b*	*E, J/kmol*
(1) Original WD: Westbrook & Dryer 2-step mechanism for methane combustion in air					
1	$CH_4+1.5O_2 \rightarrow CO+2H_2O$	$d[CH_4]/dt=ATbexp(-E/RT)[CH_4]^{0.7}[O_2]^{0.8}$	5.012×10^{11}	0	200.0
2	$CO+0.5O_2 \rightarrow CO_2$	$d[CO]/dt=AT^{b}exp(-E/RT)[CO][O_2]^{0.25}[H_2O]^{0.5}$	2.239×10^{12}	0	170.0
(3) Refined WD: refined Westbrook & Dryer 2-step mechanism for oxy-fuel combustion of methane					
1	$CH_4+1.5O_2 \rightarrow CO+2H_2O$	$d[CH_4]/dt=AT^{b}exp(-E/RT)[CH_4]^{0.7}[O_2]^{0.8}$	5.03×10^{11}	0	200.0
2	$CO+0.5O_2 \rightarrow CO_2$	$d[CO]/dt=AT^{b}exp(-E/RT)[CO]\ [O_2]^{0.25}[H_2O]^{0.5}$	2.239×10^{6}	0	41.8
3	$CO_2 \rightarrow CO+0.5O_2$	$d[CO]/dt=AT^{b}exp(-E/RT)[CO_2]\ [O_2]^{-0.25}[H_2O]^{0.5}$	1.10×10^{13}	-0.97	328.0
(3) Hydrogen oxidation					
1	$H_2+0.5O_2 \rightarrow H_2O$	$d[H_2]/dt=AT^{b}exp(-E/RT)[H_2][O_2]$	9.87×10^{8}	0	31.0

The methane oxidation kinetics was used for volatile oxidation in air and oxy-fuel modes.

5.2 CFD modeling of ignition and flame propagation in a lab-scale Drop-Tube Furnace

5.2.1 Modelling geometry and grid of Drop Tube Furnace

A lab-scale DTF with a detailed schematic in figure 5.1 was used for oxy-fuel coal combustion experiments. As detailed elsewhere, the furnace is 2.0 m long and consists of six heating sections with the same length that are controlled individually. The modeling geometry was created by GAMBIT 2.4.6 preprocessor based on the size of the furnace, as illustrated in figure 5.2. A grid independence test was first conducted to elucidate the minimum cell number in a grid to ensure the accuracy of modelling results and least calculation time. The grid of 231,000 cells yielded almost the same results with the grid with 482,000 cells. It was thus selected and used throughout this study.

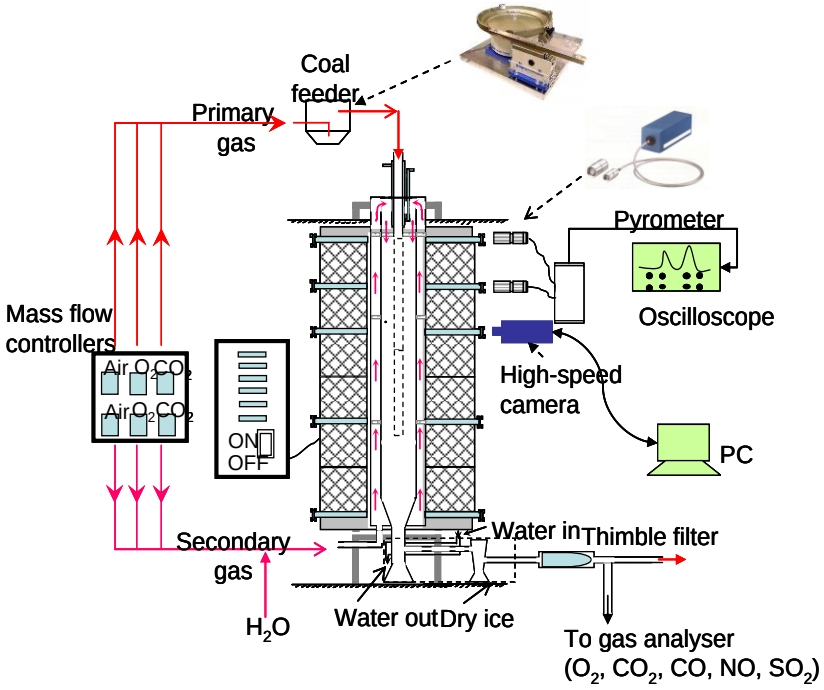

Figure 5.1 Schematic diagram of the drop tube furnace

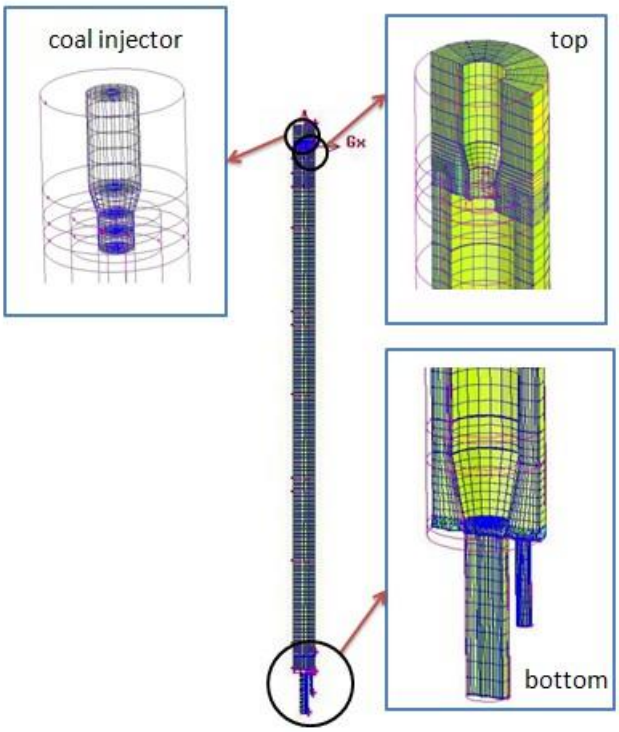

Figure 5.2. Modeling geometry and local expansion diagrams for drop tube furnace

For each run, coal was entrained by primary air and fed at a rate of approximately 0.5 g/min. The temperature of furnace wall was kept at 1073 K or 1273 K. The fluxes of primary and secondary gas were set as 1.0 L/min (cold) and 9.0 L/min (cold), respectively. The average oxygen content in bulk gas varies from 21% to 30% in volume, balanced by either N_2 or CO_2. Apart from the sampling of unburnt carbon, imaging of flame ignition and propagation was also taken during experiments.

5.2.2 Comparison of modelling results and experimental observation

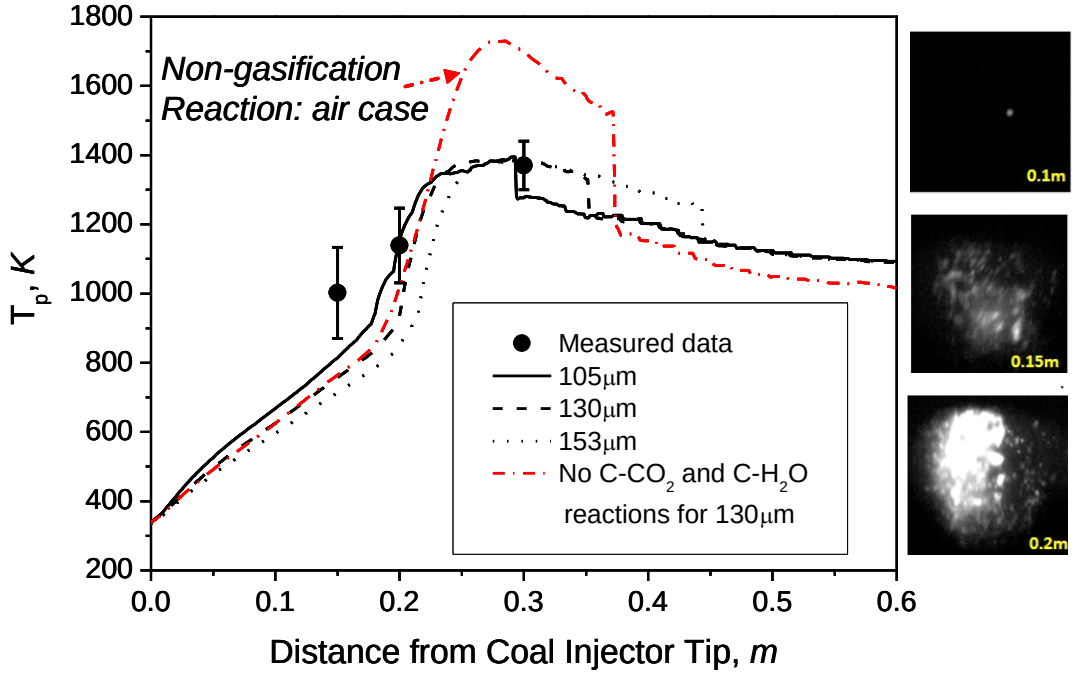

Figure 5.3 Burning coal particle temperature as a function of lab-scale drop-tube furnace distance from coal injector tip to char sampling point. The coal used is Loy Yang coal, air-dried, and furnace temperature 1073 K.

Figure 5.3 confirms the remarkable influence of char gasification reactions on the particle temperature. Without the occurrence of gasification reactions, the char particle temperature could be maximised at around 1700 K, relative to 1073 K for the furnace wall. The burning char particle temperatures, measured by two-colour pyrometer, are also lower than the prediction with the gasification reactions off. Instead, the pyrometer measurements are in good agreement with the prediction which took into account the char gasification reactions. The coal burnout rates in air versus 21% O_2 in CO_2, as illustrated in figure 5.4, also indicate a good agreement between

the measured points and the prediction curves by the CFD model taking into account char gasification reaction. Figure 5.5 further indicates that the two gasification reactions can account for 10% of the total coal burnout rate at the furnace temperature of 1073 K, and up to 25% at the furnace temperature 1273 K.

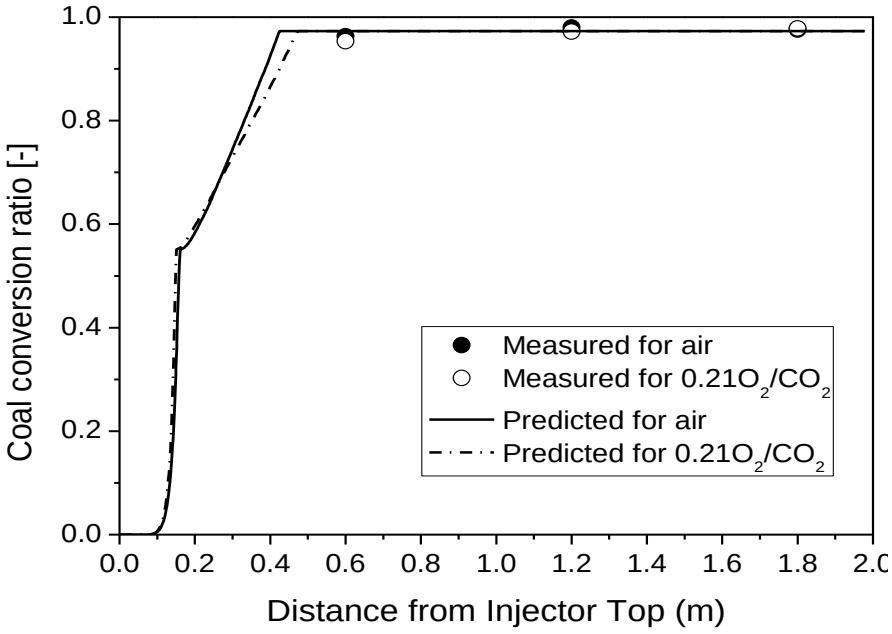

Figure 5.4 Coal burnout rate as function of drop-tube furnace distance at the furnace wall temperature o 1273 K. Air-dried Loy Yang coal.

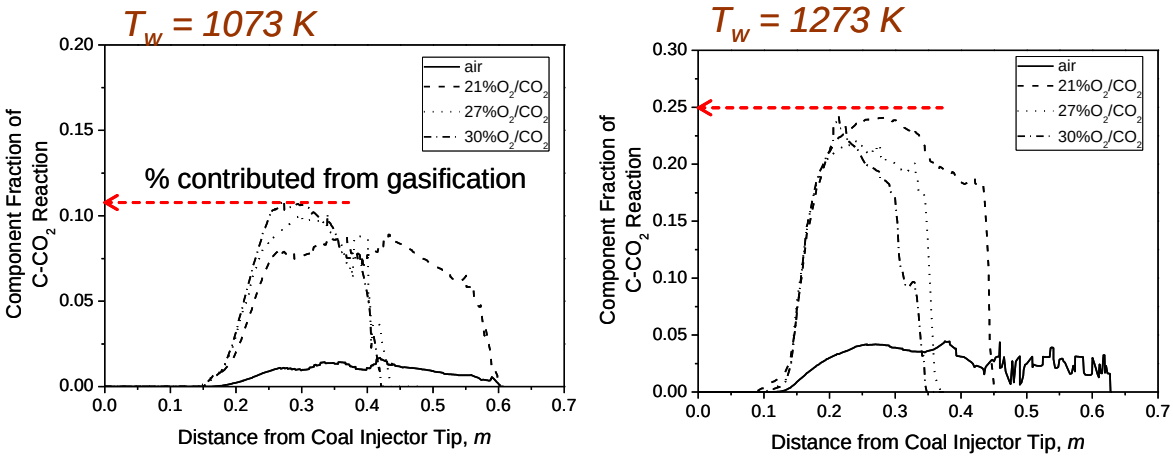

Figure 5.5 Contribution of gasification reactions on coal burnout rate, as a function of reactor length and bulk gas composition

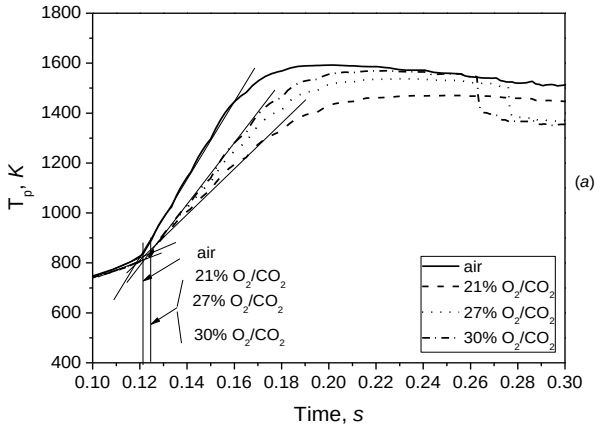

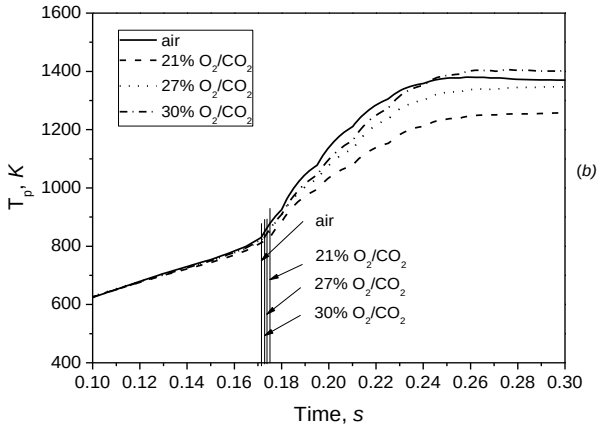

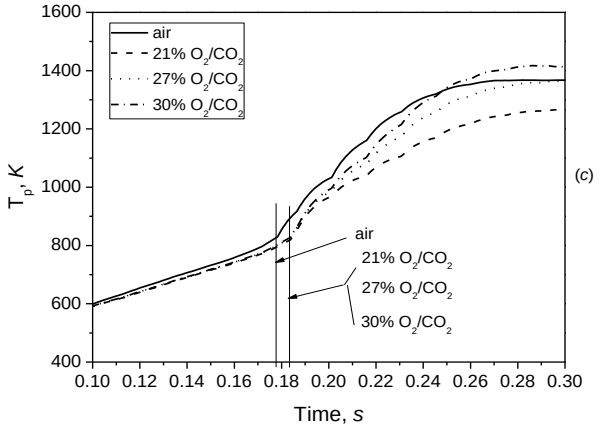

Figure 5.6. The method to determine brown coal particle ignition temperature and its variation with bulk gas composition at the secondary gas temperature of 1273K (a), 1073 K (b) and 900 K (c).

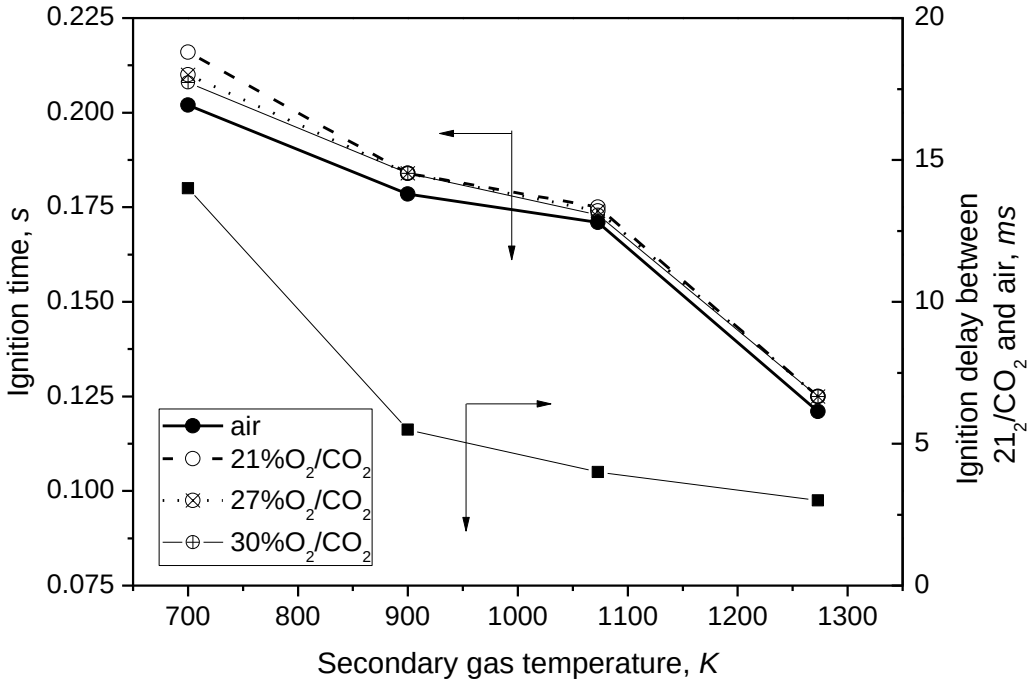

Figure 5.7 Air-dried Victorian brown coal ignition time and delay as a function of secondary gas temperature

Considering that it is very likely that both homogenous ignition and heterogeneous ignition occur simultaneously for the air-dried Victorian brown coal, the ignition time of coal was further extracted from particle temperature profiles in figure 5.3. For each panel in figure 5.6, the intersection between the tangent curves of the two sections (slow rise vs. quick rise) of a char temperature profile was deduced as coal ignition time. Clearly, at the furnace/gas temperature of 1273 K in panel (a), the brown coal ignition occurred at approximately 0.121 s in air, relative to ~0.125 s in 21% O2/CO2, 27% O2/CO2 and 30% O2/CO2 with insignificant difference amongst the three oxy-firing cases. Figure 15(b) and (c) illustrate the analysis on coal ignition temperatures at two lower temperatures for the secondary gas, 1073 K and 900 K. The former temperature was achieved by simply setting the size zones of the furnace at 1073 K, whereas the latter two were achieved by turning off the top two and four zones of the furnace, respectively. By reducing the secondary gas temperature, one can see that the discrepancy of coal ignition time between air and 21% O2 in CO2 and other oxy-fuel cases is clearly widened.

This was further quantified in Figure 5.7, where plotted were the ignition times of Victorian brown coal for four cases, and the ignition delay between 21% O2/CO2 and air as a function of the secondary gas temperature. Irrespective of bulk gas

composition, increasing the secondary gas temperature shortened the coal ignition time quickly as well as narrowed down the ignition delay between air and 21% O2 balanced in CO_2. At the gas temperature of 700 K, a coal ignition time of 0.235 s was required in air, which changed little at 900 K but was reduced to 0.184 s, then 0.171 s and 0.121 for 1073 K and 1273 K, respectively. In addition, at the low gas temperature 700 K, the ignition delay between 21% O2/CO2 and air reached ~14 ms, which was narrowed remarkably down to about 5 ms, 4 ms and 3.5 ms at 900 K, 1073 K and 1273 K, respectively. Clearly, the temperature of the secondary gas plays a critical role in particle ignition. It has the potential to offset the negative impact of the large specific heat capacity of CO2. Here, it can be concluded that, the coal ignition delay upon gas shift from air to 21% O2/CO2 can be eliminated by increasing the second gas temperature to approximately 1273 K. Apparently, such a high temperature can be achieved by employing a regenerator via the use of internal flue gas recirculation to efficiently preheat the combustion gas, same as the concept of high-temperature air combustion. The application of such a technology to the oxy-fuel combustion of Victorian brown coal may be plausible, as the low ash content in Victorian brown coal can assist in minimising the ash fouling in the regenerator.

5.2.3 Flue gas temperature profile and radiative heat flux

The match of flue gas temperature profile and radiative heat flux in a furnace is crucial for the retrofitting of oxy-fuel technology to an existing air-fired boiler in which the heat flux must be match. As shown in figure 5.8 for the flue gas temperature extracted from the CFD model, for the same O_2 concentration of 21%, the substitution of N_2 by CO_2 led to the disappearance of the highest temperature 1350 K corresponding to coal flame in air. Instead, the flue gas remained hotter close to the bottom of the furnace. This is attributed to delay on coal ignition and oxidation. Increasing the O_2 fraction in CO_2 caused an upward shift of flue gas temperature and the increase in flue gas temperature at coal flame zone, as expected. For the use of 30% O_2/CO_2 in place of air, the highest flame temperature 1350 K was achieved at nearly the same distance as in air, whereas in the bottom post-flame zone the flue gas temperature was dropped quickly, due to an intensified and quicker burnout of coal in the furnace.

Figure 5.9 further substantiates a much stronger radiation heat flux for the 30% O_2 in CO_2 than in air. Instead, the use of 27% O_2 in CO_2 shows a good match with the air in radiation heat flux in the furnace, although its flue gas temperature is lower than the air case.

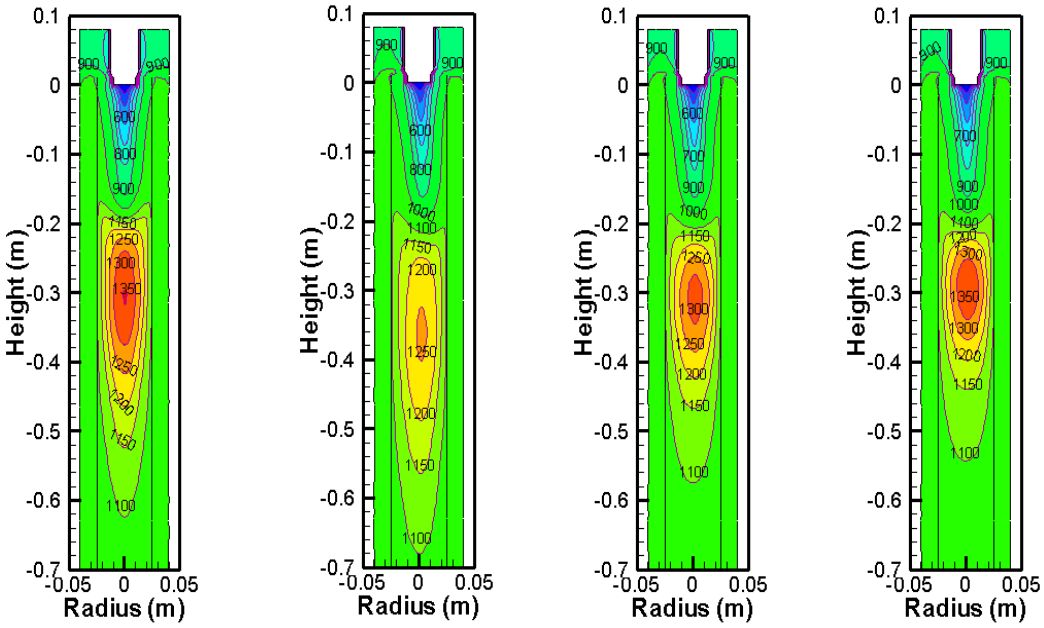

Air 21%O_2/CO_2 27%O_2/CO_2 30%O_2/CO_2

Figure 5.8 Predicted gas temperature distribution at the DTF furnace temperature of 1073 K

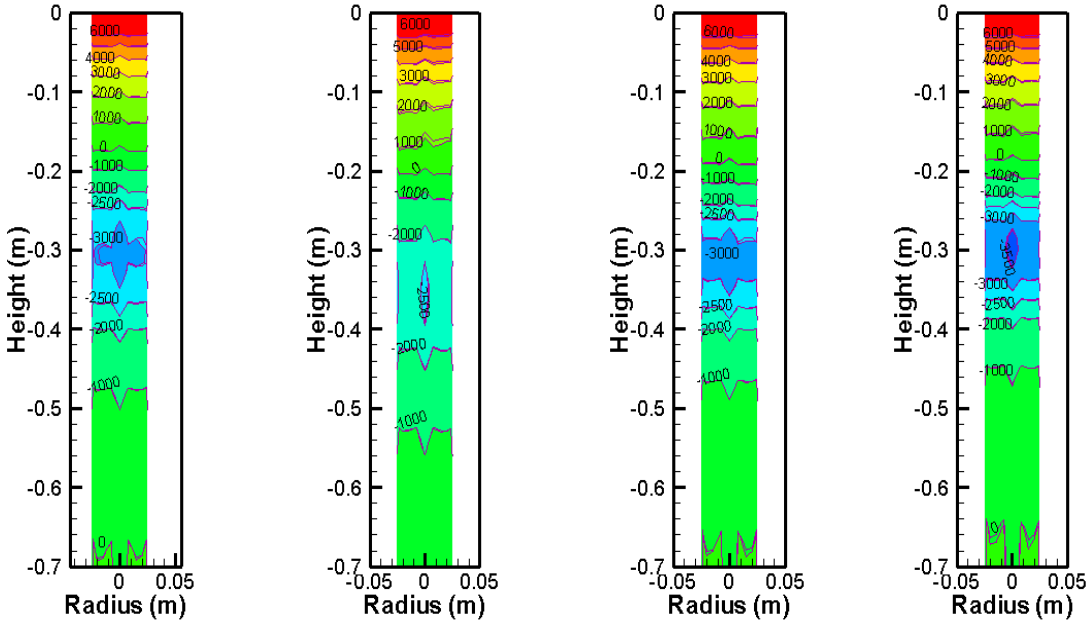

air 21%O_2/CO_2 27%O_2/CO_2 30%O_2/CO_2

Figure 5.9. Predicted radiation heat flux distribution at the furnace temperature of 1073 K, J/m^2

5.3 CFD modeling results of oxy-fuel combustion in 3MWth pilot-scale furnace

5.3.1 Modeling Geometry and grid of 3MW pilot-scale furnace

The detail size and description was stated in Chapter 3.1. And the geometry and grid generated was shown in Figure 5.10. Considering the decrease of false numerical diffusion error, the grid of cross-section of burner zone and OFA zone were drawn in Figure 5.11. The grid consists of hexahedra cells and is dense in the near burner region where the actual flame is present and coarsened toward the outlet of the furnace. Care was taken in achieving grid independent solutions, and this resulted in the use of a grid with a total number of around 286,000 cells. A random trajectory model is utilized for particle motion. Around 7,200 particles are track in the present pilot-scale furnace simulation.

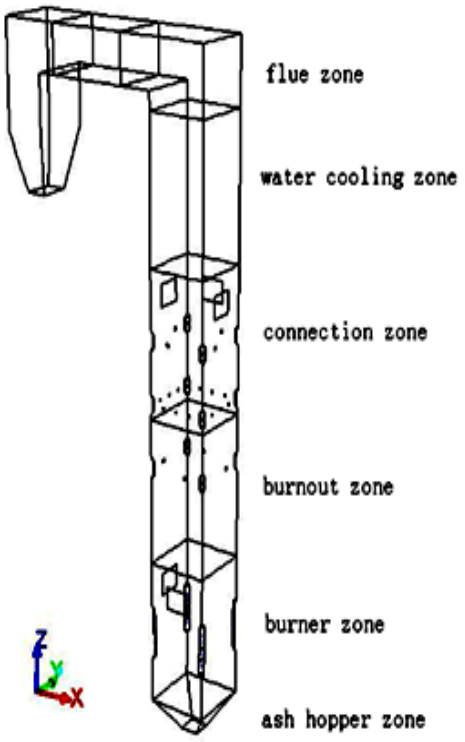

Figure 5.10 Schematic drawing of 3MW boiler

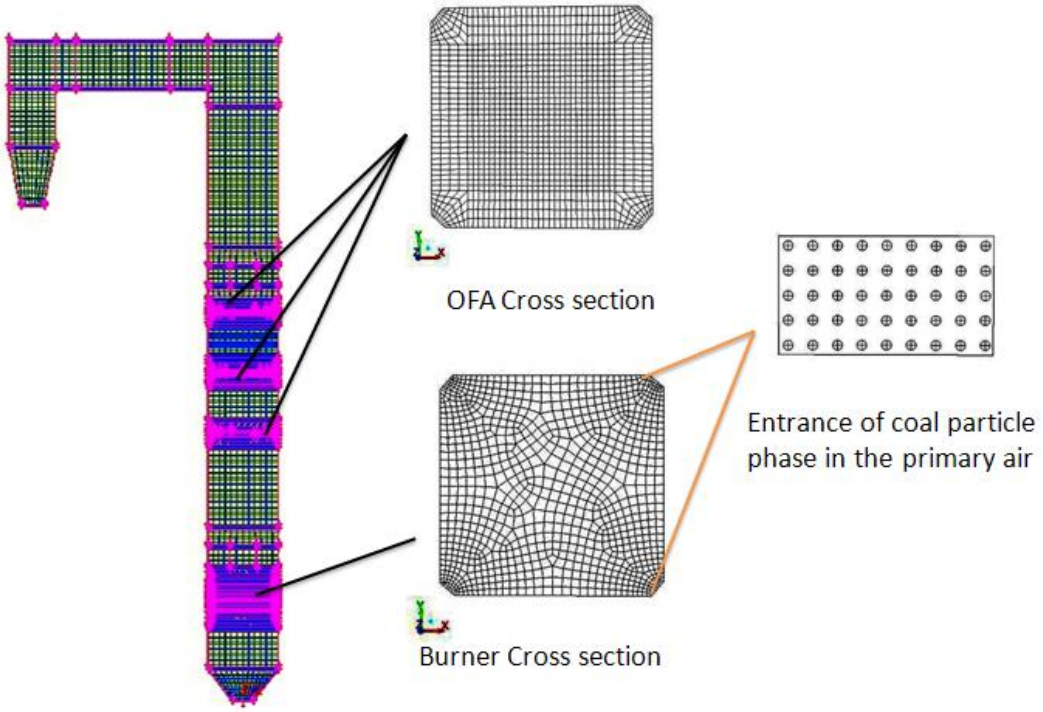

Figure 5.11 Modelling geometry of 3MW boiler

5.3.2 Predicted CO distribution and unburnt carbon profiles

Figure 5.12 shows the predicted distributions of CO volume fraction (vol %) in the hopper and combustion zone on the mid-plane. Although oxy-27% O2 and oxy-30% O2 match the air-firing of brown coal (dry and wet, respectively) in terms of flue gas temperature, one can see that, the CO concentration distributions differs dramatically between air and its matched oxy-fuel case. For the dried coal, its combustion in air is completed rapidly, generating maximum 2% CO in a very narrow flame zone. However, the use of oxy-27% O2 to replace air led to a much broader range for the presence of CO from the bottom of coal boiler to the upper burner zone, with the maximum CO concentration being tripled. This should be largely attributed to the large C-CO2 and C-H2O gasification reactions that readily occur for Victorian brown coal. The use of wet coal caused the noticeable rise on CO concentration and broadened its distribution range even in the air - firing case. It is much worse for the oxy-30% case that matches air in terms of flue gas temperature. As can be noticed, the maximum CO concentration raised to 10%, which is distributed broadly in the burner

zones. The abundant CO is not only hazardous, but it is also influential in promoting ash melting and slagging. This has been observed by our characterization on oxy-fuel ash.

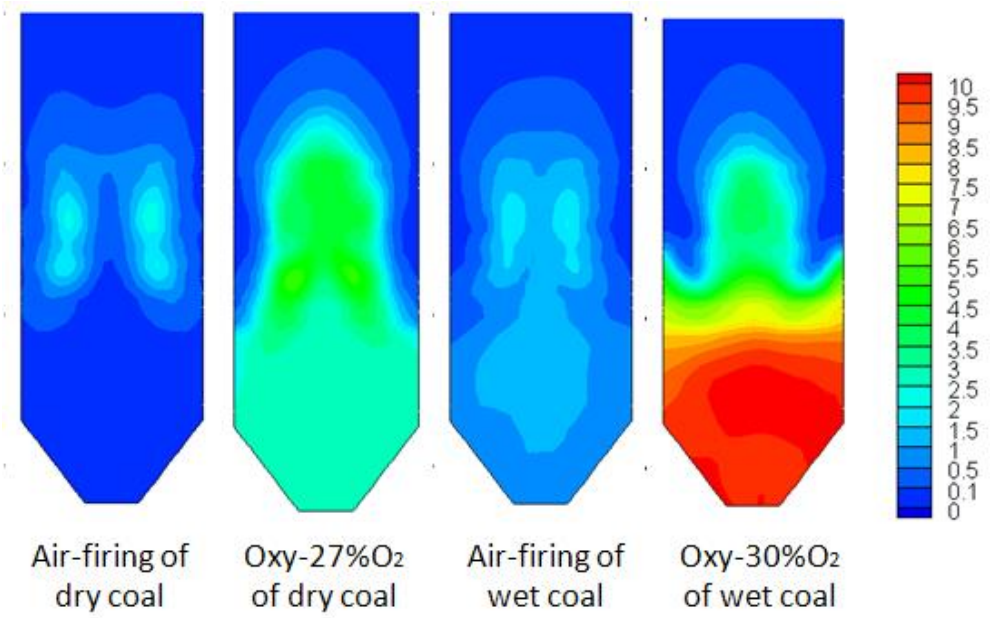

Figure 5.12 CFD predicted CO emission contour in burner vicinity

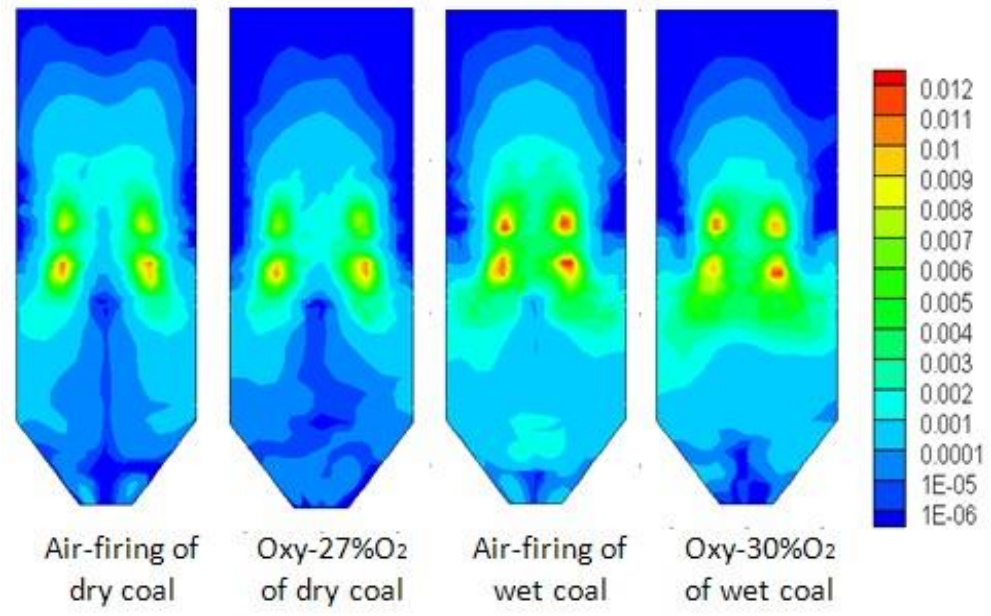

Figure 5.13 CFD predicted unburnt carbon contour in burner vicinity

Figure 5.13 demonstrates the predicted unburnt carbon content distribution for the same four cases mentioned in Figure 5.12. For either dried or wet coal, the difference of its unburnt carbon between air and matched oxy-fuel case is rather small and negligible, when compared to CO emission profile. This further strengthened the high reactivity of Victorian brown coal char for both exothermic C-O_2, and endothermic C-H2O and C-CO2 gasification reactions. For the wet coal fly ash sample collected, the unburnt carbon content is only 0.72 % and 0.91% for air case and oxy-30% case, respectively. This supports the CFD modeling prediction. For the broader distribution of unburnt carbon for wet coal than dried coal in a given case, it can be attributed to a slightly lower particle temperature for wet coal in Figure 3.11, and a larger feeding rate of wet coal that is required to achieve the same thermal output of the boiler as dried coal.

5.3.3 Design optimisation of oxy-burners

Modeling work was further carried out to provide insight on the influence of oxygen content in primary flue gas on coal ignition. This is supposed to be helpful for the oxy-burner design. The information for the particles was extracted along particle travel and interpreted statistically for the ignition characteristics of char particles.

Figure 5.14 (a) demonstrates 1800 char particle trajectories from two burners and its burnout rate, as a function of oxygen content in the primary RFG stream. As has been justified, the char ignition occurs from a particle residence time of approximately 10.5 ms in air for the average char particle size of 80 μm. With the replacement of air by oxy-fuel mode, the particle ignition is delayed to 13.5 ms for 3% O2 in primary gas stream, 12.2 ms in 21% O2 and 11.5 ms for 30% O2 in the primary RFG stream, respectively, as shown in Figure 5.14(b). Clearly, a higher oxygen content in primary gas is essential to trigger the ignition of wet brown coal timely. However, this causes the undesirable rise on the emission of NO, which is favoured by the enhanced reducing environment near coal burner. From our measurement, it has been noticed that the NO emission was increased from 230 mg/m^3 (153 mg/mJ equivalent) in air-firing mode to 764 mg/m3 (107 mg/mJ) in oxy-fuel mode case, as summarised in table 5.3 below. Apparently, the development of low-NOx oxy-fuel burner and staged oxygen injection are crucial.

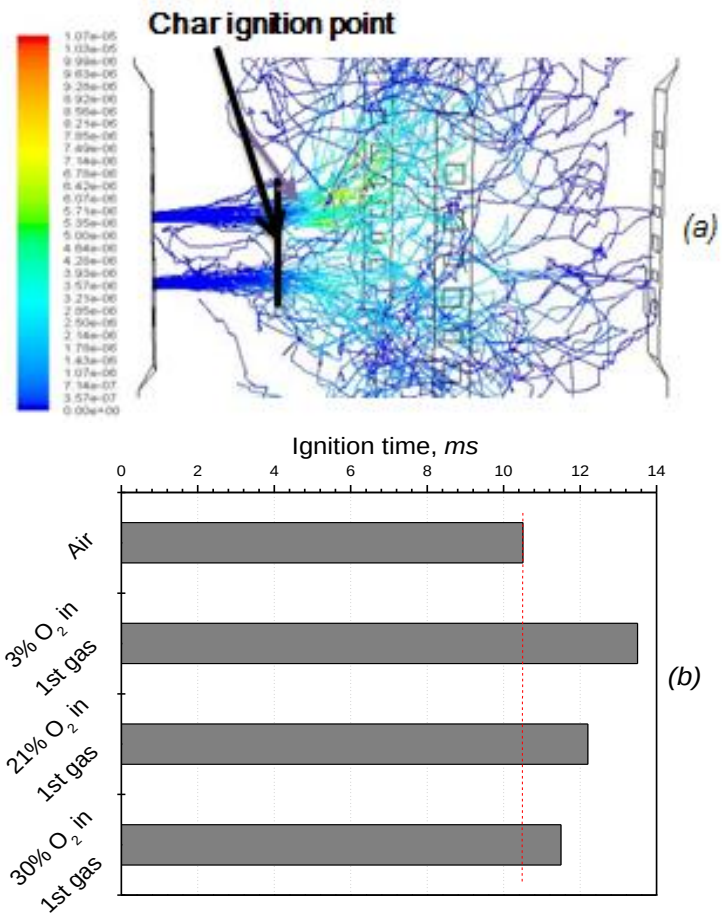

Figure 5.14 CFD predicted particle ignition point as a function of oxygen percentage in primary gas

Table 5.3 NOx data measured in 3 MWth facility

Coal	MW	mode	Flue gas				
			O_2, vol%	temp °C	NO, ppm	NO, mg/m^3	NO, mg/mJ
Yallourn	0.95	Air-firing	4.3	160	262.0	229.9	152.9
Yallourn	0.95	Oxy-firing (30% O_2)	5.0	160	870.3	763.7	106.5
Hazelwood	0.8	Air-firing	5.0	160	379.0	233.4	156.2
Hazelwood	1.0	Air-firing	5.0	160	457	295.4	192.8
Hazelwood	0.8	Oxy-firing (30%O_2)	5.0	160	1259.0	736.6	102.7

5.4 Appendix of one-dimensional Matlab code for coal drying and ignition and user-defined function (UDF) codes for CFD modelling

5.4.1 Appendix 1 – Matlab code for coal drying and ignition

```
%Main Code

%GAsification modelling based on the single film model
clc
clear

fout = fopen('semioxy26co2vsh2o_30steam.txt','w+');

fprintf('Coal Moisture Content');
mcoinput = input('\nMoisture (Fraction)=');
fprintf('\n1.Air\n2.Oxy16\n3.Oxy21\n4.Oxy26\n5.Oxy31\n');
comb = 4;
alphas = 0.3;       %Extent of External Steam gasification
inher = 0.09;       %Amount of inherent moisture remaining
alpha = 0:0.025:0.5;
n = length(alpha);
inherremo = linspace(0,inher/2,n);
fprintf(fout,'CO2\tinherent\tpercentageremoval\t50mm\t75mm\n');
for i = 1:n
   alphac = alpha(i);
   for j = 1:n
      inherrem = inherremo(j);
      alphasurf = inherrem/inher;
      [tpf,tff] = Comb_V3_gasmodel(mcoinput,comb,alphac,alphas,alphasurf,inher,inherrem);
      if comb == 1
         a = 6088;
         b = 7706;
      elseif comb == 2||comb == 3||comb == 4||comb == 5
         a = 8254;
         b = 10116;
      end
      tpfinal(i,j) = tpf(a);
      tpfinal2(i,j) = tpf(b);
      percent(j) = inherrem/inher*100;
   fprintf(fout,'%10.4g\t%10.4g\t%10.4g\t%10.4g\t%10.4g\n',alphas,inherrem,percent(j),tpfinal(i,j),tpfinal2(i,j));
   end
end
% fclose(fout);
alphass = alpha(1:i)*100;
alphacc = alpha(1:j)*100;
p = surf(alphass,percent,tpfinal);
xlabel('Contribution of Internal steam gasification (%)');
ylabel('Contribution of CO2 gasification (%)');
zlabel('Particle Temperature(K)');
set(p,'edgecolor','none');
```

%Function Code

```
function [tpf,tff] = Comb_V3_gasmodel(mcoinput,comb,alphac,alphas,alphasurf,inher,inherrem)
%One-Dimensional Code for Coal Combustion and Gasification Study

diam = 0.000084;
alphadevol = 0.08;
if inherrem == 0
   alphasurf = 0;
end
if (alphac+alphas) < 1 || (alphas+alphasurf)<1|| (alphac +alphasurf)<1
   alphao = 1-alphac-alphas-alphasurf;
end

%Problem Constant
hd = 2.26E6;           %Heat of water evaporation (J/kgK)
hco = 9.208*10^6;      %Heat of CO formation (J/kgK)
hcd = 3.28*10^7;       %Heat of CO2 formation (J/kgK)
hcdg = 1.438*10^7;     %Heat of CO2 gasification (J/kgK)
hsg = 1.094*10^7;      %Heat of steam gasification (J/kgK)
hh = 1.43*10^8;        %Heat of H2 combustion (J/kgK)
hpyro = 8.37*10^5;     %J/kgK of coal
hms = 1.145*10^7;      %Methane Steam Reforming Endothermic Reaction (J/kgK)
e = 0.8;               %Particle Emissivity
sig = 5.67E-8;         %Stefan-Boltzmann Constant
tw = 773;              %Wall temperature (K)
r = 8.314;             %Universal gas constant (J/kgK)
cpcoal = 1150;         %Lignite Heat Capacity from Fluent (J/kgK)
pdried = 1150;         %Dried Coal Density (kg/m3)
ta = 365;              %Wet bulb temperature(K)
na = 0.3468;           %Total Time in air (s)
no = 0.4132;           %Total Time in CO2 (s)
fv = 0.4495;           %Volatile Fraction in air-dried
fvdb = fv/0.88;        %Vol Fractionin dry  basis
P = 101325;            %Total Pressure (Pa)
dt = 0.000005;         %Integration time step
hchar = 3.28E7;        %Heating value of Carbon Char (J/kg)

%Coal Properties dried basis
FC = 0.470455;         %Fixed carbon
VM = 0.510795;         %Volatile matter
A = 0.018750;          %Ash
C = 0.657;             %Carbon
H = 0.068;             %Hydrogen
N = 0.06;              %Nitrogen
S = 0.05;              %Sulphur
O = 0.258;             %Oxygen

%Method 1
%Conversion ratio btu/lb to kJ/kg
ratio = 2.326;
coalhhvdb = (146.58*C*100+568.78*H*100+29.4*S*100-6.58*A*100-51.53*(O+N)*100)*ratio*1000;
coalhhvar = coalhhvdb*(1-mcoinput);
coallhvdb = coalhhvdb-(1+H/2*18)*hd;
coallhvar = coalhhvar-(1+H/2*18)*hd;
```

```
hvol2 = (coallhvar-(hchar*FC*(1-mcoinput)))/(VM*(1-mcoinput));
hvol3 = (coallhvdb-(hchar*FC))/VM;

%Method 2
Cvol = C - FC;
hvol = ((3.55*Cvol^2-232*Cvol - 2230*H +51.2*Cvol*H+131*N + 20600))*1000-hd;

if comb == 1
   fo = 0.2103;fn=0.4404;fc = 0.1644;fs = 0.1849;n = (0:dt:na);limit = na;
elseif comb == 2
   fo = 0.1664;fn = 0;fc = 0.649;fs = 0.1846;n = (0:dt:no);limit = no;
elseif comb == 3
   fo = 0.2157;fn = 0;fc = 0.5992;fs = 0.185;n = (0:dt:no);limit = no;
elseif comb == 4
   fo = 0.2654;fn = 0;fc = 0.5492;fs = 0.1855;n = (0:dt:no);limit = no;
elseif comb == 5
   fo = 0.3154;fn = 0;fc = 0.4989;fs = 0.1859;n = (0:dt:no);limit = no;
end

%Solution Initialization
tf = zeros(length(n),1);tp = zeros(length(n),1);Tm = zeros(length(n),1);
tgas = zeros(length(n),1);
mv = zeros(length(n),1);
rat = zeros(length(n),1);
qo = zeros(length(n),1);qc = zeros(length(n),1);qs = zeros(length(n),1);
qssurf = zeros(length(n),1);
qt = zeros(length(n),1);
devolrate = zeros(length(n),1);
area = zeros(length(n),1);
b = zeros(length(n),1);
psi = zeros(length(n),1);
vco = zeros(length(n),1);vco2 = zeros(length(n),1);
hcomb = zeros(length(n),1);mech = zeros(length(n),1);
distance = zeros(length(n),1);conv = zeros(length(n),1);tconv = zeros(length(n),1);
nn = zeros(length(n),1);dryrate = zeros(length(n),1);totconv = zeros(length(n),1);
massrem = zeros(length(n),1);tc = zeros(length(n),1);

%Input Parameter
d((1:length(n)),1) = diam;
mco(1:length(n),1) = mcoinput;
%pwc = pdried+(mcoinput*1000);%Wet coal density
pwc = pdried*(1-mcoinput)+mcoinput*1000;
mdried = (pdried*3.14/6*diam^3);
mi = (pdried*3.14/6*diam^3)+(mcoinput*mdried/(1-mcoinput));
% mi = pwc*3.14/6*diam^3;
% ft = fvdb*(1-mcoinput)*mdried;%Total Volatile amount
ft = fvdb*mdried;
unburnt = A*mdried;
% unburnt = A*(1-mcoinput)*mdried;%Mass of Coal unburnt
carbon = mdried-ft-unburnt;
mt(1:length(n),1) = mi;
tp(1) = 298;
tf(2) = tf(1) +dt;
i = 2;
iagain = 1;
```

```
m = 2;
err(1:length(n),1) = 0;
pchar = 615;%kg/m3

%Input Drying Model
% fprintf('\n1.McIntosh model\n2.General Model\n');
Drying = 1;
% fprintf('\n1.Kinetic model\n2.Kinetic-diffusion model\n');
% gasmode = input('Gasification Mechanism :');
% fh = fs;

clc
fprintf('Time Step: %6d%10s:%10.4f Char Conversion: %10.4f Coal Conversion:%10.4f Total
Conversion:%10.4f\n',1,'Error',0,0,0,0);
while iagain == 1
   if tf(i) == 0
      distance(i) = 0;
   elseif tf(i) > 0 && tf(i) <= 0.048
      if comb == 1
         distance(i) = (-0.0003*(tf(i)*1000)^3+0.0411*(tf(i)*1000)^2+0.7678*(tf(i)*1000)-2.7809)/10;
      elseif comb >=2&&comb<=5
         distance(i) = (-0.0003*(tf(i)*1000)^3+0.0468*(tf(i)*1000)^2-0.2070*(tf(i)*1000)+1.0267)/10;
      end
   elseif tf(i)>0.048
      if comb == 1
         distance(i) = (0.0041*(tf(i)*1000)^2+2.3791*(tf(i)*1000)-29.012)/10;
      elseif comb >=2&&comb<=5
         distance(i) = (0.0045*(tf(i)*1000)^2+1.8867*(tf(i)*1000)-37.528)/10;
      end
   end
   if distance(i) < 0
      distance(i) = distance(i-1)+0.0001;
   end
   if comb == 1
      tgas(1) = 414.96 + 820.13576;
      tgas(i) = 414.96 + 820.13576*exp(-distance(i)/30.77);
   elseif comb >=2&&comb<=5
      tgas(1) = 276.465 + 930.52797;
      tgas(i) = 276.465 + 930.52797*exp(-distance(i)/43.834);
   end%-- from if comb == 1 loop --%

   if tgas(i) <=tw
      tgas(i) = tw;
   end

   if tf(i)<=0.0025
      parvel = 0;
   elseif tf(i)>0.0025
      if comb == 1
         parvel = 0.7224*log(tf(i)*1000)-0.1205;
      elseif comb >=2&& comb <=5
         parvel = 0.897*log(tf(i)*1000)-1.3227;
      end
   end
```

```
%Kinetic Parameter
   %A is in s-1 and E is J/mole
   %Devolatilisation
   av = 5.16e16;ev=217270;
   %Char oxidation kinetic
   ao = 0.0024;eo = 69060;
   %CO2 gasification kinetic
   ac = 0.0053;ec = 125500;
   %Steam Gasification Kinetic
   as = 0.00635;es = 162000;
   %Arthur Coefficient for CO/CO2 Ratio
   at = 2511.9;bt = 52080;

   %Guess the particle temperature at t + dt
   tpi = tp(i-1)+10;
   err(i) = 1;
   b(m) = 0;

   %Iterative procedure
   for m = 1:10
      %Dimensionless Coefficient
      Tm(1) = (tpi+tgas(1))/2;
      Tm(i) = (tpi+tgas(i))/2;
      [miut,pt,cpt,lt,do2m,dn2m,dco2m,dh2om,cvt] = Gprop(Tm,i,fo,fs,fc,fn);
      kdo = 24*do2m*(1/(293)^1.75*1/r);kdc = 24*dco2m*(1/(293)^1.75*1/r);
      kds = 24*dh2om*(1/(293)^1.75*1/r);
      psat = P*exp(hd/1000*18/r*((1/373)-(1/tpi)));
      pssurf = psat;

      %Dimensionless Correlation
      gasvel = (11.7/60*10^-3)*(tgas(i)/298)/(pi*0.115^2);
      urel = abs(parvel-gasvel);
      Re = pt*urel*d(i)/miut;
      Pr = cpt*miut/lt;
      Scs = miut/(pt*dh2om);
      Shs = 2 + 0.6*Re^0.5*Scs^(1/3);
      kcs = Shs*dh2om/d(i);
      Nu = 2 + ((0.555*Re^0.5*Pr^(1/3))/(1+(1.232*(1/Re)*(Pr)^(-4/3)))^0.5);
      h = Nu*lt/d(i);

      %Constant Calculation
      area(1) = pi*d(1)^2;
      area(i) = pi*d(i)^2;

      %Rate of Drying
      if Drying == 1
         nn(i) = (6*h*(tgas(i)-ta))/(hd*pwc*(mco(1)/(1+mco(1)))*d(i));
         dryrate(i) = mco(1)*nn(i)*mi/area(i);
      elseif Drying == 2
         dryrate(i) = h*(tgas(i)-ta)/hd;
      end

      %Rate of Devolatilisation
      kv(i) = av*exp(-ev/(r*tpi));
      devolrate(i) = kv(i)*(ft-mv(i));
```

```
%Kinetic Parameter
   %A is in s-1 and E is J/mole
   %Devolatilisation
   av = 5.16e16;ev=217270;
   %Char oxidation kinetic
   ao = 0.0024;eo = 69060;
   %CO2 gasification kinetic
   ac = 0.0053;ec = 125500;
   %Steam Gasification Kinetic
   as = 0.00635;es = 162000;
   %Arthur Coefficient for CO/CO2 Ratio
   at = 2511.9;bt = 52080;

   %Guess the particle temperature at t + dt
   tpi = tp(i-1)+10;
   err(i) = 1;
   b(m) = 0;

   %Iterative procedure
   for m = 1:10
      %Dimensionless Coefficient
      Tm(1) = (tpi+tgas(1))/2;
      Tm(i) = (tpi+tgas(i))/2;
      [miut,pt,cpt,lt,do2m,dn2m,dco2m,dh2om,cvt] = Gprop(Tm,i,fo,fs,fc,fn);
      kdo = 24*do2m*(1/(293)^1.75*1/r);kdc = 24*dco2m*(1/(293)^1.75*1/r);
      kds = 24*dh2om*(1/(293)^1.75*1/r);
      psat = P*exp(hd/1000*18/r*((1/373)-(1/tpi)));
      pssurf = psat;

      %Dimensionless Correlation
      gasvel = (11.7/60*10^-3)*(tgas(i)/298)/(pi*0.115^2);
      urel = abs(parvel-gasvel);
      Re = pt*urel*d(i)/miut;
      Pr = cpt*miut/lt;
      Scs = miut/(pt*dh2om);
      Shs = 2 + 0.6*Re^0.5*Scs^(1/3);
      kcs = Shs*dh2om/d(i);
      Nu = 2 + ((0.555*Re^0.5*Pr^(1/3))/(1+(1.232*(1/Re)*(Pr)^(-4/3)))^0.5);
      h = Nu*lt/d(i);

      %Constant Calculation
      area(1) = pi*d(1)^2;
      area(i) = pi*d(i)^2;

      %Rate of Drying
      if Drying == 1
         nn(i) = (6*h*(tgas(i)-ta))/(hd*pwc*(mco(1)/(1+mco(1)))*d(i));
         dryrate(i) = mco(1)*nn(i)*mi/area(i);
      elseif Drying == 2
         dryrate(i) = h*(tgas(i)-ta)/hd;
      end

      %Rate of Devolatilisation
      kv(i) = av*exp(-ev/(r*tpi));
      devolrate(i) = kv(i)*(ft-mv(i));
```

```
            timedry = 0;
            disdry = 0;
         end
         mco(i) = inher;
         if (mv(i-1) == 0)
            mt(i) = mt(i-1)-devolrate(i-1)*dt;
            mv(i) = mv(i-1)+devolrate(i-1)*dt;
%              if ((devolrate(i-1)*dt) < (0.01*ft))
%                 tp(i) = tp(i-1) + area(i-1)/(mt(i-1)*cpcoal)*dt*(e*sig*(tw^4-tp(i-1)^4)+h*(tgas(i-1)-tp(i-1)));
%              elseif devolrate(i-1)*dt>=0.01*ft
            tp(i) = tp(i-1) + area(i-1)/(mt(i-1)*cpcoal)*dt*(e*sig*(tw^4-tp(i-1)^4)+h*(tgas(i-1)-tp(i-1))-
devolrate(i-1)/area(i-1)*hpyro);
%              end
         elseif (mv(i-1)>0 && mv(i-1)<=0.1*ft)
            mt(i) = mt(i-1)-devolrate(i-1)*dt;
            mv(i) = mv(i-1)+devolrate(i-1)*dt;
            tp(i) = tp(i-1) + area(i-1)/(mt(i-1)*cpcoal)*dt*(e*sig*(tw^4-tp(i-1)^4)+h*(tgas(i-1)-tp(i-1))-
devolrate(i-1)/area(i-1)*hpyro);
            tdevol = tf(i);
            disdevol = distance(i);
            tempdevol = tp(i);
         elseif (mv(i-1)>0.1*ft &&mv(i-1)<ft)
            mv(i) = mv(i-1)+devolrate(i-1)*dt;
            mts = mt(i-1)-devolrate(i-1)*dt;
            if mts >=(mt(1)-(mco(1)*mt(1))-ft)
               mt(i) = mts;
            elseif mts <(mt(1)-(mco(1)*mt(1))-ft)
               mt(i) = mt(1)*(1-mco(1))-ft;
            end
            tp(i) = tp(i-1) + area(i-1)/(mt(i-1)*cpcoal)*dt*(e*sig*(tw^4-tp(i-1)^4)+h*(tgas(i-1)-tp(i-1))-
devolrate(i-1)/area(i-1)*hpyro+ alphadevol*devolrate(i-1)/area(i-1)*hvol2);
            tvol = tf(i);
            disvol = distance(i);
         elseif mv(i-1) >=ft
            mv(i) = ft;
            if mt(i-1)> unburnt
               tp(i) = tp(i-1) + area(i-1)/(mt(i-1)*cpcoal)*dt*(e*sig*(tw^4-tp(i-1)^4)+h*(tgas(i-1)-tp(i-
1))+alphao*qo(i-1)*hcomb(i-1)-alphas*qs(i-1)*hsg-alphasurf*qssurf(i-1)*hsg-alphac*qc(i-1)*hcdg);
               mt(i) = mt(i-1) - qt(i-1)*area(i-1)*dt;
               d(i) = d(i-1)-2*qo(i-1)*dt/pdried;
            else
               mt(i) = unburnt;
               tp(i) = tp(i-1) + area(i-1)/(mt(i-1)*cpcoal)*dt*(e*sig*(tw^4-tp(i-1)^4)+h*(tgas(i-1)-tp(i-1)));
            end
            conv(i) = (carbon-(mt(i)-inher*mi))/carbon;
            if conv(i)<=0
               conv(i) = 0;
            end
            if mt(i) <= unburnt,break,end
         end
         tconv(i) = (mdried-(mt(i)-inher*mi))/mdried;
         if tconv(i)<=0
            tconv(i) = 0;
         end
      end%-- exit from if mco < inher loopx
      err = abs((tp(i)-tpi)/tpi);
```

```
tpi = tp(i);
      tgasi = tgas(i);
      totconv(i) = (mi-mt(i))/mi;
   end%-- Exit from for m= 1:50 loop
   fprintf('Time Step: %6d%10s:%10.4f Char Conversion: %10.4f Coal Conversion:%10.4f Total
Conversion:%10.4f\n',i,'Error',err,conv(i),tconv(i),totconv(i));
   i = i+1;
   if distance(i-1) <= 100
      iagain = 1;
      tf(i) = tf(i-1)+dt;
      if mt(i-1) <= unburnt
         iagain = 0;
         i = i-1;
      end
      converge = (conv(i-1)-conv(i-2))/conv(i-2);
      if conv(i-1)&&conv(i-2) > 0
         if abs(converge) <=1E-6
            iagain = 0;
            i = i-1;
         end
      end
      if tf(i) >=0.051
         iagain = 0;
         i = i-1;
      end
   else
      i = i-1;
      iagain = 0;
   end% -- Exit from if i > length(n)
   z = i;
end%-- From while iagain == 1

%Final Solution
tff = tf(1:i,1);tpf = tp(1:i,1);
mtf = mt(1:i,1);mvf = mv(1:i,1);mcof = mco(1:i,1);
qof = qo(1:i,1);qcf = qc(1:i,1);qsf = qs(1:i,1);qssurff = qssurf(1:i,1);qtf = qt(1:i,1);
df = d(1:i,1);areaf = area(1:i,1);tgasf = tgas(1:i,1);
devolratef = devolrate(1:i,1);distancef = distance(1:i,1);
convf = conv(1:i,1);tconvf = tconv(1:i,1);totconvf = totconv(1:i,1);

end

% fprintf('\nEnd of Calculation\n');
% fprintf('\nWriting File To Report \n');


%Write output file to Report

% fout = fopen('results.txt','w+');
% if comb == 1
%     fprintf(fout,'Combustion case =\t%10s\n','Air Combustion');
% elseif comb >1 && comb <=5
%     fprintf(fout,'Combustion case =\t%10s\n','Oxy-Fuel Combustion');
% end
% % fprintf(fout,'(1) C + O2 only\n');
```

```
% % fprintf(fout,'(2) C + O2 & C + CO2\n');
% % fprintf(fout,'(3) C + O2 & C + H2O\n');
% % fprintf(fout,'(4) C + O2& C + CO2 & C + H2O\n');
% % fprintf(fout,'Correction Factor Applied :\t%10d\n',stefcorr);
% fprintf(fout,'\nThe Reactor operating conditions are as follows:\n');
% fprintf(fout,'\nParticle diameter :\t%12.6g\t(m)\n',diam);
% fprintf(fout,'Initial Moisture Content :\t%10g\t(wt)\n',mco(1));
% fprintf(fout,'Inherent Moisture  :\t%10g\t(wt)\n',inher);
% fprintf(fout,'O2 Concentration :\t%11.4g\nN2 Concentration :\t%11.4g\nCO2 concentration :\t%10.4g\nH2O
concentration :\t%10.4g\n',fo,fn,fc,fs);
% fprintf(fout,'Wall temperature :\t%10g\t(K)\n',tw);
% if Drying == 1
%     fprintf(fout,'\n Drying Model Used:\t McinTosh Model\n');
% elseif Drying == 2
%     fprintf(fout,'\n Drying Model Used:\t General Model\n');
% end
% fprintf(fout,'\n Calculation Results\n');
% fprintf(fout,'\nDrying time :\t%10.4g\t(ms)\t%10.4g\t(cm)\nStart of Devolatilisation
:\t%10.4g\t(ms)\t%10.4g\t(cm)\n Devolatilisation Temperature :\t%10.4g\t(K)\nEnd of Devolatilisaiton
:\t%10.4g\t(ms)\t%10.4g\t(cm)\n',timedry,disdry,tdevol,disdevol,tempdevol,tvol,disvol);
% fprintf(fout,'Extent of Devolatilization:\t%15g\nExtent of  CO2 Gasification:\t%10g\nExtent of Steam
Gasification:\t%10g\nExtent of In-Moisture Gasification:\t%10g\n',alphadevol,alphac,alphas,alphasurf);
% fprintf(fout,'Partial Pressure at the Char Surface:\t%10g\t(Pa)\n',pssurf);
% fprintf(fout,'\nTime(s)\tDistance(cm)\tParticle Temperature(K)\tGas Temperature(K)\tMass(kg)\tMoisture
Content(wt)\tDiameter(m)\tDevolatilization Rate(kg/s)\tVolatile
matter\tQo(kg/m2s)\tQs(kg/m2s)\tQc(kg/m2s)\tQinherent(kg/m2s)\tChar Conversion\tCoal Conversion\t Total
Conversion\n');
% for i = 1:z
%
fprintf(fout,'%10.4g\t%10.4g\t%10.4g\t%10.4g\t%10.4g\t%10.4g\t%10.4g\t%10.4g\t%10.4g\t%10.4g\t
%10.4g\t%10.4g\t%10.4g\t%10.4g\t%10.4g\n',tff(i),distancef(i),tpf(i),tgasf(i),mtf(i),mcof(i),df(i),devolratef(i),m
vf(i),qof(i),qsf(i),qcf(i),qssurff(i),convf(i),tconvf(i),totconvf(i));
% end
% fclose(fout);
% fprintf('\nRun Completed \n');
```

5.4.2 Appendix 2 – CFD codes used in FLUENT modelling

(1) Refined radiation property in air-firing condition.

The program is used as user-define function in FLUENT, written by C++ .

```
/* UDF for estimating the effective gas absorption coeff using Yin's WSGGM for air-firing combustion
*/
/* written by Jian Zhang, Anthony De Girolamo, Monash University, in Oct 2013 */

#include "udf.h"
#include "materials.h"

DEFINE_WSGGM_ABS_COEFF(user_wsggm_abs_coeff, c, t, xi, p_t, s, soot_conc,Tcell, nb,
ab_wsggm, ab_soot)
{
 Material *m = THREAD_MATERIAL(t);
 int ico2, ih2o;
 real co2_molf, h2o_molf;
 real p_e, p_c, p_w;
 real k1, k2, k3, k4;
 real b11, b21, b31, b41;
 real b12, b22, b32, b42;
 real b13, b23, b33, b43;
 real b14, b24, b34, b44;
 real a_1, a_2, a_3, a_4;
 real emi;

 s=0.964;

 ico2 = mixture_specie_index(m,"co2");
 ih2o = mixture_specie_index(m,"h2o");
 co2_molf = xi[ico2];
 h2o_molf = xi[ih2o];
 p_c = (p_t/101325.0+1.0)*co2_molf;
 p_w = (p_t/101325.0+1.0)*h2o_molf;
 p_e=p_c+p_w;

  if (p_w <= (p_c * 0.01))   /* p_c=0 atm  */
 {
  k1 = 0.163233;
  k2 = 13.096584;
  k3 = 175.474735;
  k4 = 1310.847307;
  b11 = 0.204623;
  b21 = -0.020227;
  b31 = 0.044221;
  b41 = 0.039311;
  b12 = -0.378060;
  b22 = 0.256006;
  b32 = 0.003850;
  b42 = -0.054832;
  b13 = 0.666639;
  b23 = -0.195201;
  b33 = -0.020175;
  b43 = 0.025370;
  b14 = -0.203453;
  b24 = 0.040493;
```

```
  b34 = 0.004919;
  b44 = -0.003891;
}

else if (p_w <= (p_c * 0.5))    /* p_w/p_c=0.05, p_c=0.1 atm  */
{
  k1 = 0.352505;
  k2 = 8.210621;
  k3 = 137.410012;
  k4 = 1269.710976;
  b11 = 0.315106;
  b21 = 0.092474;
  b31 = 0.031702;
  b41 = 0.046138;
  b12 = 0.023475;
  b22 = 0.109146;
  b32 = 0.037396;
  b42 = -0.061392;
  b13 = -0.057930;
  b23 = -0.121000;
  b33 = -0.040731;
  b43 = 0.027164;
  b14 = 0.008408;
  b24 = 0.027145;
  b34 = 0.008742;
  b44 = -0.003996;
}

else if (p_w <= (p_c * 1.5))   /* p_w/p_c=1, p_c=0.1 atm  */
{
  k1 = 0.261021;
  k2 = 3.147817;
  k3 = 54.265868;
  k4 = 482.900353;
  b11 = 0.500119;
  b21 = 0.071592;
  b31 = 0.155320;
  b41 = 0.072615;
  b12 = -0.447068;
  b22 = 0.508252;
  b32 = -0.104294;
  b42 = -0.100601;
  b13 = 0.286878;
  b23 = -0.384253;
  b33 = 0.014096;
  b43 = 0.046681;
  b14 = -0.059165;
  b24 = 0.073477;
  b34 = 0.001643;
  b44 = -0.007224;
}

else if (p_w <= (p_c * 2.5))  /* p_w/p_c=2, p_c=0.1 atm  */
{
  k1 = 0.179160;
  k2 = 2.388971;
  k3 = 28.415805;
  k4 = 253.059089;
  b11 = 0.542458;
  b21 = 0.101734;
```

```
  b31 = 0.146066;
  b41 = 0.129511;
  b12 = -0.658411;
  b22 = 0.518429;
  b32 = -0.008745;
  b42 = -0.187993;
  b13 = 0.466444;
  b23 = -0.386151;
  b33 = -0.058325;
  b43 = 0.090709;
  b14 = -0.100186;
  b24 = 0.073453;
  b34 = 0.015984;
  b44 = -0.014493;
}

else if (p_w <= 0.01)    /* p_w=0 atm  */
{
  k1 = 0.085523;
  k2 = 0.475777;
  k3 = 8.549733;
  k4 = 201.906503;
  b11 = 0.966357;
  b21 = 0.662059;
  b31 = 0.060870;
  b41 = 0.103568;
  b12 = -0.790165;
  b22 = -2.262877;
  b32 = 0.436788;
  b42 = -0.153135;
  b13 = -0.050144;
  b23 = 2.309473;
  b33 = -0.395493;
  b43 = 0.074910;
  b14 = 0.115202;
  b24 = -0.572895;
  b34 = 0.085146;
  b44 = -0.012091;
}

else if (p_w <= 0.2)    /* p_w=0.05 atm  */
{
  k1 = 0.232724;
  k2 = 2.134299;
  k3 = 9.266065;
  k4 = 134.988332;
  b11 = 0.340618;
  b21 = 0.175818;
  b31 = 0.044325;
  b41 = 0.126628;
  b12 = -0.105469;
  b22 = -0.063466;
  b32 = 0.288376;
  b42 = -0.186480;
  b13 = 0.068051;
  b23 = 0.086631;
  b33 = -0.258205;
  b43 = 0.090755;
  b14 = -0.017828;
  b24 = -0.026581;
```

```
  b34 = 0.054333;
  b44 = -0.014569;
 }

 else        /* p_w=1 atm  */
 {
  k1 = 0.065411;
  k2 = 0.696552;
  k3 = 4.862610;
  k4 = 60.255980;
  b11 = -0.077336;
  b21 = 0.506777;
  b31 = -0.079989;
  b41 = 0.373898;
  b12 = 0.661776;
  b22 = -0.758948;
  b32 = 0.851078;
  b42 = -0.540887;
  b13 = -0.362515;
  b23 = 0.516146;
  b33 = -0.604264;
  b43 = 0.258923;
  b14 = 0.053534;
  b24 = -0.102909;
  b34 = 0.113500;
  b44 = -0.040957;
 }
          a_1 = b11+b12*(Tcell/1200.0)+b13*pow((Tcell/1200.0),2.0)+b14*pow((Tcell/1200.0),3.0);
          a_2 = b21+b22*(Tcell/1200.0)+b23*pow((Tcell/1200.0),2.0)+b24*pow((Tcell/1200.0),3.0);
          a_3 = b31+b32*(Tcell/1200.0)+b33*pow((Tcell/1200.0),2.0)+b34*pow((Tcell/1200.0),3.0);
          a_4 = b41+b42*(Tcell/1200.0)+b43*pow((Tcell/1200.0),2.0)+b44*pow((Tcell/1200.0),3.0);

emi = a_1*(1.0-exp(-k1*p_e*s))+a_2*(1.0-exp(-k2*p_e*s))+ a_3*(1.0-exp(-k3*p_e*s))+a_4*(1.0-
exp(-k4*p_e*s));    /*total emissivity*/

          *ab_wsggm = -1.0/s*log(1.0-emi);  /*gray absorption coefficient,m-1*/

}
```

(2) Refined radiation property in oxy-firing condition.

The program is used as user-define function in FLUENT, written by C++ .

```
/* UDF for estimating the effective gas absorption coeff using Yin's WSGGM  */
/* written by Jian Zhang, Anthony De Girolamo, Monash University, in Aug 2013 */
/* referring the example of non-gray abs_coeff in HELP */

#include "udf.h"
#include "materials.h"

DEFINE_WSGGM_ABS_COEFF(user_wsggm_abs_coeff, c, t, xi, p_t, s, soot_conc,Tcell, nb,
ab_wsggm, ab_soot)
{
 Material *m = THREAD_MATERIAL(t);
 int ico2, ih2o;
 real co2_molf, h2o_molf;
```

```
real p_e, p_c, p_w;
real k1, k2, k3, k4;
real b11, b21, b31, b41;
real b12, b22, b32, b42;
real b13, b23, b33, b43;
real b14, b24, b34, b44;
real a_1, a_2, a_3, a_4;
real emi;

s= 0.964;

ico2 = mixture_specie_index(m,"co2");
ih2o = mixture_specie_index(m,"h2o");
co2_molf = xi[ico2];
h2o_molf = xi[ih2o];
p_c = (p_t/101325.0+1.0)*co2_molf;
p_w = (p_t/101325.0+1.0)*h2o_molf;
p_e=p_c+p_w;

  if ((p_w + p_c) <= 0.1)
{
  k1 = 0.009422;
  k2 = 0.415646;
  k3 = 11.617018;
  k4 = 319.911168;

  b11 = 0.778969;
  b21 = -0.011449;
  b31 = -0.007627;
  b41 = 0.080082;

  b12 = -1.342848;
  b22 = 0.343754;
  b32 = 0.242233;
  b42 = -0.049280;

  b13 = 0.964858;
  b23 = -0.234886;
  b33 = -0.173738;
  b43 = 0.001861;

  b14 = -0.195747;
  b24 = 0.044008;
  b34 = 0.033868;
  b44 = 0.002232;
}

else if ((p_w + p_c) <= 0.3)
{
  k1 = 0.256738;
  k2 = 3.108033;
  k3 = 52.585782;
  k4 = 440.845718;

  b11 = 0.492304;
  b21 = 0.082686;
  b31 = 0.144385;
  b41 = 0.079515;

  b12 = -0.433789;
```

```
  b22 = 0.486294;
  b32 = -0.083662;
  b42 = -0.110361;

  b13 = 0.279329;
  b23 = -0.369752;
  b33 = 0.002003;
  b43 = 0.051379;

  b14 = -0.057770;
  b24 = 0.070509;
  b34 = 0.003902;
  b44 = -0.007983;
 }

 else if ((p_w + p_c) <= 0.5)
 {
  k1 = 0.132242;
  k2 = 14.660767;
  k3 = 1.750654;
  k4 = 165.763926;

  b11 = 0.478371;
  b21 = 0.101065;
  b31 = 0.185155;
  b41 = 0.191665;

  b12 = -0.608643;
  b22 = 0.204118;
  b32 = 0.299794;
  b42 = -0.277448;

  b13 = 0.475098;
  b23 = -0.202202;
  b33 = -0.240346;
  b43 = 0.133514;

  b14 = -0.109044;
  b24 = 0.042771;
  b34 = 0.046968;
  b44 = -0.021280;
 }

 else if (p_w <= (p_c * 0.2))
 {
  k1 = 0.051237;
  k2 = 0.688383;
  k3 = 13.763205;
  k4 = 289.841885;

  b11 = 0.515415;
  b21 = 0.199807;
  b31 = 0.138767;
  b41 = 0.087511;

  b12 = -0.618162;
  b22 = 0.298581;
  b32 = -0.001851;
  b42 = -0.067295;
```

```
  b13 = 0.430921;
  b23 = -0.265758;
  b33 = -0.049353;
  b43 = 0.013489;

  b14 = -0.092082;
  b24 = 0.052910;
  b34 = 0.013012;
  b44 = -5.54E-06;
 }

 else if (p_w <= (p_c * 0.4))
 {
  k1 = 0.052694;
  k2 = 0.752776;
  k3 = 11.543306;
  k4 = 252.938841;

  b11 = 0.486247;
  b21 = 0.213959;
  b31 = 0.181991;
  b41 = 0.106180;

  b12 = -0.644137;
  b22 = 0.306543;
  b32 = -0.020460;
  b42 = -0.096088;

  b13 = 0.485654;
  b23 = -0.264417;
  b33 = -0.053791;
  b43 = 0.028114;

  b14 = -0.107808;
  b24 = 0.051889;
  b34 = 0.015058;
  b44 = -0.002443;
 }

 else if (p_w <= (p_c * 0.6))
 {
  k1 = 0.052378;
  k2 = 0.712283;
  k3 = 8.067637;
  k4 = 195.892573;

  b11 = 0.383225;
  b21 = 0.251481;
  b31 = 0.208239;
  b41 = 0.147259;

  b12 = -0.510937;
  b22 = 0.161562;
  b32 = 0.070697;
  b42 = -0.156339;

  b13 = 0.442201;
  b23 = -0.150405;
  b33 = -0.135668;
  b43 = 0.057698;
```

```
  b14 = -0.106398;
  b24 = 0.028982;
  b34 = 0.032090;
  b44 = -0.007266;
 }

 else if (p_w <= (p_c * 0.9))
 {
  k1 = 0.051639;
  k2 = 0.617739;
  k3 = 6.051770;
  k4 = 150.875915;

  b11 = 0.255953;
  b21 = 0.340392;
  b31 = 0.160253;
  b41 = 0.201452;

  b12 = -0.276222;
  b22 = -0.126902;
  b32 = 0.289548;
  b42 = -0.233937;

  b13 = 0.311285;
  b23 = 0.051357;
  b33 = -0.284144;
  b43 = 0.095159;

  b14 = -0.084903;
  b24 = -0.010259;
  b34 = 0.060344;
  b44 = -0.013302;
 }

 else if (p_w <= (p_c * 1.1))
 {
  k1 = 0.051487;
  k2 = 0.571797;
  k3 = 5.398936;
  k4 = 130.622859;

  b11 = 0.164048;
  b21 = 0.412652;
  b31 = 0.112364;
  b41 = 0.238339;

  b12 = -0.087793;
  b22 = -0.339810;
  b32 = 0.450929;
  b42 = -0.288619;

  b13 = 0.195253;
  b23 = 0.197886;
  b33 = -0.388486;
  b43 = 0.121962;

  b14 = -0.063573;
  b24 = -0.038963;
  b34 = 0.079862;
```

```
  b44 = -0.017651;
}

else if (p_w <= (p_c * 2.5))
{
  k1 = 0.054480;
  k2 = 0.555304;
  k3 = 5.040174;
  k4 = 100.372663;

  b11 = -0.002188;
  b21 = 0.546857;
  b31 = -0.001911;
  b41 = 0.317219;

  b12 = 0.286129;
  b22 = -0.714799;
  b32 = 0.764177;
  b42 = -0.415470;

  b13 = -0.048594;
  b23 = 0.452812;
  b33 = -0.581819;
  b43 = 0.186570;

  b14 = -0.016243;
  b24 = -0.088841;
  b34 = 0.115069;
  b44 = -0.028335;
}

else
{
  k1 = 0.060800;
  k2 = 5.608831;
  k3 = 0.676040;
  k4 = 84.540632;

  b11 = -0.053999;
  b21 = -0.094953;
  b31 = 0.606525;
  b41 = 0.369661;

  b12 = 0.434975;
  b22 = 0.952010;
  b32 = -0.853216;
  b42 = -0.517493;

  b13 = -0.152413;
  b23 = -0.696161;
  b33 = 0.545562;
  b43 = 0.244011;

  b14 = 0.005094;
  b24 = 0.136316;
  b34 = -0.107328;
  b44 = -0.038451;
}

        a_1 = b11+b12*(Tcell/1200.0)+b13*pow((Tcell/1200.0),2.0)+b14*pow((Tcell/1200.0),3.0);
```

```
        a_2 = b21+b22*(Tcell/1200.0)+b23*pow((Tcell/1200.0),2.0)+b24*pow((Tcell/1200.0),3.0);
        a_3 = b31+b32*(Tcell/1200.0)+b33*pow((Tcell/1200.0),2.0)+b34*pow((Tcell/1200.0),3.0);
        a_4 = b41+b42*(Tcell/1200.0)+b43*pow((Tcell/1200.0),2.0)+b44*pow((Tcell/1200.0),3.0);

        emi = a_1*(1.0-exp(-k1*p_e*s))+a_2*(1.0-exp(-k2*p_e*s))+ a_3*(1.0-exp(-
k3*p_e*s))+a_4*(1.0-exp(-k4*p_e*s));    /*total emissivity*/

        *ab_wsggm = -1.0/s*log(1.0-emi);  /*gray absorption coefficient,m-1*/

}
```

(3) Steady flow-sheet calculation in oxy-fuel system

The system schematic of 3MW pilot scale boiler is shown in Figure 5.15. The flow rates of primary/secondary air and recycled flue gas can be calculated based on mass and elemental balance. In calculation, the releases of nitrogen and sulfur from coal were not considered.

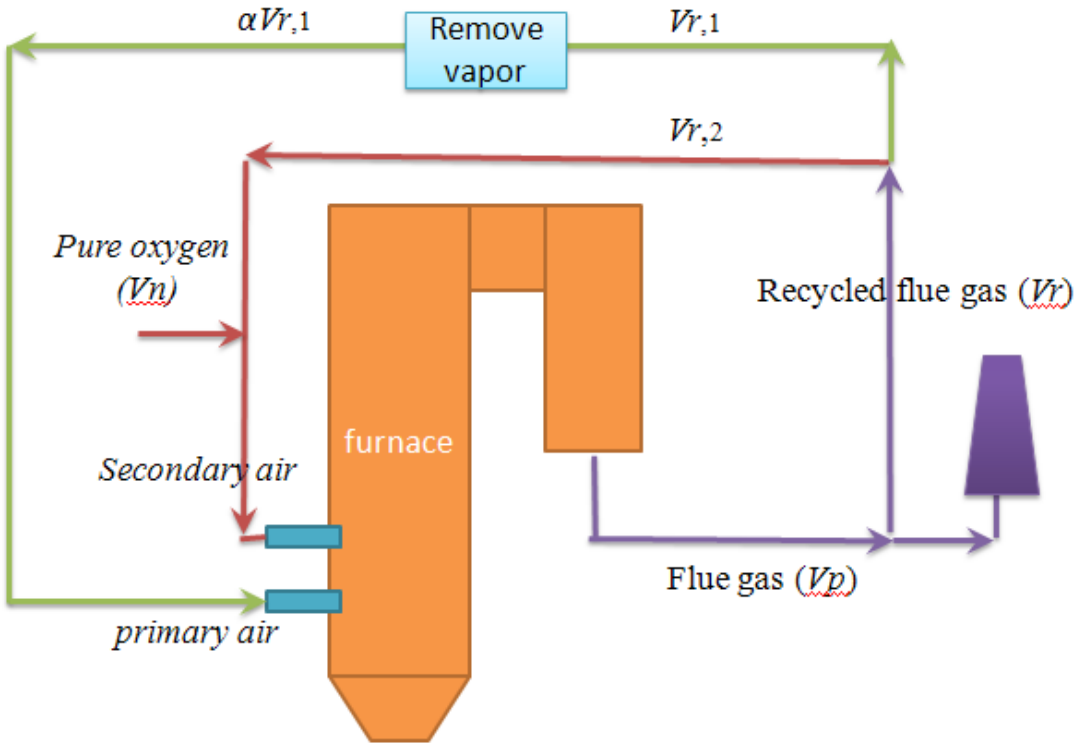

Figure 5.15 Schematic chart of oxy-fuel combustion system

The new pure oxygen flow is calculated as

$$V_n = \frac{V_{O_2,th}\varepsilon}{X_{n,O_2}} \qquad (5\text{-}21)$$

Where $V_{O_2,th}$ is theoretical O_2 amount, ε is excess pure O_2 parameter, X_{n,O_2} is purity of pure oxygen.

The recycled flue gas stream is divided into two parts. The first stream is used to entrain coal particles. The second recycled gas stream is first mixed with pure oxygen and then entering furnace as secondary air. Hence the total recycle flue gas is

$$V_r = V_{r,1} + V_{r,2} \qquad (5\text{-}22)$$

Then the secondary air is ($V_{r,2} + V_n$).

The solid-gas ratio (c) is usually set as 0.5 kg/kg in primary air. This configuration could keep the particles flow continuously into the furnace. Therefore total primary air flow is calculated as

$$\alpha V_{r,1} = \frac{m_{coal}}{c \cdot \rho} \qquad (5\text{-}23)$$

Where ρ is primary-gas density, α is a coefficient considering removed vapour. The Equation (5-24) can be derived from vapour mass balance.

$$\alpha = \frac{1 - X_{p,H2O}}{1 - X_{inlet,H2O}} \qquad (5\text{-}24)$$

Where $X_{inlet,H2O}$ is volume fraction of water vapour in primary air, $X_{p,H2O}$ is volume fraction in produced flue gas . And $\alpha = 1$ means that no vapour removed.

Recycled ratio is defined as

$$re = \frac{V_r}{V_p} \qquad (5\text{-}25)$$

The oxygen concentration entering furnace ($X_{inlet,O2}$) could be set as 27%. On basis of mass balance of oxygen, then:

$$\beta = \frac{X_{in,O2} - X_{inlet,O2}}{X_{in,O2} - X_{p,O2}} = \frac{V_r}{V_n} \qquad (5\text{-}26)$$

Besides above equation, the elemental balances of coal combustion are considered. So the flue gas composition and flow rates can be calculated.

The program is used in FORTRAN software.

```
c    Steady flow-sheet calculation in oxy-fuel system
c    by Jian Zhang, in Aug 2012 in Monash University

          real AR_M,db_a,db_vm,db_fc,db_c,db_h,db_n,db_S,db_o
          real ar_a,ar_vm,ar_fc,ar_c,ar_h,ar_o,ar_n,ar_s
          real dfa_c,dfa_h,dfa_o,dfa_n,dfa_s
          real hhv_ar,lhv_ar,mwt,w_coal,w_coal_pe,V_o2_th
          integer n_1air,n_2air
          real x_n_o2,ex_o2,Vn,nn_o2,nn_n2,x_in_o2,alfa,vr,x_r_o2
          real nr_o2,nr_n2,nr_co2,nr_h2o, c_c,wp_a,wp_c,c_flyash
          real np_co2,np_h2o,np_o2,np_n2
          real vp,recy,np_total,x_p_co2,x_p_h2o,x_p_n2,x_p_o2
          real c_guqi,den_1,v_1,x_1_h2o,beta,vr_1,vr_2,n_remove_h2o
          real r_v1,r_v2,vrr
          real nv1_co2,nv1_h2o,nv1_o2,nv1_n2,nv1_total
          real x_v1_co2,x_v1_h2o,x_v1_o2,x_v1_n2
          real nv2_co2,nv2_h2o,nv2_o2,nv2_n2,nv2_total
          real x_v2_co2,x_v2_h2o,x_v2_o2,x_v2_n2
          real nrr_co2,nrr_h2o,nrr_o2,nrr_n2,nrr_total
          real x_rr_co2,x_rr_h2o,x_rr_o2,x_rr_n2
          real hv_c,hv_vm,wm_vm,n_vm_c,n_vm_h,n_vm_o,n_vm_n,n_vm_s
          real vm_c_0,vm_h_0,vm_o_0,vm_n_0,vm_s_0
          real vm_c,vm_h,vm_o,vm_n,vm_s
          real cvm_vm,cvm_o2,cvm_co2,cvm_h2o,cvm_n2,cvm_so2,h0_vol
          real wcoal_1air
          real f_per1air,f_per2air,c_2air_ccofa,
     +   c_2air_3,c_2air_2,c_2air_1,t_1air,t_2air
          real v_1air,v_real_1air,uu_1air,uu_2air_1
          real v_2air,v_real_2air,uu_2air_ccofa,uu_2air_3,uu_2air_2
          real n2air_o2,n2air_co2,n2air_h2o,n2air_n2,n2air_total
          real x_2air_o2,x_2air_co2,x_2air_h2o,x_2air_n2
          real n1air_o2,n1_air_co2,n1air_h2o,n1air_n2,n1air_total
          real x_1air_o2,x_1air_co2,x_1air_h2o,x_1air_n2
          real np_h2o_dep,np_co2_t,np_h2o_t,np_n2_t,np_o2_t
          real np_total_t,time,x_p_co2_t,x_p_o2_t,x_p_n2_t,x_p_h2o_t

          open(10,file='output.dat')

C------- 1.input   ------------------------------------c
                    open(1,file='input.dat')
                    READ(1,1001) AR_M,db_a,db_vm,db_fc,db_c,db_h,db_n,db_S
                    READ(1,1001) hhv_ar,lhv_ar
                    READ(1,1001) MWT,x_n_o2,c_guqi,ex_o2, X_IN_O2,c_c
                    READ(1,1001) beta,x_1_h2o
                    read(1,1001) time
                    CLOSE(1)
1001                FORMAT(52X,E12.5)
```

```
            x_n_o2=x_n_o2/100.0
            X_IN_O2=X_IN_O2/100.0
            c_c=c_c/100.0
            x_1_h2o=x_1_h2o/100.0

c           den_1=1.293         ! gas density in 1st gas for air-firing
            den_1=1.7           ! gas density in 1st gas for oxy-firing

C-------- 2. Coal property calculation  ----------------------------------------C

            db_o=100.-db_c-db_h-db_n-db_S-db_a

            ar_a=(100.-ar_m)/100.*db_a
            ar_vm=(100.-ar_m)/100.*db_vm
            ar_fc=(100.-ar_m)/100.*db_fc

            ar_c=(100.-ar_m-ar_a)*db_c/(db_c+db_h+db_o+db_n+db_s)
            ar_h=(100.-ar_m-ar_a)*db_h/(db_c+db_h+db_o+db_n+db_s)
            ar_o=(100.-ar_m-ar_a)*db_o/(db_c+db_h+db_o+db_n+db_s)
            ar_n=(100.-ar_m-ar_a)*db_n/(db_c+db_h+db_o+db_n+db_s)
            ar_s=(100.-ar_m-ar_a)*db_s/(db_c+db_h+db_o+db_n+db_s)

            dfa_c=db_c/(100.-db_a)*100.
            dfa_h=db_h/(100.-db_a)*100.
            dfa_o=db_o/(100.-db_a)*100.
            dfa_n=db_n/(100.-db_a)*100.
            dfa_s=db_s/(100.-db_a)*100.

            if(hhv_ar.eq.0.0)then
            hhv_db=(146.58*db_c+568.78*db_h+29.4*db_s-6.58*db_a-
     +   51.53*(db_o+db_n))*0.002326*1000000.
            hhv_ar=hhv_db*(100.-ar_m)/100.
            endif

            if(lhv_ar.eq.0.0)then
            lhv_ar=(hhv_ar-2.25e6*ar_m/100.)-ar_h/100./1./2.*18.*2.25e6
            endif

C-------- 3. Coal feeding rate and gas supplies  ----------------------------------------C

            w_coal=mwt*1.0e6/lhv_ar*3600.

            V_o2_th=(0.0889*(ar_c+0.375*ar_s)+0.265*ar_h-0.0333*ar_o)
     +       *w_coal*0.21

            x_r_o2_0=0.05
            x_r_co2=0.67
            x_r_h2o=0.18
            x_r_o2=x_r_o2_0

100         Vn=V_O2_th*EX_O2/x_n_o2
            nn_o2=vn*x_n_o2/22.4
            nn_n2=vn*(1.-x_n_o2)/22.4

            v_1=w_coal/c_guqi/den_1

            IF(BETA.NE.1)THEN
            beta=(1.-x_r_h2o)/(1.-x_1_h2o)
            ENDIF
```

```
      vr_1=v_1/beta
      n_remove_h2o=(vr_1-v_1)/22.4

      alfa=(x_n_o2-X_IN_O2)/(X_IN_O2-x_r_o2)
      vr=vn*alfa
      x_r_n2=1.-x_r_o2-x_r_co2-x_r_h2o
      nr_o2=x_r_o2*vr/22.4
      nr_n2=x_r_n2*vr/22.4
      nr_co2=x_r_co2*vr/22.4
      nr_h2o=x_r_h2o*vr/22.4

      vr_2=vr-vr_1
      r_v1=vr_1/vr
      r_v2=vr_2/vr

      wp_a=w_coal*(ar_a/100.+ar_s/100.+ar_n/100.)
      wp_c=w_coal*ar_c/100.*(1.-c_c)
      c_flyash=wp_c/(wp_c+wp_a)

      np_co2=w_coal*ar_c/100./12.*c_c + nr_co2
      np_h2o=w_coal*ar_h/100/1./2. +w_coal*ar_m/100./18. +nr_h2o
+     - n_remove_h2o
      np_n2=nr_n2+nn_n2
      np_o2=nn_o2+ nr_o2        + w_coal*ar_o/100./16./2.
+    -(w_coal*ar_c/100./12.*c_c )
+    -(w_coal*ar_h/100./1./4.)
      np_total=np_co2+np_h2o+np_n2+np_o2
      vp=np_total*22.4
      recy=vr/vp

      x_p_co2=np_co2/np_total
      x_p_o2=np_o2/np_total
      x_p_n2=np_n2/np_total
      x_p_h2o=np_h2o/np_total

      rex1=0.5

      if(abs(x_p_co2-x_r_co2)/x_r_co2.gt.1.0e-6.or.
+  abs(x_p_h2o-x_r_h2o)/x_r_h2o.gt.1.0e-6
+   .or.abs(x_p_o2-x_r_o2)/x_r_o2.gt.1.0e-6
+   ) then
      x_r_co2=x_r_co2*(1.-rex1)+x_p_co2*(rex1)
      x_r_h2o=x_r_h2o*(1.-rex1)+x_p_h2o*(rex1)
      x_r_o2=x_r_o2*(1.-rex1)+x_p_o2*(rex1)
      goto 100
      endif

      v_1air=v_1
      v_real_1air=v_1air*t_1air/273.15
      uu_1air=v_real_1air/3600./n_1air/f_per1air
      v_2air=vr_2+vn
      v_real_2air=v_2air*t_2air/273.15
      uu_2air_ccofa=v_real_2air*c_2air_ccofa/4./f_per2air/3600.
      uu_2air_3=v_real_2air*c_2air_3/4./f_per2air/3600.
      uu_2air_2=v_real_2air*c_2air_2/4./f_per2air/3600.
      uu_2air_1=v_real_2air*c_2air_1/4./f_per2air/3600.
      n2air_o2=nn_o2+np_o2*recy*r_v2
      n2air_co2=np_co2*recy*r_v2
      n2air_h2o=np_h2o*recy*r_v2
      n2air_n2=nn_n2+np_n2*recy*r_v2
```

```
      n2air_total=n2air_o2+n2air_co2+n2air_h2o+n2air_n2
      x_2air_o2=n2air_o2/n2air_total
      x_2air_co2=n2air_co2/n2air_total
      x_2air_h2o=n2air_h2o/n2air_total
      x_2air_n2=n2air_n2/n2air_total
      n1air_o2=np_o2*recy*r_v1
      n1air_co2=np_co2*recy*r_v1
      n1air_h2o=np_h2o*recy*r_v1-n_remove_h2o
      n1air_n2=np_n2*recy*r_v1
      n1air_total=n1air_o2+n1air_co2+n1air_h2o+n1air_n2
      x_1air_o2_0=n1air_o2/n1air_total
      x_1air_co2_0=n1air_co2/n1air_total
      x_1air_h2o_0=n1air_h2o/n1air_total
      x_1air_n2_0=n1air_n2/n1air_total
      x_1air_h2o=1.0-(1.0-x_r_h2o)/beta
      x_1air_o2=(1.-x_1air_h2o)*x_1air_o2_0
     +  /(x_1air_co2_0+x_1air_o2_0+x_1air_n2_0)
      x_1air_co2=(1.-x_1air_h2o)*x_1air_co2_0
     +  /(x_1air_co2_0+x_1air_o2_0+x_1air_n2_0)
      x_1air_n2=(1.-x_1air_h2o)*x_1air_n2_0
     +  /(x_1air_co2_0+x_1air_o2_0+x_1air_n2_0)

C-------- 4. Water vapor deposition in furnace  ------------------------------C

      np_h2o_dep=w_coal*ar_h/100./1./2. +w_coal*ar_m/100./18.
     +  - n_remove_h2o-(1.0-recy)*vr*x_p_h2o/22.4

      np_co2_t=np_co2
      np_h2o_t=np_h2o+np_h2o_dep*time
      np_n2_t=np_n2
      np_o2_t=np_o2
      np_total_t=np_co2_t+np_h2o_t+np_n2_t+np_o2_t

      x_p_co2_t=np_co2_t/np_total_t
      x_p_o2_t=np_o2_t/np_total_t
      x_p_n2_t=np_n2_t/np_total_t
      x_p_h2o_t=np_h2o_t/np_total_t

C-------- 5. output  ----------------------------------------C

      write(10,*)'Properties of coal:'
      write(10,*)'high heating value of ar coal (J/kg) =',hhv_ar
      write(10,*)'low heating value of ar coal  (J/kg) =',lhv_ar
      write(10,*)
      write(10,*)'operating conditions:'
      WRITE(10,*)'total coal mass              (kg/h) =',W_COAL
      write(10,*)'total primary air flux      (Nm3/h) =',v_1air
      write(10,*)'total secondary air         (Nm3/h) =',v_2air
      write(10,*)'pure O2 in secondary air    (Nm3/h) =',Vn
      write(10,*)'total flue gas produced     (Nm3/h) =',Vp
      write(10,*)'backflow ratio              (vol%)  =',recy*100.
      write(10,*)'total recycled flue gas     (Nm3/h) =',Vr
      write(10,*)'remove H2O                  (Kmol/h) =',n_remove_h2o
      write(10,*)'carbon content in fly ash     (wt%) =',c_flyash*100.
      write(10,*)

      if(BETA.NE.1)then
      write(10,*)'component of primary air:'
      write(10,*)'x_o2  in primary air         (vol%) =',x_1air_o2*100.
      write(10,*)'x_co2 in primary air         (vol%) =',x_1air_co2*100
```

```
      write(10,*)'x_h2o in primary air         (vol%) =',x_1air_h2o*100
      write(10,*)'x_n2  in primary air         (vol%) =',x_1air_n2*100.
      write(10,*)
      write(10,*)'Component of secondary air:'
      write(10,*)'x_o2  in secondary air       (vol%) =',x_2air_o2*100.
      write(10,*)'x_co2 in secondary air       (vol%) =',x_2air_co2*100
      write(10,*)'x_h2o in secondary air       (vol%) =',x_2air_h2o*100
      write(10,*)'x_n2  in secondary air       (vol%) =',x_2air_n2*100.
      write(10,*)
      endif

      write(10,*)'Component of flue gas:'
      write(10,*)'x_co2 in flue gas            (vol%) =',x_p_co2*100.
      write(10,*)'x_h2o in flue gas            (vol%) =',x_p_h2o*100.
      write(10,*)'x_o2  in flue gas            (vol%) =',x_p_o2*100.
      write(10,*)'x_n2  in flue gas            (vol%) =',x_p_n2*100.
      write(10,*)

      if(time.ne.0.0)then
      write(10,*)'h2o deposited in furnace (kmol/h) =',np_h2o_dep
      write(10,*)'Component of flue gas after hours:'
      write(10,*)'x_co2 in flue gas       (vol%) =',x_p_co2_t*100
      write(10,*)'x_h2o in flue gas       (vol%) =',x_p_h2o_t*100
      write(10,*)'x_o2  in flue gas       (vol%) =',x_p_o2_t*100.
      write(10,*)'x_n2  in flue gas       (vol%) =',x_p_n2_t*100.
      endif

200   continue
      close(10)
      end
```

(4) Transient flow-sheet calculation in oxy-fuel system.

The program is used in FORTRAN software.

```
c  Transient flow-sheet calculation in oxy-fuel system for 3MW pilot-scale facility
c        For the transient progress of mode shift , form air-firing to oxy-firing
c  by Jian Zhang, in January 2013 in Monash University

      real AR_M,db_a,db_vm,db_fc,db_c,db_h,db_n,db_S
      real hhv_ar,lhv_ar,MWT,ex_air,c_c
      real t_1,t_2,t_3,t_4,h_1,h_2,h_3,h_4,s_1,s_2,s_3,s_4
      real db_o,ar_a,ar_vm,ar_fc
      real ar_c,ar_h,ar_o,ar_n,ar_s
      real dfa_c,dfa_h,dfa_o,dfa_n,dfa_s
      real w_coal,v_air_th,v_air,V_o2
      real n_air_co2,n_air_so2,n_air_h2o,n_air_n2,n_air_o2
      real N_AIR_TOTAL,v_air_fluegas
      real X_AIR_CO2,X_AIR_O2,X_AIR_SO2,X_AIR_H2O,X_AIR_N2
      real x_air_no,n_air_no,c_air_leak,v_air_leak
      REAL v_oxy_fluegas,vel_1,dt_1,vel_2,dt_2
      real vel_3,dt_3,vel_4,dt_4,dtime,time
      real r_recycle,v_oxy_o2,c_o2
      real X_oxy_CO2,X_oxy_O2,X_oxy_SO2,X_oxy_H2O,X_oxy_N2,x_oxy_no
      REAL V_OXY_RECYCLE,V_OXY_INLET
      real n_in_o2,n_in_n2,n_in_co2,n_in_h2o,n_in_so2,n_in_no,n_in_total
```

```
      real x_in_o2,x_in_n2,x_in_co2,x_in_h2o,x_in_so2,x_in_no
      real c_oxy_leak,v_oxy_leak,N_oxy_TOTAL
      real n_oxy_co2,n_oxy_so2,n_oxy_h2o,n_oxy_no,n_oxy_n2,n_oxy_o2


      open(10,file='output-aircombust.dat')
      open(20,file='output-oxycombust.dat')
c     open(30,file='output-oxy-checkcode.dat')

            open(1,file='input.dat')
            READ(1,1001) AR_M,db_a,db_vm,db_fc,db_c,db_h,db_n,db_S
            READ(1,1001) hhv_ar,lhv_ar
            READ(1,1001) MWT,ex_air,c_air_leak
            read(1,1001) r_recycle, V_oxy_o2, c_o2, c_oxy_leak
            read(1,1001) c_c

      read(1,1001) t_1, t_2, t_3, t_4     !c, gas temperature in burner zone, burnout zone, rest furnace
   zone and recycled flue gas pipe
      read(1,1001) h_1, h_2, h_3, h_4  !m, height in burner zone, burnout zone, rest furnace zone
   and recycled flue gas pipe

            CLOSE(1)
1001        FORMAT(52X,E12.5)


      if((db_a+db_vm+db_fc-100.00).gt.1e-3)then
      write(*,*)'Pls check the proximate analysis!','  total=',
     +    db_a+db_vm+db_fc
      endif

      c_c=c_c/100.0

c size
      S_1=1.2*1.2          !m2, cross-section square in burner zone
      S_2=1.2*1.2          !m2, cross-section square in burnout zone
      s_3=1.2*0.8          !m2, cross-section square in rest furnace
      s_4=3.1415926*(0.46/2)**2   !m2, cross-section square in recycled flue gas pipe

C-------- 1. Coal property calculation  ----------------------------------------C

      db_o=100.-db_c-db_h-db_n-db_S-db_a
      ar_a=(100.-ar_m)/100.*db_a
      ar_vm=(100.-ar_m)/100.*db_vm
      ar_fc=(100.-ar_m)/100.*db_fc
      ar_c=(100.-ar_m-ar_a)*db_c/(db_c+db_h+db_o+db_n+db_s)
      ar_h=(100.-ar_m-ar_a)*db_h/(db_c+db_h+db_o+db_n+db_s)
      ar_o=(100.-ar_m-ar_a)*db_o/(db_c+db_h+db_o+db_n+db_s)
      ar_n=(100.-ar_m-ar_a)*db_n/(db_c+db_h+db_o+db_n+db_s)
      ar_s=(100.-ar_m-ar_a)*db_s/(db_c+db_h+db_o+db_n+db_s)
      dfa_c=db_c/(100.-db_a)*100.
      dfa_h=db_h/(100.-db_a)*100.
      dfa_o=db_o/(100.-db_a)*100.
      dfa_n=db_n/(100.-db_a)*100.
      dfa_s=db_s/(100.-db_a)*100.

      if(hhv_ar.eq.0.0)then
      hhv_db=(146.58*db_c+568.78*db_h+29.4*db_s-6.58*db_a-
     +  51.53*(db_o+db_n))*0.002326*1000000.      !j/kg(db) mason & Gandhi
      hhv_ar=hhv_db*(100.-ar_m)/100.               !j/kg(ar)
      endif
```

```
      if(lhv_ar.eq.0.0)then
      lhv_ar=(hhv_ar-2.25e6*ar_m/100.)-ar_h/100./1./2.*18.*2.25e6  !j/kg(ar), fluent
      endif

      write(10,*)'(1)Properties of coal:'
      write(10,11)'volatile       ar     (wt*100%) =',ar_vm/100.
      write(10,11)'fixed carbon   ar     (wt*100%) =',ar_fc/100.
      write(10,11)'ash            ar     (wt*100%) =',ar_a/100.
      write(10,11)'moisture       ar     (wt*100%) =',ar_m/100.
      write(10,11)'C              ar     (wt*100%) =',ar_c/100.
      write(10,11)'H              ar     (wt*100%) =',ar_H/100.
      write(10,11)'O              ar     (wt*100%) =',ar_O/100.
      write(10,11)'N              ar     (wt*100%) =',ar_N/100.
      write(10,11)'S              ar     (wt*100%) =',ar_S/100.

      write(10,11)'C             DAF     (wt*100%) =',dfa_c/100.
      write(10,11)'H             DAF     (wt*100%) =',dfa_h/100.
      write(10,11)'O             DAF     (wt*100%) =',dfa_o/100.
      write(10,11)'N             DAF     (wt*100%) =',dfa_n/100.
      write(10,11)'S             DAF     (wt*100%) =',dfa_s/100.
      write(10,*)'high heating value of ar coal (J/kg) =',hhv_ar
      write(10,*)'low heating value of ar coal  (J/kg) =',lhv_ar
      write(10,*)
11              FORMAT(A35,f10.4)
12              FORMAT(A35,f10.2)

C-------- 2. Air-firing calculation  ----------------------------------------C

      w_coal=mwt*1.0e6/lhv_ar*3600.        !kg(AR)/h
      v_air_th=(0.0889*(ar_c+0.375*ar_s)+0.265*ar_h-0.0333*ar_o)*w_coal  !nm3(air)/h
      v_air=v_air_th*ex_air
      V_o2=v_air*0.21      !NM3(o2)/h

      write(10,*)'(2)air combustion operating conditions:'
      WRITE(10,*)'total coal mass         (kg/h)  =',W_COAL
      write(10,*)'total air flux          (Nm3/h) =',v_air
      write(10,*)'total o2 flux           (Nm3/h) =',v_o2

      v_air_leak=v_air*c_air_leak  !nm3/h
      n_air_co2=ar_c/100.0*c_c*w_coal/12.0   !KMOL/H
      n_air_so2=ar_s/100.0*c_c*w_coal/32.0
      n_air_h2o=ar_h/100.0*w_coal/1.0/2.0+ar_m/100.0*w_coal/18.0
      n_air_no=ar_n/100.0*w_coal/14.0/2.0
      n_air_n2=v_air*0.79/22.4 +v_air_leak/22.4*0.79
      n_air_o2=ar_o/100.0*w_coal/16.0/2.0+V_o2/22.4-n_air_co2-
     +         ar_h/100.0*w_coal/1.0/4.0-n_air_so2-n_air_no/2.0
     +         +v_air_leak/22.4*0.21
      N_AIR_TOTAL=n_air_co2+n_air_so2+n_air_h2o+n_air_n2+n_air_o2
     +        +n_air_no
      v_air_fluegas=n_air_total*22.4    !nm3/h

      X_AIR_CO2=N_AIR_CO2/N_AIR_TOTAL
      X_AIR_O2=N_AIR_O2/N_AIR_TOTAL
      X_AIR_SO2=N_AIR_SO2/N_AIR_TOTAL
      X_AIR_H2O=N_AIR_H2O/N_AIR_TOTAL
      X_AIR_N2=N_AIR_N2/N_AIR_TOTAL
      x_air_no=N_AIR_no/N_AIR_TOTAL
```

```
      write(10,12)'total leakage air flux   (Nm3/h) =',
     +      v_air_leak
      write(10,12)'real exess air parameter        =',
     + (v_air+v_air_leak)/v_air_th

            WRITE(10,*)
            WRITE(10,*)'(3)fluegas in air combustion:'
      write(10,12)'total flue gas flux     (Nm3/h) =',
     +      v_air_fluegas
      WRITE(10,12)'o2   con in flue gas     (vol%) =',X_AIR_O2*100.
      WRITE(10,12)'co2  con in flue gas     (vol%) =',X_AIR_cO2*100.
      WRITE(10,12)'h2o  con in flue gas     (vol%) =',X_AIR_h2o*100.
      WRITE(10,12)'n2   con in flue gas     (vol%) =',X_AIR_n2*100.
      WRITE(10,12)'so2  con in flue gas     (vol%) =',X_AIR_sO2*100.
      WRITE(10,12)'no   con in flue gas     (vol%) =',X_AIR_no*100.


C-------- 3. Mode shift to oxy-firing  ----------------------------------------C

      v_oxy_fluegas=v_air_fluegas   !nm3/h
      X_oxy_CO2=x_air_co2
      X_oxy_O2=X_AIR_O2
      X_oxy_SO2=X_AIR_sO2
      X_oxy_H2O=X_AIR_h2o
      X_oxy_N2=X_AIR_n2
      x_oxy_no=X_AIR_no
      time=0.0 ; dtime=0.0

      write(20,21)'time(s)','dtime(s)','r_ryl(vol%)','v_in(nm3/h)',
     +  'v_ryl(nm3/h)',
     +  'v_o2(nm3/h)','V_gas(nm3/h)',
     +  'X_in_o2','X_in_co2','X_in_H2O','X_in_N2',
     +  'x_oxy_o2','x_oxy_co2','x_oxy_H2O','x_oxy_N2'
21      format(2A9,5A13,8a10)

      write(20,22)time,dtime,'0.0',v_air,'0.0',
     +  v_air_o2,v_air_fluegas,
     +  '0.21','0.0','0.0','0.79',
     +  x_air_o2,x_air_co2,x_air_H2O,x_air_N2
22      format(1x,f6.1,1x,f8.1,a13,f13.3,a13,2f13.3,4a10,4f10.3)

100     CONTINUE

      vel_1=v_oxy_fluegas/3600.0*(273.0+t_1)/273.0/s_1
      dt_1=H_1/vel_1
      vel_2=v_oxy_fluegas/3600.0*(273.0+t_2)/273.0/s_2
      dt_2=H_2/vel_2
      vel_3=v_oxy_fluegas/3600.0*(273.0+t_3)/273.0/s_3
      dt_3=H_3/vel_3
      vel_4=v_oxy_fluegas/3600.0*(273.0+t_4)/273.0/s_4
      dt_4=H_4/vel_4
      dtime=dt_1+dt_2+dt_3+dt_4
      time=time+dtime


      v_oxy_recycle=r_recycle*v_oxy_fluegas
      v_oxy_inlet=v_oxy_recycle+v_oxy_o2
      v_oxy_leak=v_oxy_inlet*c_oxy_leak

      n_in_o2=v_oxy_recycle/22.4*x_oxy_o2 +v_oxy_o2/22.4*c_o2
```

```
      n_in_n2=v_oxy_recycle/22.4*x_oxy_n2 +v_oxy_o2/22.4*(1.0-c_o2)
      n_in_co2=v_oxy_recycle/22.4*x_oxy_co2
      n_in_h2o=v_oxy_recycle/22.4*x_oxy_h2o
      n_in_so2=v_oxy_recycle/22.4*x_oxy_so2
      n_in_no=v_oxy_recycle/22.4*x_oxy_no
      n_in_total=n_in_o2+n_in_n2+n_in_co2+n_in_h2o
     +  n_in_so2+n_in_no

      x_in_o2=n_in_o2/n_in_total
      x_in_n2=n_in_n2/n_in_total
      x_in_co2=n_in_co2/n_in_total
      x_in_h2o=n_in_h2o/n_in_total
      x_in_so2=n_in_so2/n_in_total
      x_in_no=n_in_no/n_in_total

      n_oxy_co2=ar_c/100.0*c_c*w_coal/12.0  +
     +    v_oxy_recycle/22.4*X_oxy_Co2  !KMOL/H
      n_oxy_so2=ar_s/100.0*c_c*w_coal/32.0 +
     +    v_oxy_recycle/22.4*X_oxy_so2  !KMOL/H
      n_oxy_h2o=ar_h/100.0*w_coal/1.0/2.0+ar_m/100.0*w_coal/18.0+
     +     v_oxy_recycle/22.4*X_oxy_h2o  !KMOL/H
      n_oxy_no=ar_n/100.0*w_coal/14.0/2.0 +
     +   v_oxy_recycle/22.4*X_oxy_no
      n_oxy_n2=v_oxy_leak/22.4*0.79 +
     +   v_oxy_recycle/22.4*X_oxy_n2  +
     +   v_oxy_o2/22.4*(1-c_o2)
      n_oxy_o2=ar_o/100.0*w_coal/16.0/2.0-n_air_co2-
     +        ar_h/100.0*w_coal/1.0/4.0-n_air_so2-n_air_no/2.0
     +        +v_oxy_leak/22.4*0.21 +
     +       v_oxy_recycle/22.4*X_oxy_o2   +
     +       v_oxy_o2/22.4*c_o2
      N_oxy_TOTAL=n_oxy_co2+n_oxy_so2+n_oxy_h2o+n_oxy_n2+n_oxy_o2
     +       +n_oxy_no
      v_oxy_fluegas=n_oxy_total*22.4

      X_oxy_CO2=N_oxy_CO2/N_oxy_TOTAL
      X_oxy_O2=N_oxy_O2/N_oxy_TOTAL
      X_oxy_SO2=N_oxy_SO2/N_oxy_TOTAL
      X_oxy_H2O=N_oxy_H2O/N_oxy_TOTAL
      X_oxy_N2=N_oxy_N2/N_oxy_TOTAL
      x_oxy_no=N_oxy_no/N_oxy_TOTAL

      write(20,23)time,dtime,r_recycle,v_oxy_inlet,v_oxy_recycle,
     +  v_oxy_o2,v_oxy_fluegas,
     +  X_in_o2,X_in_co2,
     +  X_in_H2O,X_in_N2,
     +  x_oxy_o2,x_oxy_co2,x_oxy_H2O
     +  ,x_oxy_N2
23      format(1x,f6.1,1x,f8.1,5f13.3,2f10.3,2f10.3
     +  ,3f10.3 ,f10.3 )


      if(time.lt.3600.00)then
      goto 100
      endif

      close(10)
      close(20)
c     close(30)
      end
```

5.5 Conclusions

The numerical modeling of the combustion of air-dried Victorian brown coal in O_2/N_2 and O_2/CO_2 mixtures has been conducted via the use of computational fluid dynamics (CFD), Ansys-Fluent 13.0, in which a series of updated sub-models have been added into the codes. And the main conclusions or achievements are summarized as follows.

(1) The advanced oxy-fuel models are employed in the FLUENT modeling, including the refined Weighted-Sum-of-Grey-Gases (WSGG) model, the single-film model with multiple surface reactions (i.e. char-O_2, char-CO_2, and char-H_2O) for char particle as well as the refined two-step mechanism for the oxy-firing of methane to mimic the volatile oxidation.

(2) The purposes of the modeling based on the experimental data in a lab-scale drop-tube furnace (DTF) are to promote the understanding on the details underpinning the combustion characteristics of Victorian brown coal. The air-dried Victorian brown coal bears an extremely high reactivity for devolatilisation, char-O_2 and char-CO_2 reactions. As has been confirmed, the modeling results show good agreement with the experimental measurements on particle temperature, coal ignition delay photographed by high-speed camera, carbon burnout rate and particle velocity.

(3) Increasing the secondary gas temperature greatly narrowed down coal ignition delay caused by the substitution of 21% O_2 balanced in CO_2 for air. At the furnace temperatures of 1073 K and 1273 K, the contribution of char-CO2 to coal burnout reached approximately 10% and 25% in the oxy-fuel mode, respectively, which in turn reduced coal particle temperature by maximum 300 K.

6. Properties of fly ash, slagging/fouling and deposition propensity in oxy-fuel combustion process

Ash formation during coal combustion is complex, which is governed by a variety of factors including the mode of occurrence of the inherent ash-forming elements in the raw coal, combustion temperature, and local gas environment on char surface. As discussed in the subsection for coal burnout, the C-CO_2 and C-H_2O gasification reactions are supposed to occur on char surface, which in turn reduce char particle temperature, whilst enhance the concentrations of reducing gases (CO and H_2) on char surface. These two consequences affect the ash formation in an opposite manner, *i.e.* reducing particle temperature favours weakening ash melting propensity, whilst enhancing the concentrations of reducing gases favours ash melting. In this sense, the ash formation under oxy-firing is expected to differ noticeably from air-firing case. Moreover, the deposition mechanisms for ash in a coal-fired boiler are determined by three forces, inertia impaction, thermopherisis, and diffusion, each of which applies to different ash particle size, *i.e.* inertia impaction for the ash size >10 μm, thermopherisis for ash particle in the range of 1-10 μm, and diffusion for the size <1 μm. Except the thermopherisis force is affected by gas temperature, the other two are affected by gas flow rate and the slip velocity of ash particles. Given the fact that the total gas flow rate in the oxy-firing mode is 1.3 less than the air-firing mode, it is very likely that the ash inertia impaction force for coarse ash particle size would be reduced, which in turn minimises the amount of ash that could deposit on the water tube surface. The proposed project targets clarifying these special issues and their changes upon coal moisture content and flue gas composition, and eventually, provides credible datasets for design/modification and optimised operating conditions to incorporate both dry and wet Victorian brown coal for oxy-fuel combustion.

6.1 Ash sampling and analysis

During the past two years, we did several experiment runs on 3MW boiler with our collaboration partners Shanghai Boiler Works. To clarify the ash slagging/fouling and deposition properties, both silicon rod and probe with cooling oil were used for ash sampling in typical different temperature zone along the furnace. Figure 6.1 shows the silicon carbide and probe with cooling oil which were used for ash deposit sampling.

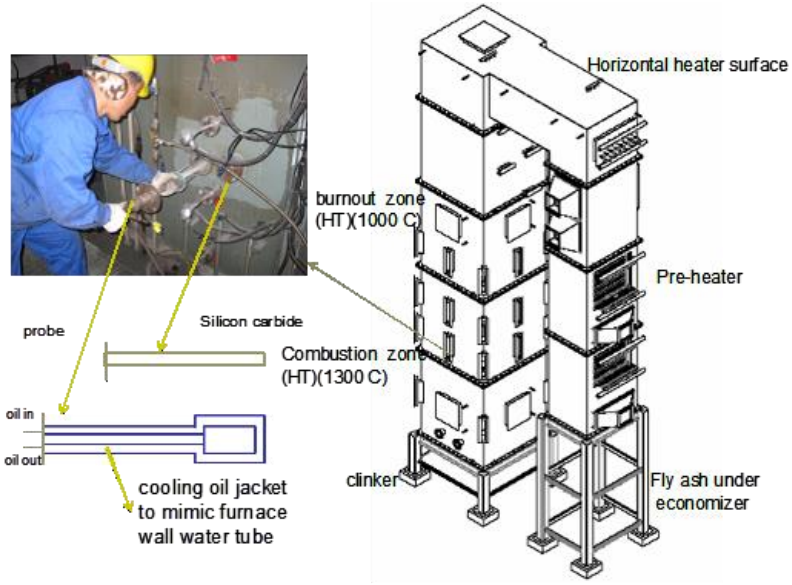

Figure 6.1 Ash deposition probes used for ash collection through the boiler

For each condition, apart from on-line sampling of flue gas components, around 20-36 ash samples was generated, all of which were characterised by the combination of a number of advanced facilities including XRD, XRF, ICP-OES, TMA and XAS, as detailed on next page for Yallourn coal.

Figure 6.2 visualises the ash deposits collected from the probes installed at the flame size in the combustion zone, for the combustion of fully dried Yallourn coal under the air-firing mode at a thermal capacity of 0.9 MW_{th}. The flue gas temperature achieved is around 1300^{o}C that is similar with the industrial boiler. The combustion lasted five hours. As can be seen, the reddish ash powders form thick layer on the silicon carbide probe without the use of cooling water jacket. However, once the combustion mode was changed to the oxy-firing mode, less ash was deposited on the tubes, as illustrated in figure 7.3. One major reason is the lower flue gas temperature achieved under the oxy-firing mode. Due to the low flue gas temperature, less of ash particles were melted, and hence, stacked loosely on the probe. As the exposure time was very short, a concrete conclusion on if less ash was melted in oxy-firing mode can not yet be achieved here. However, it is very promising that the ash slagging and fouling propensity for brown coal could be minimised under the oxy-firing mode, given the facts that flame/gas/particle temperatures are lower, and gas flow rate is smaller in the oxy-firing mode. Both of them are in favour of minimising ash slagging and fouling propensity. It is interesting to further explore this issue in the future research.

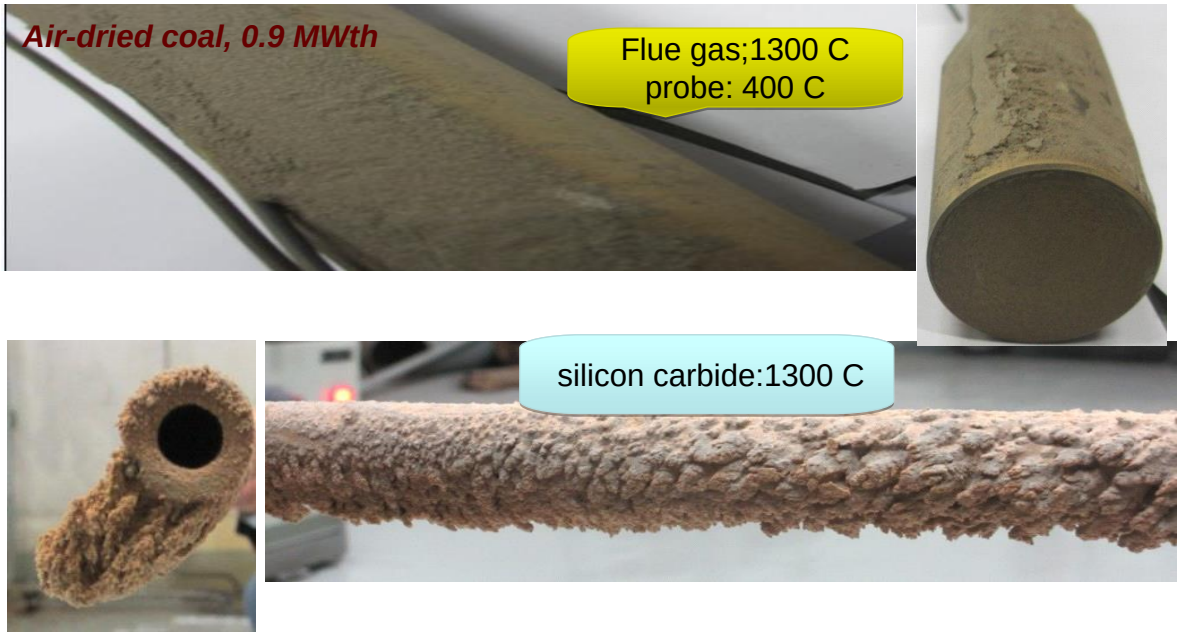

Figure 6.2 Ash deposits collected on the probes installed at flameside in the combustion zone, for the combustion of fully dried Yallourn coal in air

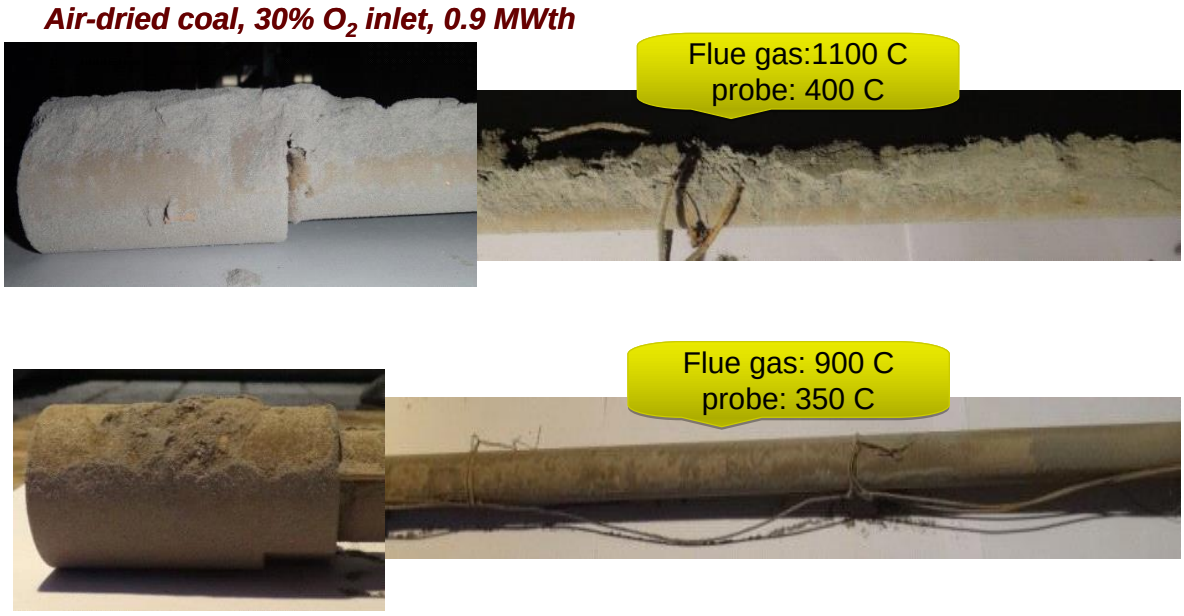

Figure 6.3 Ash deposits collected on the probes installed at flame-side in the combustion zone, for the combustion of fully dried Yallourn coal in oxy-firing mode with 30% O_2 in the furnace.

6.2 Properties of air-firing ash samples

Three dried Victorian brown coal samples with a moisture content of around 20 *wt%* were further burned in May 2013 to collect their fly ash and deposits under the air-fired conditions. The furnace thermal load is 0.9 M with a maximum flue gas temperature of around 1099^{o}C in the combustion zone. The oxygen excess ratio remains at 20% for all the tests.

The fly ash collected from the three coals bear a very fine particle size distribution, as shown in figure 6.4. There are two major peaks formed, one being around 7 μm and another one ~50 μm. The former peak size refers to the condensed fine/ultra-fine ash particles formed by vaporisation-condensation route. The latter one should be formed by particle agglomeration. The typical sizes are further visualised in figure 6.5, which is the SEM pictures for Yallourn fly ash.

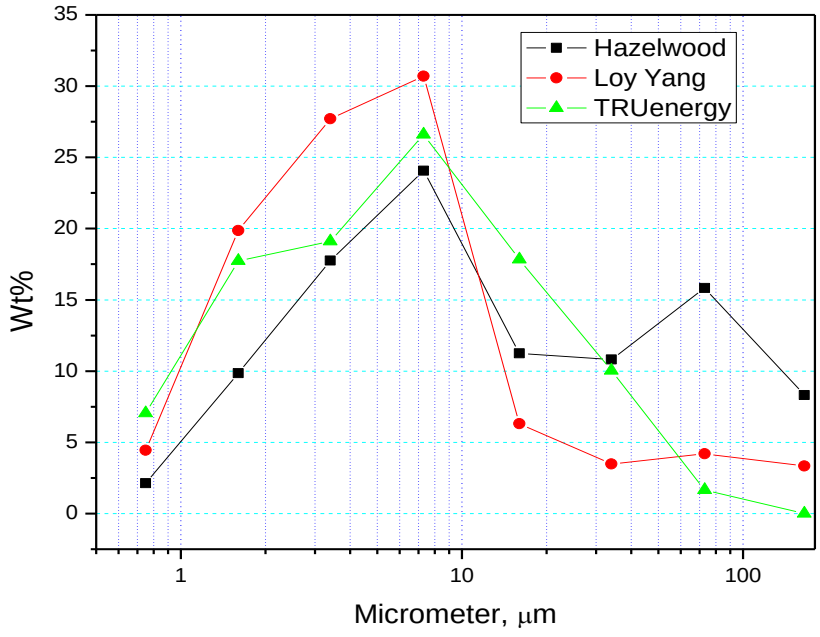

Figure 6.4 particle size distribution of fly ash samples collected from Air combustion of three coals.

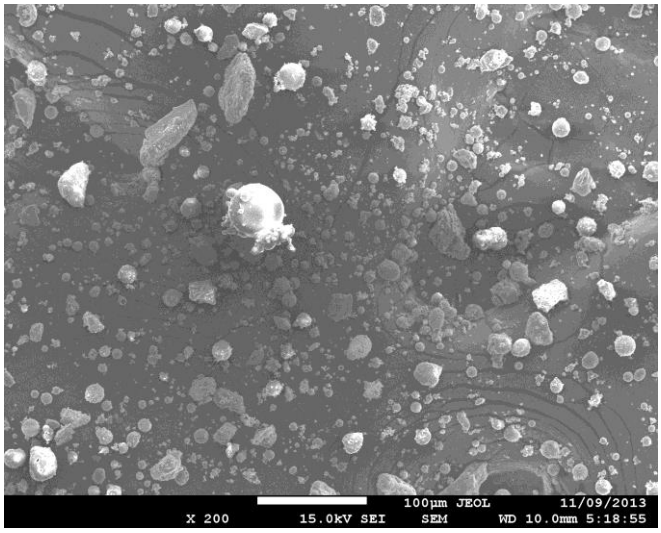

Figure 6.5 SEM photo for Yallourn coal fly ash

The XRF characterisation results for elemental composition of three fly ashes are tabulated in table 6.1. Calcium and magnesium are rich in Hazelwood and Loy Yang fly ash samples, whereas in TRUenergy fly ash both iron and magnesium oxides are abundant. In particular, iron oxide accounts for 43.9 *wt%* in TRUenergy fly ash. XRF analysis on the bottom ash and ash deposits collected from Yallourn coal combustion is further tabulated in table 6.2, where one can see the abundance of iron in the other two ash samples as well. Magnesium oxide and SO_3 are less present in bottom ash, most of which are present in fly ash. This implies the sulfation of alkali and alkaline earth metals during flue gas cooling in post-flame zones in the furnace. Instead, silicon is most prevalent in bottom ash, suggestive of the agglomeration of this refractory metal with others upon melting and coalescence.

Table 6.1 XRF results for air-fired fly ash compositions, *wt%*

	Int'l Power Hazelwood	Loy Yang	TruEnergy
SiO2	5.36	2.11	11.30
Al2O3	2.60	2.14	6.98
Fe2O3	0.03	9.66	43.90
CaO	30.00	27.40	8.49
MgO	25.80	23.50	23.00
TiO2	0.43	0.00	0.54
NaO	6.58	8.91	1.01
K2O	0.48	0.46	0.32
P2O5	0.04	0.00	0.07
SO3	15.10	22.80	2.63
MnO	11.20	0.21	0.63
ZnO	0.03	0.03	0.00
BaO	0.00	0.00	0.86

Table 6.2 XRF results for bottom ash and ash deposits collected from Yallourn coal combustion, *wt%*.

	Bottom ash	Deposit	Fly ash
Na2O	0	4.5	5
MgO	5.1	14.1	16.4
Al2O3	8.1	16.4	4.2
SiO2	34.4	18.1	6.2
Fe2O3	39.1	31.6	46.3
P2O5	0.12	0.13	0
SO3	4.3	6.4	11.1
Cl	0.86	0.34	0.18
K2O	0.85	1.3	0.23
CaO	5.8	6.3	9.7
TiO2	1	1.3	0.34
Cr2O3	0.23	0.083	0
MnO	0.34	0.77	0.64
NiO	0	0.045	0

To examine the chemical structures in all the ash samples, the combination of X-ray diffraction (XRD) and sequential acid leaching was conducted. The sequential leaching follows a classic scheme for the speciation of modes of occurrence of individual metals in fly ash matrix, as shown in figure 6.6. For each leaching, it takes around 1 hr and the liquid to solid ratio remains at 10. The residue from each leaching step was analysed by both XRF and XRD. The resulting XRD spectra for Hazelwood fly ash are summarised in figure 6.7. Quartz (SiO_2) and anhydrite ($CaSO_4$) are the major species formed, followed by lime (CaO) and periclase (MgO). The latter two species were readily washed away by ammonia acetate mixed with acetic acid. The similar results apply to Loy Yang fly ash as shown in figure 6.8. The periclase (MgO) is Loy Yang ash is more prevalent than in Hazelwood fly ash. The ash properties of Yallourn coal fly ash are very different. As illustrated in figure 6.9, magnesia ferrite ($MgFe_2O_4$) is most prevalent, followed by quartz, anhydrite and a small amount of lime (CaO). The peaks for magnesia ferrite overlap significantly with magnetite (Fe_3O_4) and maghemite (γ-Fe_2O_3).

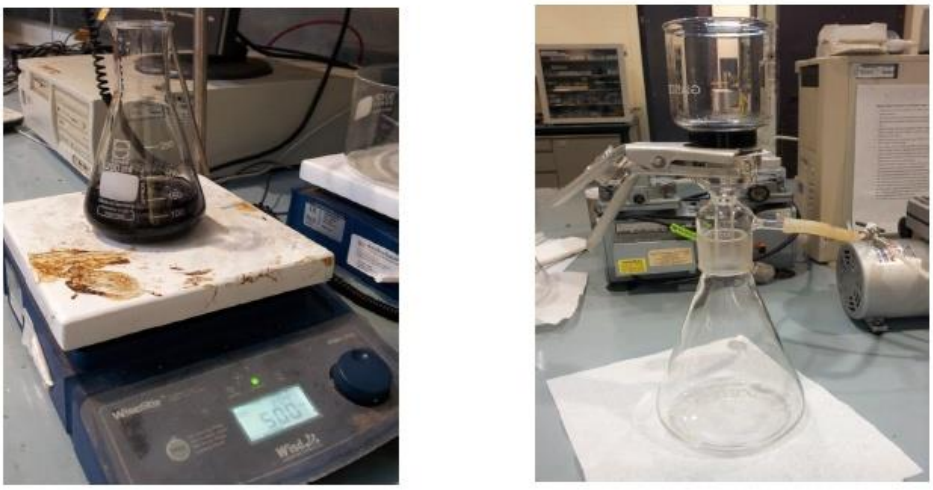

Figure 6.6 The process of coal washing and leaching

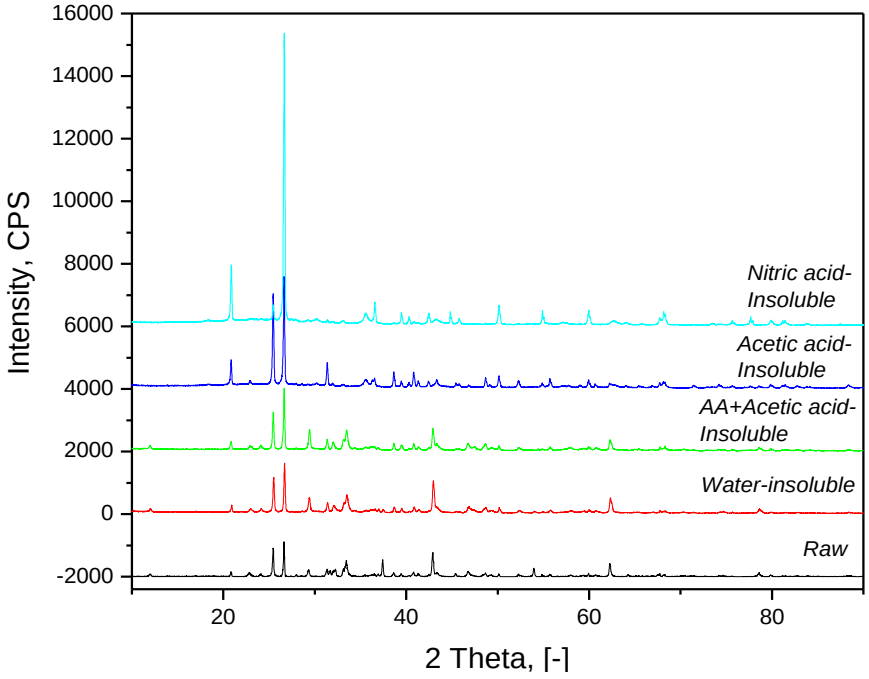

Figure 6.7 Hazelwood fly ash XRD spectra.

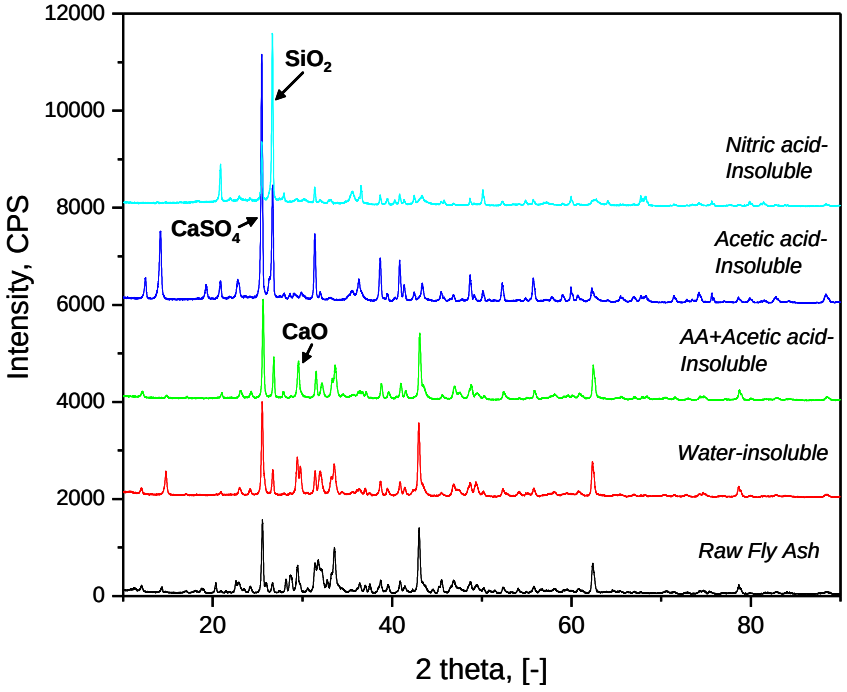

Figure 6.8 Loy Yang coal fly ash spectra

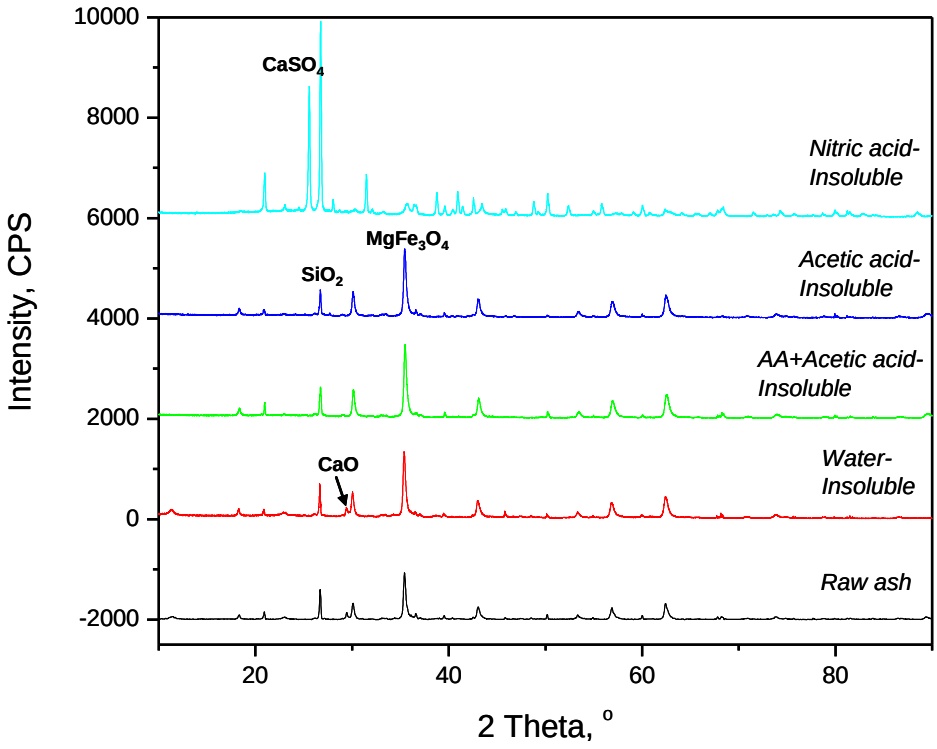

Figure 6.9 Yallourn coal fly ash XRD spectra.

Table 6.3 CCSEM results for Hazelwood fly ash sample

Category	Size (μm)								Totals
	0.5-1.	1-2.2	2.2-4.6	4.6-10.	10.-22.	22.-46.	46.-100.	100.-211.	
Quartz	0.12	0.49	0.33	0.51	0.03	0.34	1.59	2.25	5.66
Iron Oxide	0.01	0.00	0.00	0.05	0.36	0.00	0.00	0.00	0.43
Periclase	0.01	0.00	0.00	0.00	0.00	0.00	0.00	0.00	0.01
Rutile	0.00	0.00	0.00	0.10	0.00	0.00	0.00	0.00	0.10
Alumina	0.03	0.00	0.00	0.00	0.00	0.00	0.00	0.00	0.03
Calcite	0.00	0.00	0.00	0.00	0.00	0.00	0.00	0.00	0.00
Dolomite	0.20	0.34	0.27	0.06	0.01	0.04	0.00	0.00	0.90
Ankerite (Ca, Fe, Mg)CO_3	0.41	2.38	7.78	12.17	2.69	0.46	0.00	0.00	25.89
Kaolinite	0.01	0.04	0.09	0.53	0.14	0.12	0.21	0.00	1.14
Montmorillonite	0.03	0.15	0.24	0.66	0.42	0.37	0.82	0.00	2.70
K Al-silicate	0.00	0.03	0.14	0.00	0.02	0.05	0.14	0.00	0.39
Fe Al-silicate	0.27	1.22	0.30	0.34	0.24	0.04	0.12	0.00	2.53
Ca Al-silicate	0.01	0.05	0.03	0.00	0.00	0.00	0.00	0.00	0.10
Na Al-silicate	0.00	0.08	0.29	0.34	0.03	0.03	0.27	0.52	1.56
Aluminosilicate	0.00	0.00	0.00	0.00	0.00	0.00	0.00	0.00	0.00
Mixed Aluminosilicate	0.02	0.00	0.09	0.03	0.01	0.03	0.00	0.00	0.18
Fe silicate	0.07	0.00	0.16	0.12	0.00	0.00	0.00	0.00	0.35
Ca silicate	0.01	0.04	0.34	0.00	0.03	0.00	0.00	0.00	0.42
Ca Aluminate	0.00	0.00	0.00	0.00	0.00	0.00	0.00	0.00	0.00
Pyrite	0.00	0.00	0.00	0.00	0.00	0.00	0.00	0.00	0.00
Pyrrhotite	0.00	0.00	0.00	0.00	0.00	0.00	0.00	0.00	0.00
Oxidized pyrrhotite	0.00	0.00	0.00	0.00	0.00	0.00	0.00	0.00	0.00
Gypsum	0.12	0.43	0.12	0.00	0.00	0.03	0.00	0.00	0.69
Barite	0.00	0.00	0.00	0.00	0.00	0.00	0.00	0.00	0.00
Apatite	0.00	0.00	0.00	0.00	0.00	0.00	0.00	0.00	0.00
Ca-Al-P	0.00	0.00	0.00	0.00	0.00	0.00	0.00	0.00	0.00
NaCl	0.00	0.00	0.00	0.05	0.00	0.00	0.00	0.00	0.05
KCl	0.00	0.00	0.00	0.00	0.00	0.00	0.00	0.00	0.00
Gypsum/Barite	0.00	0.00	0.00	0.00	0.00	0.00	0.00	0.00	0.00
Gypsum/Al-silicate	0.03	0.00	0.00	0.00	0.00	0.00	0.00	0.00	0.03
Si-Rich	0.12	0.44	0.21	0.42	0.03	0.04	0.15	0.00	1.40
Ca-Rich	0.00	0.02	0.00	0.00	0.00	0.00	0.00	0.00	0.02
Ca-Si Rich	0.00	0.00	0.02	0.00	0.00	0.00	0.00	0.00	0.02
Unknown	2.96	14.17	17.29	15.33	2.29	1.93	0.90	0.56	55.42
Totals	4.44	19.87	27.70	30.69	6.30	3.48	4.20	3.33	100.00

The Hazelwood fly ash was further analysed by computer-controlled scanning electron microscopy (CCSEM) in Chubu University. The results are shown in table 6.3. This further confirms the abundance of ultra-fine and fine ash particles in the air-fired fly ash sample. The distribution of each species is also highly size-dependent.

Synchrotron X-ray adsorption spectroscopy (XAS) for the speciation of sulfur was also carried out at National Synchrotron Radiation Research Center (NSRRC), Taiwan. As illustrated in figure 6.10, sulfate such as Na_2SO_4 and $CaSO_4$ is prevalent in each fly ash sample. However, for the Yallourn coal fly ash, a small amount of pyrite (FeS_2) is also present in it. This is indicative of the strong reducing environment in the burner vicinity when this coal was burnt. The pyrite should be fully embedded in ash slag matrix where iron is dominant. To further clarify the presence of the strong reducing environment in coal burner, the ash deposit near coal burner and bottom ash were analysed by XRD, as shown in figure 6.11. Wustite (FeO) is present in both bottom ash and ash deposit in coal burner vicinity, which is a direct sign of the reducing environment near coal burner. Otherwise, wustite should be fully oxidised to hematite (Fe_2O_3). The strong reducing environment near coal burner should be caused by the evaporation of coal moisture, and/or the low ratio of primary air (for coal particle entrainment) to coal mass.

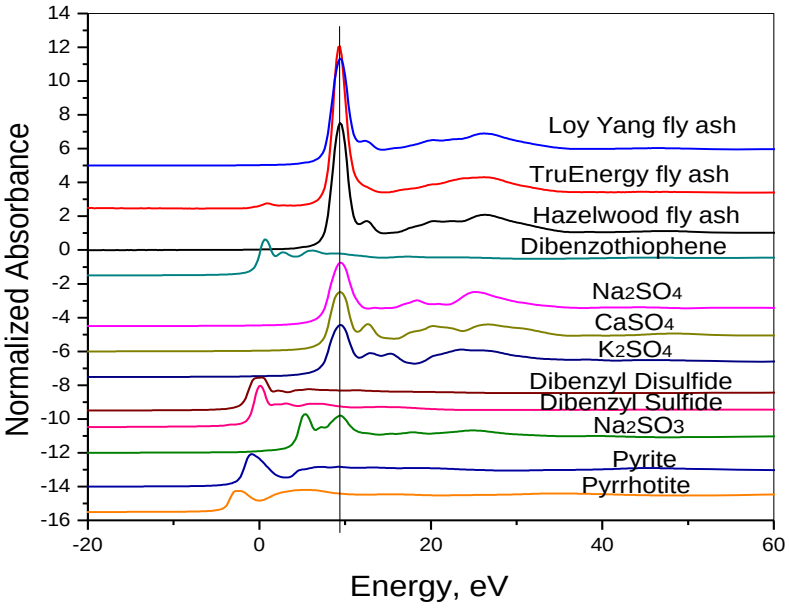

Figure 6.10 Synchrotron sulfur K-edge spectra for three fly ash samples.

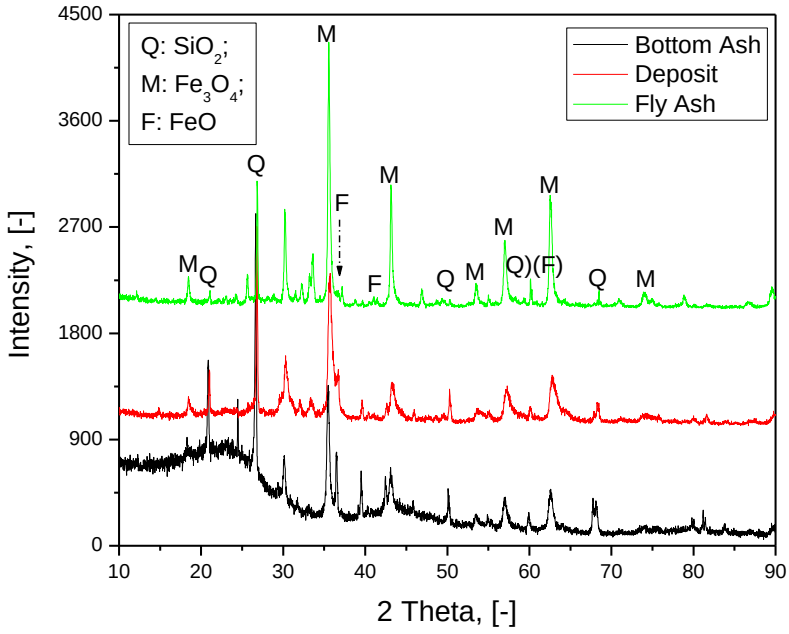

Figure 6.11 XRD spectra for bottom ash and ash deposit collected from the combustion of Yallourn coal in air in pilot-scale facility.

6.3 Characterization of oxy-fuel ash samples

The photos of probe with deposited ash under both air and oxy-fuel combustion conditions indicate the great difference between these two ash deposits, as visualised in Figure 6.12. It can be seen that, the appearance of the deposited ash (loose and powdery) is very similar under both conditions. However, the deposit thickness was notably different. Under the oxy-firing conditions, more of ash particles were found depositing on the probe. This should be due to a lower flow rate for flue gas and a larger ash particle density in flue gas as well.

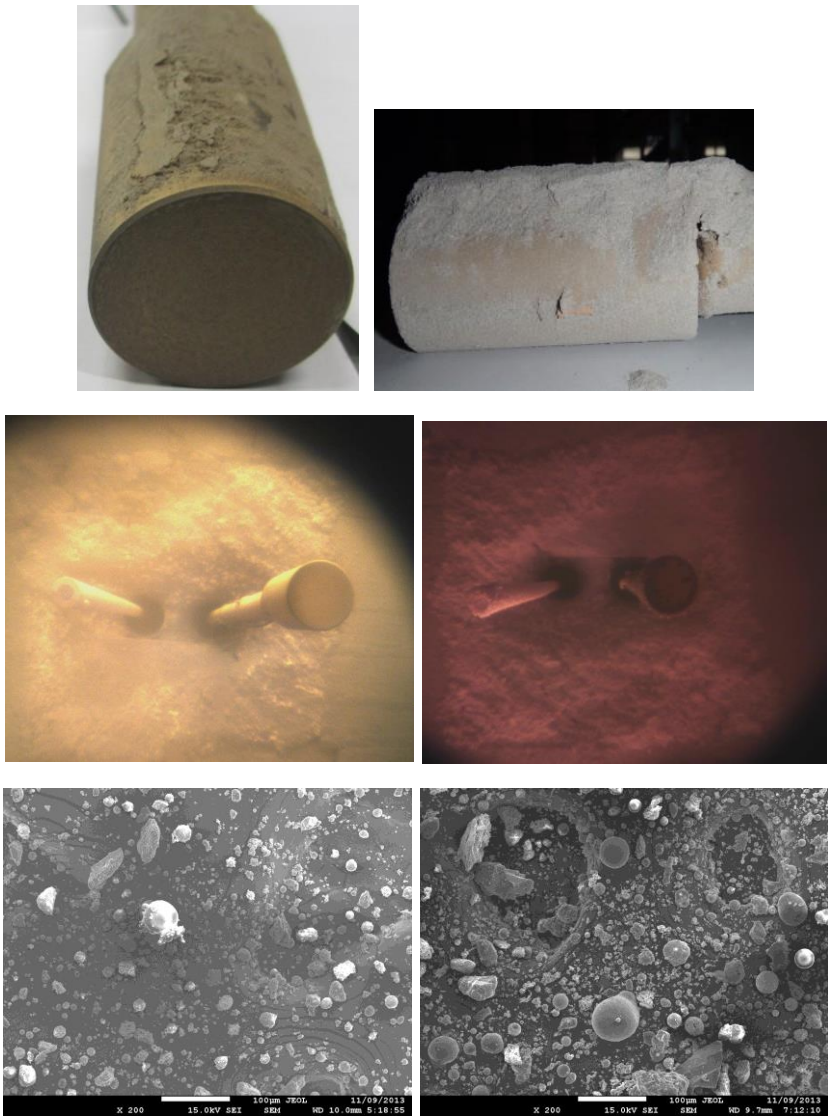

(a) Air firing (b) Oxy firing

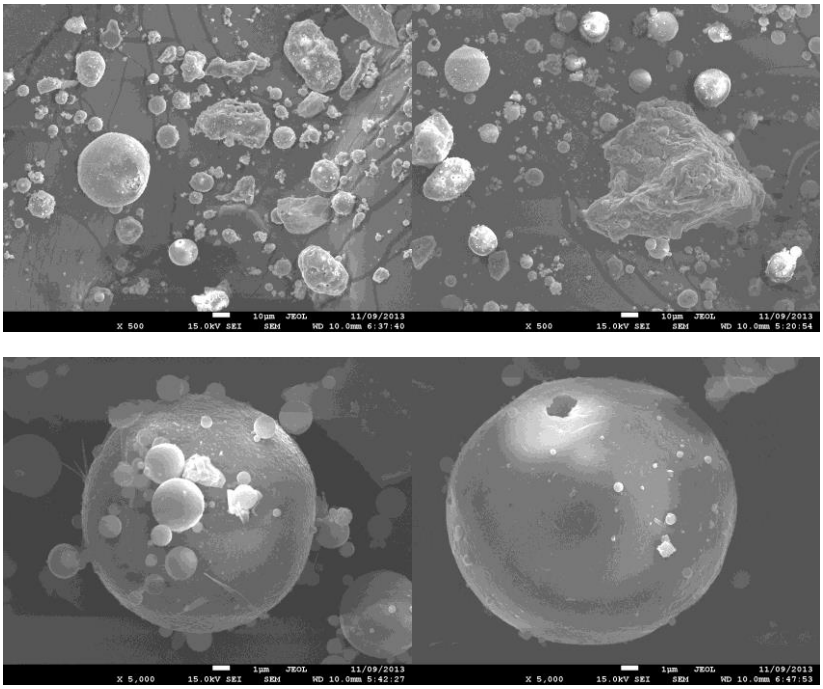

(a) Air firing (b) Oxy firing

Figure 6.12 Photos of deposited ash separately under air and oxy-fuel combustion conditions (flue gas Temp. 1300℃; Probe Temp. 400℃)

The particle size distribution for fly ash and ash deposits from air- and oxy-fuel modes, as determined by Malvern particle analyser, is shown in figure 6.13. Here we can clearly see a much smaller peak size for oxy-fuel fly ash, which suggests the preferred vaporization of fly ash due to the strong reducing environment in coal burner vicinity, under the oxy-fuel condition. The strong reducing environment is in favor of the vaporization of inherent ash-forming metals in a coal, particularly the organically bound metals which are abundant in low-rank brown coal. The condensed particulates usually bear a sub-micron size less than *1 μm*. This is clearly the case as observed for oxy-fuel fly ash.

The elemental compositions were identified by using X-ray fluorescence spectroscopy (XRF). The enrichment factor EF_i was also used to describe the relative enrichment of an element in the sampled ash relative to its concentration in the laboratory ash achieved by ashing coal at 600^{o}C (air condition). The enrichment factor EF is definite as follows:

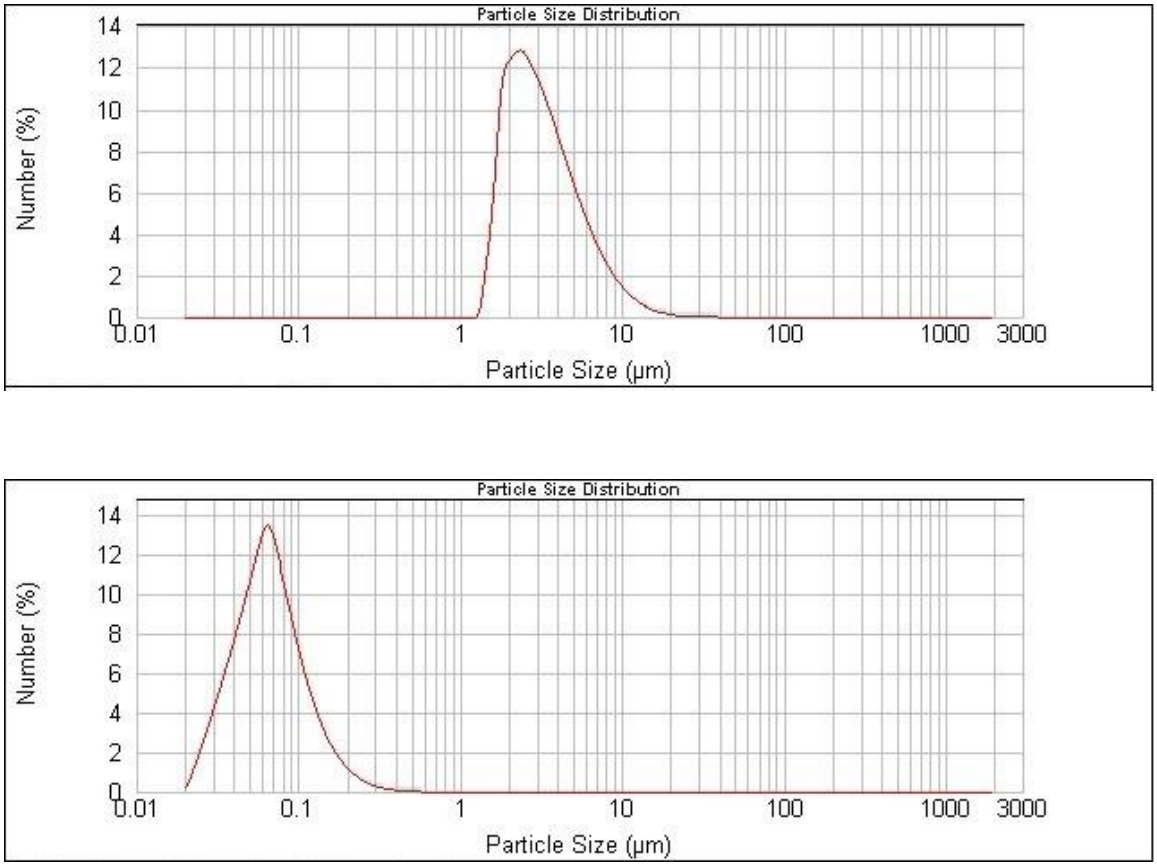

Figure 6.13 Particle size distribution of fly ash samples collected from air-firing and oxy-fuel combustion of dried Loy Yang coal, 0.9 MW.

$$EF_i = \frac{X_{dep,i}}{X_{ash,i}}$$

Where, $X_{dep,i}$ is the mass fraction of the element *i* (expressed as oxide) in the either the deposit or fly ash and $X_{ash,i}$ is the its corresponding mass fraction of the element i (expressed as oxide) in the laboratory ash, which resemble the bulk chemical composition of raw ash. The EF of individual metals and elements their mass concentrations of sampled ash under different conditions are illustrated in Figure 6.14, respectively. For the enrich factor (EF), the enrichment factor, for most elements does not seem to change between air and oxy-fuel conditions, except for the element of K (seen from *Fig. 6.14*). Elemental composition in figure 6.15 indicate that the ash deposit as well as fly ash are enriched in Si, Al, K, and Ca under the both conditions, while slightly depleted in sodium, sulfur and iron. This indicates that a portion of sodium enters the gas phase, likely in Na_2O or Na and the sulfur is mainly existed as SO_2 as gas phase. While for the iron element, the main reason for its depletion in ash

deposit could be the formation of lower melting temperature of iron-bearing minerals and caused that prefer to drop out of the boiler as bottom slag. The chemical compositions of ash deposit and fly ash are shown in Figure 6.15 separately ((a) and (b)). It can be seen that the fly ash contents and ash deposition characteristics in oxy-firing case differ from air-firing case. The higher content of SO_3 and Fe_2O_3 and lower content of SiO_2 and Al_2O_3 were observed for the fly ash collected under oxy-fuel combustion condition. Accordingly, the oxy-fuel fly ash sample has a higher base/acid ratio, as demonstrated in *figure 6.16*. While the similar ash contents and ash deposition characteristic has been confirmed in the deposited ash in the combustion zone of experimental furnace under two conditions. The altered flue gas components and temperature distribution is the main reason for that phenomena.

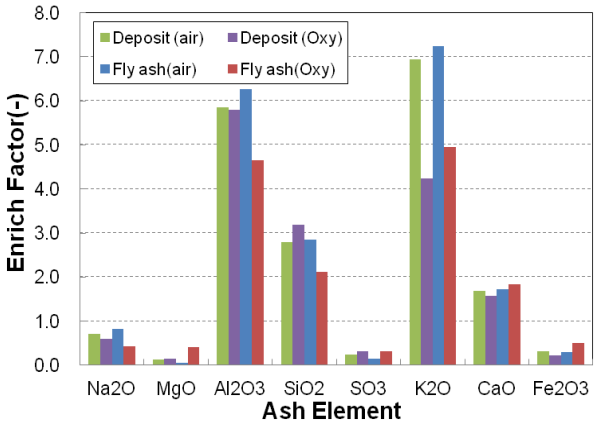

Figure 6.14 EF of deposited and fly ash separately under air and oxy-fuel combustion condition

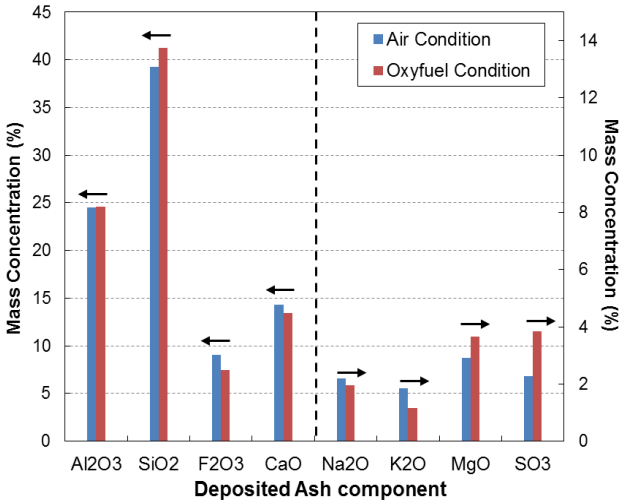

(a) Deposited ash (Flue gas temp. 1300℃)

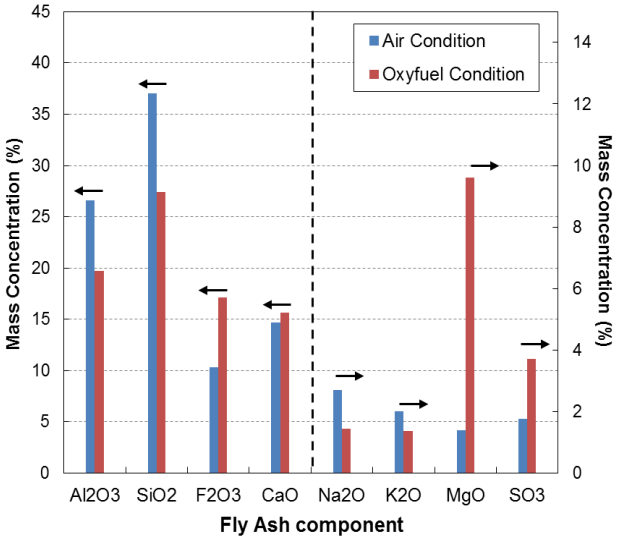

(b) Fly ash (flue gas temp. 250℃)

Figure 6.15 Chemical composition of ash samples under air and oxy-fuel combustion condition

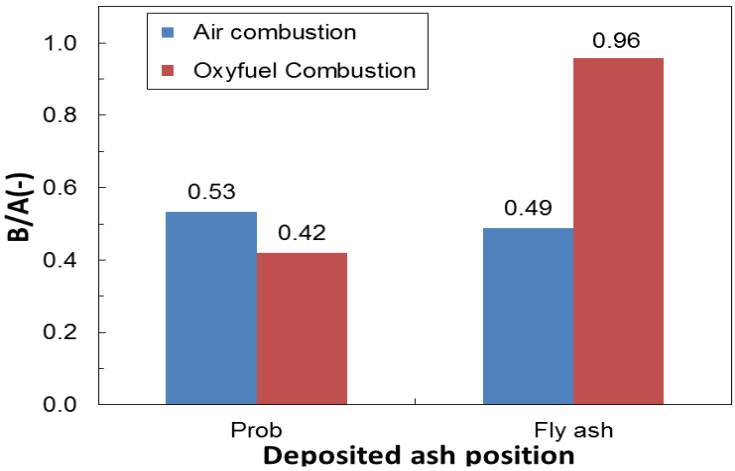

Figure 6.16 base/acid value of ash samples under both conditions

In order to obtain the detailed information on ash melting behavior of YL coal under both air-firing and oxy-firing conditions, a thermodynamic equilibrium analysis and viscosity calculations were conducted, considering that the amount of liquid phases present as well as viscosity affects the rate of ash sintering and deposition. The FToxid-slagA liquid/glass solution database and flue gas composition in boiler were used in each calculation, which contain the system of six components SiO_2-Al_2O_3-CaO-Fe_2O_3-MgO-Na_2O-K_2O-SO_3 in solid phase and four gases (O_2; CO_2; N_2:73; H_2O) in gas phase. The modified Urbain equation (Kalmanovitch model) has been used for

viscosity estimation. For each calculation, its input includes ash compositions, flue gas composition (either oxidizing environment or reducing gas composition for 50% H_2 and 50% CO_2) and temperature. The calculations were performed for a temperature range between 800 and 1800℃ and atmospheric pressure. The possible products selected are the entire compound species (ideal gases, pure solids and pure liquids) from the software database. Figure 6.17 shows the thermodynamic equilibrium predictions of molten slag fraction (*wt%*) and viscosities (poise) for both ashes from 200℃ to 1800℃. According to chemical equilibrium calculation results for air and oxy-fuel combustion conditions, the higher amounts of slag phase for two kinds of ash samples under oxy-fuel condition are predicted as comparing with that under air firing condition. The slagging behavior of the deposited ash formed in oxy-firing and air-firing cases are very similar, reflecting the similarity of their compositions as shown in figure 7.15(a). While for the fly ash, the different chemical component caused the remarkably different melting behavior in the two cases. The maximum amount of slag for oxy-firing fly ash reaches around 85 gram from 1200^{o}C onwards, relative to only 60 gram from 1500^{o}C for the air case. This implies the intensified slagging issue for the oxy-firing ash, although the flue gas temperature in oxy-firing case is slightly lower than the air case. The enrichment of S and Fe in the fly ash under oxy-fuel combustion condition should be the main reason for this issue. A detailed investigation on the structure of these two elements is underway.

The strong deposit region was defined as the value of viscosity ranges from 250 poises to 3300 poises. A liquid with a viscosity of 250 poises should readily flow on a flat surface, while the value of 3300 poises should be mostly present like sticky honey that is hard to blow off on the surface. The temperature window of strong deposition for deposit ash under oxy-firing condition is ranged from 1050℃ to 1260℃, which 40 ℃ lower than that under air-firing condition. Whereas, for fly ash, the temperature window of its strong deposition under oxy-firing condition is about 170~180℃ (880~1080℃) lower than that under air-firing condition, as shown in *table 7.4*. The lower temperature window of strong deposition and higher percentage of molten phase in ash under oxy-firing condition seems to be the main reason for its relative more serious deposition problems in the section of super heater and re-heater (800~1150℃) in boiler.

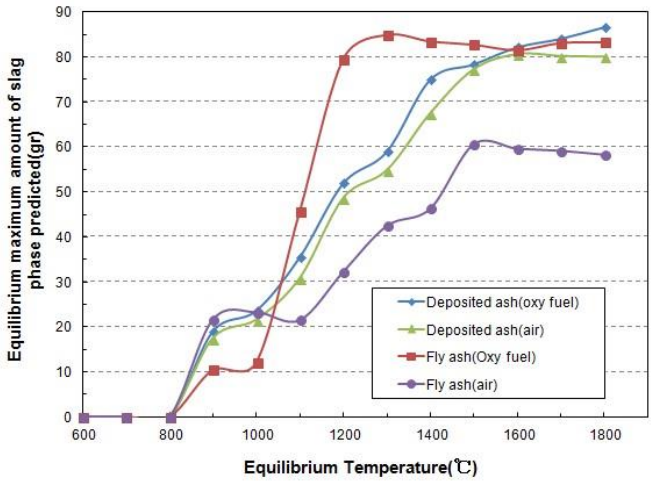

(a) Percentage of liquid phase in ash along with temperature

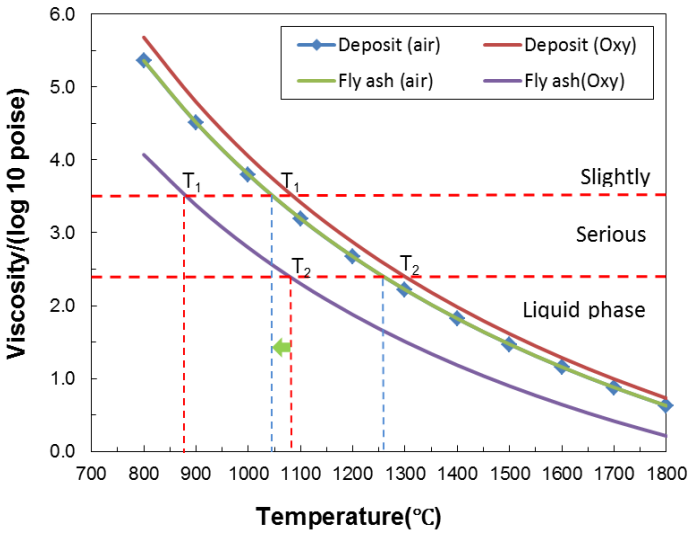

(b) Viscosity of ash samples under both two conditions

Figure 6.17 Predictions of molten slag fraction and viscosities for ash samples under both air-firing and oxy-firing conditions

Table 6.4 Strong deposition temperature window of ash under both conditions

	T_1	T_2	ΔT
Deposited (air)	1090	1300	210
Deposited (Oxy fuel)	1050	1260	210
Fly ash(air)	1050	1260	210
Fly ash(Oxy fuel)	880	1080	200

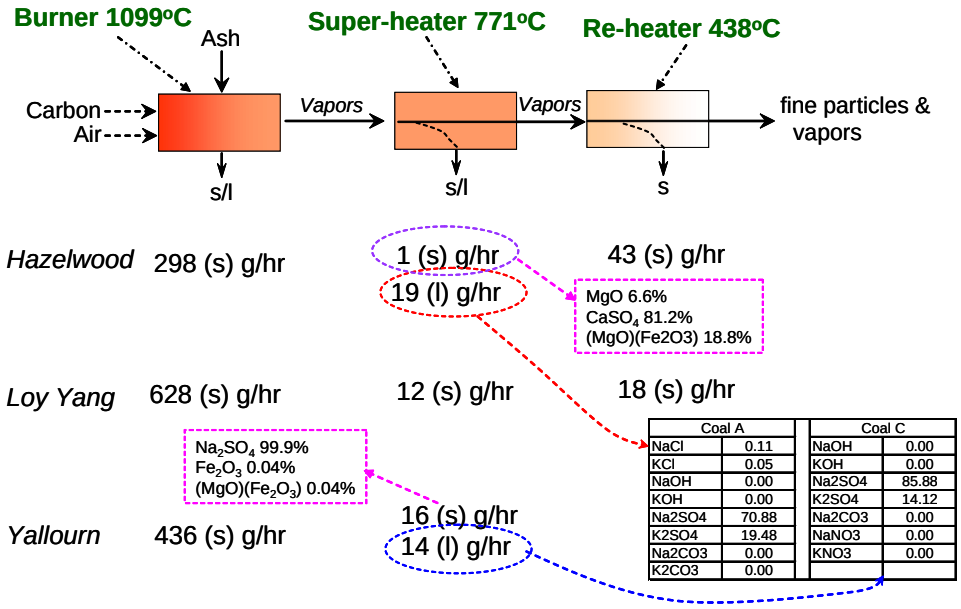

Figure 6.18 Ash mass balance and distribution estimated for the combustion of three coals in air-firing.

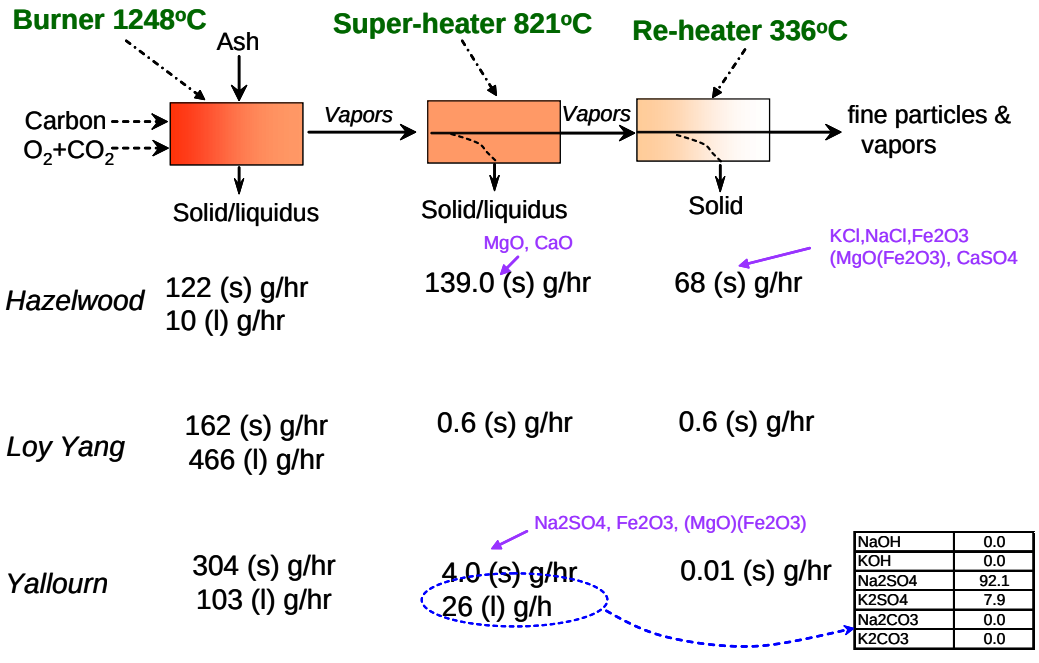

Figure 6.19 Ash mass balance and distribution estimated for the combustion of three coals in oxy-firing with 30% oxygen in the furnace and the use of dried coal with 20% moisture.

.

For both ash deposit and fly ash collected from oxy-fuel case, the fraction of liquidus species within either of them is larger than the respective air-fired samples. This can be attributed to the stronger reducing environment in the vicinity of coal burner in the oxy-fuel case than air-firing case. The stronger reducing environment is caused by the extra char-CO_2 and char-steam gasification reactions near coal burner. This is proven by the CFD modeling results in the subsection 4 later. This strong reducing environment not only affects ash properties, but it also affects ash distribution along the furnace.

Based on ash mass balance, the ash distribution of ash-forming metals for the combustion of three coals in oxy-fuel versus air-firing is summarised in figures 6.18 and 6.19, respectively. For the air-firing, the majority of fly ash particles is supposed to be formed in the combustion zone where the average temperature is around 1100^{o}C, irrespective of coal sample property. In particle, the Loy Yang coal ash formed in the combustion zone accounts for nearly all the final fly ash in the exhausted flue gas. This should be attributed to the presence of abundant refractory SiO_2 and Al_2O_3 in this coal sample. Regarding the ash deposit on super-heater zone, it is rich in sulfates including Na_2SO_4, K_2SO_4 and oxide spinel such as $(MgO)(Fe_2O_3)$. With the shift of coal combustion from air to oxy-firing, the total amount of ash generated in combustion zone wasn't changed noticeably. However, the fraction of liquidus species is increased notably. For Loy Yang coal ash, its liquid amount in ash was increased to around 466 g/h in oxy-fuel case, compared to a negligible value for air-firing case. Similarly, for Yallourn coal, its ash generated in the oxy-fuel combustion zone is composed of 103 g/h liquidus phase, relative to nearly zero in the air-firing case. Regarding ash deposit amount, it was increased in the oxy-fuel case for Hazelwood coal, compared to its air-firing case. This could be attributed to a small flue gas amount and high ash particle density in the oxy-firing boiler. The changes on the other two coal ash deposit amount are relatively small. Regarding ash carbonation, we did not notice any carbonate formed in the ash deposit. This should be due to a very short exposure time (maximum 5 *hr*) for the ash particles in the boiler.

6.4 Conclusions

Through the short-term ash exposure test for maximum 5 *hr*, the major conclusions regarding Victorian brown coal ash deposition propensity and properties can be drawn as follows:

1 The higher content of SO_3 and Fe_2O_3 and lower content of SiO_2 and Al_2O_3 were found in the oxy-firing fly ash, whereas the similar composition and ash deposition characteristic have been found in the combustion zone for air-firing versus oxy-fuel combustion;

2 The ash fusion temperature of oxy-firing fly ash is approximately 200^{o}C lower than the air case. The enrichment of S and Fe in the oxy-firing sample is supposed to be the main reason.

3 The basic and acid ratio (B/A) value (0.9) of fly ash is around 2 times than that in the air case, due to the relative higher content of SO_3 and Fe_2O_3 and lower content of SiO_2 and Al_2O_3, whereas the similar B/A value (~0.4) of deposited ash at high temperature in the both case;

4 Based on the equilibrium and viscosity calculation, the serious deposition temperature zone of fly ash in the oxy-fuel case is around 880 ~1080 ℃, which is around 180 ℃ earlier than that in the air case. Again, the enrichment of S and Fe in the oxy-firing sample is supposed to be the main reason for this issue.

7. Future works

To reiterate, this project is based on oxy-fuel combustion technology, a process for the burning of coal, either dried or as-received wet, in a mixture of high-purity oxygen with recirculated flue gas. Through a prior removal of nitrogen, and the optimisation of boiler operating parameters, oxy-fuel combustion has proven to be able to provide purity up to 95% for CO_2 in flue gas, which can thus be sequestered or utilised with minimal treatment. Through this two-year ANLEC R&D/BCIA project in 2012-13, we have proven the stable and quicker combustion of wet Victorian brown coal with up to 40 *wt%* moisture in a 3 MWth pilot-scale furnace, the high-purity of CO_2 (>80% dry) in flue gas, the distinct radiative heat flux and flue gas temperature profile in the oxy-firing boiler, the remarkably low concentrations of impure trace metals in flue gas, and the potentially distinct slagging/fouling propensity for brown coal ash in oxy-fuel mode. In addition, we have successfully established the process flowsheet for a virtual 600 MWth brown coal-fired oxy-fuel plant coupled with external dryer and supercritical steam condition, and successfully refined and validated the computational fluid dynamics (CFD)-based codes to incorporate the distinct properties relating to oxy-fuel combustion of Victorian brown coal.

For a detailed system design in the future deployment stage, extra efforts should be made to continue the R&D of oxy-fuel combustion of Victorian brown coal through both experimental investigations and computational modelling, to further optimise the oxy-firing process for Victorian brown coal, and to clarify the unknown/unclear issues that may deter the deployment of brown coal oxy-fuel combustion technology. That is:

a) Optimisation of burner aerodynamic and staged oxygen injection to strike the balance between the stability of brow coal combustion and the emissions of NOx/SOx/unburnt carbon/CO and mercury;

b) Elucidation of ash slagging/fouling propensity and water tube corrosion rate as a function of brown coal oxy-firing conditions, combined with subcritical or supercritical steam conditions, under long-term ash exposure conditions; and

c) Completion of the fully validated modelling programs on oxy-lignite burner configuration and lignite ash deposition prediction under both airfiring and oxy-fuel modes.

8. Intellectual Properties and Publication

Modeling Programs/Codes Developed

1) Brown coal drying code as user defined function (UDF) added into CFD Fluent;

2) Computing code for the radiation coefficients of oxy-fuel flue gas;

3) Computing codes for the simulation of char-CO_2, char-steam and volatile-CO_2 oxidation rates.

Published Journal Papers:

4) Wirhan Prationo, Jian Zhang, Xiaojiang Wu, Xiaodong Chen, Lian Zhang, Influence of external clay and inherent minerals on lignite optical ignition and volatile flame propagation in air-firing and oxy-firing, ***Industrial & Engineering Chemistry Research*** 2014, 53(7): 2594-2604.

5) Jian Zhang, Wirhan Prationo, Lian Zhang, Zhongxiao Zhang, Computational fluid dynamics modelling on the air-firing and oxy-fuel combustion of dried Victorian brown coal, ***Energy Fuels*** 2013, 27: 4258-69.

6) Baiqian Dai, Fiona Low, Anthony De Girolamo, Xiaojiang WU, Lian Zhang, Characteristics of ash deposits in a pulverised lignite coal-fired boiler and the mass flow of major ash-forming inorganic elements, ***Energy Fuels*** 2013, 27(10): 6198-6211.

7) Juan Chen, Facun Jiao, Lian Zhang, Yong Hao, Yoshihiko Ninomiya, Elucidating the mechanism of Cr(VI) formation upon the interaction with metal oxides during coal oxy-fuel combustion, ***Journal of Hazardous Materials***, 2013, 261: 260-8.

8) Fiona Low, Lian Zhang, Arsenic emissions and speciation in the oxy-fuel fly ash collected from lab-scale drop-tube furnace, ***Proc. Comb. Inst***, 2013, 34, 2877-84.

9) Fiona Low, Lian Zhang, Microwave Digestion for the Quantification of Inorganic Elements in Coal and Coal Ash using ICP-OES, ***Talanta*** 2012, 101, 346-52.

10) Juan Chen, Baiqian Dai, Fiona Low, Lian Zhang, XANES investigation on sulphur evolution during Victorian brown coal char gasification in oxy-fuel combustion mode, ***Energy Fuels***, 2012, 26, 4775-82.

11) Juan Chen, Facun Jiao, Lian Zhang, Hong Yao, Yoshihiko Ninomiya, Use of synchrotron XANES and Cr-doped coal to further confirm the vaporization of organically bound Cr and the formation of Cr(VI) during coal oxy-fuel combustion, ***Environ. Sci. Technol.*** 2012, 46, 3567-3573.

12) Juan Chen, Hong Yao, Lian Zhang, A study on the calcination and sulphation behaviour of limestone during oxy-fuel combustion, ***Fuel*** 2012, 102, 386-395.

13) Submitted Journal Papers Under Peer Review:

14) Fiona Low, Anthony De Girolamo, Baiqian Dai, Lian Zhang, Emission of organically bound metals during the pyrolysis and char oxidation of lignites in oxy-fuel combustion mode. ***Energy Fuels***, submitted in Feb 2014.

15) Baiqian Dai, Xiaojiang Wu, Anthony Der Girolamo, Lian Zhang, Inhibition of lignite ash slagging and fouling upon the use of silica-based additive in industrial pulverised coal-fired boiler: part 1 change on the properties of ash deposits along the furnace, ***Fuel***, submitted in Feb 2014.

16) Baiqian Dai, Xiaojiang Wu, Anthony Der Girolamo, Lian Zhang, Inhibition of lignite ash slagging and fouling upon the use of silica-based additive in industrial pulverised coal-fired boiler: Part 2 speciation of iron in ash deposits and separation of magnetite and ferrite, ***Fuel***, submitted in Feb 2014.

17) Wirhan Prationo, Jian Zhang, Xiaodong Chen, Lian Zhang, Clarifying the influence of moisture on the ignition and combustion of wet Victorian brown coal in air-firing and oxy-fuel modes: experimental and modelling study, ***Fuel***, Dec 2013.

18) Jian Zhang, Lian Zhang, Pilot-scale oxy-fuel combustion of Victorian brown coal, ***Proceedings of the Combustion Institute***, Dec 2013.

19) Xiaojiang Wu, Jian Zhang, Baiqian Dai, Lian Zhang, Ash slagging and fouling during high-alkali coal combustion in pilot-scale facility, ***Proceedings of the Combustion Institute***, Dec 2013.

20) Peer-reviewed Conference Papers:

21) Jian Zhang, Lian Zhang, Pilot-scale oxy-fuel combustion of Victorian brown coal, 3rd International Oxy-Fuel Combustion Conference, Sept 2013, Panferrade, Spain.

22) Lian Zhang, Fiona Low, The chemistry of chromium in coal and its transformation during coal combustion – use of synchrotron XAS and high-temperature XRD for molecular-scale investigation, 10th Australian Coal Science Conference, October 2013, Brisbane.

23) Jian Zhang, Lian Zhang, *In-situ* optical diagnosis and continuous-film modelling on homo-heterogeneous ignition of lignite in air-firing and oxy-firing modes, 10th Australian Coal Science Conference, October 2013, Brisbane.

24) Xiaojiang Wu, Bai-qian Dai, Kai Yan, Jian Zhang, Xiang Zhang, Jianwen Zhang, Lian Zhang, Experimental study on ash deposition characteristics of Victorian brown coal in pilot-scale oxy-fuel combustion, 2013 Chemeca, Sept 29 – Oct 2, 2013, Brisbane.

25) Kai Yan, Huan Wang, Qiang Fan, Defu Che, Xiaojiang Wu, Lian Zhang, A universal model for the hydrodynamics performance design of steam generation system, 2013 Chemeca, Sept 29 – Oct 2, 2013, Brisbane.

26) Zhang L, Zhang J, Wu XJ, Zhang J, Ninomiya Y, Experimental and modeling investigation on the pilot-scale oxy-fuel combustion of Victorian brown coal, Proceedings of the 30th International Pittsburgh Coal Conference, Sept 15-18, 2013, Beijing, China.

27) De Girolamo A, Dai B-Q, Zhang L, Wu XJ, A study of slagging and fouling: current theory and experimental chracterisation of deposits, Proceedings of the 30th International Pittsburgh Coal Conference, Sept 15-18, 2013, Beijing, China.

28) Prationo W, Zhang L, Zhang J, Ignition and combustion characteristics of wet Victorian brown coal in oxy-firing and air-firing conditions, Proceedings of the 30th International Pittsburgh Coal Conference, Sept 15-18, 2013, Beijing, China.

29) Yan K, Wang H, Fan Q, Che D, Wu XJ, Zhang L, A universal model for the thermal hydraulic performance design of steam generation system, Chemeca 2013, Sept 29-Oct 2 2013, Brisbane, Australia.

30) Wu XJ, Dai BQ, Yan K, Zhang K, Zhang X, Zhang J, Zhang L, Experimental study on ash deposition characteristics of Victorian brown coal in pilot-scale oxy-fuel combustion, Chemeca 2013, Sept 29-Oct 2 2013, Brisbane, Australia.

31) Wu XJ, Zhang J, Zhang L, Yan K, *et al*, Investigation on the oxy-fuel combustion of Victorian brown coal in a 3 MW pilot-scale facility, Proceedings of the Australian Combustion Symposium, November 6-8, 2013, Perth, Western Australia.

32) Yan K, Wu XJ, Hoadley A, Xu XY, Zhang j, Zhang L, Sensitivity analysis of oxy-fuel power plant performance, Proceedings of the Australian Combustion Symposium, November 6-8, 2013, Perth, Western Australia.

33) Zhang J, Prationo W, Zhang L, CFD modelling of the oxy-fuel combustion of Victorian brown coal in drop tube furnace and 3 MW pilot scale boiler, Proceedings of the 9th International Conference on CFD in the Minerals and Process Industries, CSIRO, 10-12 Dec 2012, Melbourne, Australia.

34) Zhang L, Zhang J, Prationo W, Oxy-fuel combustion of Victorian brown coal, AIChE Annual Meeting, Oct 28- Nov 2, 2012, Pittsburgh, USA.

35) Chen J, Yao H, Xu M, Wu X, Zhang L, Mechanisms for calcination and sulfation of limestone during oxy-fuel combustion, the 2nd oxy-fuel combustion conference, 12-16 September 2011, Brisbane, Australia.

36) Zhang L, Jiao F, Ninomiya Y, Bhattacharya S and Li C-Z, Ash formation and trace metal emissions during oxy-fuel combustion, the 2nd oxy-fuel combustion conference, 12-16 September 2011, Brisbane, Australia.

Workshop organised:

Australia-China oxy-fuel combustion workshop, February 6-8, 2014, Hotel Bruce County, Mount Waverley, Melbourne, Australia.

This paper is left blank intentionally.